DEVELOPMENT AND CHARACTERIZATION OF UF MEMBRANES
AND
RELATION OF MEMBRANE PROPERTIES TO ADSORPTIVE FOULING

Prepared by:

Mark M. Clark,

Corine Combe, Elisabeth Molis, Yonghun Lee,

Kerry Howe, Kwang-Soo Kim, Manish Kumar, Pascale Lucas, and Yingge Wang

The University of Illinois

At Urbana-Champaign

205 N. Mathews Avenue

Urbana, IL 61801

Sponsored by:

National Water Research Institute

and Lyonnaise de Eaux

CONTENTS

Part I

Diffusion and Partitioning of Humic Acid in a Porous Ultrafiltration Membrane, published in Journal of Membrane Science, 1998

and

The Effect of CA Membrane Properties on Adsorptive Fouling of Humic Acid, published in Journal of Membrane Science, 1999

ELSEVIER

Journal of Membrane Science 154 (1999) 73–87

journal of MEMBRANE SCIENCE

The effect of CA membrane properties on adsorptive fouling by humic acid

C. Combe[a], E. Molis[a], P. Lucas[a], R. Riley[b], M.M. Clark[a,*]

[a]*Department of Civil and Environmental Engineering, University of Illinois, 205 North Mathews Avenue, Urbana, IL 61801, USA*
[b]*Separation Systems Technology, 4901 Morena Blvd, San Diego, CA 92117, USA*

Received 9 April 1998; received in revised form 28 May 1998; accepted 31 August 1998

Abstract

Cellulose acetate membranes with varied charge, hydrophobicity, porosity, and pore size have been developed by annealing, hydrolysis and oxidation of a basic cellulose acetate membrane. The effects of these modifications were characterized by poly(ethylene glycol) retention, contact angle and streaming potential measurements, and atomic force microscopy. The behavior of the membranes during humic acid adsorption experiments has also been studied. The results show that humic acid adsorption occurs both inside the pore and on the membrane surface. Experiments at different pH show the importance of solution properties on humic acid adsorption through modification of membrane and humic acid charge. Although many membrane characteristics are modified by hydrolysis and oxidation, neither treatment prevented humic acid adsorption on the CA membranes. The most effective surface treatment was with an anionic polymer, which significantly reduced adsorption of humic acid.

Keywords: Humic acid; Membrane preparation and structure; Water treatment; Surface characterization

1. Introduction

Humic substances are abundant in natural waters. They are the result of chemical and biological degradation of plant and animal residues and the synthesis activities of microorganisms [1]. Humic and fulvic acids represent the major fraction of dissolved natural organic matter in aquatic environments. They are responsible for natural water color and for initiating photochemical transformations of both organic compounds and trace metals [2]. These substances are also important constituents of the organic colloidal phase and are one of the major fouling agents during filtration of surface waters in reverse osmosis [3], nanofiltration [4], ultrafiltration [5,6], and microfiltration [7]. Although membrane fouling by relatively well characterized macromolecules such as proteins has been extensively studied [8,9], mechanisms of fouling by humic substances are not yet well understood because of the heterogeneous nature of these macromolecules. According to previous studies, membrane fouling by humic substances is influenced by the characteristics of the humic substances and membrane, the hydrodynamic conditions, and the chemical composition of the feed water. Understanding of these factors is essential for better control of membrane fouling by humic acid and other types of natural organic matter.

*Corresponding author. Tel: +1-217-333-3629; fax: +1-217-333-6968; e-mail: m-clark3@uiuc.edu

0376-7388/99/$ – see front matter
PII: S0376-7388(98)00268-3

Several studies have focussed on humic acid properties. Cornel et al. [1] found that pH and ionic strength affect the molecular size distribution of humic acid. Because of the presence of numerous carboxylic and phenolic –OH functional groups, humic substances are usually negatively charged in aqueous solutions at neutral to high pH. This charge also varies with physico-chemical properties of the solution such as ionic strength and humic concentration. The theory proposed by Ghosh and Schnitzer [10] suggests two configurations for humic acid macromolecules: a flexible linear macromolecule at very low ionic strength, high pH, and low solution concentration, and a rigid compact spherocolloidal macromolecule at high ionic strength, low pH, and high solution concentration. Membrane fouling by humic substances may be explained in part by the effect of solution chemistry on molecular configuration.

Membrane pore size, porosity, charge, and hydrophobic/hydrophilic character will affect fouling by organic matter. For example, adsorption of humic acid seems to be enhanced on hydrophobic membranes [11]. Hong and Elimelech [12] remark that fouling on nanofiltration membranes cannot be explained by the same mechanisms as those used in the case of fouling of ultrafiltration or microfiltration membranes. For charged molecules transport phenomena like back-diffusion or charge repulsion are enhanced in nanofiltration compared to ultrafiltration and microfiltration.

The objective of this work is to investigate the effect of membrane properties on humic acid adsorption. Several variations of the basic cellulose acetate membrane were developed by surface modification of the membrane. The effects of modifications of pore hydrophobicity, charge, pore size, and porosity on humic acid adsorption were studied. Electrostatic and hydrophobic interactions between humic acid and the membrane surface were taken into account to explain adsorption results.

2. Experimental

2.1. Membrane preparation and structure

Cellulose acetate is the result of esterification of cellulose by acetic acid or anhydride. The most common cellulose acetate is cellulose triacetate. This ester results from the replacement of all or portion of the hydroxyl units on the cellulose chain with acetyl groups. The acetyl content affects the hydrophobicity of the membrane.

Table 1
Polymer mixture composition for the membrane synthesis

CA solids	15%
CA 39.8-3 (77.446%)	
CTA Eastman 2314~44% Acetyl (22.54%)	
Average acetyl content (40%)	
Dioxane	47.86%
Acetone	24.88%
Methanol	9.17%
Maleic acid	3.09%

The membranes used in this research were manufactured by Separation Systems Technology, San Diego, CA. They are made from cellulose acetate using the phase inversion process, in which a polymer is dissolved in an appropriate solvent and cast as a 0.1–1 mm thick film. The polymer mixture composition is presented in Table 1. A non-solvent is then contacted with this liquid film, causing phase separation and precipitation. In our case the film is immersed into a cold water gelation bath. The membranes are cast on the surface of a non-woven polyester support, which is commonly used in the industry. The membranes were fabricated on both a laboratory casting machine and a continuous commercial-type casting machine.

2.2. Membrane surface modification

In order to study the influence of membrane surface properties on fouling, several series of modified CA membranes have been developed.

2.2.1. Annealing: modification of porosity, and pore size

Cellulose acetate has a negative coefficient of expansion, and it is possible to increase the density of the skin layer by annealing the membrane at different temperatures. In our work CA membranes have been annealed at temperatures varying between 40°C and 80°C by immersion in a water bath. The effect of annealing temperature is then measured in terms of porosity and pore size modification.

2.2.2. Hydrolysis and oxidation: modification of hydrophilic/hydrophobic nature

Increased hydrophobicity is generally correlated with increased fouling by humic acid. Hydrophobicity is directly related to the acetyl content of the membrane and can be reduced by breaking the ester link between cellulose and acetyl groups. Treatment with caustic effectively reduces acetyl content of the membrane below 39.8%, a level that cannot normally be achieved in the phase inversion process because of the insolubility of cellulose acetate in common organic solvents at these acetyl levels. In our research, hydrolysis was carried out by treating the CA membrane with a solution of 0.1 M NaOH with 1% MeOH for varying times of 1, 5, and 10 min. Membrane hydrophobicity is estimated by contact angle measurements.

Surface oxidation can also be used to decrease CA membrane hydrophobicity by increasing carboxyl content. Oxidation has been carried out with a strong oxidizing agent, 35% H_2O_2. Oxidation takes place at the anhydroglucose linkages, and should affect hydrophobicity and pore/surface charge by replacing hydroxyl groups by acid groups. In our study the oxidation times were 30, 60, and 120 min.

After hydrolysis and oxidation treatments, the CA membranes were annealed by immersion in a water bath at a fixed temperature between 40°C and 80°C.

2.2.3. Polymer treatment: surface charge modification

After annealing, some of the membranes were contacted with a dilute solution of a vinyl acetate/acrylic acid copolymer, called "Colloid 189". At pH=4, this anionic polymer adsorbs onto the surface of cellulose acetate, but can desorb above pH=7. This treatment will increase the hydrophilic character of the membrane surface and increase the negative charge. This treatment is called sizing and is known in the industry to increase the rejection of reverse osmosis membranes. Sizing is investigated here to see if it affects adsorptive fouling of CA membranes by humic acid.

After membrane casting and treatment, water permeation rate was measured at different pressures; then the CA membranes were characterized with the different methods presented below.

Table 2
Solute radius calculated by empirical Lentsch's equation [13]

MW (Da)	300	600	3350	10000
r_s (nm)	0.5	0.75	1.6	2.6

2.3. PEG retention

In order to characterize the membrane pore size, molecular weight cut-off (MWCO) was determined using model solutes. Synthetic polymers, such as polyethylene glycol (PEG), dextran, polyvinylpyrrolidone are usually chosen because they do not interact strongly with the membrane material. In this study we used a group of four PEG, with molecular weights of 300, 600, 3350 and 10000 Da purchased from Sigma (St Louis, MO). Lentsch [13] used an empirical equation to calculate the Stokes radius of PEG. Experimental PEG diffusion coefficient measurements were combined with the Stokes–Einstein law to give the following relation:

$$r_s = 0.045\, M^{0.44}, \tag{1}$$

where r_s is the PEG Stokes radius (nm); M is the molecular weight (Da). The Stokes radii calculated for the PEG used in this study are presented in Table 2.

Filtration tests were performed using a 28.7 cm^2 diameter UF cell with magnetic stirrer (Amicon, Minnetonka, MI). The pressure was applied via a compressed nitrogen tank, and was varied between 103.4 and 344.7 kPa (15 and 50 psi). The concentration of PEG was 10 mg/l and the pH=6.5. Membrane water permeability was measured before and after each filtration experiment in order to check for membrane fouling by PEG. For each applied pressure, PEG concentrations in the retentate and permeate were measured by a TOC analyzer (Phoenix 8000, Dohrmann) and PEG retentions were calculated using the following equation:

$$R = 1 - \frac{C_p}{C_0}. \tag{2}$$

Because of concentration polarization occurring in the retentate side, an intrinsic retention must be defined by

$$R^* = 1 - \frac{C_p}{C_m}, \tag{3}$$

where C_m represents the concentration at the membrane surface [14]. The film model is used to relate R and R^*:

$$\ln\left(\frac{1-R}{R}\right) = \ln\left(\frac{1-R^*}{R^*}\right) + \frac{J}{k}. \quad (4)$$

R^* is obtained by the intercept of the slope of $\ln((1-R)/R)$ versus flux J. The plot of intrinsic retention versus flux is used to determine the membrane MWCO.

In order to get the average corresponding pore radius, we used a model of steric exclusion as presented by Ferry [15]. When size exclusion is the only selectivity phenomena the intrinsic retention extrapolated to no flux is equal to

$$R^*_{J=0} = (1-(1-\lambda)^2)^2 \quad (5)$$

with $\lambda = (r_s/r_p)$ where r_s is the solute radius and r_p is the pore radius.

The first approximation is to consider that the membrane pores are all the same size. In this case an average pore radius can be calculated from the values of R^* determined by the retention experiments and PEG radius. This method allows the calculation of the pore radius of the homogeneous membrane equivalent to the membrane tested. This is a good method in our case where we want to compare different membranes.

2.4. AFM characterization

Atomic force microscopy (AFM) is used for direct analysis of membrane surface properties, such as pore size distribution, pore shape, and surface roughness. This technique does not require any special preparation of the sample, and the sample can be imaged in either air or liquid.

The CA membranes were imaged under water since the membranes should be studied in their working environment in order to get the best resolution [16,17]. The wet membranes are studied in contact mode. In this case the probe tip scans across the sample surface and is in direct physical contact with the sample. It can then respond to very short-range repulsive interactions with the sample.

The AFM observations were performed on a Topometrix TMX 2001 instrument. Cantilevers, made from silicon nitride, are 200 μm long and have a triangular shape. The spring constant of the narrow cantilever is k=0.032 N/m. The tip is also made of silicon nitride and has a pyramidal shape. Square pieces (5 mm× 5 mm) of the membrane were cut and attached to the magnetic holder using doubled-sided tape. The wet membrane surface was studied by contacting the surface with a drop of ultrapure water after sample mounting. For studies in liquids, a liquid tube scanner is used. The liquid tube scanner allows simple and routine imaging in liquids, without the need for ancillary equipment or a closed chamber [18].

Pore sizes are estimated from AFM images and calculated by AFM surface analysis software (SPM v.3.06). Line profiles are selected to traverse the AFM image and pass through the pores. To determine pore size, the operator must choose points on each height profile where the pore is considered to start and end. The pore radius is then the horizontal distance between these points [18]. The porosity of the membraue was estimated using the measured average pore diameter and the "lakes analysis" included with the software.

2.5. Contact angle measurements

The basis contact angle measurement is related to the three-phase equilibrium that occurs at the contact point of the solid/liquid/vapor or solid/liquid/liquid interface [19]. In our case, where the phases are membrane/water/air, the contact angle is a measure of wettability of the membrane, i.e., the capacity of water to be adsorbed on the membrane [20]. This can be interpreted as the hydrophobicity/hydrophilicity of the membrane. A contact angle of 0° corresponds to an ideal hydrophilic surface.

The sessile drop method was used in our research [21]. This method, also called the water droplet method, is based on measuring the contact angle between a water droplet and the membrane surface using a goniometer. Prior to measurement, membranes were stored in petri dishes at 4°C. They were soaked in milli-Q water for 3 h, with three water changes, and then soaked in 5% NaCl solution for 1 h. All membranes were then flushed in the stirred cell in order to remove any trace organic compounds used by the manufacturer to prevent drying and preserve the membrane. The membranes were cut into 20 mm× 1.5 mm strips and mounted in a holder that was placed

in a glass chamber. A water droplet (1.8 μl) was deposited on the membrane with a microliter syringe. A light source was placed behind the sample and the light was focussed through a slit. The contact angle was measured with the goniometer. Reported contact angles are the average of 7–10 measurements. The error on the measurement is equal to 15%.

2.6. Streaming potential measurements

In the case of charged membranes, the charges are distributed on the membrane surface and on the pore surface. When a charged solute passes through a membrane, the charges located on the pore surface can be important. It is possible to have some information about the net charge of the pore surface, and therefore about the charge distribution inside the electrochemical double layer, by measuring the zeta potential. The zeta potential represents the potential located at the shearing plane between the compact layer attached to the pore wall and the mobile diffuse layer. It can be calculated from streaming potential measurements with the Helmholtz–Smoluchowski equation [22]:

$$\xi = \frac{\eta\kappa\Delta E}{\epsilon_0\epsilon_r\Delta P} \tag{6}$$

with ξ is the zeta potential, η the viscosity, κ the conductivity, ϵ_0 the conductivity, ϵ_0 the permittivity of vacuum, ϵ_r the relative dielectric constant of the solution, ΔE the electrical field potential and ΔP is the differential pressure.

This equation shows a linear relation between the differential pressure ΔP applied across the membrane and the electrical field ΔE measured because of charged species accumulation. This equation implies there is no overlap of double layers inside the pore, that is the ratio between the pore radius and Debye length is assumed to be very large. The streaming potential is measured at constant ionic strength, I=0.01 in our experiments. Considering the membrane pore radius and the solution velocity through the pores, the pore flow is laminar [11]. It is important to recall here that this equation only applies to an ideal case.

Nyström et al. [23] have described the principle of streaming potential measurement and its application. The instrument constructed for this research consists of two half-cylindrical cells of 42 cm^3, connected to a Capsuhelic differential pressure gage (Dwyer Instrument, Michigan City, IND). The accuracy of the gage is 0.34 kPa (0.05 psi). Silver chloride electrodes, placed in each half-cell, measure the potential drop across the membrane. They are made of copper mesh (0.01 mm width opening) cut into disks (17 and 29 mm diameter) soldered to a copper wire, silver plated and chloridized following the method of Brown [24].

The electrical field ΔE is measured with a Fluke 45 Dual Multimeter (Fluke and Phillips, Everett, WA) characterized by an impute impedance of 1 MΩ. For each measurement, the membrane is cut into a circle and placed on the larger lower electrode that acts as a support. Trapped air bubbles are removed from the cell. The solution (I=0.01, various pH) is constantly flowing through the cell at about 350 ml/min. The temperature is maintained constant at 24±0.5°C between the different experiments. For each differential pressure ΔP, the conductivity κ and the potential drop ΔE are measured. Streaming potential data obtained by this method are function of physicochemistry (ionic strength and pH).

2.7. Adsorption experiments

2.7.1. Preparation of the natural organic matter

The organic matter used for this study was a soil humic acid supplied by Aldrich (Milwaukee, WI). The cleaning procedure was described by Hering and Morel [25] with the addition of a dialysis step, as explained by Hong and Elimelech [12]. The humic salt was dissolved in deionized water and precipitated by the addition of concentrated HCl. The suspension was centrifuged, and following centrifugation, the supernatant was discarded and the precipitate resuspended in 3 M HCl. The supernatant gives an intense color on addition of potassium thiocyanate solution (KSCN), indicating the presence of Fe(III) contamination. The procedure was repeated 10 times with acid and twice with a water rinse. This cleaning procedure was followed by dialysis against water to further purify the precipitate. The solid was placed in a regenerated cellulose dialysis bag having a MWCO of 50 000 Da (Fisher Scientific) and was dialyzed against deionized water until the conductivity of the solution was less than 10 μS/cm (more than 7 days). The dialysis solution was replaced every day.

2.7.2. Adsorption experiments

An 8 mg/l solution of humic acid, prepared in 10^{-3} M calcium chloride was used in the experiments. The pH was adjusted with 0.1 M HCl. The solution was placed in a glass jar with the membrane on the top, the skin side facing the interior of the jar. A Teflon sheet covered by five sheets of aluminum foil was then placed on the membrane. The jar was closed and turned upside down, in order to contact the solution and membrane. The aluminum sheets are required to avoid any leakage from the jar. The jar is than placed on a gyrator shaker in the dark at 22±2°C and it is shaken during 3 days.

After the adsorption period, the humic acid concentration of the supernatant was measured by UV absorption (254 nm). However, the very small difference between the concentration of the solution before and after the adsorption experiments could not be resolved by this technique. Hence, the membrane was rinsed and placed in a 20 ml of 0.1 M NaOH during 5 h in order to recover all the adsorbed humic acid by desorption [26]. The concentration of this solution was then measured by UV absorption analysis.

The fractional uptake of humic acid in the membrane at equilibrium was calculated by

$$\text{fractional uptake} = \frac{UV_0 - UV_f}{UV_0}, \tag{7}$$

where UV_0 is the absorbance before adsorption experiment and UV_f is the absorbance after adsorption experiment.

Clark and Lucas [18] proposed a model based on diffusion and adsorption of humic acid materials from a mixed solution into a one-dimensional porous medium. They introduced a interaction parameter, *Km*, given by

$$Km = \frac{h}{\alpha}, \tag{8}$$

where K is the partition coefficient, h is the solution depth (in the jar), m is the membrane thickness, and where α is calculated from

$$\frac{UV_0 - UV_f}{UV_0} = \frac{1}{1+\alpha}. \tag{9}$$

For a given membrane, *Km* characterizes the strength of interaction between the humic acid and the membrane. The main benefit of the parameter *Km* over simply presenting the fractional uptake is that *Km* takes into account the solution volume.

Kinetic experiments were performed with a solution of 8 mg/l humic acid prepared in 10^{-3} M calcium chloride, pH=5.5, 6.5, 7.5, on the following membranes:

- Membranes annealed at 40°C, 60°C and 80°C.
- Membranes hydrolyzed during 5 min and then annealed at 40°C, 60°C and 80°C.
- Membranes oxidized during 1 h and then annealed at 40°C, 60°C and 80°C.
- Annealed membranes sized with Colloid 189.

3. Results

3.1. Annealing

The water fluxes are presented in Fig. 1 for the different annealing temperatures. The decrease of membrane permeability with increased annealing temperature was expected because of the negative coefficient of expansion of cellulose acetate. In order to find if this decrease is due to pore radius and/or porosity modification, the retention at ΔP=344.7 kPa (50 psi) for four different PEG fractions was carried out; this is presented in Fig. 2. The increase of retention with increasing annealing temperature is related to a decrease of pore radius. According to these results, the molecular weight cut-off (MWCO) of membranes annealed at 40°C, 60°C and 80°C are 520, 410 and 300 Da, respectively. Bouchard et al. [4] found a similar MWCO around 400 Da for CA nanofiltration membranes. The pore radii calculated from PEG retention and PEG Stokes–Einstein radii are presented in Table 3. It is also possible to calculate porosity by assuming that the fluid follows Poiseuille's law inside the pores. The porosity values are calculated according to the equation:

$$\epsilon = \frac{8\eta l L_p}{r_p^2} \tag{10}$$

with η is the water viscosity [$0.89.10^{-3}$ kg/ms (T=20°C)], l is the assumed membrane thickness (0.25 μm), L_p is the water permeability (slope of membrane flux versus ΔP), and r_p is the pore radius determined by PEG retention experiments.

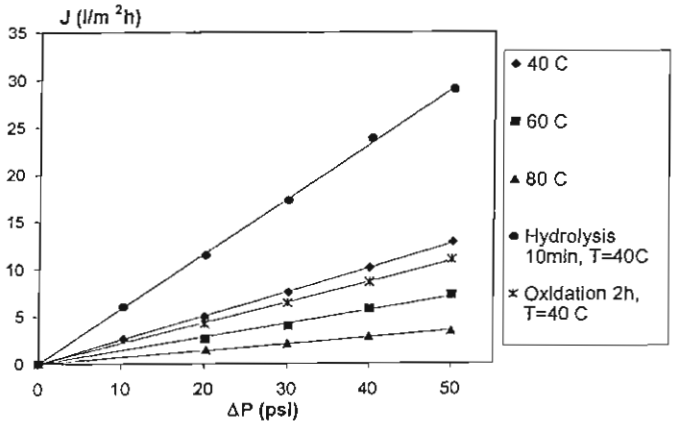

Fig. 1. Water flux for different membranes. Effect of annealing temperature and treatment (hydrolysis and oxidation).

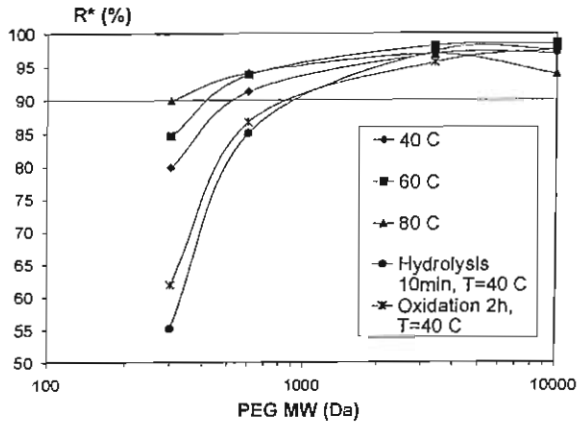

Fig. 2. PEG retention curves for different membranes. Effect of annealing temperature and treatment (hydrolysis and oxidation). PEG concentration: 10 mg/l.

The value chosen to approximate the membrane thickness comes from the literature, where thickness values between 0.05 and 0.3 μm have been determined for ultrafiltration and nanofiltration membranes [27,28]. Using this method, Table 3 indicates a slight decrease of porosity with increased annealing temperature.

AFM images of the 40°C, 60°C, and 80°C annealed membranes are presented in Fig. 3(a)–(c). We do not see a great difference between the membranes. From the AFM images, pore radii can be calculated by the Topometrix software (Table 3). They follow the expected order, i.e., a decrease of pore radius with increasing annealing temperature. However, pore radii calculated from the AFM images are very large compared to those calculated from PEG retention curves. It seems probable that the AFM software overestimates pore radius because of the difficulty in determining the edge of the pore on the image. Dietz et al. [29] studied the influence of tip shape on AFM images of membranes. They proposed a model taking into account pore and tip shape and showed that AFM measurements can overestimate pore diameter by 13–80% in the case of pores with rounded edges. The tip tends to measure the pore diameter at the pore entrance, which leads to overestimation of pore diameter. The tip size

Table 3
MWCO and pore radius calculated from PEG retention, and porosity, calculated by Poiseuille's law and AFM software

Membrane	MWCO (g/mol)	Pore radius from rejection (nm)	Porosity from Poiseuille law (%)	Pore radius from AFM (nm)	Porosity from AFM (%)
Annealed 40°C	520	1.62	0.7	13.2	6.2
Annealed 60°C	410	1.56	0.4	9.1	3.1
Annealed 80°C	300	1.57	0.2	3	4
Hydrolyzed 10 min, annealed 40°C	930	1.7	1.4	11.5	6.5
Oxidized 2 h, annealed 40°C	830	1.69	0.5	15	9

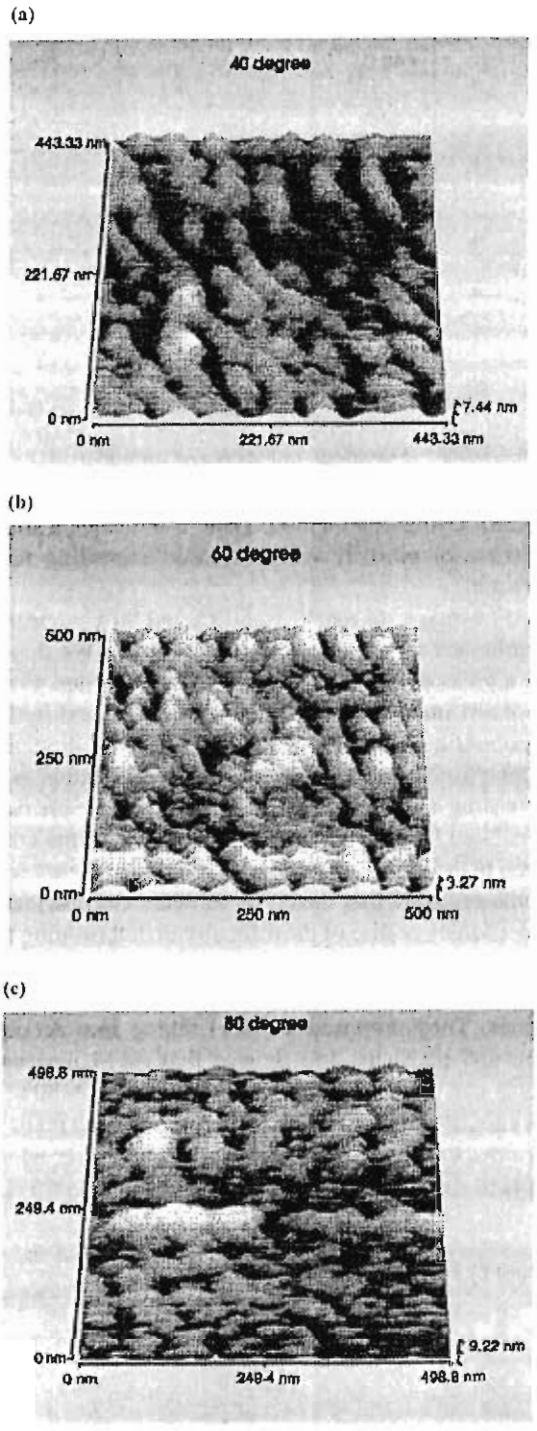

Fig. 3. AFM images of membranes annealed at: (a) 40°C; (b) 60°C; (c) 80°C.

and shape also affect the measurement of membrane surface roughness. The same observation has been obtained with track-etched polycarbonate membranes [30]. In this case the pores are rectilinear but with a slight incline compared to the actual membrane surface. They show that resolution in depth depends on tip thickness and shape, with an increase in resolution of depth with reduced thickness. The pore radii determined by the AFM software are often larger than those determined by calibrated molecule retention [31]. These results show the complexity of using AFM to determine membrane pore radius.

Contact angle data, presented in Table 4, show that the membrane surface is not very hydrophilic. Pure cellulose acetate is usually considered a hydrophilic material. However, as explained in Section 2.1, cellulose acetate is commonly cellulose triacetate where the hydroxyl units have been replaced by acetyl groups. Compared to pure cellulose acetate, this modification decreases the free OH-groups, and hence the hydrophilicity. Comparable values have been measured by Jucker and Clark [32]. Zhang et al. [33] also show the difficulty in interpreting contact angle data because of changes in membrane surface energies and because of the variation of contact angle with membrane roughness. Annealing has a negligible effect on contact angle and hydrophobicity, with only a slight increase in contact angle with decreasing pore size.

The curves for zeta potential versus pH show that zeta potential does not vary with annealing temperature (Fig. 4). Membrane pores are negatively charged in the range of pH=5.5–8.5, decreasing with pH. Therefore, we conclude that annealing has no effect on the surface chemistry of the pores.

The results of adsorption experiments show that the amount of humic acid adsorbed is lower when annealing temperature is increased (Table 5). Therefore, adsorption could be related to pore radius, since the results presented above show that pore radius is the only parameter affected by annealing [32]. This could mean that adsorption occurs inside the pores. With the 40°C and 60 annealed membranes the adsorption decreases with increasing pH. Zeta potential measurements showed an increase of the negative charge of membrane pores with increasing pH. Humic acid is negatively charged at high pH because of ionized COOH groups. The electrostatic repulsion between the negative pore charge and the negative macro-

Table 4
Effect of annealing temperature on average contact angle data

Annealing temperature (°C)	40	50	60	70	80
Contact angle (°)	54.1±8.2	56±8.4	54.7±8.2	56.3±8.4	58.2±8.7

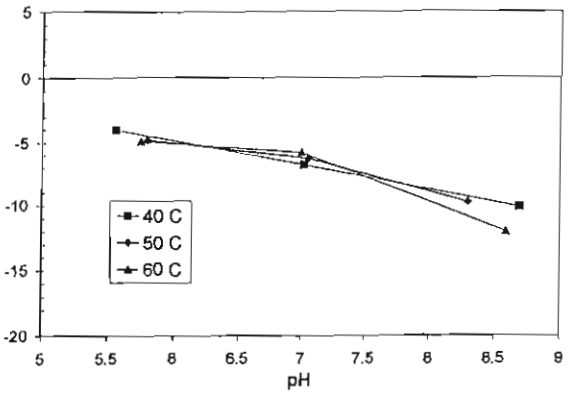

Fig. 4. Variation of zeta potential with pH for membranes annealed at different temperatures.

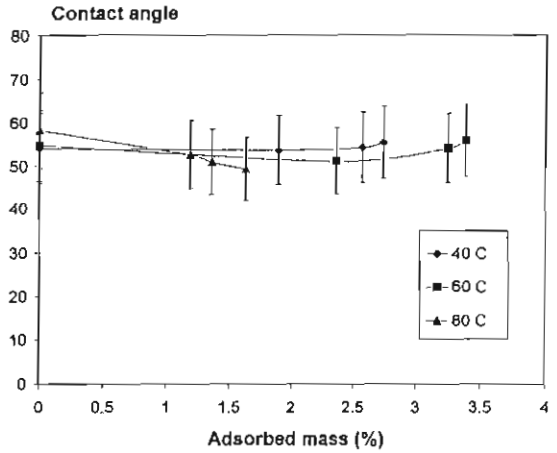

Fig. 5. Contact angle on membranes fouled by humic acid. Effect of annealing temperature and comparison with clean membranes.

molecule leads to a decrease in adsorption of humic acid on the membrane surface [32]. No effect of pH on adsorption is visible with the 80°C annealed membrane. In this case, the pore size has a more important influence than pore charge.

Contact angles have been measured on fouled membrane (Fig. 5). The values are close to those determined on clean membranes. The hydrophobic/hydrophilic character of the membrane is not really affected by fouling. It is interesting to compare these results with those obtained by Jucker and Clark [32] on two hydrophobic ultrafiltration membranes. They reported a significant decrease of contact angle with increasing adsorbed mass. In that study, membranes were contacted with Suwannee River humic and fulvic acid. In our experiments, the humic acid (Aldrich) is extracted from the soil. The average molecular weight of this humic acid as reported by different authors is usually larger than 50 000 Da [12]. Typically the hydrophobicity of humic substances increases with increasing molecular weight and decreasing acidity. Hong and Elimelech [12] found a higher carboxylic acidity for Suwannee River humic acid than for Aldrich humic acid. These results suggest that Aldrich

Table 5
Effect of annealing temperature and hydrolysis on adsorption results (*Km* and % of adsorbed mass)

Membrane	pH=5.5		pH=6.5		pH=7.5	
	Km	% Adsorbed mass	*Km*	% Adsorbed mass	*Km*	% Adsorbed mass
Annealed 40°C	0.155	2.74 (2.78, 2.68)	0.145	2.57 (2.52, 2.62)	0.106	1.89 (1.85, 1.93)
Annealed 60°C	0.193	3.39 (3.33, 3.46)	0.185	3.25 (3.18, 3.31)	0.133	2.36 (2.31, 2.41)
Annealed 80°C	0.066	1.19 (1.16, 1.21)	0.076	1.36 (1.33, 1.39)	0.091	1.63 (1.6, 1.66)
Hydrolyzed 5 min, annealed 40°C	0.133	2.36 (2.41, 2.31)	0.107	1.91 (1.87, 1.95)	0.123	2.19 (2.15, 2.23)
Hydrolyzed 5 min, annealed 60°C	0.205	3.59 (3.52, 3.66)	0.137	2.43 (2.38, 2.48)	0.131	2.33 (2.28, 2.38)
Hydrolyzed 5 min, annealed 80°C	0.107	1.91 (1.87, 1.95)	0.131	2.33 (2.28, 2.38)	0.143	2.53 (2.48, 2.58)

Humic acid concentration=8 mg/l, pH=5.5, 6.5, and 7.5, hydrolysis time=5 min.

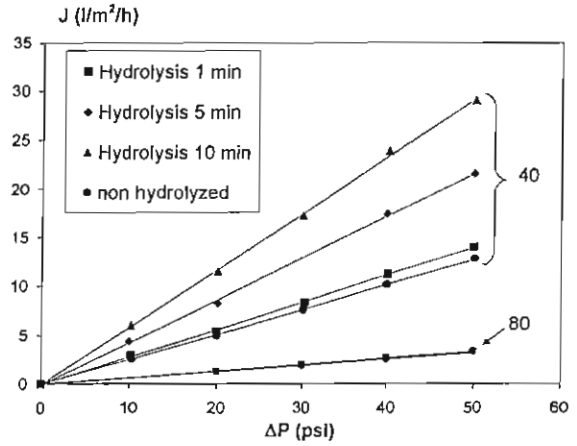

Fig. 6. Water flux for hydrolyzed membranes. Effect of hydrolysis time and annealing temperature

humic acid may be more hydrophobic than Suwannee River humic acid. Therefore, the lack of decline in contact angle observed on fouled membranes may be due to the greater hydrophobicity of the soil humic acid. These results underline the difference in behavior of these two humic acids.

3.2. Hydrolysis

Fig. 6 shows that hydrolysis can have a great effect of permeability on the more porous membranes. Experiments for different times of hydrolysis show an increase of water flow of as much as 100% for membranes annealed at 40°C and 60°C. This effect is not visible for the membrane annealed at 80°C. The MWCO of the hydrolyzed 40°C annealed membrane determined from PEG retention is estimated to be 930 Da, which corresponds to a pore radius of 0.94 nm (Fig. 2). Porosity calculated by Poiseuille's law increases with hydrolysis, from 3.8% to 4.7% (Table 3). The comparison between pore radius calculated from PEG retention and AFM measurements shows again a higher value for AFM (Table 3).

According to contact angles measurements hydrolysis has a dramatic effect on hydrophobicity (Table 6). The longer the treatment the smaller the contact angle. Treatment by a caustic agent to reduce acetyl content is used in the industry to produce more hydrophilic regenerated cellulose acetate membranes. We have found very low contact angles for a commercial regenerated cellulose acetate membrane [32]. We do not see a great change of contact angle with annealing temperature, which supports our previous observations that annealing does not affect pore surface chemistry.

For 40°C and 60°C annealing temperatures, zeta potential of the hydrolyzed membranes decreases in absolute value and becomes positive after a certain time of hydrolysis (>10 min). The data presented in Fig. 7 are for an annealiug temperature of 60°C. Therefore hydrolysis reduces the pore charge, and the membrane becomes more neutral. Since negative membrane charge is often considered to reduce organic fouling, hydrolysis may increase adsorptive fouling.

Table 6
Contact angle data for membranes after hydrolysis or oxidation and annealing at different temperature

Annealing temperature (°C)	Type of treatment	Contact angle (°)	Annealing temperature (°C)	Type of treatment	Contact angle (°)
40	None	54.1	40	None	54.1
	Hydrolysis 1 min	28.2		Oxidation 30 min	30.5
	Hydrolysis 5 min	23.3		Oxidation 1 h	30.3
	Hydrolysis 10 min	20.8		Oxidation 2 h	30
60	None	54.7	60	None	54.7
	Hydrolysis 1 min	30		Oxidation 30 min	31.4
	Hydrolysis 5 min	28		Oxidation 1 h	31.7
	Hydrolysis 10 min	26		Oxidation 2 h	31.7
80	None	58.2	80	None	58.2
	Hydrolysis 1 min	28.3		Oxidation 30 min	31
	Hydrolysis 5 min	18.6		Oxidation 1 h	31
	Hydrolysis 10 min	15.7		Oxidation 2 h	31.4

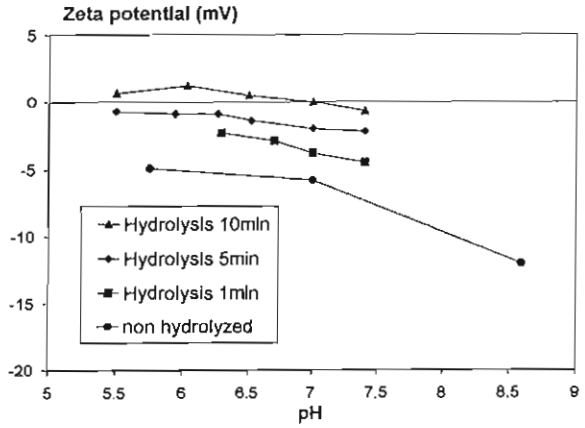

Fig. 7. Variation of zeta potential with pH for hydrolyzed membranes. Effect of hydrolysis time for membranes annealed at 60°C.

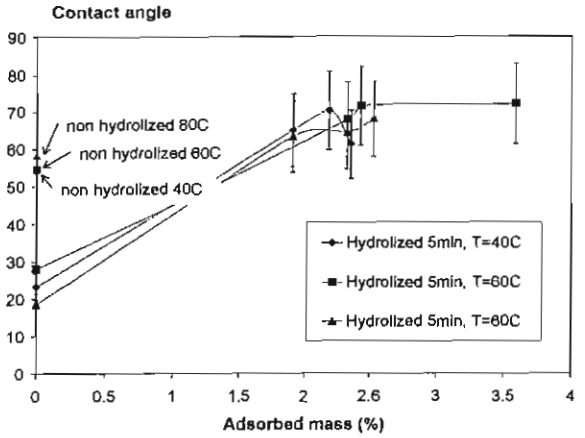

Fig. 8. Effect of hydrolysis on contact angle. Evolution with annealing temperature and adsorbed mass.

However, no significant change in humic acid adsorption was observed with hydrolysis (Table 5). Although hydrophobicity decreases with hydrolysis (according to contact angle measurements), we do not observe any decrease in adsorption. This result is discussed in Section 4. Fig. 8 shows that the contact angle increases with the mass of humic acid adsorbed, reaching an asymptotic value similar to the values on the annealed (unhydrolyzed) membranes.

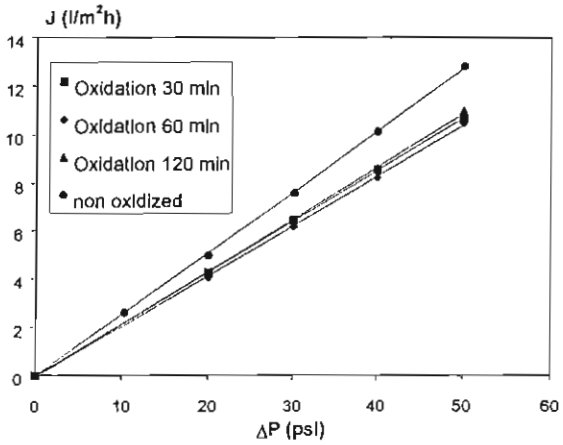

Fig. 9. Water flux for oxidized membranes. Effect of oxidation time on membrane annealed at 40°C.

3.3. Oxidation

A slight decline of water permeability is observed after oxidation of the membrane (Fig. 9). Unreported data for membranes annealed at 60°C and 80°C also show that oxidation time has little effect on membrane permeability: the main effect of treatment by H_2O_2 is already visible after 30 min. Although a decrease of water permeability is observed by comparing the 40°C annealed membranes before and after oxidation, PEG retention experiments show an increase in pore radius (Table 3). A lower porosity value is calculated for the oxidized membrane compared to the membrane annealed at the same temperature without treatment. According to these results oxidation leads to somewhat ambiguous increase in pore size and decrease in membrane porosity. In this case also, AFM overestimates pore radius.

The contact angle measurements presented in Table 6 show a significant decrease of contact angle values after oxidation. Oxidation times greater than 30 min have no effect on contact angle, and therefore no effect on surface hydrophilicity. By comparing results obtained on hydrolyzed and oxidized membranes the ultimate hydrophilicity is greater after hydrolysis than oxidation (Table 6).

Although time of oxidation does not seem to have any affect on water permeability and membrane hydrophobicity, its effect on pore charge is visible (Fig. 10). Streaming potential measurements show a

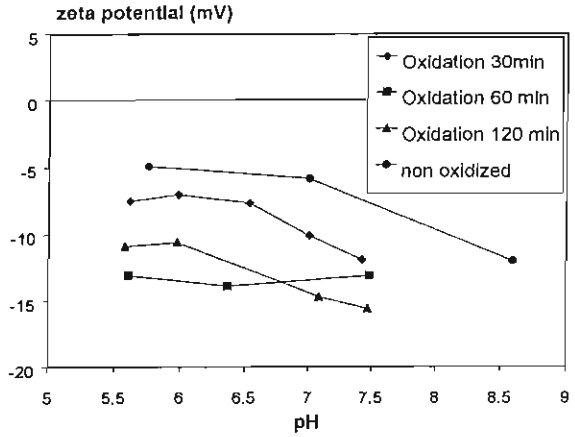

Fig. 10. Variation of zeta potential with pH for oxidized membranes. Effect of oxidation time for membranes annealed at 60°C.

more negative pore charge when oxidation time increases. This effect is just the opposite to what was observed for hydrolysis. We might, therefore, anticipate that oxidation of cellulose acetate will decrease fouling by humic acid.

However, adsorption experiments results show an increase of NOM adsorption on the oxidized membranes (Table 7). Despite the decrease in membrane hydrophobicity and the more negative pore charge, adsorption of NOM increases on oxidized CA membrane surfaces.

3.4. Treatment with anionic polymer

Some of the previously studied membranes were treated by a polymer, in order to see if there would be an effect on adsorption of humic acid. Adsorption experiments carried out on these membranes show a great decrease of humic acid adsorption (Table 8). The data are obtained at pH=4 for the treated membrane and at pH=5.5 for untreated membranes. In nearly all cases adsorption on the treated membranes is lower than adsorption on untreated membranes. At pH=4 the polymer adsorbs on the membrane surface, and appareutly prevents or greatly decreases the ability of humic acid to interact with the membrane surface.

4. Discussion

In the membrane literature, it is common to associate increased negative charge and increased hydrophilicity with decreased adsorptive fouling by natural organic matter. Yet in this study of adsorption of humic acid on modified CA membranes, this view was not at all clearly supported. For the hydrolyzed membranes, the apparent hydrophilicity was increased according to sessile drop contact angle measurements, but the negative charge as measured with streaming potential was reduced. There was little change in adsorbability of humic acid compared to the unhydrolyzed membranes. One could postulate a cancellation of beneficial effects here, i.e., the positive effect of increased hydrophilicity was offset by the negative effect of decreased negative charge. On the other hand, oxidation of the membrane surface increased the apparent hydrophilicity and increased the negative charge, two effects that would normally be considered beneficial; yet, adsorption of humic acid was increased.

Table 7
Effect of annealing temperature and oxidation on adsorption results (*Km* and % of adsorbed mass)

Membrane	pH=5.5		pH=6.5		pH=7.5	
	Km	% Adsorbed mass	*Km*	% Adsorbed mass	*Km*	% Adsorbed mass
Annealed 40°C	0.155	2.74 (2.68, 2.79)	0.145	2.57 (2.52, 2.62)	0.106	1.89 (1.85, 1.93)
Annealed 60°C	0.193	3.39 (3.32, 3.46)	0.185	3.25 (3.18, 3.31)	0.133	2.36 (2.31, 2.41)
Annealed 80°C	0.066	1.19 (1.17, 1.21)	0.076	1.36 (1.33, 1.39)	0.091	1.63 (1.6, 1.66)
Oxidized 1 h, annealed 40°C	0.277	4.79 (0.47, 0.49)	0.229	4.00 (3.92, 4.08)	0.247	4.30 (4.21, 4.4)
Oxidized 1 h, annealed 60°C	0.351	6.00 (5.88, 6.12)	0.363	6.19 (6.07, 6.31)	0.217	3.80 (3.72, 3.88)
Oxidized 1 h, annealed 80°C	0.339	5.81 (5.69, 5.93)	0.314	5.40 (5.29, 5.51)	0.295	5.09 (4.99, 5.19)

Humic acid concentration=8 mg/l, pH=5.5, 6.5, and 7.5, oxidation time=1 h. The values in parenthesis represent the maximum and minimum values of adsorbed mass.

Table 8
Effect of treatment by Colloid 189 on adsorption (*Km* and % of adsorbed mass)

Non-treated with Colloid 189 membranes	Adsorbed mass (%)	*Km*	Treated with Colloid 189 membranes	Adsorbed mass (%)	*Km*
Annealed 40°C	2.6 (2.55, 2.65)	0.155	Annealed 40°C	2.9 (2.84, 2.96)	0.105
Hydrolyzed 5 min, annealed 40°C	2.3 (2.25, 2.35)	0.133	Hydrolyzed 10 min, annealed 40°C	1.52 (1.49, 1.55)	0.054
Oxidized 1 h, annealed 40°C	4.8 (4.7, 4.9)	0.277	Oxidized 4 h, annealed 40°C	3.56 (3.49, 3.63)	0.129
Annealed 60°C	3.6 (3.53, 3.67)	0.193	Annealed 60°C	2.7 (2.64, 2.75)	0.097
Annealed 80°C	1.3 (1.27, 1.33)	0.066	Annealed 80°C	1.92 (1.88, 1.96)	0.068
Hydrolyzed 5 min, annealed 80°C	1.8 (1.76, 1.84)	0.107	Hydrolyzed 10 min, annealed 80°C	3.49 (3.42, 3.56)	0.126
Oxidized 1 h, annealed 80°C	5.8 (5.68, 5.92)	0.339	Oxidized 4 h, annealed 80°C	3.99 (3.91, 4.07)	0.145

Humic acid concentration=8 mg/l, pH=4. Comparison with untreated membranes. The values in parenthesis represent the maximum and minimum values of adsorbed mass.

To explain these results, we consider more carefully the role of calcium in adsorption of humic acid, and the measurement and interpretation of zeta potential. First, several investigators [12,18,32] have shown that calcium has an important role in increasing adsorption of humic acid on membranes. In the soil science literature, calcium is known to complex with humic materials. Hence, calcium is often considered to act as a bridge between the negatively charged membrane surface and negatively charged carboxyl groups on the humic acid. Although calcium concentration was not varied in this study of CA membranes, calcium was present in the background electrolyte during adsorption experiments. Regarding streaming potential measurements, it should be recalled that there has not been a clear explanation of the negative charge of many presumably uncharged membrane surfaces like cellulose acetate (recall Fig. 4). One of the most likely explanations is that the negative charge is due to the adsorption of hydroxyl ions or chloride ions from the strong electrolyte (0.01 M KCl) used in the streaming potential measurement [32,34]. Probstein explains that the negative charge of hydrocarbons is caused by the preferential adsorption of anions such as Cl^-, over simple cations. This adsorption is enhanced by the hydrophobic nature of the interface with the water [35]. A study of the structure of adsorbed water in cellulose acetate membranes shows the importance of H-bonds between the membrane and the water or hydroxyl groups; the lower the acetyl content (comparable to the more hydrolyzed membranes in our study), the greater the sorption of water and the more hydrophilic the membrane [36]. Our results show that the zeta potential is less negative after hydrolysis, that is when the membrane hydrophobicity is decreased. According to Probstein this can be explained by the decrease in adsorption of chloride ions, due to the increased hydrophilicity. Therefore, if it is postulated that adsorption of humic acid is dominated by charge interactions, then as observed, adsorption of humic acid (in the absence of the strong KCl electrolyte) is not affected by hydrolysis, since there is really no change in charged surface groups during hydrolysis – only an apparent change due to interactions of the membrane surface with chloride or hydroxyl ions. On the other hand, for the oxidized membranes, oxidation is a clear mechanism for increasing the concentration of charged surface carboxyl groups; this leads to the significantly increased negative charge measured after oxidation. If as has been suggested, calcium forms a bridge between negative surface groups on the membrane and negative groups on the humic acid, then oxidation increases the number of adsorption sites, which leads to increased adsorption (which is indeed observed).

5. Conclusion

Several variations of a basic cellulose acetate membrane have been developed by surface modification of the membrane. The results of this study show that techniques like AFM, streaming potential, contact angle measurements, and PEG retention charted changes in membrane surface properties. Annealing has a great effect on membrane permeability, without changing pore charge or hydrophobicity. Hydrolysis greatly increases membrane porosity, decreases the

charge of the membranes, and increases hydrophilicity, but has little effect on adsorption of humic acid. Oxidation had a small effect on porosity, but significantly increased hydrophilicity and the negative membrane charge; adsorption of humic acid was increased on the oxidized membranes. Only by pre-adsorption of an anionic polymer on the membrane surface is adsorption of humic acid on the membrane surface decreased.

Finally, the results of this work have challenged some of the conventional wisdom on fouling of membranes by natural organic matter. Normally, decreased membrane hydrophobicity and increased (negative) charge are assumed to reduce fouling by negatively charged organic foulants. We found exactly these desirable characteristics for the oxidized membranes studied here, nevertheless, adsorptive fouling by humic acid was actually increased on the oxidized membranes. We have attempted to explain this behavior by a careful consideration of charge-related adsorption and the role of calcium in adsorption of humic acid.

6. Nomenclature

C_m	solute concentration at the surface of the membrane (mol/l or mol/m)
C_p	concentration in the permeate (mol/l)
C_0	solute concentration in the feed (mol/l)
ΔE	electric field potential (V)
J	flow density, called the total volume flow rate (μm/s)
k	mass transfer coefficient (m/s)
Km	adsorption parameter (m)
l	membrane thickness (m)
L_p	membrane hydraulic permeability (m^2 s/Kg)
M	molecular weight (Da)
ΔP	pressure gradient (Pa)
r_p	pore radius (m)
r_s	Stokes solute radius (m)
R^*	intrinsic retention coefficient
R	observed retention coefficient

Greek symbols

ϵ	membrane porosity: empty volume/total volume
ϵ_0	permittivity of vacuum (F/m)
ϵ_r	relative dielectric constant of the solution
κ	conductivity (S)
η	viscosity of the solvent (Poise)
σ_m	surface charge of the powder (eq/m)
ξ	zeta potential (V)

Acknowledgements

The authors thank the National Water Research Institute, Lyonnaise des Eaux, and the American Water Works Association Research foundation for their financial support. The assistance of visiting students Karin Dassas and Philippe Molis with the experimental work is appreciated. The comments of an anonymous referee were also appreciated.

References

[1] P.K. Cornel, R.S. Summers, P.V. Roberts, Diffusion of humic acid in dilute aqueous solution, J. Colloid Interface Sci. 110(1) (1986) 149.
[2] S.A. Green, F.M.M. Morel, N.V. Blough, Investigation of the electrostatic properties of humic substances by fluorescence quenching, Environ. Sci. Technol. 26 (1992) 294.
[3] M. Elimelech, X. Zhu, A.E. Childress, S. Hong, Role of membrane surface morphology in colloidal fouling of cellulose acetate and composite aromatic polyamide reverse osmosis membranes, J. Membr. Sci. 127 (1997) 101.
[4] C.R. Bouchard, J. Jolicoeur, P. Kouadio, M. Britten, Study of humic acid adsorption on nanofiltration membranes by contact angle measurements, Can. J. Chem. Eng. 75 (1997) 339.
[5] M. Nyström, K. Ruohomäki, L. Kaipia, Humic acid as a fouling agent in filtration, Desalination 106 (1996) 79.
[6] V. Turcaud Lahoussine, M.R. Wiesner, Y.J. Bottero, Fouling in tangential-flow filtration: the effect of colloid size and coagulation treatment, J. Membr. Sci. 52 (1990) 173.
[7] Y. Kaiya, Y. Itoh, K. Fujita, S. Takizawa, Study on fouling materials in the membrane treatment process for potable water, Desalination 106 (1996) 71.
[8] P. Aimar, S. Baklouti, V. Sanchez, Membrane–solute interactions: influence on pure solvent transfer during ultrafiltration, J. Membr. Sci. 29 (1986) 207.
[9] W.S. Opong, A.L. Zydney, Diffusive and convective protein transport through asymmetric membranes, AIChE J. 37 (1991) 1497.
[10] K. Ghosh, M. Schnitzer, Macromolecular structures of humic substances, Soil Sci. 129(5) (1980) 266.
[11] C.A. Jucker, Interactions between aquatic substances and ultrafiltration membranes, Master's thesis, University of Illinois at Urbana–Champaign, 1993.

[12] S. Hong, M. Elimelech, Chemical and physical aspects of NOM fouling on nanofiltration membranes, J. Membr. Sci. 132 (1997) 159.
[13] S. Lentsch, P. Aimar, J.L. Orozco, Separation albumin-PEG: transmission of PEG through ultrafiltration membranes, Biotechnol. Bioeng. 41 (1993) 1039.
[14] W.M. Deen, Hindered transport of large molecules in liquid-filled pores, AIChE J. 33 (1987) 1409.
[15] J.D. Ferry, Ultrafilter membranes and ultrafiltration, Chem. Rev. 18 (1936) 373.
[16] P. Dietz, P. Hansma, K. Herrmann, O. Inacker, H. Lehmann, Atomic force microscopy in air and under water, Ultramicroscopy 35 (1991) 155.
[17] A. Bessières, Etude des propriétés fonctionnelles et structurales des membranes synthétiques par rétention de molécules calibrées et microscopies à champ proche, Thèse de doctorat, Université Paul Sabatier, Toulouse, France, 1994.
[18] M.M. Clark, P. Lucas, Diffusion and partitioning of humic acid in a porous ultrafiltration membrane, J. Membr. Sci. 143 (1998) 13.
[19] J.D. Andrade, L.M. Smith, D.E. Gregonis, The contact angle and interface energetics, in: J.D. Andrade (Ed.), Surfaces and Interfacial Aspects of Biomedical Polymers, Plenum Press, New York, 1985, p. 249.
[20] P.C. Hiemenz, in: J.J. Lagowski (Ed.), Principles of Colloid and Surface Chemistry, 2nd ed., Dekker, New York, 1986, p. 287.
[21] J.D. Chen, N. Wada, Edge profiles and dynamic contact angles of a spreading drop, J. Colloid Interface Sci. 148 (1992) 207.
[22] R.J. Hunter, in: R.H. Otterwill, R.L. Rowell (Eds.), Zeta Potential in Colloid Science, Principle and Applications, Academic Press, London, 1981.
[23] M. Nyström, M. Lindström, E. Mathiasson, Streaming potential as a tool in the characterization of ultrafiltration membranes, Colloids Surf. 36 (1989) 297.
[24] A.S. Brown, A type of silver chloride electrode suitable for use in dilute solutions, J. Am. Chem. Soc. 56 (1934) 646.
[25] J.G. Hering, F.M.M. Morel, Humic acid complexation of calcium and copper, Environ. Sci. Technol. 22(10) (1988) 1234.
[26] K.L. Jones, PhD thesis, the John Hopkins University, Baltimore, MD, 1996.
[27] R. Riley, J.O. Gardner, U. Merten, Cellulose acetate membranes: electron microscopy of structure, Science 143(3608) (1964) 801.
[28] A. Braghetta, F.A. DiGiano, W.P. Ball, Nanofiltration of natural organic matter: pH and ionic strength effects, J. Environ. Eng. (1997) 628.
[29] P. Dietz, P.K. Hansma, O. Inacker, H.-D. Lehmann, K.-H. Herrmann, Surface pore structures of micro- and ultrafiltration membranes imaged with the atomic force microscope, J. Membr. Sci. 65 (1992) 101.
[30] A. Chahboun, R. Coratger, F. Ajustron, J. Beauvillain, P. Aimar, V. Sanchez, Comparative study of micro- and ultrafiltration membranes using STM, AFM and SEM techniques, Ultramicroscopy 41 (1992) 235.
[31] A. Bessieres, M. Meireles, R. Coratger, J. Beauvillain, V. Sanchez, Investigations of surface properties of polymeric membranes by near field microscopy, J. Membr. Sci. 109 (1996) 271.
[32] C. Jucker, M.M. Clark, Adsorption of aquatic humic substances on hydrophobic ultrafiltration membranes, J. Membr. Sci. 97 (1994) 37.
[33] W. Zhang, M. Wahlgreen, B. Sivik, Membrane characterization by the contact angle technique. II. Characterization of UF-membranes and comparison between the captive air bubble and sessile drop as methods to obtain water contact angles, Desalination 72 (1989) 263.
[34] M. Nyström, P. Järvinen, Modification of polysulfone ultrafiltration membranes with UV irradiation and hydrophilicity increasing agents, J. Membr. Sci. 60 (1991) 275.
[35] R.F. Probstein, Physicochemical Hydrodynamics: An Introduction, 2nd ed., Wiley, New York, 1994, p. 212.
[36] W.A.P. Luck, K. Rangsriwatananon, The structure of adsorbed water in cellulose acetate membranes, Colloid Polym. Sci. 275 (1997) 1018.

ELSEVIER

Journal of Membrane Science 143 (1998) 13–25

journal of MEMBRANE SCIENCE

Diffusion and partitioning of humic acid in a porous ultrafiltration membrane

Mark M. Clark*, Pascale Lucas

Department of Civil and Environmental Engineering, University of Illinois, 205 N. Mathews Avenue, Urbana, IL 61801, USA

Received 23 June 1997; received in revised form 8 December 1997; accepted 9 December 1997

Abstract

Surface imaging of wet polysulfone (PM30) ultrafiltration membranes with atomic force microscopy indicates a relatively smooth but porous surface in the aqueous environment. The average pore radius was 9.7±0.8 nm, and the average porosity was 10%. Therefore, for the case of adsorption of humic acid on the membrane (J. Membr. Sci. 97 (1994) 37–52), we hypothesize here that the transport of humic materials in the membrane can be modeled as one-dimensional diffusion and linear partitioning in a porous medium. An interaction parameter was developed using the model to characterize the strength of interaction between the humic acid and the membrane as a function of pH and calcium concentration. The mass of humic acid adsorbed and the calculated interaction parameter were found to increase with decreasing pH and increasing calcium concentration; hence, the strength of interaction between humic acid and membrane is now simply parameterized. The kinetics of adsorption of humic acid was also modeled, and fitted diffusion time scales showed that the humic acid diffusion coefficient increased with decreasing pH and increasing calcium concentration, which is consistent with a compaction of the humic molecule. These effects were also consistent with a previous study of humic acid diffusion coefficients in activated carbon (J. Colloid Interface Sci. 110 (1) (1986) 149–164). © 1998 Elsevier Science B.V.

Keywords: Diffusion; Fouling; Ultrafiltration; Atomic force microscopy; Adsorption

1. Introduction

Clark and Jucker [1] and Jucker and Clark [2] studied the adsorption of aquatic humic substances on PM30 (polysulfone, 30,000 Da MWCO) and XM50 (poly(acrylonitrile-co-vinyl chloride), 50,000 Da MWCO) ultrafiltration membranes in a shaken cell without permeation. It was found that the degree of adsorption of humic and fulvic acid depended on several physicochemical factors. First, adsorbed mass was considerably higher on the more porous of the two membranes (PM30). Measurements of apparent pore zeta potential for both membranes showed that the initially negative pore zeta potential increased (became less negative) rather quickly with amount of mass adsorbed, but then plateaued as humic materials continued to adsorb. This was interpreted to mean that pore adsorption sites (or other roughness features) adsorbed humic materials quickly; a weaker and longer-term adsorption continued either on lower energy sites or as a second layer deposited on the first.

*Corresponding author. Fax: 217 333-9464; e-mail: m-clark3@uiuc.edu

PII S0376-7388(97)00332-3

The chemistry of the system also strongly affected adsorption of humic materials. As pH was lowered from 6 to 4.8, mass adsorbed increased significantly. Jucker and Clark [2] showed using octanol/water partition coefficients that the soluhility and hydrophilicity of humic substances decreases from pH 6 to 4, which is due likely to the protonation of phenolic and carboxylic hydroxyl groups on the humic materials. Streaming potential measurement showed that the pore zeta potential of virgin membranes also increases significantly (becomes less negative) for that same pH change. So the following picture emerges: The humic materials have a net negative charge at neutral pH; as the pH is lowered, the pore zeta potential increases (becomes less negative), the negative charge of the humic materials is neutralized, and the electrostatic barrier to adsorption of humic materials is decreased. Jones and O'Melia [3] found a parallel increase in adsorption of Suwannee humic acid on a regenerated cellulose acetate UF membrane as pH was lowered.

Calcium is an important environmental component, and its complexation by humic materials has been long recognized [4]. Calcium is also implicated in fouling of hydrophobic membranes [2,5,6]. In Jucker and Clark's [2] work, calcium was also found to significantly enhance adsorption of humic materials. X-ray Photoelectron Spectroscopy (XPS) measurements on the PM30 membrane surface after adsorption suggested that the calcium was complexed with the humic acid. The role of calcium was interpreted as either a bridge between the negative surface and humic materials, or as a means of altering the ionic strength, hence, compacting or coiling the humic polymer chain [7]. A smaller polymer conformation could also permit a more dense adsorbed layer [8].

Jucker and Clark [2] did not attempt to model the kinetics of humic acid adsorption on the membranes, nor did they parameterize the strength of the humic-membrane interaction. In this follow-up to their work, we model adsorption kinetics assuming a linear isotherm, and consider that adsorption proceeds in a manner similar to one-dimensional diffusion and partitioning in a porous medium [9]. We focus in this paper on the adsorption of humic acid on the PM30 membrane, a system for whieh excellent kinetic data are available [10]. Comparison of humic acid molecular sizes with pore size statistics gathered with atomic force microscopy imaging of the PM30 membrane support the modeling of humic acid transport as diffusion and partitioning in a porous medium. A parameter related to the classical partition coefficient is developed to characterize the strength of the humic acid–membrane interaction, while the model permits us to interpret the effects of solution chemistry on the humic acid diffusion coefficient.

2. Experimental

The polysulfone PM30 membrane had a nominal molecular-weight cutoff of 30 kDa. The PM30 membranes were cleaned in a multistep process with Milli-Q water and 5% NaCl [2]. The cleaned membranes were stored skin side down in Milli-Q water in a dark 6°C chamber, and membranes were never allowed to dry prior to any analyses.

A Topometrix, TMX 2000 Explorer, atomic force microscope was used to acquire images of the PM30 membrane surface in the contact mode. Square pieces (5 mm × 5 mm) of the membrane were cut and attached to the magnetic holder using double-sided tape. The wet membrane surface was studied by contacting the surface with a drop of ultrapure water after sample mounting. For the studies in liquids, a liquid tube scanner was used. The liquid tube scanner allows simple imaging in liquids, without ancillary equipment or closed chambers.

The cantilevers were 200 μm long and of triangular shape; the spring constant of the cantilever used here was K=0.032 N/m. The tips were made from silicon nitride, and had a pyramidal shape. Scans were made on more or less randomly selected membrane areas of 1000 × 1000, 500 × 500, and 200 × 200 nm.

The manufacturer's software allowed computation of various statistics related to the surfaee roughness, including the average height, arithmetic mean deviation from the average height, the RMS roughness height, the bearing ratio, and the ratio of surface area to projected area. The roughness statistics reported in the next section were based on two scanned areas of 500 × 500 nm. Pore size was also determined. In this analysis, line profiles are selected to traverse the AFM image and pass through the pores. To determine pore size, the operator must choose the point on each height profile where the pore is considered to start and end. In

the analysis reported here, the pore radius is then simply the distance between two cursors, one at the bottom of the pore profile, and the other at the vertical location corresponding to the local 50% bearing ratio. The statistics on pore radius reported in the next section were based on measurement of more than 74 pores on 5 images of 500×500 nm and 200×200 nm membrane areas. The number of pores and porosity of the membrane were estimated using the "lakes" analysis included with the software. In this analysis, two 500×500 nm and one 200×200 nm areas were analyzed using a bearing ratio of 75%.

The reader is referred to the previous paper [2] for a thorough discussion of the adsorption experiments. Solutions of either 8 or 25 mg/l humic acid solutions were made up using reference standards from the International Humic Substances Society (USA) dissolved in distilled-deionized water. Solutions were buffered with 10^{-3} M sodium phosphate dibasic, and pH was adjusted with 10^{-1} M HCl. Calcium concentration was varied by adding the appropriate amount of calcium chloride. A 250 ml solution of humic acid was poured into a 473 ml (16 oz) clear medium round glass jar, and a cleaned membrane was placed skin side down on the top of the glass bottle, which nearly perfectly supported the membrane along its outside edge. A Teflon sheet was then placed over the top of the jar, followed by several sheets of aluminum foil to ensure a good final seal between the glass threads and the plastic cap. After the plastic cap was screwed on, the jar was inverted and placed on a gyratory shaker used extensively in carbon adsorption studies in our laboratories. Therefore, in our adsorption experiments, humic substances are contacted with the skin side of the membrane under non-permeation conditions, where the solution overlying the membrane is effectively mixed over relatively short time scales. Blank solutions (everything the same except no membrane), were used to correct for any humic acid adsorbed to the glass (negligible). Every day, the shaker was stopped, and 5 ml of solution was withdrawn for ultraviolet (UV) absorption analysis (254 nm) and computation of depletion of humic acid from the solution. Kinetic experiments were performed with new membranes after each change in chemical conditions. The temperature for all adsorption experiments was 22±2°C, and all long-term adsorption and kinetics experiments were conducted in a dark chamber.

3. Model development

Bornzin and Miller [11] and Jones and O'Melia [3] modeled adsorption of organic compounds on various polymer and membrane surfaces as diffusion from an unmixed liquid phase to a flat and non-porous surface, so-called "static adsorption". In their systems, the concentration gradient at the membrane surface declines over time as more organic material diffuses to the membrane surface. However, as microscopic analyses show (Section 4), the surface of PM30 UF membranes studied here is quite porous. In addition, like most adsorption experiments, the adsorption experiments of Jucker and Clark [2] were performed with a mixed liquid phase. Therefore, in this work, we model adsorption of humic materials from a mixed solution into a one-dimensional porous medium, where the concentration boundary condition at the membrane surface is determined by the overall depletion of organics from solution. Diffusion in a porous medium can be described with the one-dimensional diffusion equation,

$$\frac{\partial c}{\partial t} = D_{\text{eff}} \frac{\partial^2 c}{\partial x^2} \tag{1}$$

where D_{eff} is interpreted as an effective diffusion coefficient and x is perpendicular to the membrane surface. The boundary conditions for diffusion from a well-mixed reservoir are (1) $C=0$ throughout the membrane at time=0, and (2) the flux of material into the membrane results in a uniform decrease in concentration of humic materials in the well-mixed reservoir of depth h,

$$h \frac{\partial c}{\partial t} = D_{\text{eff}} \frac{\partial c}{\partial x}\Big|_{x=0} \tag{2}$$

Crank [12] provides an analytical solution to this problem in terms of the mass adsorbed at some time t, M_t, divided by the mass adsorbed at equilibrium, M_e:

$$\frac{M_t}{M_e} = 1 - \sum_{n=1}^{\infty} \frac{2\alpha(1+\alpha)}{1+\alpha+\alpha^2 q_n^2} \exp\left(-\frac{q_n^2 t}{\tau}\right) \tag{3}$$

Here α is related to the fractional uptake of adsorbate

in the membrane at equilibrium,

$$\text{fractional uptake of humic materials by membrane at equilibrium} = \frac{1}{1+\alpha} \quad (4)$$

The q_n are the roots of the generating function,

$$\tan q_n = -\alpha q_n \quad (5)$$

and τ is the diffusion time scale,

$$\tau = \frac{m^2}{D_{\text{eff}}} \quad (6)$$

where m is the effective membrane thickness for adsorption. The model described by Crank [12] assumes a linear isotherm, which was generally observed in the experiments of Jucker and Clark [2]. The linear partition coefficient K is related to α, the solution depth h, and the membrane thickness as

$$K = \frac{h}{\alpha m} \quad (7)$$

Since m is difficult to characterize in adsorption experiments, we will later use a parameter which is the product of K and m,

$$Km = \frac{h}{\alpha} \quad (8)$$

The product of K and m is subsequently referred to as the "interaction parameter". The equilibrium fractional uptake in Eq. (4) was determined from the UV measurement as,

$$\text{fractional uptake of humic materials by membrane at equilibrium} = \frac{UV_0 - UV_f}{UV_0} \quad (9)$$

where UV_0 is the initial UV absorbance of the humic acid solution, and UV_f is the final UV measurement at the end of the kinetics experiments. For a value of α determined from Eq. (9) and the experiments, Eq. (5) was plotted and the local roots were determined using the secant method (Mathcad, Mathsoft, Cambridge, MA). For non-zero values of M_t/M_e, the series in Eq. (3) converged quickly. The best fit of Eq. (3) to the experimental data was found by adjusting the parameter τ to minimize the variance between measured and modeled M_t/M_e.

The summary, our model assumes that the solution above the membrane is well mixed over time scales which are short relative to diffusion and adsorption in the membrane itself. It is reasonable to expect that time scales for mixing in the overlying fluid are of the order of seconds to minutes, whereas it is observed in the following section that time scales for uptake of humic acid by the membranes are of the order of days. Hence in our modeling, mass transfer limitation is assumed to occur only within the membrane itself (i.e., no liquid-phase mass transfer limitation).

4. Results

4.1. AFM images and surface statistics for PM30 membrane

Fig. 1 shows a scan of a 500 nm square section of the surface of a new, wet, PM30 membrane. The average of the roughness heights is Z_{ave}=0.12 nm, with a maximum roughness height of Z_{max}=0.23 nm. The arithmetic mean of the deviation in height from the average height is R_a=0.04 nm, while the RMS height is Z_{rms}=0.05 nm. The ratio of surface area to projected area is A/A_p=1.004. Comparison of these roughness statistics with other studies is complicated by the fact that different AFM manufacturers do not always calculate equivalent roughness statistics, and because to our knowledge, there are no other AFM studies of the PM30 membrane. Bowen et al. [13] studied a 25,000 MWCO polyethersulfone membrane with non-contact AFM. Although they did not report quantitative roughness statistics, the apparent Z_{max} values on a 100 × 100 nm scan were very similar to those reported in this work. Our Z_{ave}, Z_{max}, R_a and Z_{rms} values are approximately an order of magnitude less than comparable statistics from tapping mode AFM analysis of dry PPO gas separation membranes cast from chloroform and TCE [14]. Non-contact AFM scans of comparable areas of dry Nucleopore polycarbonate (N0015) UF membranes also indicated roughness statistics about an order of magnitude greater than the PM30 results presented here [15]. There is evidence which suggests that roughness statistics are influenced by the area of the scanned sample. On scans of larger 1 μm square areas of the PM30 membrane, some roughness statistics were found to increase (Z_{ave}=0.20 nm, Z_{max}=0.37 nm, R_a=0.06 nm). Prádanos et al. [15] found roughly an

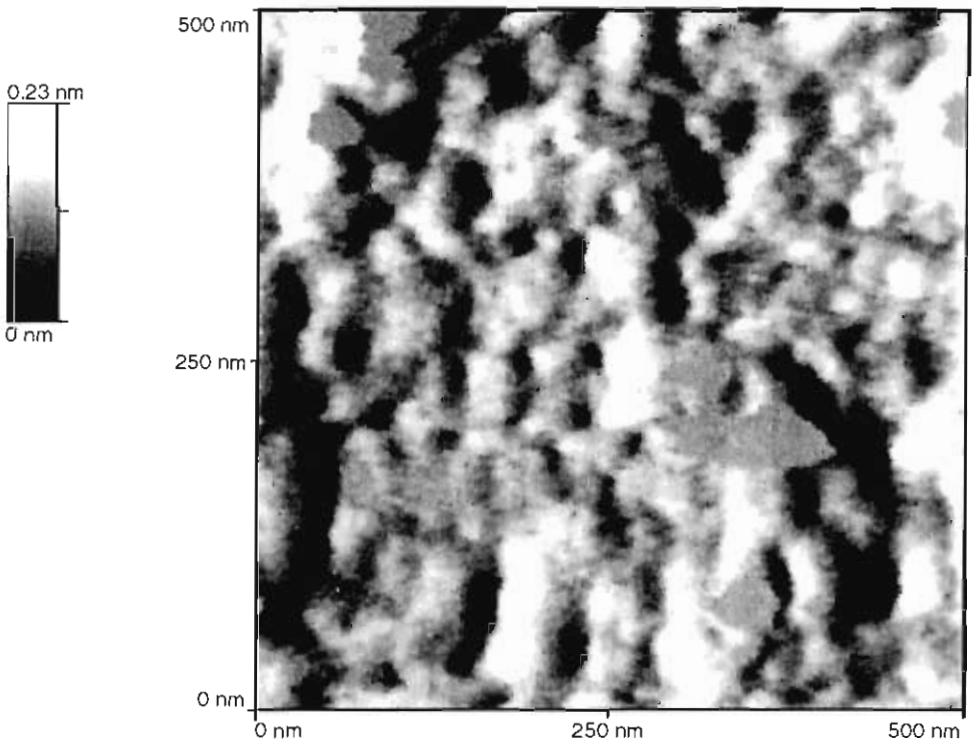

Fig. 1. Top view of 500 × 500 nm section of wet PM30 membrane using atomic force microscopy.

order of magnitude larger R_a values on 1 μm square areas than on 200 nm square areas of the Nucleopore membrane. On AFM scans of 5 μm square pieces of polypiperazineamide fully aromatic polyamide nano- and brackish water filtration membranes, Safarik [16] found a very grainy surface with much greater roughness statistics than those for the PM30 UF membrane studied here. The variation in roughness statistics with scanned area is probably caused by two factors. First, statistically speaking, a larger sampling area is more likely to sample larger roughness elements than a smaller area. Second, we have found that there are different scales of roughness on a given membrane surface, and scans of progressively larger areas tend to encounter ever larger scales of roughness. Finally, the issue of the effect of wet and dry imaging environments on roughness values is beginning to receive attention in the literature; one study of a 40 kDa MWCO sulfonated polysulfone membrane indicates significantly smaller roughness elements in the aqueous environment than in the dry environment, an effect which may be related to polymer dehydration [17].

Results for pore size analysis for the PM30 membrane are shown in Fig. 2. The average pore radius of the PM30 membrane was found to be 9.69±0.83 nm (95% confidence interval). The porosity of the PM30 membrane was found to be 10%, with 344 pores per μm^2. Fane et al. [18] assumed pore diameters for the PM30 membrane of 3.5–4 nm in their hydraulic estimation of PM30 porosity. Using TEM, Fane and Fell [19] found pore radii of 6 nm and porosities of 2% for the PM30 membrane, while using FESEM, Kim et al. [20] found average pore radii of 2 nm and average porosity of 5.9% for the same membrane. All techniques used to measure pore size and porosity suffer from certain limitations and artifacts. For example, both electron and atomic force microscopic techniques can not discriminate between true pores and dead-end pores or other pore-like features. The microscopic techniques are also not optimized to determine effective pore diameters which might result from

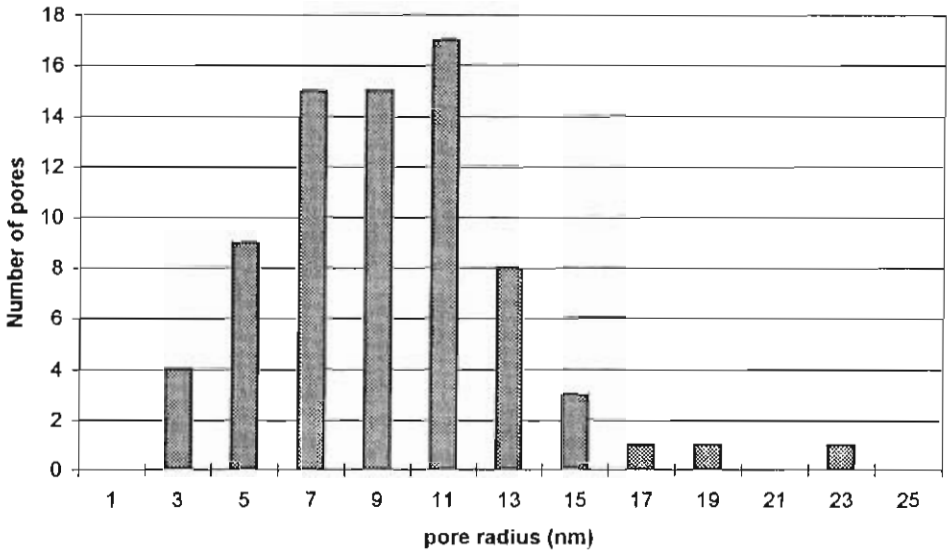

Fig. 2. Pore size distribution of PM30 membrane.

necking down of a pore at lower levels in the relatively dense skin layer. Hydraulic techniques for estimating porosity must first determine (or assume) the capillary length, diameter, and tortuosity [21]. TEM and FESEM are done on dry membranes, and pores on the dehydrated membrane may be smaller than on a hydrated membrane.

The measurements of pore size reported here are consistent with other recent AFM measurements. For example, Dietz et al. [22] found 350 pores per μm^2 on a 10,000 MWCO polysulfone membrane. Bowen et al.'s [13] study of dry 25,000 MWCO polyethersulfone membranes indicated average pore diameters of 5.1 nm. Fritzsche et al. [23] studied 30,000 MWCO polyethersulfone membranes and found pore diameters in the range of 15–25 nm. Wetted 30,000 MWCO polyacrylonitrile membranes were studied by Fritzsche et al. [24] who found pore diameters in the 12–20 nm range.

Based on small-angle X-ray scattering at high ionic strength ($I \simeq 10^{-1}$), the radius of gyration of the Suwannee humic acid molecules is given as 1.11 nm [25], with a molecular weight range of 5–10 kDa [26]. Using membrane separation techniques (Amicon YM series UF membranes) at lower ionic strengths ($I \simeq 5 \times 10^{-4}$), Jucker and Clark [2] found somewhat larger apparent molecular weight for the Suwannee humic acid of 0.5–30 kDa. (Approximately 96% of the Suwannee humic acid passed through the 30 kDa MWCO YM30 membrane.) The differences in apparent molecular weights at such widely different ionic strength is expected, since humic acid conformation is known to depend on variables like pH and ionic strength [7]. Considering the above information, it is clear that the humic acid can pass into the PM30 pores. This provides justification for our modeling of humic acid adsorption as diffusion and partitioning in a porous medium.

4.2. Interaction between humic acid and PM30 membranes

A summary of the appropriate experimental conditions and measured parameters are shown in Table 1. Note from the table the general inerease in fractional uptake of humic acid with decreasing pH; as discussed in the Section 1, these results are consistent with a decreasing electrostatic barrier between humic acid and membrane with lowered pH. Humic acid contains approximately 4.9 meq/g of carboxylic and 2.9 meq/g of phenolic hydroxyl groups [27]. The carboxylic groups are deprotonated at neutral pH. Hence, as the pH is lowered, these groups become protonated and the overall negative charge of the molecules is

Table 1
Experimental conditions, and measured and fitted model parameters

C_0	pH	[Ca]	Fractional uptake	α	τ (d)	Km (cm)
8	6.0	11	0.12	7.0	2.9	0.97
8	4.8	11	0.29	2.5	8	2.9
8	6.0	34	0.32	2.1	9.4	3.3
8	4.8	34	0.39	1.6	8.1	4.5
25	6.0	180	0.49	1.0	7.6	6.8
25	4.8	180	0.54	0.85	7.8	8.3

decreased. This decreasing solubility of the humic acid with decreasing pH was verified through measurement of octanol–water partition coefficients for the humic acid. As the pH was lowered from 6 to 4, the partition coefficient increased significantly, indicating that the humic materials become less water soluble at the lower pH [1]. Jucker and Clark [2] also found an increased (less negative) pore zeta potential as the pH was lowered over the same pH range. Hence the net effect of the pH decrease is a decreased electrostatic barrier to adsorption of humic acid. A similar interpretation of the effect of pH was employed by Matthiasson [28] for protein (BSA) adsorption on polysulfone membrane, and by Braghetta [29] for Suwannee River humic material adsorption on a sulfonated polysulfone nanofiltration membrane.

The increase in adsorption of humic acid with increasing calcium concentration is consistent with several possible mechanisms. First, it is well known from soil science that the humic materials complex or chelate metal ions such as calcium [4]. Metal ions are thought to attach to negatively charged groups like deprotonated carboxyl groups. This can result in expulsion of hydration water, coiling of the molecule, and a reduction in charge. The decreased charge of the humic acid may allow for increased adsorption through a net decrease in the electrostatic barrier between the humic acid and the membrane. In addition, if the molecular conformation is indeed smaller, this would allow for a more dense packing of humic acid during physisorption [8]. The other model for the effect of calcium is simply an ionic strength effect; the increase in ionic strength with added calcium chloride decreases the shielding between negatively charged groups on the humic material. This allows a smaller molecular conformation and a more dense adsorbed layer.

The main parameter characterizing the strength of the humic acid–membrane interaction in our model is the partition coefficient, K. To calculate this parameter, both the membrane thickness and the solution depth are required. Although the depth of solution above the membrane was known (h=7.1 cm), the thickness of the membrane m – essentially the thickness of the diffusion domain – is a more difficult parameter to specify because of the asymmetry of the membrane. There are various estimates and measurements of the thickness of asymmetric membranes and skin layers, but even with accurate estimates of such thicknesses, the *effective* diffusion thickness would still be unknown in our experiments; therefore, we have preferred the more accessible calculation of the product of the membrane thickness and the partition coefficient, Km. For lack of a better name, we call it the "interaction parameter". For experiments with the same membrane (i.e., constant m) it should be linearly related to the partition coefficient. Hence, the interaction parameter offers a direct comparison of the strength of interaction between the humic acid and PM30 membrane under different chemical conditions. As seen in Fig. 3, the interaction parameter increases

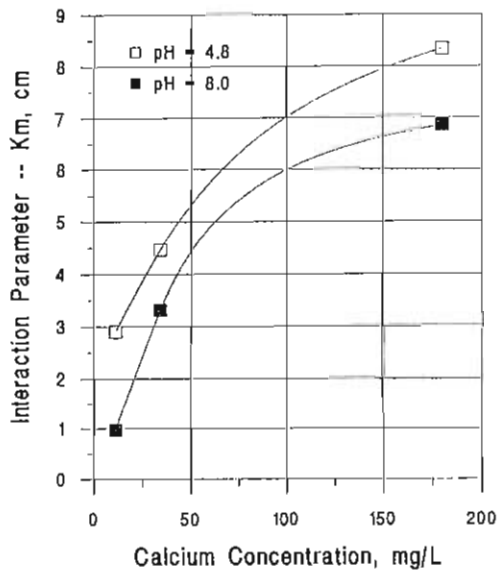

Fig. 3. Effect of pH and calcium concentration on interaction between humic acid and PM30 membrane.

significantly as the pH decreases from 6.0 to 4.8 and as the calcium concentration increases from 11 to 180 mg/l. Hence the interaction parameter parallels and parameterizes the strength of the humic acid–membrane interaction. Since it is based on an accepted adsorption model for diffusion and partitioning in a porous medium, it offers a new and logical parameter with which to characterize membrane–organic interactions.

4.3. Adsorption kinetics

Figs. 4–6 are plots of the normalized adsorbed mass (M_t/M_e) vs. time for six different conditions of pH and calcium concentration. For all experiments but one which was terminated prematurely – experiment 1 in Table 1, and Fig. 4(a) – the time scale of the adsorption process seems to be roughly of the same order of magnitude (Table 1). The model approximations of the kinetic data for experiments 1–6 are also shown in Figs. 4–6. In most cases, the fit of the model to the kinetic data is quite reasonable. The model fitting procedure yields apparent diffusion time constants, τ, and these are indicated in Table 1. Except for the prematurely terminated first experiment, the adsorption time scales are fairly tightly clustered, with an average value of 8.2 d, and standard deviation of 0.7 d; therefore, the adsorption time constants do not seem to be clearly correlated to chemical conditions. Further, the reasonable model fits suggest that the adsorption of humic acid from the mixed solution is indeed diffusion-limited in the membrane, where the intensity of

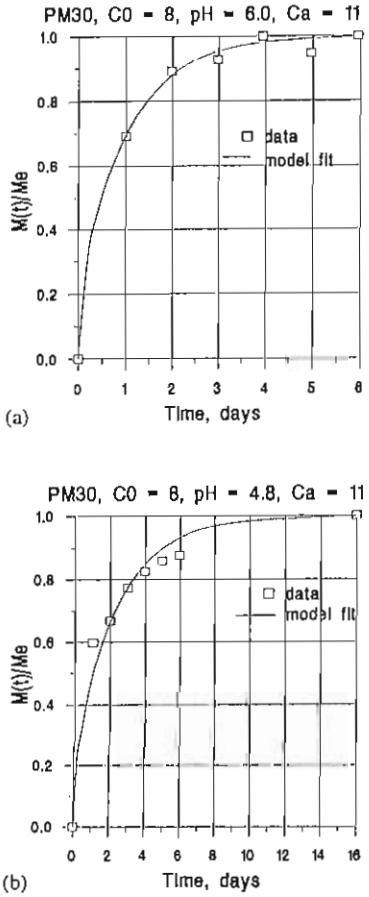

Fig. 4. Kinetics of humic acid adsorption on PM30 membrane: (a) pH 6.0, and (b) pH 4.8. C_0=8 mg/l and [Ca]=11 mg/l.

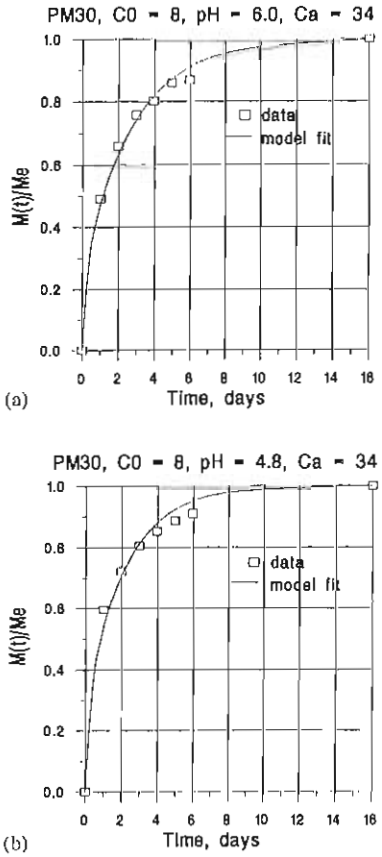

Fig. 5. Kinetics of humic acid adsorption on PM30 membrane: (a) pH 6.0, and (b) pH 4.8. C_0=8 mg/l and [Ca]=34 mg/l.

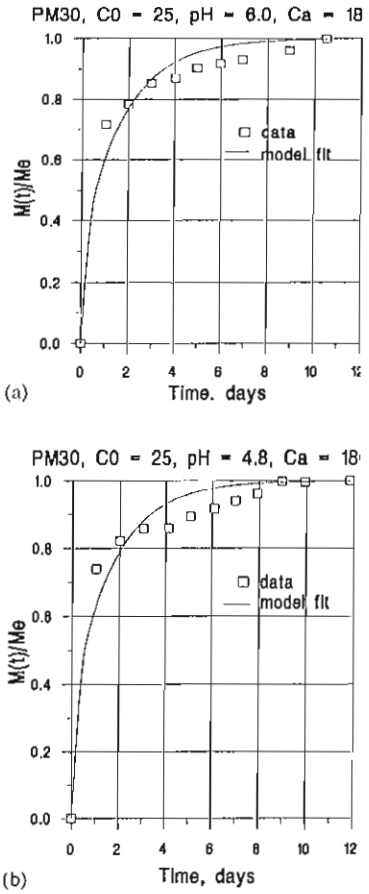

Fig. 6. Kinetics of humic acid adsorption on PM30 membrane: (a) pH 6.0, and (b) pH 4.8. C_0=25 mg/l and [Ca]=180 mg/l.

the interaction between humic acid and membrane surface is captured by the interaction parameter developed here.

5. Discussion

Studies of the fouling of membranes by naturally occurring organic compounds have been hampered by lack of a quantitative understanding of the roles of convection, diffusion, and adsorption phenomena [30]. The experiments and model presented here focus on the diffusion and adsorption aspects of the membrane fouling problem. The effective membrane thickness for diffusion was not known in the present study, and it will continue to be a difficult parameter to characterize for asymmetric membranes. However, we can at least say for the same membrane that the interaction parameter developed here should be sensitive to variations in humic material–membrane interactions caused by variations in system chemistry. This study showed marked increases in the interaction parameter with increasing calcium concentration and decreasing pH.

One can get an idea about the magnitude of the partition coefficient by substituting into Eq. (7) an estimated effective membrane thickness m. For example, we might consider that the minimum effective membrane thickness could correspond to the vertical distance between cursors used in the pore size analysis of Section 4.1. However, since the AFM tip can only chart the depth of the pore profile to a limited extent, the actual pore depths can not at present be determined with AFM. Another (probably large) estimate for the depth of the diffusion domain would be the membrane "skin thickness". Hanemaaijer et al. [31] indicate skin thicknesses for polysulfone UF membranes on the order of 100 nm from high resolution SEM. Then dividing the Km estimates in Table 1 by m=100 nm, we find partition coefficients ranging from a minimum value of $K=9.7\times10^4$ (less favorable adsorption conditions – Experiment 1) to a maximum value of $K=8.3\times10^5$ (more favorable adsorption conditions – Experiment 6). So assuming that the effective membrane thickness m of the PM30 membrane is a constant regardless of the chemical conditions studied here, the results in Table 1 suggest that variations in chemical conditions studied here can lead to changes in the partition coefficient of nearly one order of magnitude.

Because of a lack on confidence in the effective membrane thickness, we have elected to present "diffusion time scales", τ (Table 1), rather than attempt to compute an effective diffusion coefficient in Eq. (6). Considering the values of τ calculated above, and assuming a constant m, Eq. (6) yields an estimate of the ratio of the effective diffusion coefficients. However, since the effective diffusion coefficient in a porous medium is a complicated function of the porous medium tortuosity and the retardation of the diffusing species, it is useful to develop the model further to see if any clear physicochemical parameters can be estimated (viz., the molecular diffusion coefficient of the humic acid).

In porous medium, D_{eff} is often presented as [32]

$$D_{\text{eff}} = \frac{D\tau'}{R} \tag{10}$$

where D is the molecular diffusion coefficient of the humic material in water, and τ' is the tortuosity of the diffusion path. R in Eq. (10) is the retardation coefficient,

$$R = 1 + \frac{K}{\epsilon} \tag{11}$$

where ϵ is the membrane porosity. For large retardation factors ($R \gg 1$) typical of strongly adsorbing solutes, and for constant values of m and τ', Eqs. (6), (10) and (11) can be manipulated to yield for the ratio of molecular diffusion coefficients at two different pH values,

$$\frac{D^{(\text{pH}\,2)}}{D^{(\text{pH}\,1)}} = \frac{D_{\text{eff}}^{(\text{pH}\,2)}}{D_{\text{eff}}^{(\text{pH}\,1)}} \frac{Km^{(\text{pH}\,2)}}{km^{(\text{pH}\,1)}} \frac{\epsilon^{(\text{pH}\,1)}}{\epsilon^{(\text{pH}\,2)}} = \frac{\tau^{(\text{pH}\,1)}}{\tau^{(\text{pH}\,2)}} \frac{Km^{(\text{pH}\,2)}}{km^{(\text{pH}\,1)}} \frac{\epsilon^{(\text{pH}\,1)}}{\epsilon^{(\text{pH}\,2)}} \tag{12}$$

If we further assume that the membrane porosity is not affected by small variations of physicochemical conditions, i.e., $\epsilon^{(\text{pH}\,1)} = \epsilon^{(\text{pH}\,2)}$, then Eq. (12) reduces to

$$\frac{D^{(\text{pH}\,2)}}{D^{(\text{pH}\,1)}} = \frac{\tau^{(\text{pH}\,1)}}{\tau^{(\text{pH}\,2)}} \frac{Km^{(\text{pH}\,2)}}{Km^{(\text{pH}\,1)}} \tag{13}$$

Eq. (13) could also be derived for changes in calcium concentration or ionic strength at constant pH (just substitute ionic strength for pH in above formula). With Eq. (13), we can now calculate ratios of apparent molecular diffusivities of the humic acid at the different physicochemical conditions in the above tests. As suggested above, we can look at diffusivities at different pH values (for constant ionic strength), or at different ionic strength values (for constant pH). For example, using Eq. (13), we can make the following comparisons of the effect of a pH excursion from 6.0 to 4.8 at constant ionic strength:

$I = 1.5 \times 10^{-2}$ M ([Ca] = 180 mg/l):

pH 6 → 4.8 yields $D^{\text{pH}\,4.8}/D^{6.0} = 1.18$

$I = 3.97 \times 10^{-3}$ M ([Ca] = 33 mg/l):

pH 6 → 4.8 yields $D^{\text{pH}\,4.8}/D^{6.0} = 1.56$

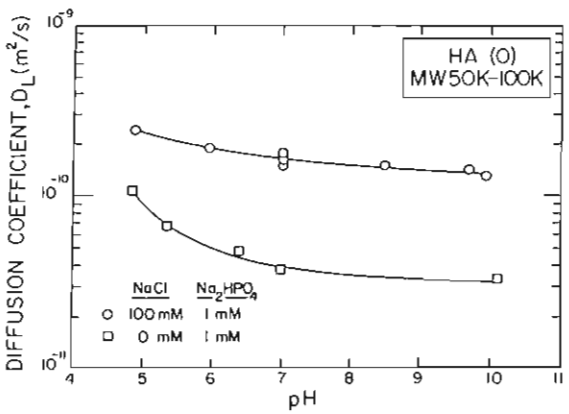

Fig. 7. Effect of pH and ionic strength on diffusion coefficient of large molecular weight fraction of Aldrich humic acid. Reproduced from Cornel, Summers, and Roberts, J. Colloid Interface Sci. 110 (1) (1986) 160. Reprinted with permission granted by Academic Press.

These calculations suggest a number of things. First, regardless of the ionic strength, the diffusivity of humic acid is increased for a decrease in pH from 6.0 to 4.8. This is consistent with a compaction of the humic molecules due to neutralization of carboxylic groups [7]. Second, the calculation suggests that the effect of a pH decrease from 6.0 to 4.8 is greater at lower ionic strength. This is also reasonable if it is hypothesized that ionic strength also causes compaction of the humic molecules, perhaps through shielding of charged groups on the molecule [4]. Data on the effect of pH and ionic strength on the diffusion coefficient of humic acid are limited. However, Cornel et al. [33] found pH and ionic strength effects very similar to the changes described above in a study of the adsorption of humic acids by activated carbon. Fig. 7 is reproduced from their study. Unfortunately, the humic acid studied by Cornel et al. (Aldrich Humic Acid, Aldrich Chemical, Milwaukee, WI) was extracted from a different source than the Suwannee humic acids used by Jucker and Clark [2]; hence, it is not useful to do more than simply note the consistency between the present predictions and the measurements of Cornel et al. [33].

With the data from Table 1, we can also calculate the effect of an ionic strength change at different pH values. For example:

$$\text{pH} = 4.8: \; I = 3.97 \times 10^{-3}\,\text{M} \rightarrow 1.5 \times 10^{-2}\,\text{M},$$
$$\text{yields } D^{0.015\,\text{M}}/D^{0.00397\,\text{M}} = 1.92$$

$$\text{pH} = 6.0: \; I = 3.97 \times 10^{-3}\,\text{M} \rightarrow 1.5 \times 10^{-2}\,\text{M},$$
$$\text{yields } D^{0.015\,\text{M}}/D^{0.00397\,\text{M}} = 2.56$$

These calculations suggest as before, an increase in ionic strength inereases the diffusivity of the humic acid. In addition, the calculations show that for a given increase in ionic strength, the effect of the increase on diffusion coefficient is greater at higher pH. These results are also very complimentary to the results of Cornel et al. [33] in Fig. 7, and support the hypothesis that increases in either (or both) hydrogen ion concentration or ionic strength serve to compact the humic acid molecules. The consistency between our results and Cornel et al. [33] is taken as one measure of support for the diffusion and partitioning model developed here.

Finally, another aspect of the results presented here which deserves attention are the plateaus evident in some of the kinetics results (especially Fig. 6(a) and (b)), which may be indicative of multiple time scale adsorption. Interestingly, it is not difficult to find other examples of kinetics with more than one plateau value. Bornzin and Miller [11] observed apparent multiple time scale adsorption kinetics for adsorption of albumin and fibrinogen on silicon rubber surfaces and porcine heart valve xenographs. They thought that this phenomenon could be related to two types of adsorption: an irreversible, hydrophobic adsorption, and a reversible, hydrophilic adsorption. The overall time scales for the adsorption experiments of Bornzin and Miller [11] was on the order of hours, in contrast to the longer kinetics observed here. Whalgren and Elofsson [34] studied adsorption of β-lactoglobulin A on non-porous methylated-silica surfaces and saw multi-time scale adsorption kinetics similar to ours, although they did not comment on these phenomenon. In their study of adsorption of humic acid on YM30 membranes, Jones and O'Melia [3] also observed plateaus which could be indicative of multiple time scale adsorption, although this was not discussed by the authors.

For the adsorption of humic acid on the polysulfone membrane, a number of phenomena could cause multiple time scale adsorption. First, the humic acid is not a single compound, but a heterogeneous mixture of compounds of different molecular weight and probably different concentrations of functional groups (see Ref. [2]). Smaller, more diffusive (or perhaps more reactive) fractions of the humic acid could reach the surface first, followed by the less diffusive or reactive fractions.

Second, although the surface of the PM30 membrane is relatively smooth compared to other membranes studied with AFM, it is a fairly porous surface. One might expect that an initially fast adsorption could occur on the non-pore surface, with a longer term adsorption occurring by molecules which had to first diffuse into the pores. Actually, the process might be just the reverse. We have stressed here that the pores are probably more energetic sites for adsorption. Therefore, it seems just as likely that after an initial period of more energetically favorable pore adsorption, there could be a longer term adsorption on the nonpore surface of the membrane. Finally, it has been suggested to us [35] that for adsorption that is quite energetically favorable, the early stages of adsorption could be dominated by a relatively small number of molecules. Over time, these molecules could change their conformation to allow greater overall adsorption.

6. Conclusions

A diffusion model with linear partitioning was found to be useful in characterizing adsorption kinetics and the strength of interaction between an aquatic humic acid and a hydrophobic UF membrane. The strength of interaction between Suwannee humic acid and the PM30 membrane increases with increasing ionic strength (increasing calcium concentration) and decreasing pH, which is consistent with a smaller conformation of the humic acid molecule, and a reduced electrostatic barrier to adsorption. Analysis of fitted diffusion time scales allowed prediction of the effect of chemical changes on the molecular diffusion coefficient of the humic acid, and these effects were found to be consistent with a previous study of humic acid.

Acknowledgements

Support of the National Science Foundation (BCS90-57387), the Electric Power Research

Institute, the National Water Research Institute, and the American Water Works Association Research Foundation is greatly appreciated. AFM studies were performed at the Beckman Institute Visualization Facility at the University of Illinois. The aid of Elisabeth Molis and Nikolai Kocherginsky in reviewing this manuscript is greatly appreciated.

References

[1] M.M. Clark, C. Jucker, Interactions between hydropbobic ultrafiltration membranes and humic substances, Proceedings of the American Water Works Association Membrane Technology Conference, Baltimore, MD, August 1–4, 1993.
[2] C. Jucker, M.M. Clark, Adsorption of aquatic humic substances on hydrophobic ultrafiltration membranes, J. Membr. Sci. 97 (1994) 37–52.
[3] K.L. Jones, C.R. O'Melia, The influence of protein and humic acid adsorption on the fouling of hydrophilic ultrafiltration membranes, American Chemical Society, Division of Environmental Chemistry, vol. 36, No. 2, 212th ACS National Meeting, Orlando, FL, August 25–29, 1996.
[4] M. Schnitzer, S.U. Khan, Humic Substances in the Environment, Marcel Dekker, New York, 1972.
[5] M. Cheryan, Ultrafiltration Handbook, Technomic Publishers, Lancaster, PA, 1986.
[6] J.M. Laîné, J.P. Hagstrom, M.M. Clark, J. Mallevialle, Effect of ultrafiltration membrane composition, J. Am. Water Works Assoc. 81(11) (1989) 61–67.
[7] K. Ghosh, M. Schnitzer, Macromolecular structures of humic substances, Soil Science 129(5) (1980) 266–276.
[8] S. Hong, M. Elimelech, Chemical and physical aspects of natural organic matter (NOM) fouling of nanofiltration membranes, J. Membr. Sci. 132 (1997) 1159–1181.
[9] M.M. Clark, C. Jucker, Diffusion and Partitioning of Humie Acid in a Hydrophobic UF Membrane, American Chemical Society, Division of Environmental Chemistry, vol. 36, No. 2, 212th ACS National Meeting, Orlando, FL, 1996, August 25–29.
[10] C.A. Jucker, Master's Thesis, University of Illinois, Urbana, Illinois, 1993.
[11] G.A. Bornzin, I.F. Miller, The kinetics of protein adsorption on synthetics and modified natural surfaces, J. Colloid Interface Sci. 86(2) (1982) 539–558.
[12] J. Crank, The Mathematics of Diffusion, Clarendon Press, Oxford, 1956.
[13] R.W. Bowen, N. Hilal, R.W. Lovitt, P.M. Williams, Visualization of an ultrafiltration membrane by non-contact atomic force microscopy at single pore resolution, J. Membr. Sci. 110 (1996) 229–232.
[14] K.C. Khulbe, B. Kruczek, G. Chowdhury, T. Gagné, T. Matsuura, S.P. Verma, Characterization of membranes prepared from PPO by Raman scattering and atomic force microscopy, J. Membr. Sci. 111 (1996) 57–70.
[15] P. Prádanos, M.L. Rodriquez, J.I. Calvo, A. Hernández, F. Tejerina, J.A. de Saja, Structural characterization of an UF membrane by gas adsorption–desorption and AFM measurements, J. Membr. Sci. 117 (1996) 291–302.
[16] J. Safarik, Personal communication, Orange County Water District, Fountain Valley, CA, 1995.
[17] A. Bessières, M. Meireles, R. Coratger, J. Beauvillain, V. Sanchez, Investigation of surface properties of polymeric membranes by near field microscopy, J. Membr. Sci. 109 (1996) 271–284.
[18] A.G. Fane, C.J.D. Fell, A.G. Waters, The relationship between membrane surface pore charaeteristics and flux for ultrafiltration membranes, J. Membr. Sci. 9 (1981) 245–262.
[19] A.G. Fane, C.J.D. Fell, Desalination 62 (1987) 117.
[20] K.J. Kim, A.G. Fane, C.J.D. Fell, T. Suzuki, M.R. Dickson, Quantitative microscopic study of surface characteristics of ultrafiltration membranes, J. Membr. Sci. 54 (1990) 89–102.
[21] F.P. Cuperous, C.A. Smolders, Characteristics of UF membranes. Membrane characteristics and characterization techniques, Adv. Colloid Interface Sci. 34 (1991) 135–173.
[22] P. Deitz, P.K. Hansma, K.H. Herrmann, O. Inaeker, H.D. Lejmann, Atomic force microscopy of synthetic ultrafiltration membranes in air and water, Ultramicroscopy 35 (1991) 155.
[23] A.K. Fritzsche, A.R. Arevalo, A.F. Connolly, V.B. Moore, K. Elings, K. Kjoller, C.M. Wu, The structure and morphology of the skin of polyethersulfone ultrafiltration membranes. A comparative atomic force microscope and a scanning electron microscope study, J. Appl. Polym. Sei. 45 (1992) 1945–1956.
[24] A.K. Fritzsche, A.R. Arevalo, V.B. Moore, C. O'Hara, The surface structure and morphology of polyacrilonitrile membranes by atomic force microscopy, J. Appl. Polym. Sci. 45 (1993) 1945–1956.
[25] G.R. Aiken, P.A. Brown, T.I. Noyes, D.J. Pinckney, Molecular size and weight of fulvic and humic acids from the Suwannee river, in: R.C. Averret, J.A. Leenheer, D.M. McNight, K.A. Thorn (Eds.), Humic Substances in the Suwannee River, Georgia: Interactions, Properties and Proposed Structure, Open-File Rep. U.S. Geol. Surv., 1989, No 87–557, pp. 163–179.
[26] E.M. Thurman, R.L. Wershaw, R.L. Malcolm, D.J. Pinckney, Molecular size of aquatic humic substances, Org. Geochem. 4 (1982) 27–35.
[27] K.A. Thorn, Nuclear magnetic resonance spectrometry investigations of fulvic and humic acids from the Suwannee river, in: R.C. Averret, J.A. Leenheer, D.M. McNight, K.A. Thorn (Eds.), Humic Substances in the Suwannee River, Georgia: Interactions, Properties and Proposed Structure, Open-File Rep. U.S. Geol. Surv., 1989, No 87-557, pp. 163–179.
[28] E. Matthiason, The role of macromolecular adsorption in fouling of ultrafiltration membranes, J. Membr. Sci. 16 (1983) 23–36.
[29] A. Braghetta, PhD thesis, University of North Carolina, Chapel Hill, NC, 1995.

[30] P. Aimar, C. Taddei, J-P. LaFaille, V. Sanchez, Mass transfer limitations during ultrafiltration of cheese whey with inorganic membranes, J. Membr. Sci. 38 (1988) 203–221.

[31] J.H. Hanemaaijer, T. Robbertson, Th. van der Boomgaard, C. Olieman, P. Both, D.G. Schmidt, Characterization of clean and fouled ultrafiltration membranes, Desalination 68 (1988) 93–108.

[32] M.M. Clark, Transport Modeling for Environmental Engineers and Scientists, Wiley, New York, 1996.

[33] P.K. Cornel, R.S. Summers, P.V. Roberts, Diffusion of humic acid in dilute aqueous solution, J. Colloid Interface Sci. 110(1) (1986) 149–164.

[34] M. Wahlgren, U. Elofsson, Simple models for adsorption kinetics and their correlation to the adsorption of β-Lactoglobulin A and B, J. Colloid Interface Sci. 188 (1997) 121–129.

[35] C. Tiller, Personal Communication, 1996.

Part II

Results of SPEES/PES-PS Series Membranes

Development and Characterization of UF Membranes and Relation of Membrane Properties to Adsorptive Fouling

Subject: SPEES/PES-PS series membranes

Principal Investigator: Mark M. Clark

Research Assistants: Corine Combe, Manish Kumar, Yingge Wang, and Yonghun Lee

January, 1999

SPEES/PES ULTRAFILTRATION MEMBRANES

CASTING PARAMETERS

% solid content ↗ →

SPEES/PES to PS ratio ↗ ↓

MC20 SPEES/PES : 0 % PS : 17.9 % NMP+PA: 82.1 %	**MC23** SPEES/PES : 0 % PS : 19.93 % NMP+PA : 80.07 %	**MC26** SPEES/PES : 0 % PS : 21.93 % NMP+PA : 79.07 %
MC21 SPEES/PES : 1.65 % PS: 16.28 % NMP+PA : 82.1 %	**MC24** SPEES/PES : 1.65 % PS : 18.28 % NMP+PA : 80.07 %	**MC27** SPEES/PES : 1.65 % PS : 20.28 % NMP+PA : 79.07 %
MC22 SPEES/PES : 3.33 % PS : 14.6 % NMP+PA : 82.1 %	**MC25** SPEES/PES : 3.33 % PS : 16.6 % NMP+PA : 80.07 %	**MC28** SPEES/PES : 3.33 % PS : 18.6 % NMP+PA : 79.07 %

What we can expect?

a) SPEES/PES to PS ratio ↗ (vertically)
- charge density ↗
- hydrophilicity ↗
- water permeability constant

b) % solid content ↗ (horizontally)
- charge density constant
- hydrophilicity constant
- water permeability ↘ (smaller pore size)

Chemical Structures of PEES/PES and PS

SPEES/PES: Sulfonated-polyethersulfone/Polyether sulfone

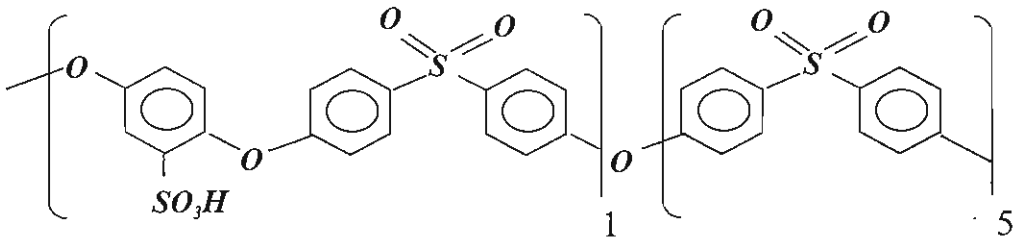

PS: Polysulfone

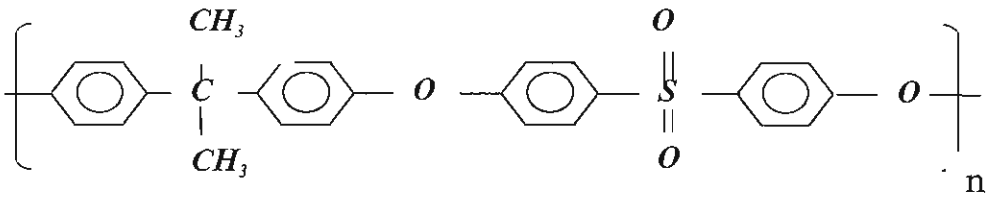

SOLVENTS: NMP: N-METHYL PYRROLIDONE (C_5H_9NO)

PA: PROPIONIC ACID CH_3-CH_2-COOH

MEMBRANE CHARACTERIZATION

- Water permeability
- XPS analysis: *elemental composition of membrane surface*
- PolyEthyleneGlycol retention: *estimation of MWCO*
- Contact angle measurements: *hydrophobic/hydrophilic character*
- Streaming potential measurements: *measurement of membrane pore charge*
  evolution of pore charge with pH
- Atomic Force Microscopy: *visualization of membrane surface*
- FTIR/FTR spectra: *chemical functional groups*

FOULING OF MEMBRANE BY HUMIC ACID

- Adsorption of humic acid without permeation: *interactions between membrane surface and humic acid*

- Cross-flow experiments: *flux decline*

WATER PERMEABILITY

Methods and Material

Filtration tests were performed using a 28.7cm^2 diameter UF cell with magnetic stirrer (Amicon, Minnetonka, MI). The pressure was applied via a compressed nitrogen tank, and was varied between 68.9 kPa and 206.7 kPa (10psi and 30psi).

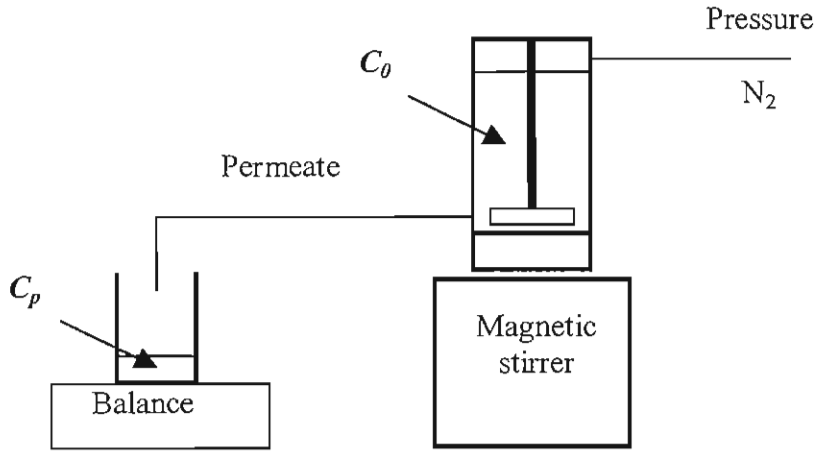

Figure 1 Amicon cell dead-end setup

The variation of water flux was plotted versus applied pressure and the slope represents the membrane water permeability symbolized by Lp.

Results and Discussion

The values for the membrane series are presented in Table 1 and Figures 2-1 thru 2-4 .

Table 1 Water permeability and thickness of membranes

MC20	**MC23**	**MC26**
Lp (10^9 m/sPa) = 1.27	Lp (10^9 m/sPa) = 0.424	Lp (10^9 m/sPa) = 0.263
Lp (10^3 LMH/Pa) = 4.57	Lp (10^3 LMH/Pa) = 1.53	Lp (10^3 LMH/Pa) = 0.95
Total Thickness (μm) = 177.8	Total Thickness (μm) = 210.8	Total Thickness (μm) = 193.0
Skin Thickness (μm) = 76.2	Skin Thickness (μm) = 109.2	Skin Thickness (μm) = 91.4
MC21	**MC24**	**MC27**
Lp (10^9 m/sPa) = 3.13	Lp (10^9 m/sPa) = 1.11	Lp (10^9 m/sPa) = 1.11
Lp (10^3 LMH/Pa) = 11.27	Lp (10^3 LMH/Pa) = 4.00	Lp (10^3 LMH/Pa) = 4.00
Total Thickness (μm) = 231.1	Total Thickness (μm) = 274.3	Total Thickness (μm) = 246.4
Skin Thickness (μm) = 129.5	Skin Thickness (μm) = 172.7	Skin Thickness (μm) = 144.8
MC22	**MC25**	**MC28**
Lp (10^9 m/sPa) = 4.37	Lp (10^9 m/sPa) = 1.89	Lp (10^9 m/sPa) = 1.43
Lp (10^3 LMH/Pa) = 15.73	Lp (10^3 LMH/Pa) = 6.8	Lp (10^3 LMH/Pa) = 5.15
Total Thickness (μm) = 241.3	Total Thickness (μm) = 304.8	Total Thickness (μm) = 269.2
Skin Thickness (μm) = 139.7	Skin Thickness (μm) = 203.2	Skin Thickness (μm) = 167.6

Figure 2 presents the variation of flux versus pressure for water filtration. By comparing membranes of the same column (MC 20/21/22, MC 23/24/25 and MC 26/27/28) we can see an increase in water permeability. This result was not expected. The only difference between those membranes is their SPEES/PES to PS ratio, that is increasing by moving down in the table, and this parameter was not expected to affect water flux. We also notice a decrease in water permeability when moving horizontally in the table, i.e. when solid content is increasing. This is in good agreement with what we expected.

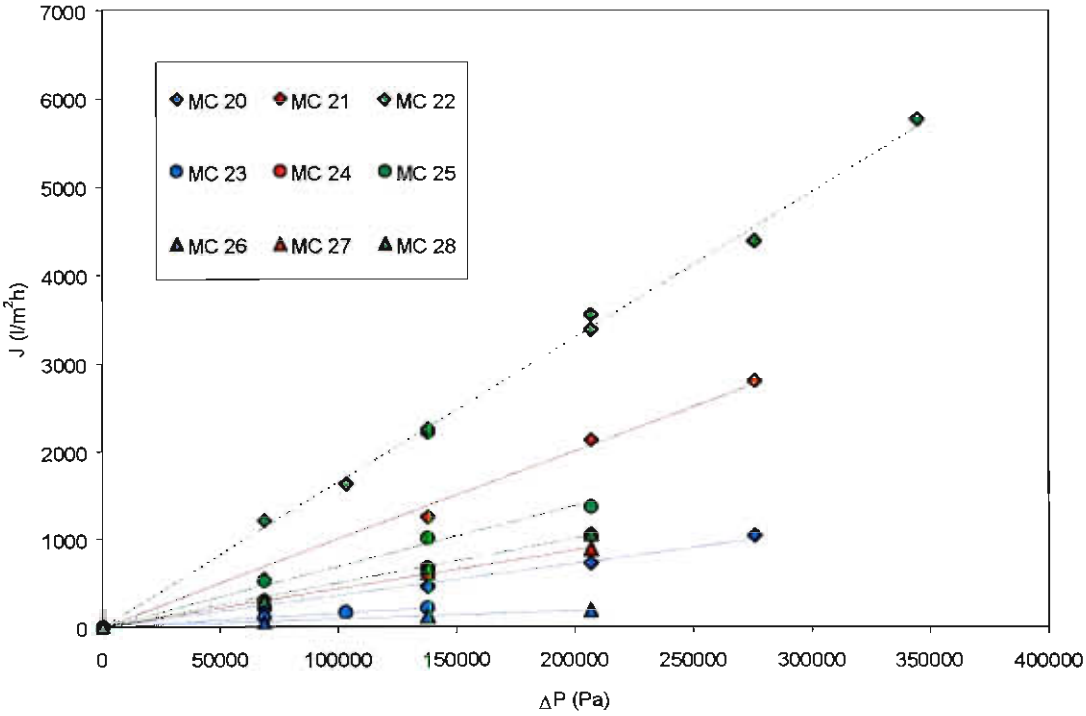

Figure 2-1 Specific water permeability

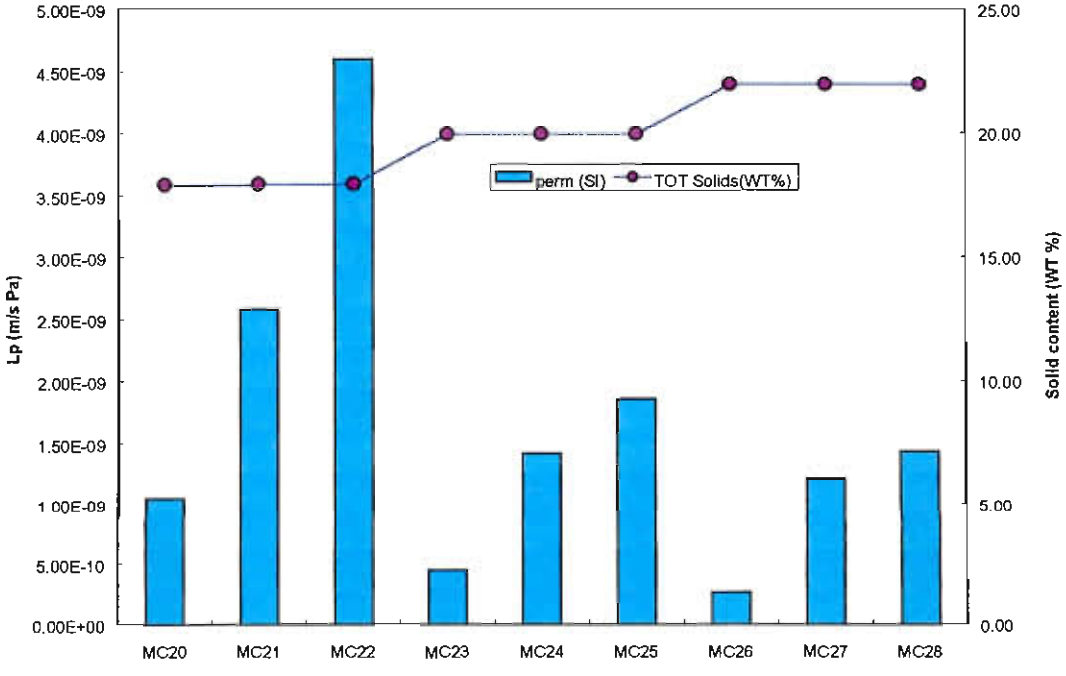

Figure 2-2 Effect of solid content on water permeability

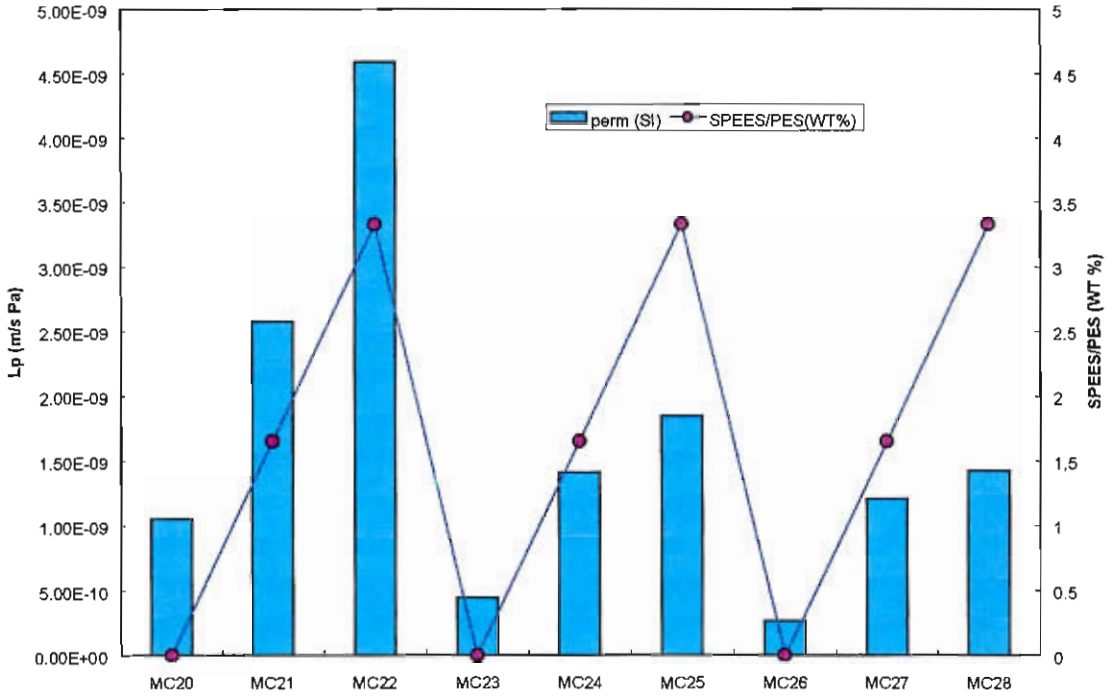

Figure 2-3 Effect of SPEES/PES content on water permeability

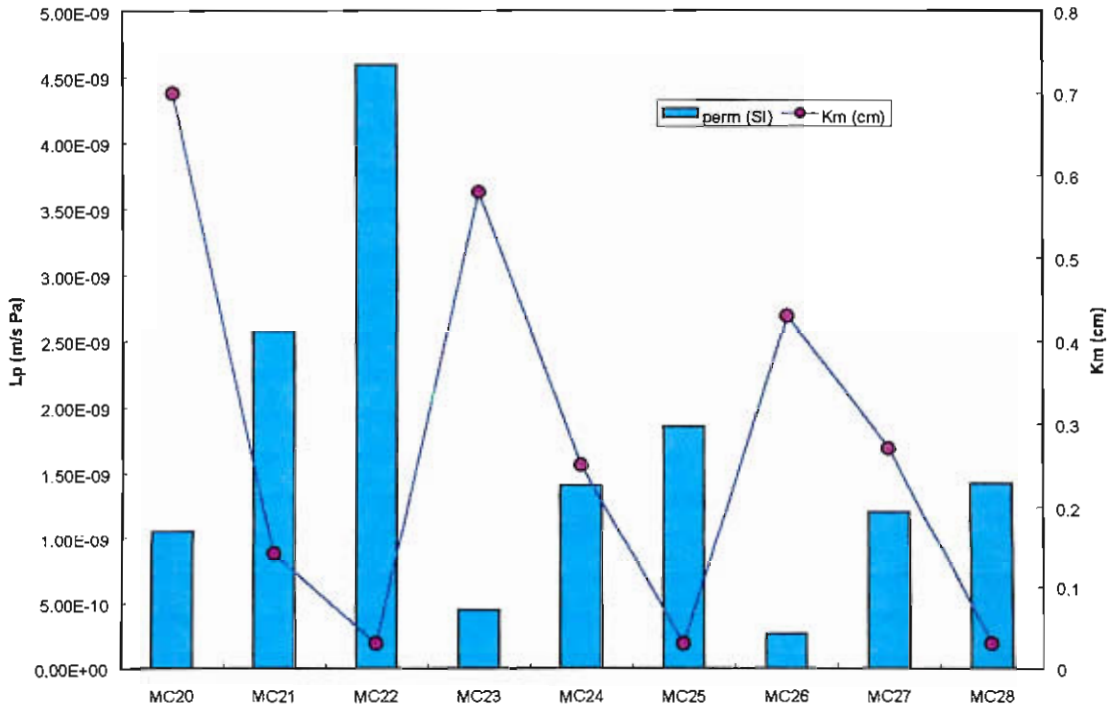

Figure 2-4 Effect of SPEES/PES content on interaction parameter

XPS ANALYSIS: SURFACE ELEMENTARY COMPOSITION

Methods and Material

This technique is used to determine the elementary composition of a surface sample. It is known under several names: X-ray photoelectron spectroscopy (XPS), electron spectroscopy for chemical analysis (ESCA), high-energy photoelectron spectroscopy (HEPS), induced emission spectroscopy (IEES0, photoelectron spectroscopy of the inner shell (PESIS) and energy dispersion system (EDS). The principle is simple: the sample surface is bombing by X-rays and the kinetic energies of photoelectrons ejected are measured. Because the binding energy of those electrons, also called core electrons, is a characteristic of an individual element, each chemical element is identifiable (Oldani and Schock, 1989; Clark and Feast, 1975). For each element, the binding energy depends on the energy level of the core electron, which can be 1s, 2s, $2p_{1/2}$, and/or $2p_{3/2}$. In general, the ESCA spectrum of a given core level consists of well resolved peaks corresponding to electrons escaping without undergoing energy losses, superimposed in a background tailing to lower kinetic energy arising from inelastically scattered electrons.

This technique provides information related to surface, subsurface, or essentially bulk properties, depending on differences in escape depths for photoemitted (or Auger) electrons corresponding to different kinetic energies. By varying the incident energy, it is possible to use ESCA to depth profile samples to investigate their homogeneity. Hence, if an element gives two or more signals from levels with very different escape depths, it ought to be possible to use the relative intensities of the signals to calculate the thickness of the layer containing that element (Clark and Feast, 1975).

The principle advantages of this technique are:

- the sample may be solid, liquid or gas, and the technique is essentially non-destructive
- the sensitivity of this technique is such that a fraction of a monolayer coverage may be detected

• high sensitivity is independent of the spin properties of any nucleus and is applicable in principle to any element of the periodic table. Hydrogen and helium are exceptions, being the only elements for which the core levels are also the valence levels

• information can be obtained on both the core and the valence energy levels of molecules

• only the top 50-100 Å of the samples are analyzed (Clark and Feast, 1975; Stengaardh, 1988)

In our experiments the data were collected by a Perkin-Elmer/Physical Electronics Division model n° 5400 X-ray photoelectron spectrometer with Mg Kα X-radiation, 1253.6 eV (15kV, 400W). For the determination of the atomic composition of each element, data were collected for multiplex spectra at 0.05 eV/step for 100 mses/step with a 35.75 pass energy. The atomic composition was determined using peak area sensitivity factors described by Wagner et al. (1979). The accuracy of the instrument is 0.1 eV, and the minimum detection limit in the relative chemical composition determination is about 0.2%. Prior to analysis pieces of membranes (about 1 cm^2) were put in petri dishes and let at room temperature for one day. Before starting the analysis the samples were placed in a vacuum for about 15 min, under a base pressure of 1 to $1.4.10^{-11}$ psi. The analysis pressure was in the range 0.2 to $1.0.10^{-11}$ psi. In our experiments ESCA measurements were carried out to determine the atomic composition (C, O, S, N) of the clean membranes.

Results and Discussion

The results are presented in Table 2.

Table 2 Elementary composition obtained by XPS of some SPEES/PES membranes

Membrane	MC 20	MC 21	MC 22	MC 24	MC 27
C (%)	76.28	74.82	75.53	72.97	70.99
O (%)	19.15	19.97	19.75	22.17	22.68
N (%)	1.87	1.94	0	3.16	1.88
S (%)	2.7	3.28	4.76	1.7	4.45

a) SPEES/PES to PS ratio ↗ % S ↗

(vertically)

b) % solid content ↗

(horizontally)

Presence of N: due to residual solvents: NMP : N-methyl pyrrolidone C_5H_9NO

PA : proprionic acid CH_3-CH_2-COOH

PEG RETENTION: DETERMINATION OF MWCO

Methods and Material

In order to characterize the membrane pore size, molecular weight cut-off (MWCO) was determined using model solutes. Synthetic polymers, such as polyethylene glycol (PEG), dextran, polyvinylpyrrolidone are usually chosen because they do not interact strongly with the membrane material. In this study we used a group of four PEG, with molecular weights of 300, 600, 3350 and 10000 Da purchased from Sigma (St Louis, MO). Lentsch et al. (1993) used an empirical equation to calculate the Stokes radius of PEG. Experimental PEG diffusion coefficient measurements were combined with the Stokes-Einstein law to give the following relation:

$$r_s = 0.045\ M^{0.44} \tag{1}$$

where r_s: PEG Stokes radius (nm)

M: molecular weight (Da)

The Stokes radii calculated for the PEG used in this study are presented in Table 3.

Table 3 Solute radius of PEG calculated by empirical Lentsch's equation (1)

MW (Da)	300	600	3350	10000
r_s (nm)	0.5	0.75	1.6	2.6

Filtration tests were performed using a 28.7cm^2 diameter UF cell with magnetic stirrer (Amicon, Minnetonka, MI). The pressure was applied via a compressed nitrogen tank, and was varied between 68.9 kPa and 206.7 kPa (10psi and 30psi). Membrane water permeability was measured before and after each filtration experiment in order to check for membrane fouling by PEG. For each applied pressure, PEG concentrations in the retentate and permeate were measured by a TOC analyzer (Phoenix 8000, Dohrmann) and PEG retentions were calculated using the following equation:

$$R = 1 - \frac{C_p}{C_0} \tag{2}$$

Because of concentration polarization occurring in the retentate side, an intrinsic retention must be defined by:

$$R^* = 1 - \frac{C_p}{C_m} \tag{3}$$

where C_m represents the concentration at the membrane surface [14]. The film model is used to relate R and R^*:

$$\ln\left(\frac{1-R}{R}\right) = \ln\left(\frac{1-R^*}{R^*}\right) + \frac{J}{k} \tag{4}$$

R^* is obtained by the intercept of the slope of $\ln\left(\frac{1-R}{R}\right)$ versus flux J. The plot of intrinsic retention versus flux is used to determine the membrane MWCO.

In order to get the average corresponding pore radius, we used a model of steric exclusion as presented by Ferry (Deen, 1987). When size exclusion is the only selectivity phenomena the intrinsic retention extrapolated to no flux is equal to

$$R^*_{J=0} = \left(1 - (1-\lambda)^2\right)^2 \tag{5}$$

with $\lambda = \frac{r_s}{r_p}$ r_s solute radius, r_p pore radius

The first approximation is to consider that the membrane pores are all the same size. In this case an average pore radius can be calculated from the values of R^* determined by the retention experiments and PEG radius. This method allows the calculation of the pore radius of the homogeneous membrane equivalent to the membrane tested. This is a good method in our case where we want to compare different membranes.

Results and Discussion

Table 4 MWCO and pore radius determined by PEG retention experiments

MC20 MWCO (Da) = 3350 r_p (nm) = 1.9	MC23 MWCO (Da) = 1000 r_p (nm) = 1.14	MC26 MWCO (Da) = r_p (nm) =
MC21 MWCO (Da) = 2700 r_p (nm) = 1.76	MC24 MWCO (Da) = 2850 r_p (nm) = 1.8	MC27 MWCO (Da) = 2850 r_p (nm) = 1.8
MC22 MWCO (Da) = 9450 r_p (nm) = 3.06	MC25 MWCO (Da) = r_p (nm) =	MC28 MWCO (Da) = r_p (nm) =

a) SPEES/PES to PS ratio ↗ pore radius ↗ ??? not expected

(vertically)

b) % solid content ↗

(horizontally)

CONTACT ANGLE (CAPTIVE AIR BUBBLE METHOD): HYDROPHOBICITY

Methods and Material

The captive air bubble method was used in this research. It is based on measuring the contact angle between an air bubble and the membrane covered with water.

Prior to measurement, membranes were stored in petri dishes at 4°C. They were soaked in milli-Q water for three hours, with three water changes, and then soaked in 5% NaCl solution for one hour. All membranes were then flushed in the stirred cell in order to remove any trace organic compounds used by the manufacturer to prevent drying and preserve the membrane.

The membranes were cut into pieces and stored in water. Membrane strips were tapped inside a glass cell. After this cell was completely filled with water, an air bubble was injected using a microliter syringe. This bubble moved vertically and rised the membrane surface. A light source was placed behind the sample and the light was focussed through a slit. The contact angle was measured with the goniometer

Results and Discussion

The results are presented in Table 5 and Figure 3.

Table 5 Contact angles obtained by captive air bubble. Comparison with data measured by Orange County District

MC20 CA = 76.6 ± 3.6 CA (Orange Dist.) = 64.9	MC23 CA = 78.4 ± 2.8 CA (Orange Dist.) = 65.4	MC26 CA = 79.55 ± 2.7 CA (Orange Dist.) = 67.1
MC21 CA = 77.6 ± 4.6 CA (Orange Dist.) = 61.5	MC24 CA = 77.8 ± 3.3 CA (Orange Dist.) = 61.6	MC27 CA = 76.17 ± 4.8 CA (Orange Dist.) = 61.8
MC22 CA = 79.6 ± 4.4 CA (Orange Dist.) = 61.2	MC25 CA = 78.4 ± 2.6 CA (Orange Dist.) = 61.6	MC28 CA = 78.8 ± 3.6 CA (Orange Dist.) = 61.6

a) SPEES/PES to PS ratio ↗ (vertically) CA constant

b) % solid content ↗ (horizontally) CA constant

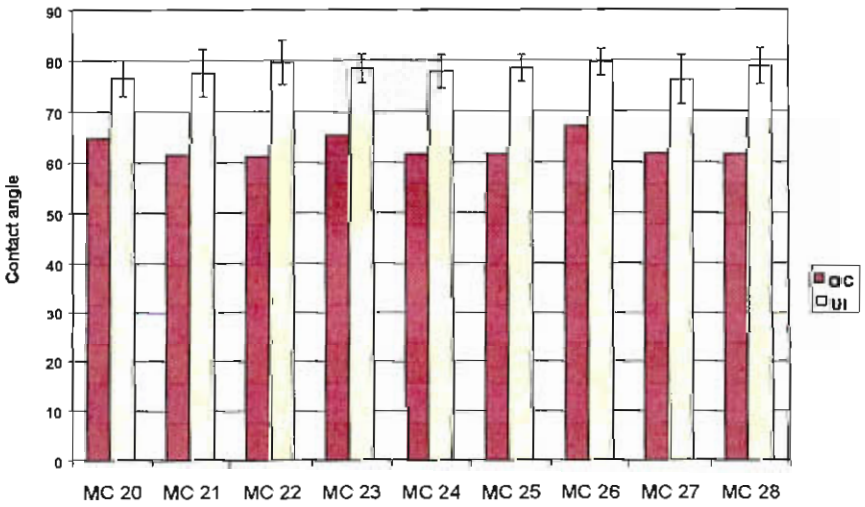

Figure 3 Comparison of contact angle measurements (Orange County vs. UI)

AFM: MEAN DIAMETER

Methods and Material

Atomic Force Microscopy (AFM) is used for direct analysis of membrane surface properties, such as pore size distribution, pore shape, and surface roughness. This technique does not require any special preparation of the sample, and the sample can be imaged in either air or liquid.

The membranes were imaged under water since the membranes should be studied in their working environment in order to get the best resolution. The wet membranes are studied in contact mode. In this case the probe tip scans across the sample surface and is in direct physical contact with the sample. It can then respond to very short-range repulsive interactions with the sample.

The AFM observations were performed on a Digital Nanoscope II instrument. Cantilevers, made from silicon nitride, are 200μm long and have a triangular shape. The spring constant of the narrow cantilever is k=0.032N/m. The tip is also made of silicon nitride and has a pyramidal shape. Square pieces (5mm*5mm) of the membrane were cut and attached to the magnetic holder using doubled-sided tape. The wet membrane surface was studied by contacting the surface with a drop of ultrapure water after sample mounting. For studies in liquids, a liquid tube scanner is used. The liquid tube scanner allows simple and routine imaging in liquids, without the need for ancillary equipment or a closed chamber.

Pore sizes are estimated from AFM images and calculated by AFM surface analysis software. Line profiles are selected to traverse the AFM image and pass through the pores. To determine pore size, the operator must choose points on each height profile where the pore is considered to start and end. The pore radius is then the horizontal distance between these points. The porosity of the membrane was estimated using the measured average pore diameter and the "lakes analysis" included with the software.

Results and Discussion

Table 6 Pore diameter (dp in nm) and average roughness (Rms in Å) measured after AFM images. Comparison with values obtained at Orange County District

MC20		MC23		MC26	
UI	OC	UI	OC	UI	OC
dp = 56	dp = 86	dp = 86.7	dp = 108	dp = 69.4	dp = 90
Rms = 40.6	Rms = 43.6	Rms = 70.8	Rms = 74.2	Rms = 65.9	Rms = 48.8
MC21		MC24		MC27	
UI	OC	UI	OC	UI	OC
dp =	dp = 92	dp =	dp = 45	dp =	dp = 58
Rms =	Rms = 14.8	Rms =	Rms = 78.9	Rms =	Rms = 24.4
MC22		MC25		MC28	
UI	OC	UI	OC	UI	OC
dp = 415	dp = 153	dp =	dp = 115	dp =	dp = 120
Rms = 308	Rms = 275	Rms =	Rms = 120	Rms =	Rms = 165.6

a) SPEES/PES to PS ratio ↗ pore diameter ↗

(vertically)

b) % solid content ↗ pore diameter constant

(horizontally)

STREAMING POTENTIEL: PORE CHARGE

Methods and Material

Zeta potential of membrane surface were obtained from streaming potential measurements on an instrument build according to Nyström's research (Nyström et al., 1989; Nyström and Zhu, 1997).

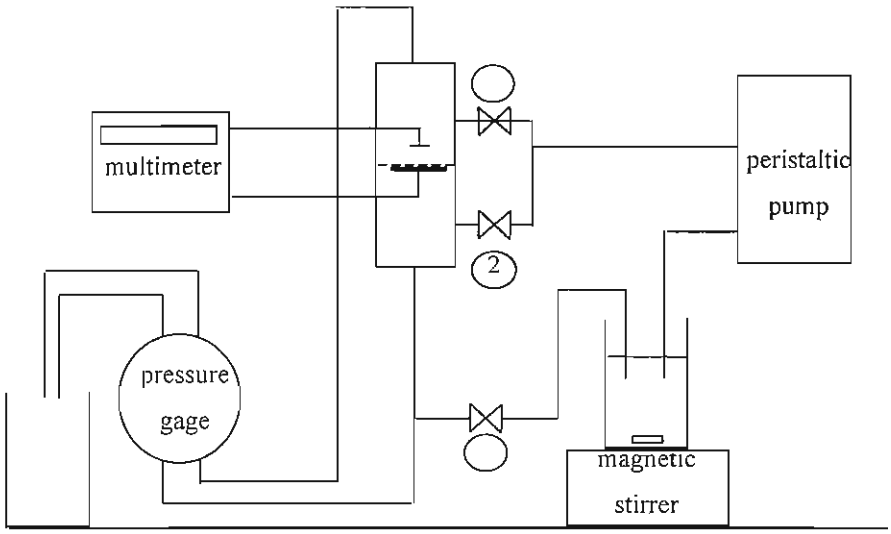

Figure 4 Experimental set-up for zeta potential measurement

The measuring cell consists of two cylindrical half-cells made in plexiglass. To prepare the electrodes 18 X 18 per linear inch copper mesh is cut into two disks of 17mm and 29mm diameter. These disks are soldered to a 0.5mm copper wire. Both disks and wire are silver plated by electrolysis and chloridized by electrolysis in 0.1N HCl at a total current of about 2mA during half an hour. After silver platting they are washed for a few hours to eliminate any excess chloride ions until the voltage is constant when no differential pressure is applied.

A peristaltic pump with a variable speed drive 6-600rpm is used to pump the liquid from the feed beaker through the cell. The speed is controlled with a speed drive system. Because of this peristaltic pump the flow is not perfectly smooth. A pulse dampener is added in the line to reduce the fluctuations of the flow. The two cell

compartments are connected to a Capsuhelic differential pressure gage (0-5psi, accuracy ± 0.05psi). The voltage is measured with a Fluke 45 dual display multimeter (resolution 0.001mV, accuracy 0.02%).

All our experiments follow the same experimental procedure: the cell is closed without membrane and placed in the instrumental set-up. All the valves are open and the electrolyte solution is pumped until there is no air bubble left in the all system (valves 1 and 2 may be closed at the end of the filling). The pump is then turned off and the cell is open, without letting air bubbles entering into the lower half-cell. A 3.3cm diameter piece of membrane is cut and placed on the lower larger electrode, which serves as a support for the membrane. The cell is closed and the solution is pumped again, in order to fill the upper part of the instrument. The instrument is ready when it is free of air bubble. Valves 1 and 3 are open, valve 2 is closed.

The solution is circulated under no differential pressure until the difference in potential between the two half cells remain constant (about 30 min). The conductivity of the solution is measured and the pressure is increased up to 4.5psi by touching valve 2. The resulting difference in potential is measured. The pressure is decreased of 0.5psi until 1psi and the potential is measured each time. At the end of the series the conductivity of the solution is checked and the pressure is released. The cells are emptied and the solution is replaced by Milli-Q water. The system is flushed with the water before any other measurement.

The Helmoltz-Smoluchowski equation was used to calculate the zeta potential from these measurements:

$$\xi = \frac{\eta \ \kappa \Delta E}{\varepsilon_0 \ \varepsilon_r \ \Delta P} \tag{6}$$

with:

- $T = 20° C \pm 1°C$
- $\eta = 1.002.10^{-3}$ ($kg.m^{-1}.s^{-1}$)
- $\varepsilon_0\varepsilon_r = 80.37$
- ξ = zeta potential (mV)
- ΔE = potential difference (mV)
- ΔP = pressure difference (psi)
- κ = conductivity ($mS.cm^{-1}$)

Results and Discussion

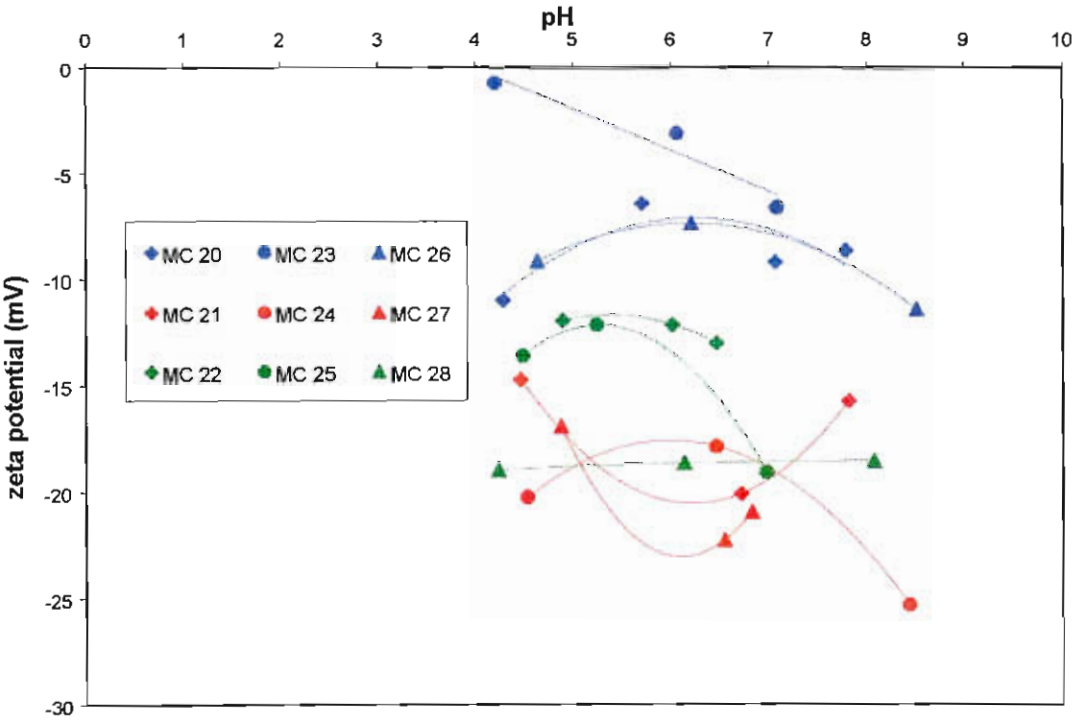

Figure 5 Zeta potential mesurements ([NaCl]=0.01M and [Na_2HPO_4]=0.0005M)

a) SPEES/PES to PS ratio ↗ (vertically) — polysulfone (MC 20-23-26) less negative; MC 21-24-27 and MC 22-25-28 same charge

b) % solid content ↗ (horizontally) — no significant evolution

ADSORPTION EXPERIMENTS

Methods and Material

First membrane water permeability was measured. In these experiments the organic matter was Suwannee River reference humic acid purchased from the International Humic Substances Society. A solution of this humic acid was placed in a glass jar with the membrane on the top, the skin side facing the interior of the jar. A Teflon sheet covered by one sheet of Parafilm and three sheets of aluminum foil was then placed on the membrane. The jar was closed and turned upside down, in order to contact the solution and membrane. The aluminum sheets were required to avoid any leakage from the jar. The jar was than placed on a gyrator shaker in the dark at 22 ± 2°C and it was shaken during the time of the experiment.

After the adsorption period the membrane was removed from the jar. The humic acid concentration of the supernatant was measured by UV absorption (254nm) and the percent of mass adsorbed was calculated by:

$$\%\ mass\ adsorbed = 100 * \frac{UV_o - UV_f}{UV_0} \tag{7}$$

with UV_0: UV measurement of feed solution before adsorption

UV_f: UV measurement of supernatant after adsorption

Water permeability was measured and compared with the value obtained with the clean membrane. The membrane resistances were calculated and the adsorptive resistance, i.e. the resistance due to the adsorbed humic acid is obtained by:

$$R_a = R_t - R_m \tag{8}$$

with R_a: membrane adsorptive resistance

R_t: total membrane resistance after adsorption

R_m: clean membrane resistance

R_a is plotted on the figures as a percent of the total resistance R_t.

Results and Discussion

Table 7 Interaction parameter (Km)

MC20 Km = 0.7	MC23 Km = 0.59	MC26 Km = 0.43
MC21 Km = 0.14	MC24 Km = 0.25	MC27 Km = 0.26
MC22 Km = 0.04	MC25 Km = 0.04	MC28 Km = 0.04

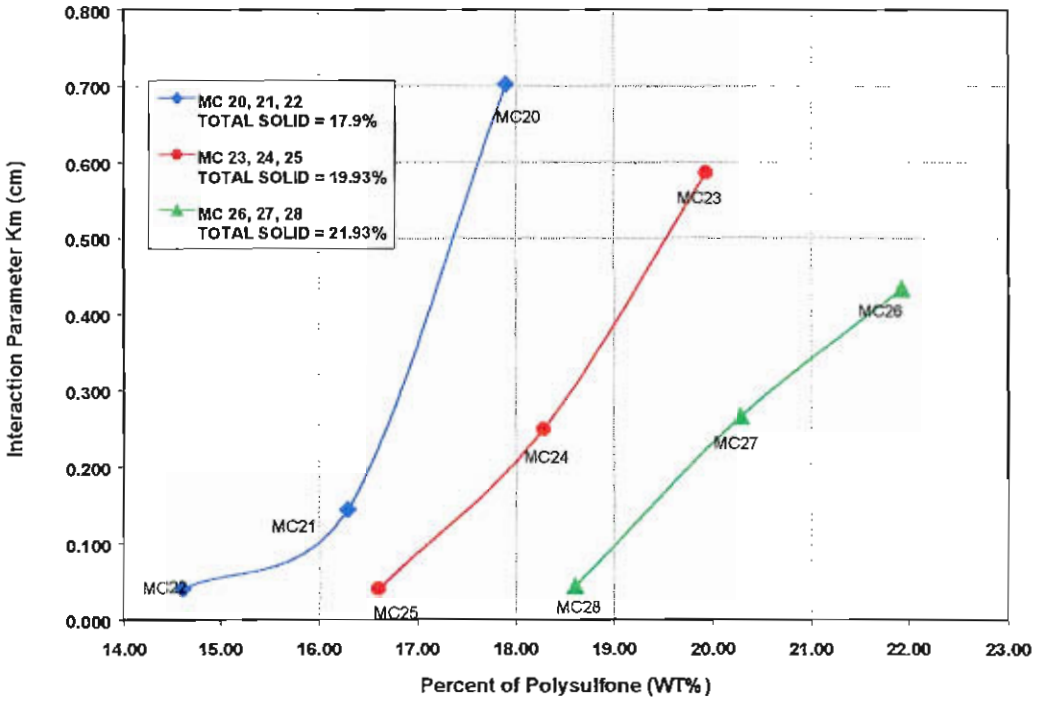

Figure 6 Effect of SPEES/PES content on interaction parameter

a) SPEES/PES to PS ratio ↗ adsorption ↘ (pore size ↘)

(vertically)

Results of adsorption kinetic experiments

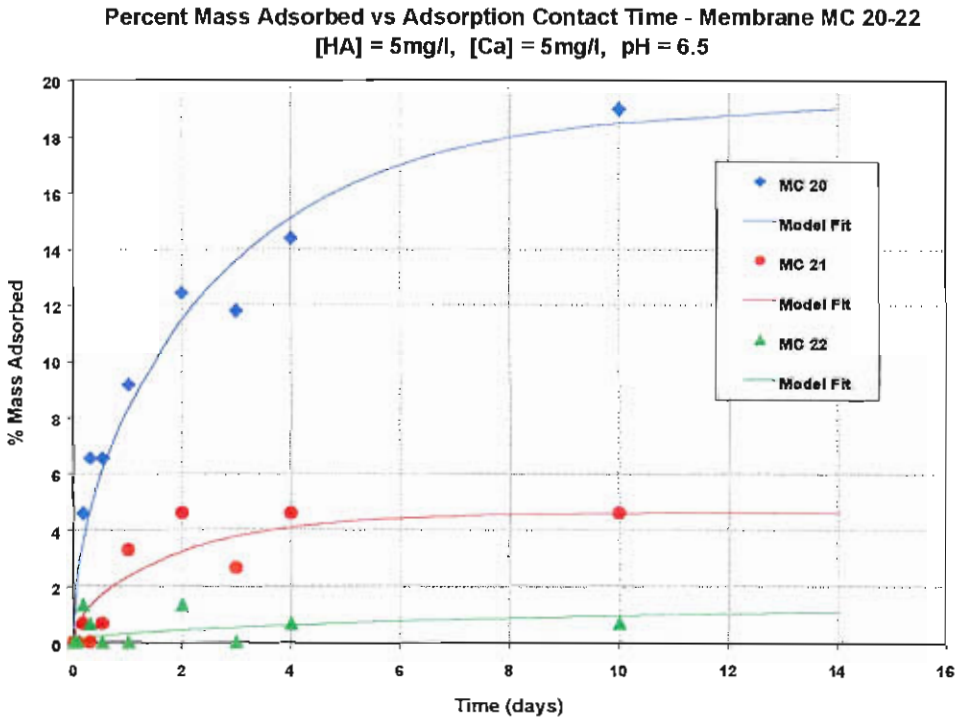

Figure 7-1 Model fitting of humic acid adsorption on MC 20-22 membranes

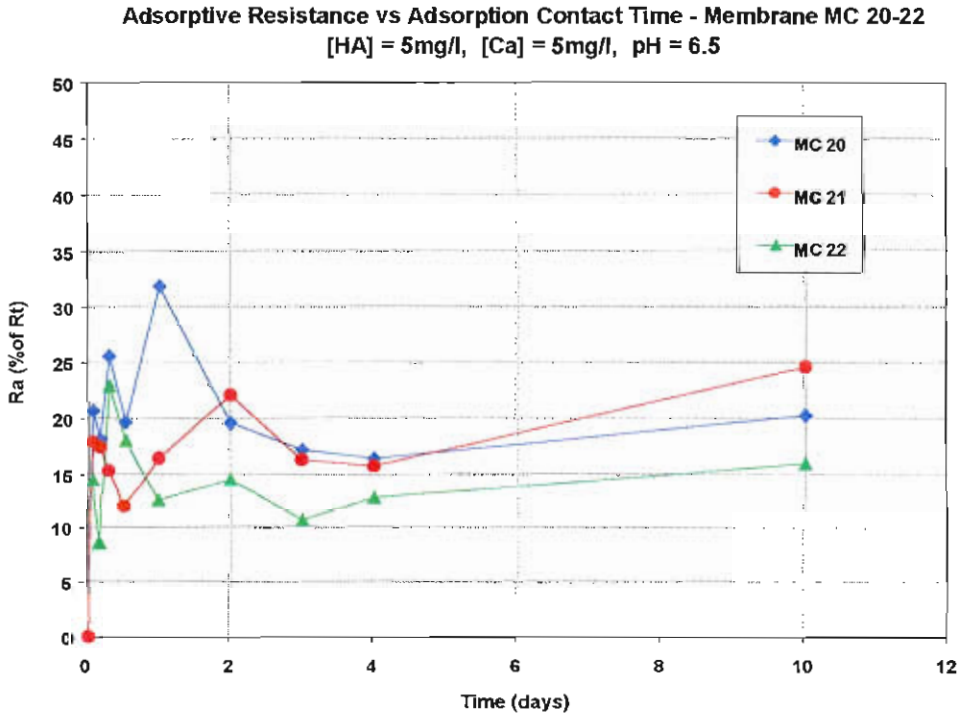

Figure 7-2 Adsorptive resistance of MC 20-22 membranes

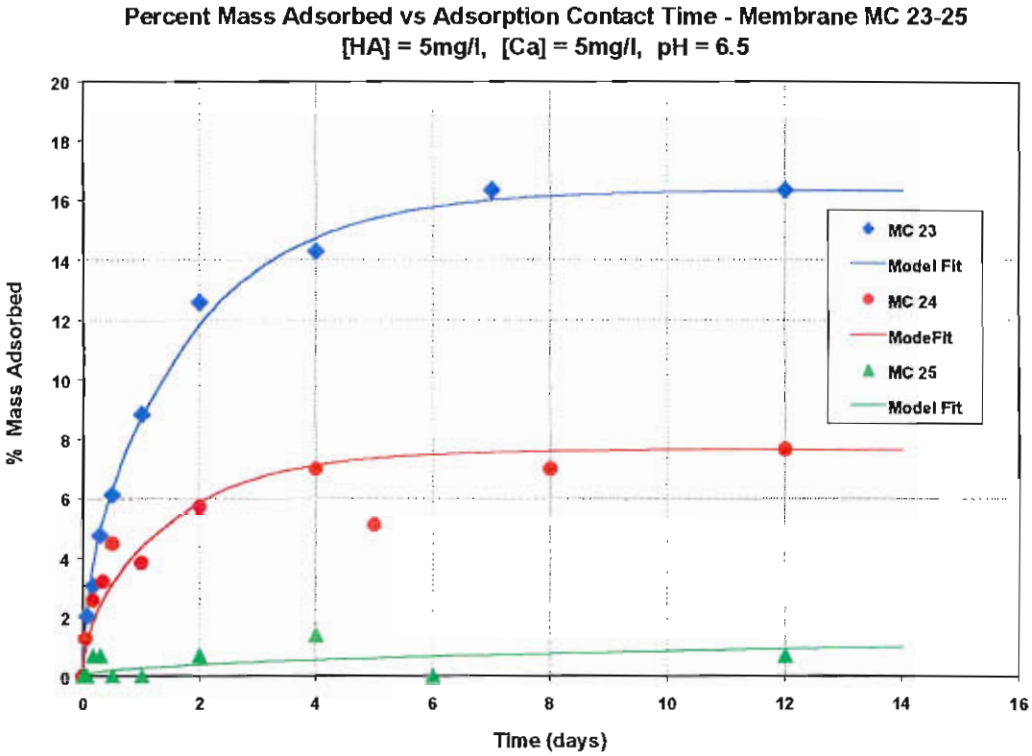

Figure 8-1 Model fitting of humic acid adsorption on MC 23-25 membranes

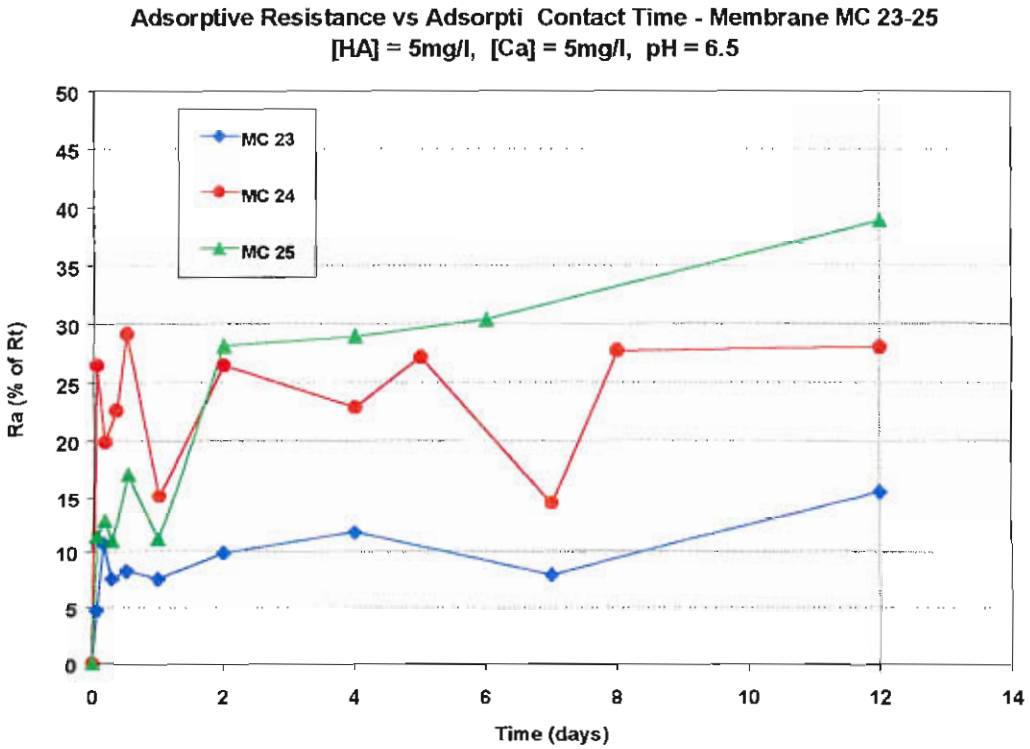

Figure 8-2 Adsorptive resistance of MC 23-25 membranes

CROSSFLOW FILTRATION EXPERIMENTS

Methods and Material

A channel-type crossflow UF/MF membrane filtration unit (Model SEPA CF System, Osmonics Inc., Minnetonka, MN) was used for crossflow filtration tests. A schematic diagram of the crossflow membrane filtration system is shown in Figure 2.12. A 12 liter glass jar served as a feed tank, and a large magnetic stirrer was used for mixing the feed tank. A Masterflex peristaltic pump (Model H-07017-00, Cole-Palmer Instruments Co., Chicago, IL) was used to drive the feed water to the membrane cell. The pump was driven by an adjustable speed gearmotor (Model Type 42DSBEPM-E1, Bodine Electric Company, Chicago, IL) and a permanent magnet control with analog interface board (Model Type FPM 856, Bodine Electric Company, Chicago, IL). Two pulsation dampeners (Model H-07596-20, Cole-Palmer Instruments Co., Chicago, IL) were installed serially close to the pump to reduce the pulsations created by the peristaltic pump. This provided almost pulsation-free feed to the channel-type crossflow UF/MF membrane filtration unit.

A general-purpose programming system called LabView was employed to control the system as well as to continuously log data onto a computer during filtration tests. All measurement instruments in the system generate analog signals, which could be logged

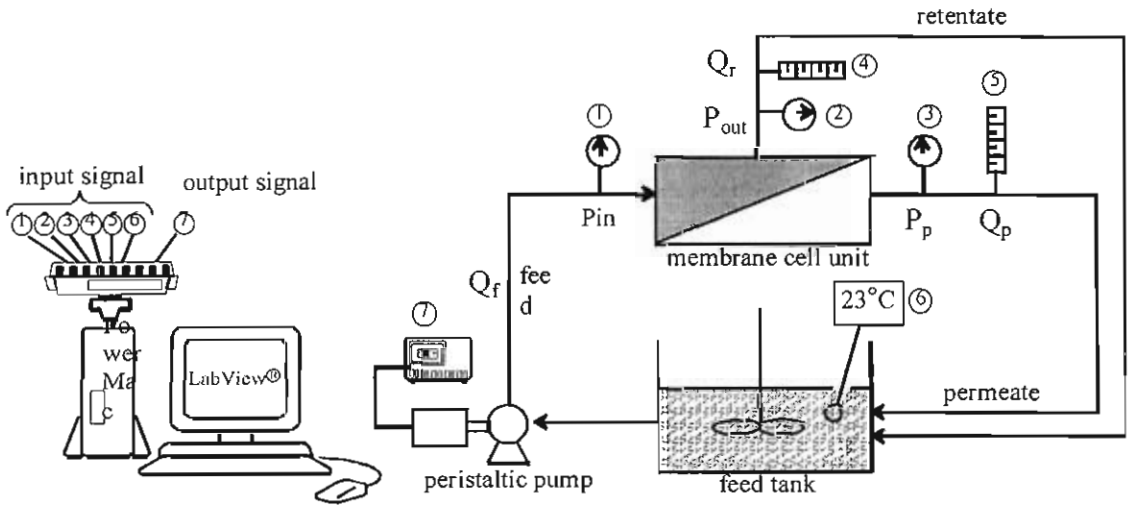

(a) data acquisition (b) membrane filtration

Figure 10 Schematic diagram of cross-flow filtration experimental set-up

onto a computer. Inlet, outlet, and permeate pressures were measured by digital pressure transmitters (Model PG-4/20, PSI-Tronix, Tulare, CA). Permeate and retentate flowrate were measured by 150 mm variable area flowmeters (Model H-03229-31 and H-03229-35, respectively, Cole-Palmer Instruments Co., Chicago, IL) equipped with flowmeter electronic conversion modules (Model H-03298 00, Cole-Palmer Instruments Co., Chicago, IL). Temperature was measured by an RTD probe (Model DD93560-02, Cole-Palmer Instruments Co., Chicago, IL), which was inserted into the permeate tube line. The temperature probe was connected to an RTD indicator-transmitter (Model H-08099-00, Cole-Palmer Instruments Co., Chicago, IL).

The membrane was cut and soaked in Milli-Q water for at least four hours, and the water was changed every half hour up to two hours. The membrane was then pre-compacted by filtration of Milli-Q water under the operating transmembrane pressure of 20 psi for 24 hours or until a constant flux was established. The variation of water flux with pressure was then measured to check the linearity.

Crossflow filtration tests were carried out in the constant transmembrane pressure mode. The humic acid solutions were filtered for 24 hours. Samples were taken from the feed, retentate and permeate during this period.

The cleaning procedure involved several steps. After humic acid filtration, the membrane was flushed for 5 minutes with clean water, in order to measure the resistance due to concentration polarization (surface wash). The membrane was then taken out of the cell and its surface was rinsed with clean water as thoroughly as possible. Then, the membrane was put back in the filtration cell with its skin side facing the permeate spacer, and the system was flushed with clean water for about 5 minutes under the same transmembrane pressure (backflush). After backflushing, the clean water flux was measured again under the same operating conditions. The last step of the cleaning procedure was to put the fouled membrane into 0.1 M NaOH solution for about 5 hours (chemical cleaning). The chemical cleaning was to remove most of the adsorbed matter in membrane pores and surface. After rinse the water permeability was measured again.

In order to prevent any bacterial growth in the system during down times, it was filled with 0.01 % NaN3 solution after each filtration test. With this procedure, we were able to get reproducible and coherent results of filtration with humic acid.

Results and Discussion

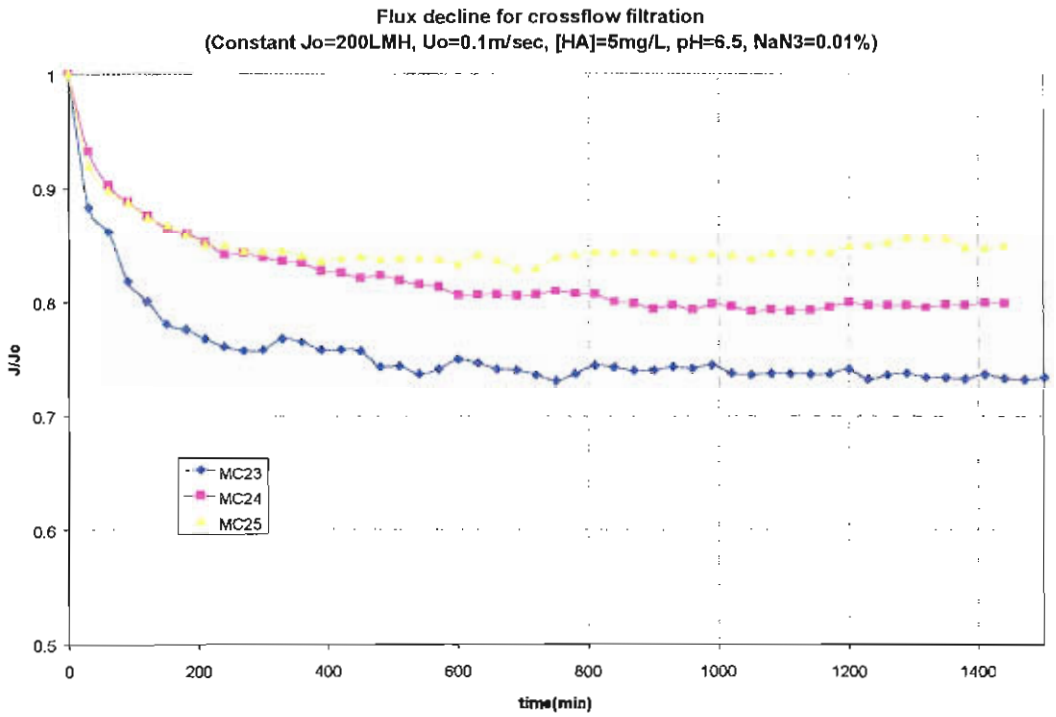

Figure 11-1 Effect of SPEES/PES contents on flux decline during crossflow filtration

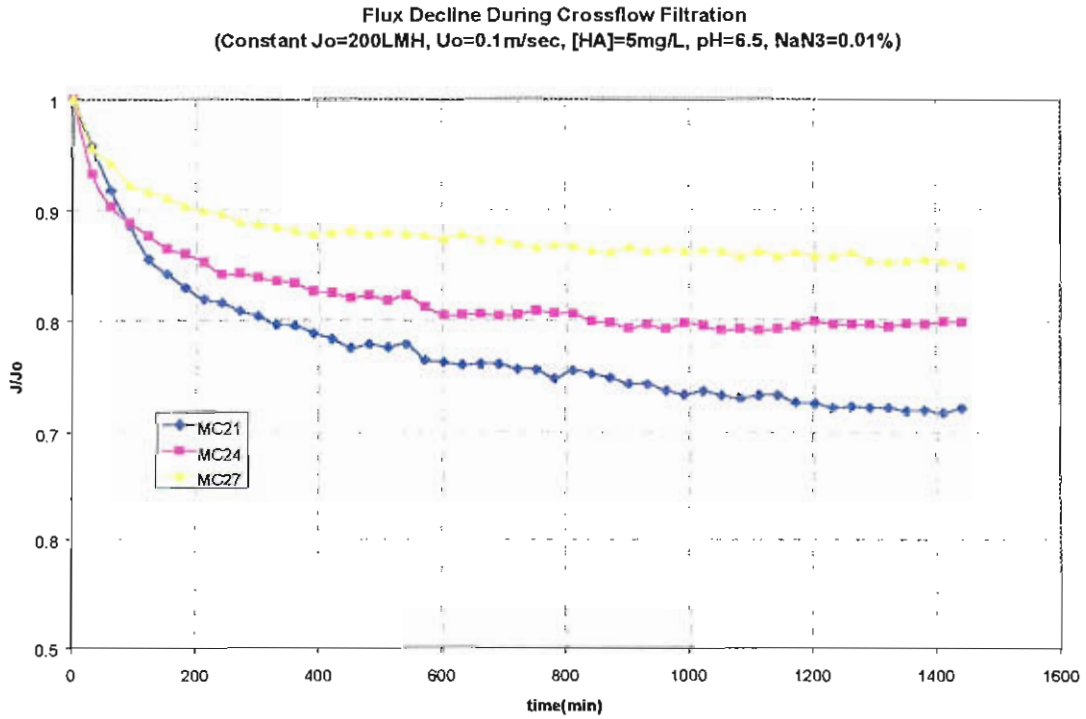

Figure 11-2 Effect of solid contents on flux decline during crossflow filtration

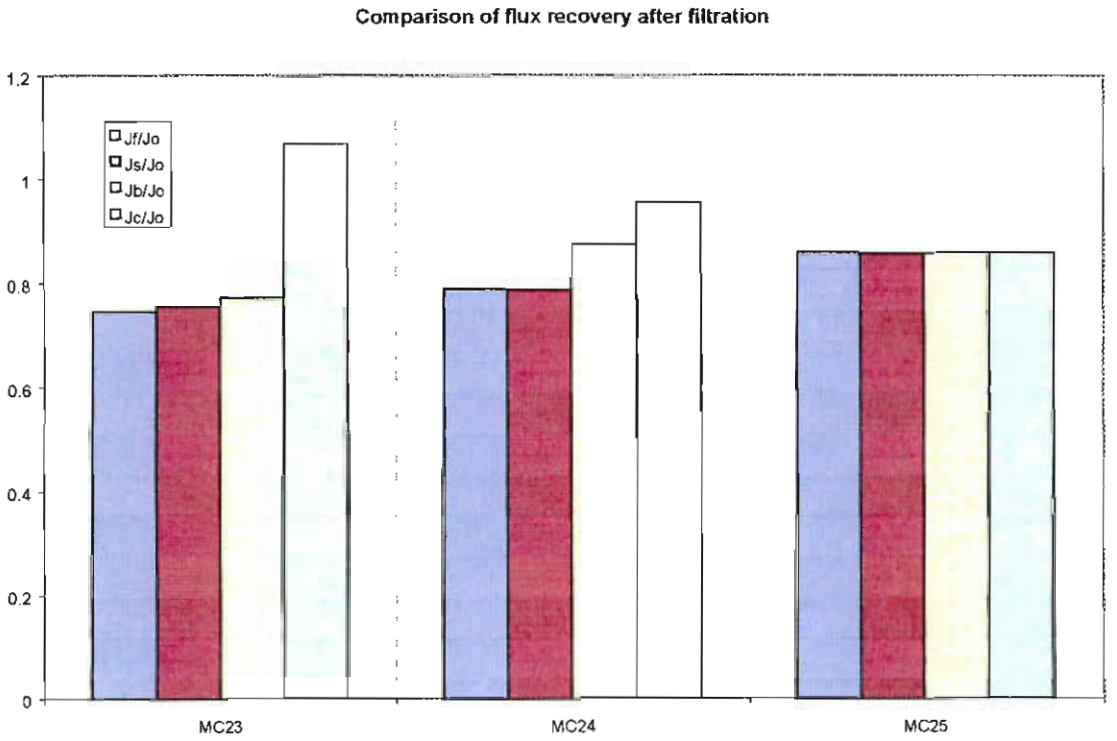

Figure 12-1 Effect of SPEES/PES contents on flux recovery

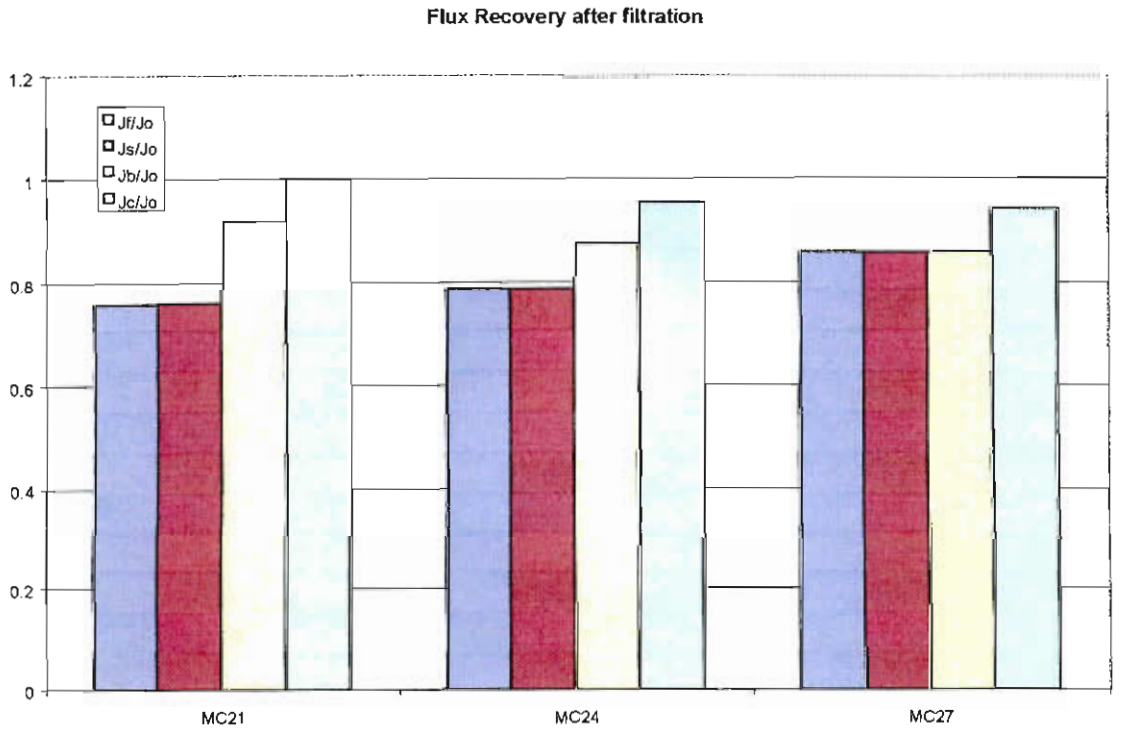

Figure 12-2 Effect of solid contents on flux recovery

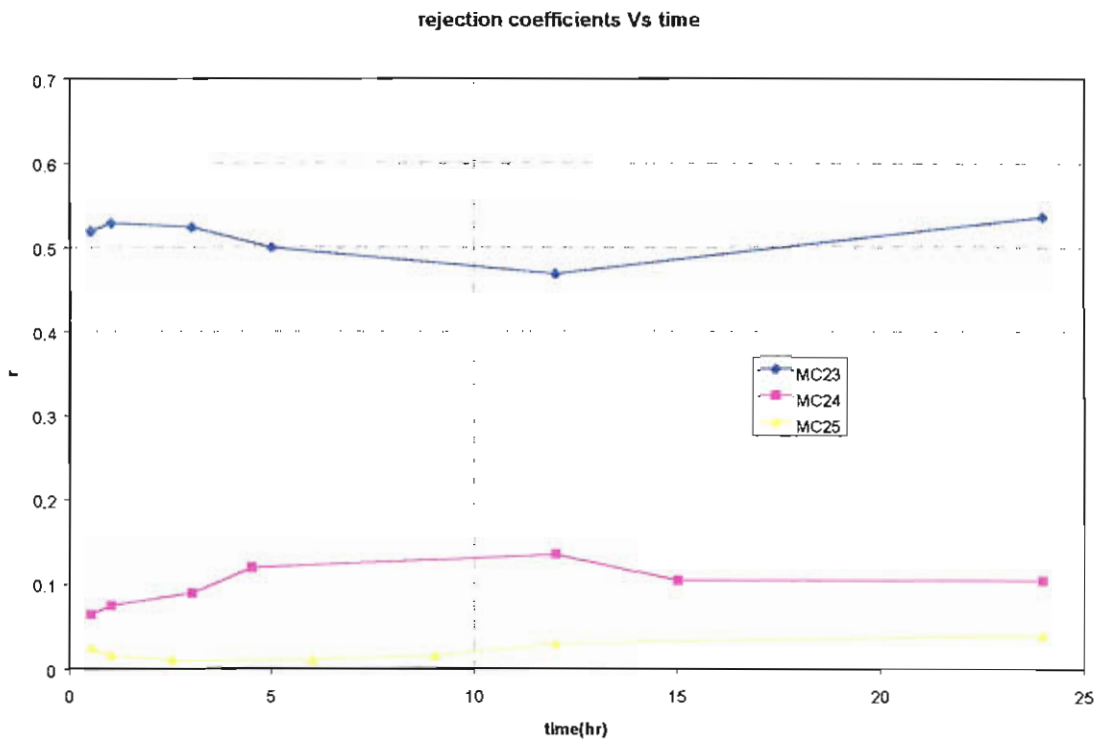

Figure 13-1 Effect of SPEES/PES contents on rejection

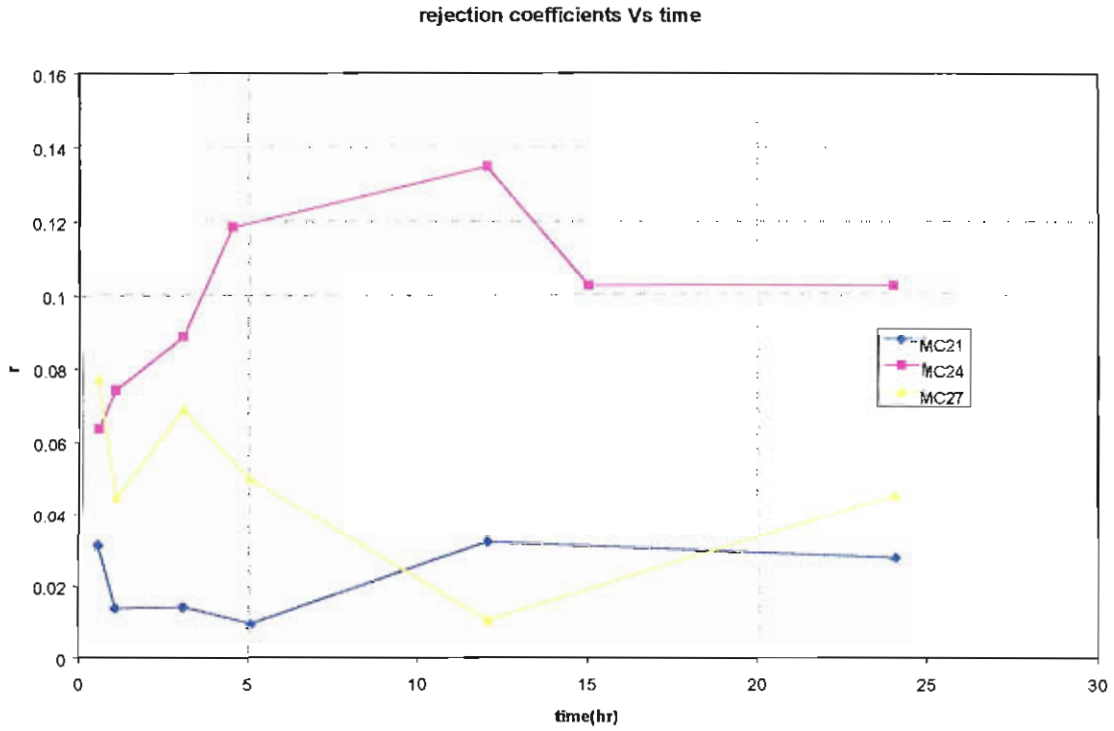

Figure 13-2 Effect of solid contents on rejection

BIBLIOGRAPHY

M. Oldani, G. Schock, *Characterization of ultrafiltration membranes by infrared spectroscopy, ESCA, and contact angle measurements*, Journal of Membrane Science, 43 (1989) 243.

D.T. Clark, W.J. Feast, *Application of ESCA to studies of structure and bonding in polymeric systems*, Rev. Macromol. Chem., C12(2) (1975) 191.

F.F. Stengaardh, *Characteristics and performance of new types of ultrafiltration membranes with chemically modified surfaces*, Desalination, 70 (1988) 207.

C.D. Wagner, W.M. Riggs, L.E. Davis, J.F. Moulder, G.E. Mullenberg, in *Handbook of X-ray photoelectron spectroscopy*, Perkin Elmer Corp., Physical Electronics Div., Eden Pririe, MN, (1979).

S. Lentsch, P. Aimar, J.L. Orozco, *Separation albumin-PEG: transmission of PEG through ultrafiltration membranes, Biotechnology and Bioengineering*, 41 (1993) 1039.

W.M. Deen, *Hindered transport of large molecules in liquid-filled pores*, AIChE Journal, 33 (1987) 1409.

M. Nyström, M. Lindström, E. Mathiasson, *Streaming potential as a tool in the characterization of ultrafiltration membranes*, Colloids Surfaces, 36 (1989), 297.

M. Nyström, H. Zhu, *Characterization of cleaning results using combined flux and streaming potential methods*, Journal of Membrane Science, 131 (1997) 195.

Appendix AFM images of SPEES/PES-PS membranes

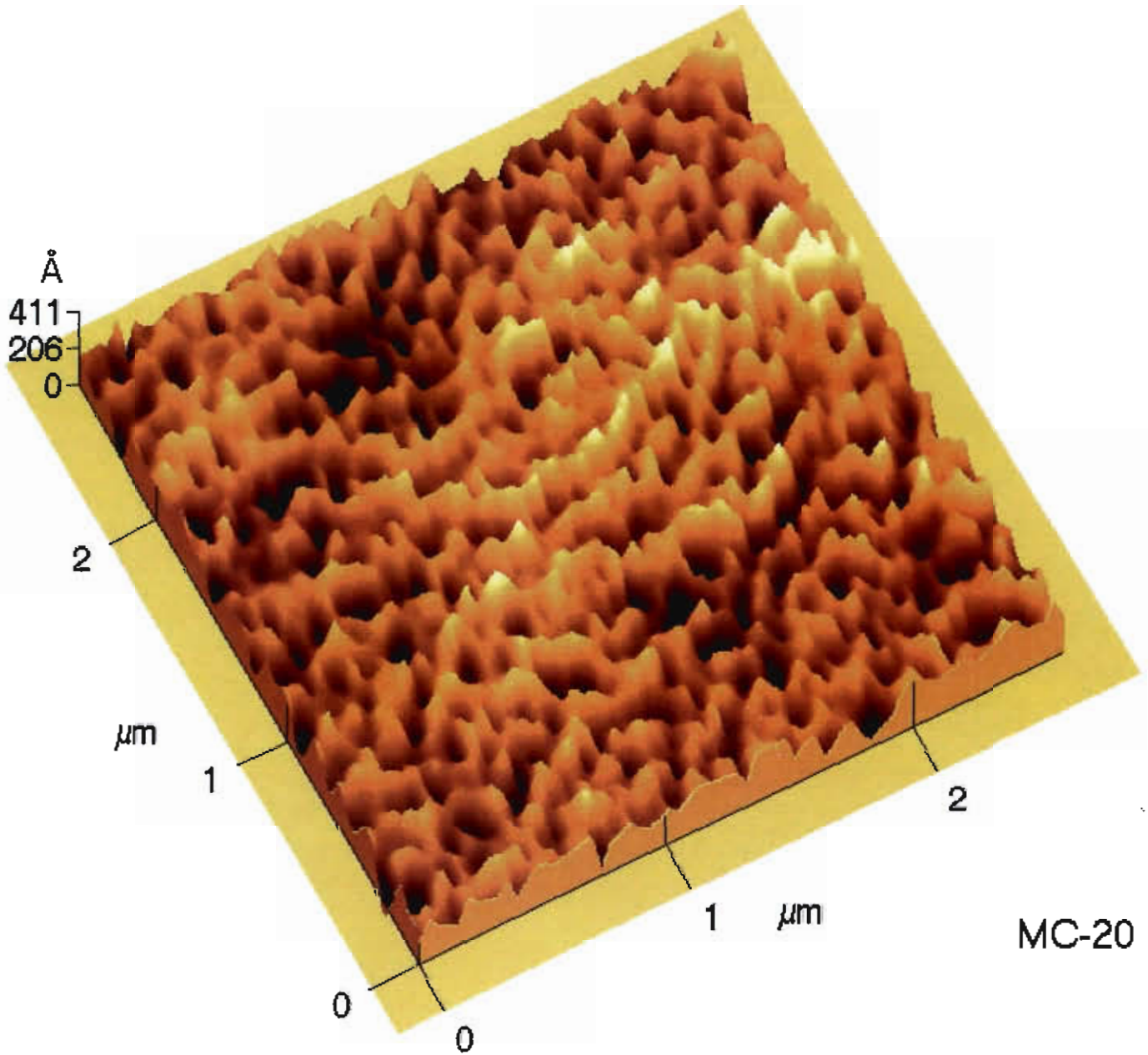
Å
411
206
0
2
µm
1
0
0
1
µm
2
MC-20

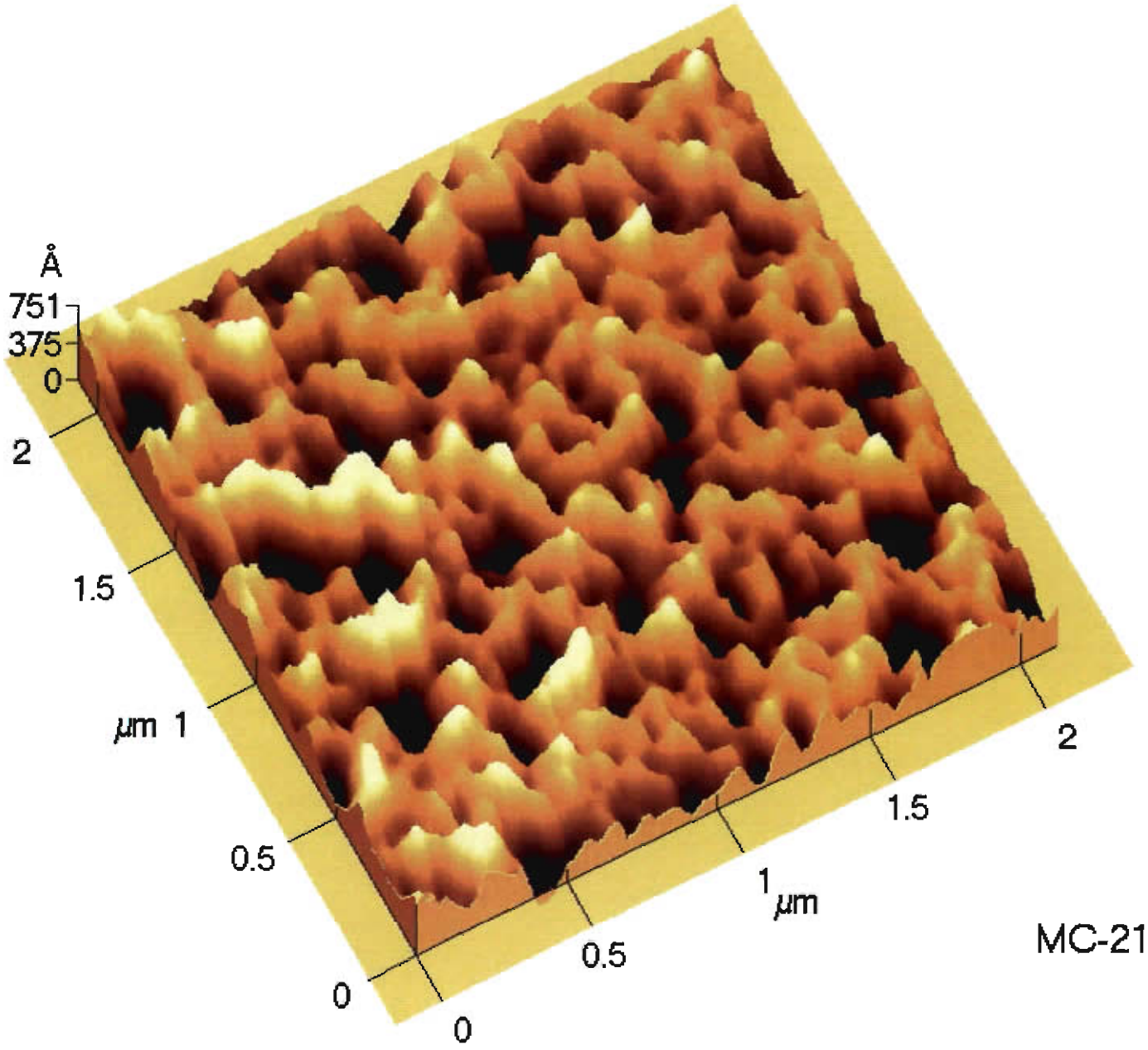
Å
751
375
0
2
1.5
µm 1
0.5
0
0
0.5
1
µm
1.5
2
MC-21

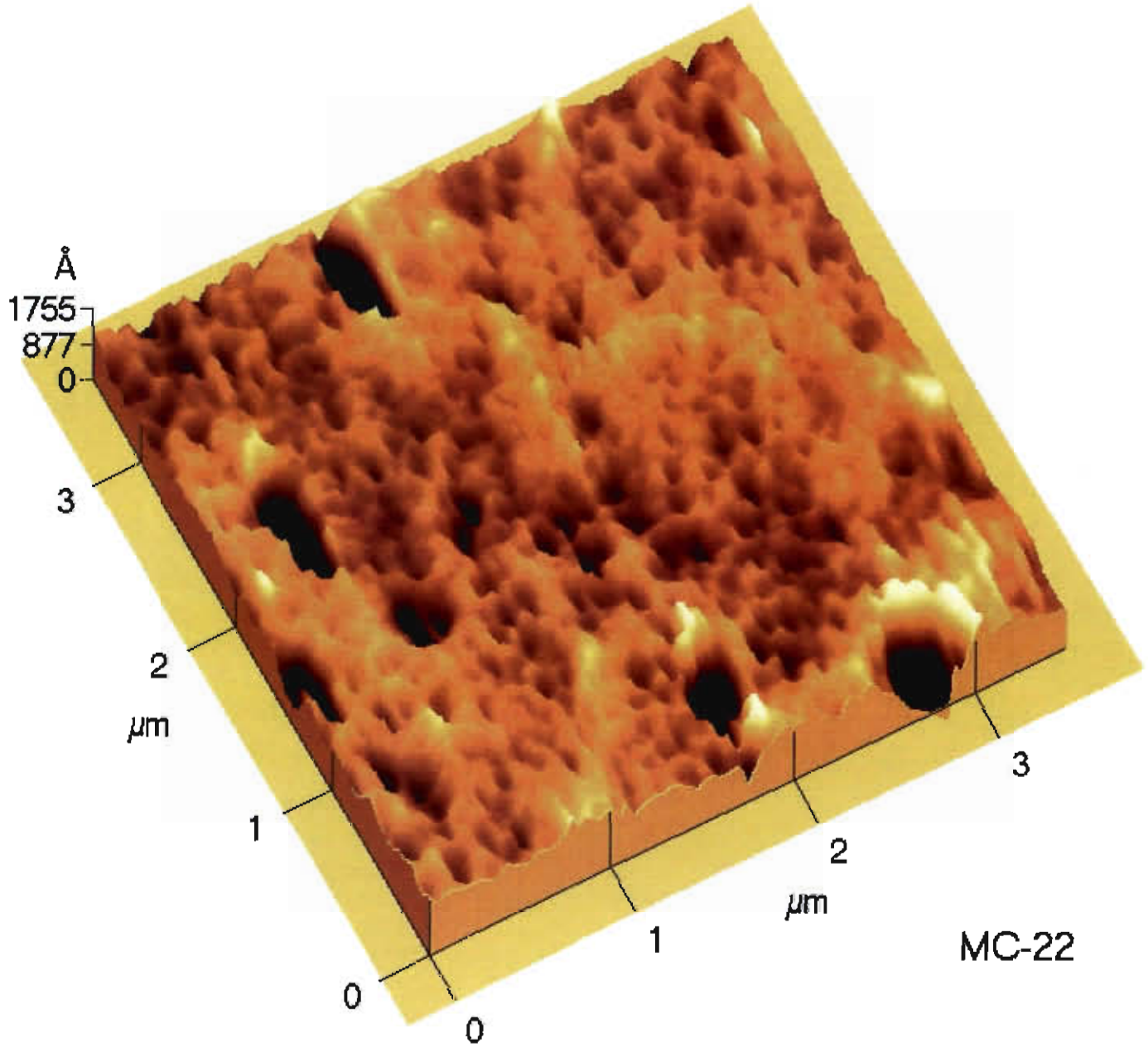
Å
1755
877
0
3
2
µm
1
0
0
1
2
µm
3
MC-22

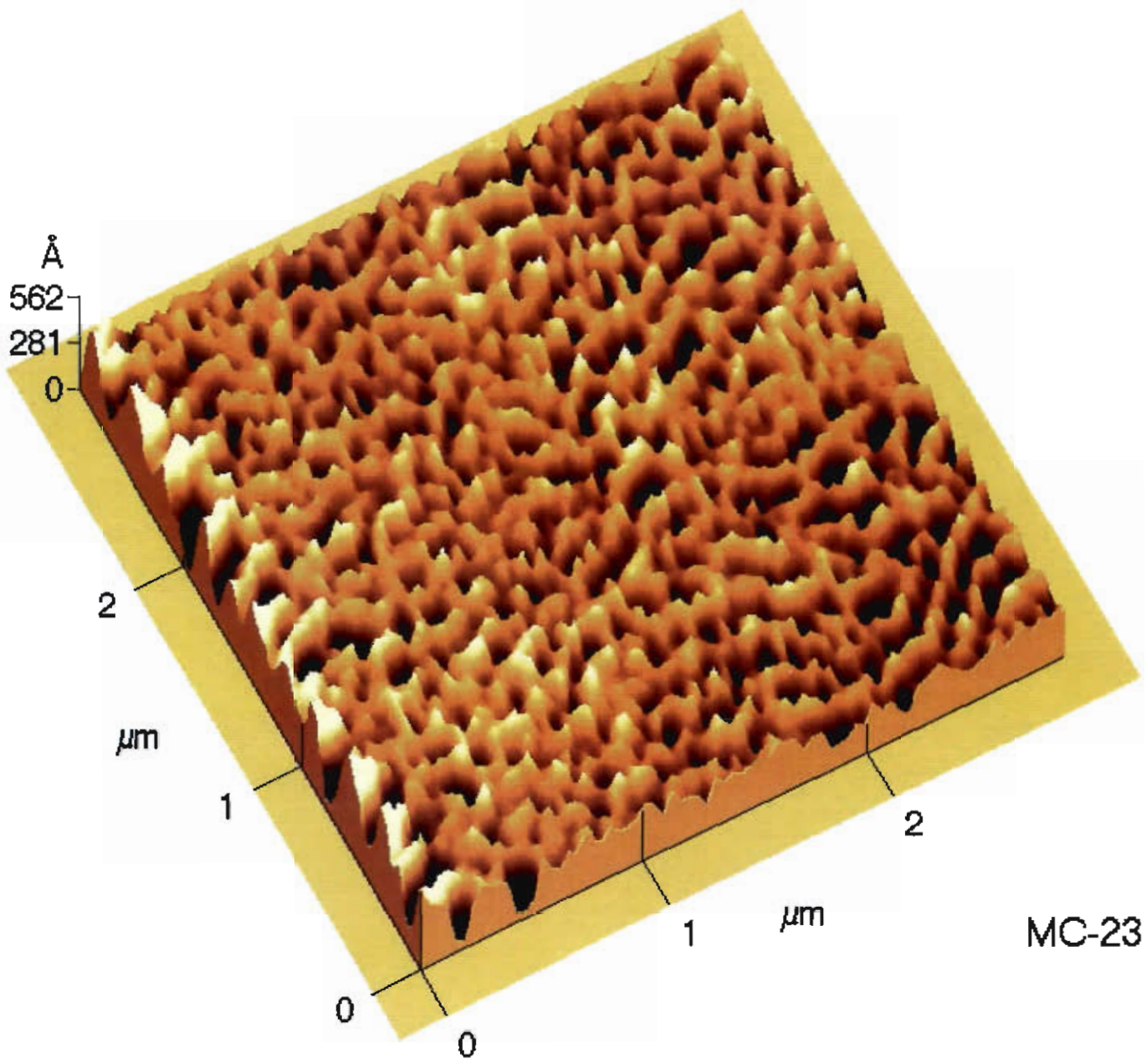
Å
562
281
0
2
μm
1
0
0
1
μm
2
MC-23

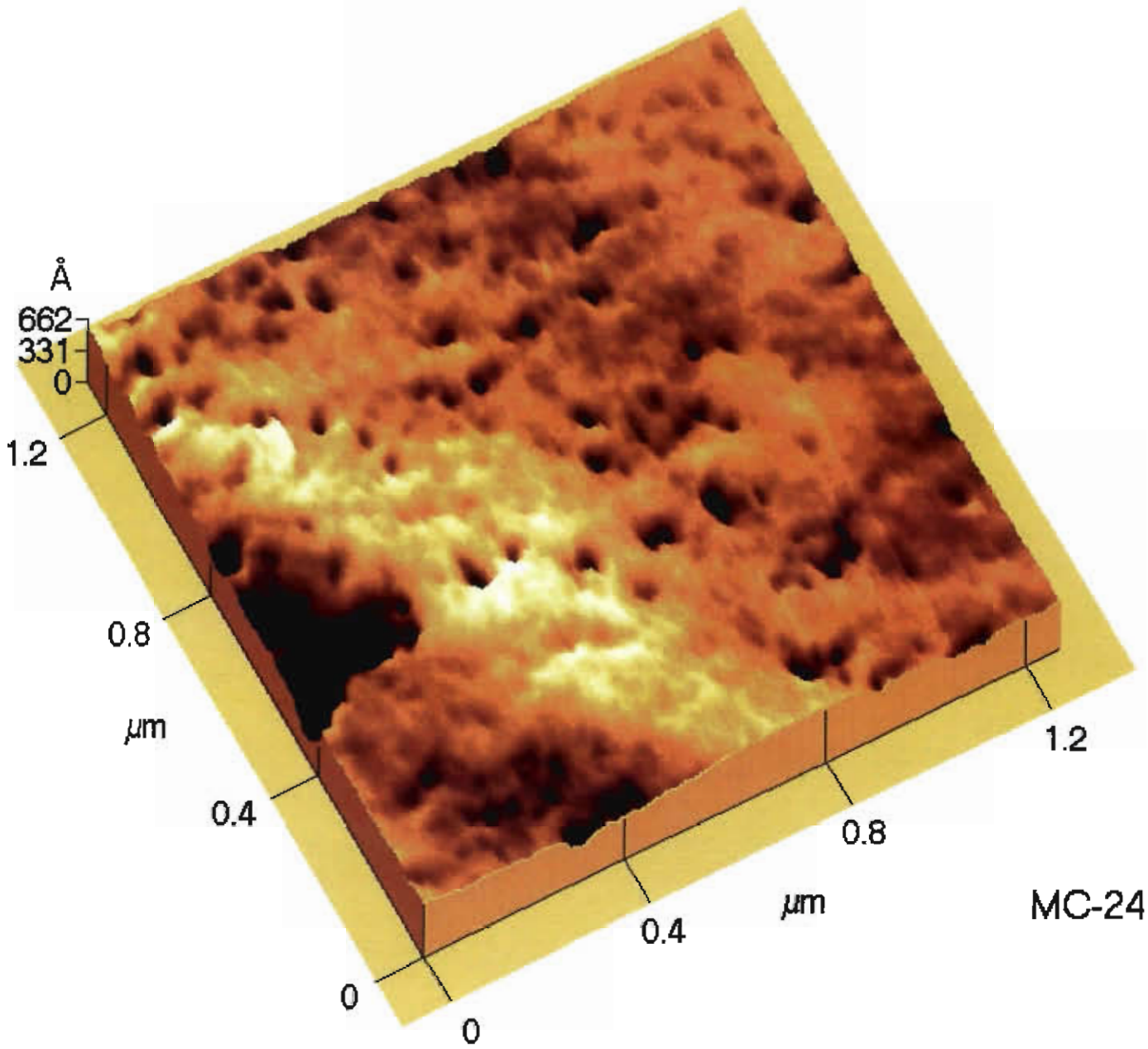
Å
662
331
0
1.2
0.8
µm
0.4
0
0
0.4
0.8
µm
1.2
MC-24

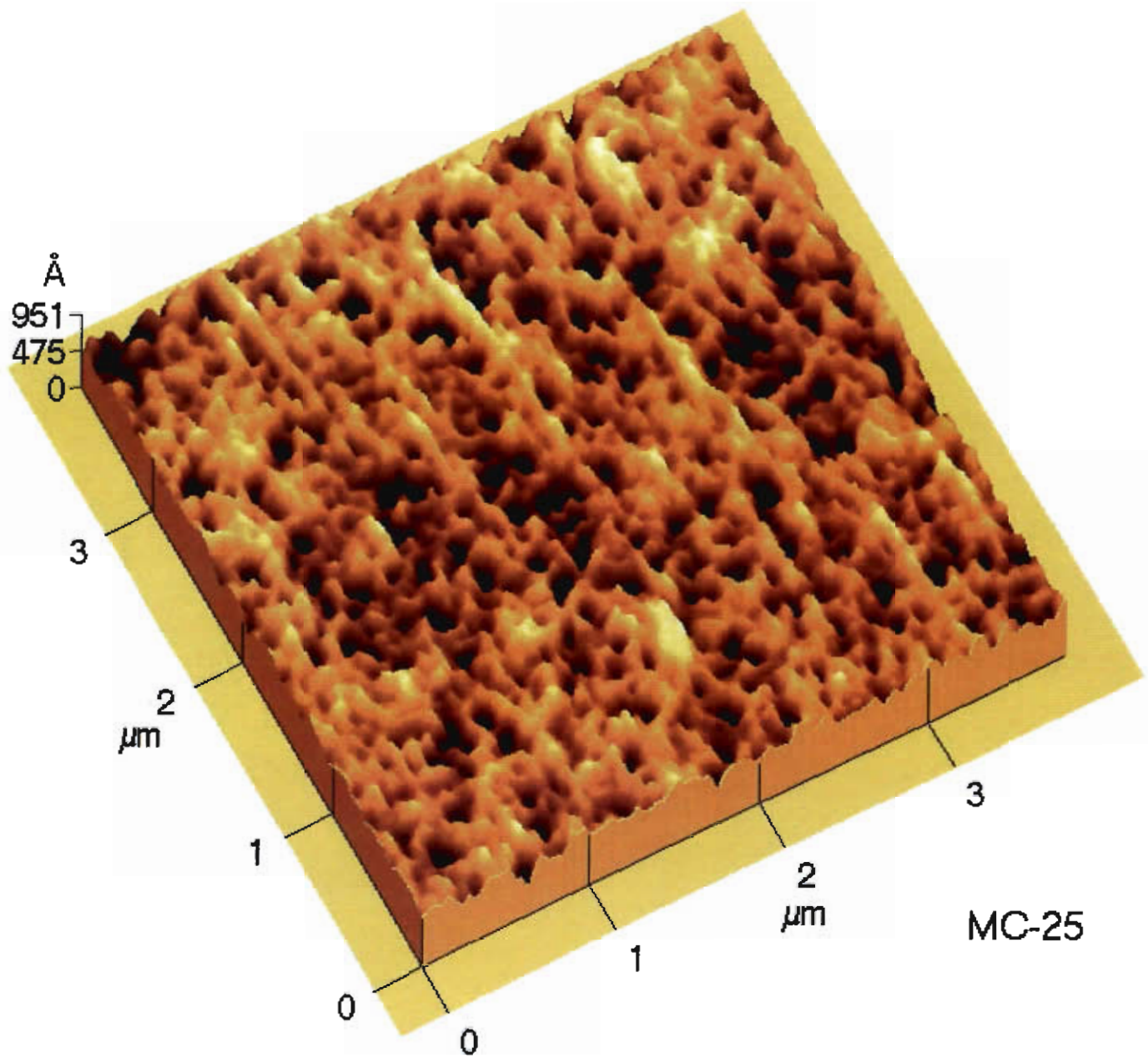
Å
951
475
0
3
2
µm
1
0
0
1
2
µm
3
MC-25

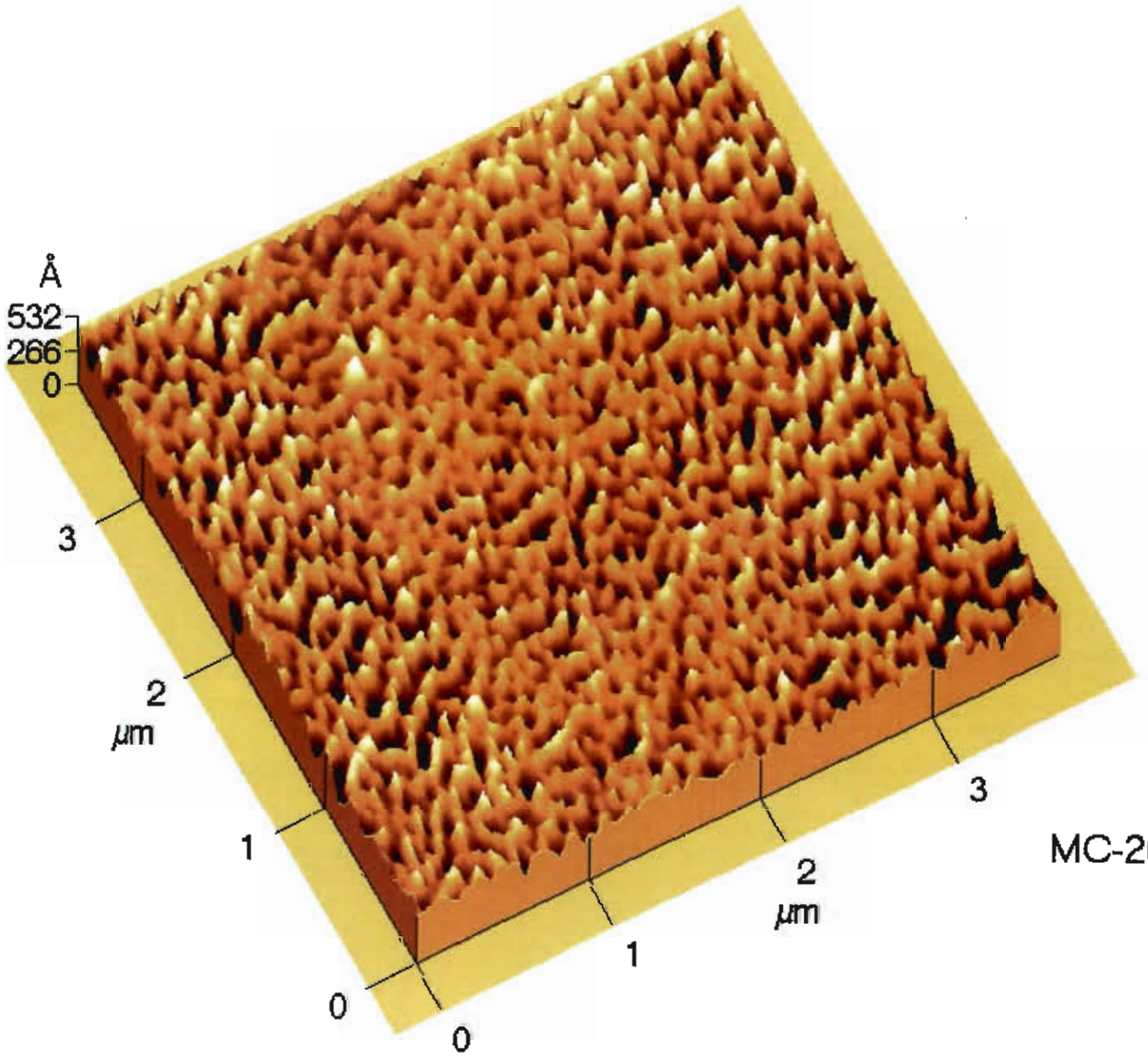

MC-26

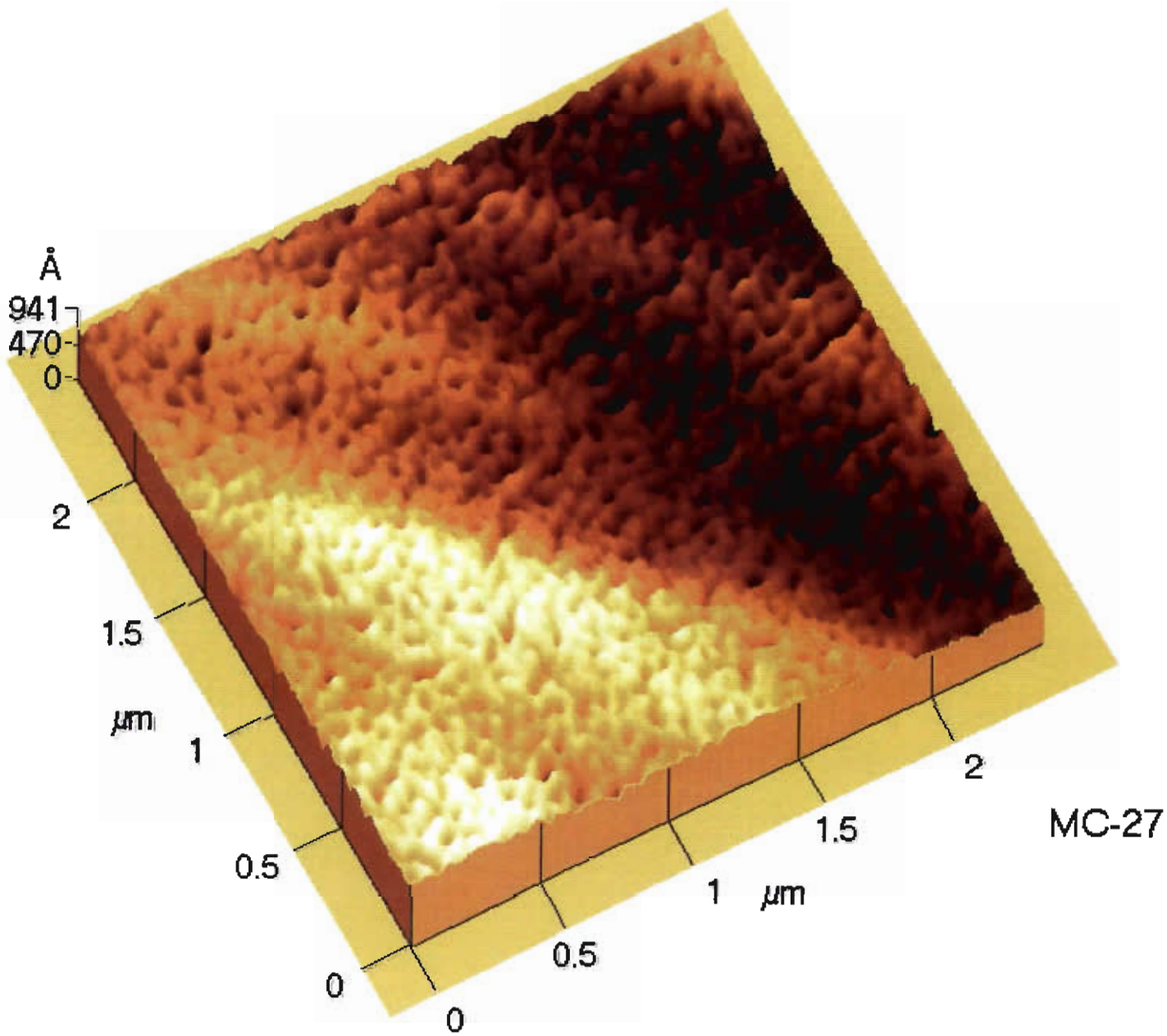
Å
941
470
0
2
1.5
µm
1
0.5
0
0
0.5
1
µm
1.5
2
MC-27

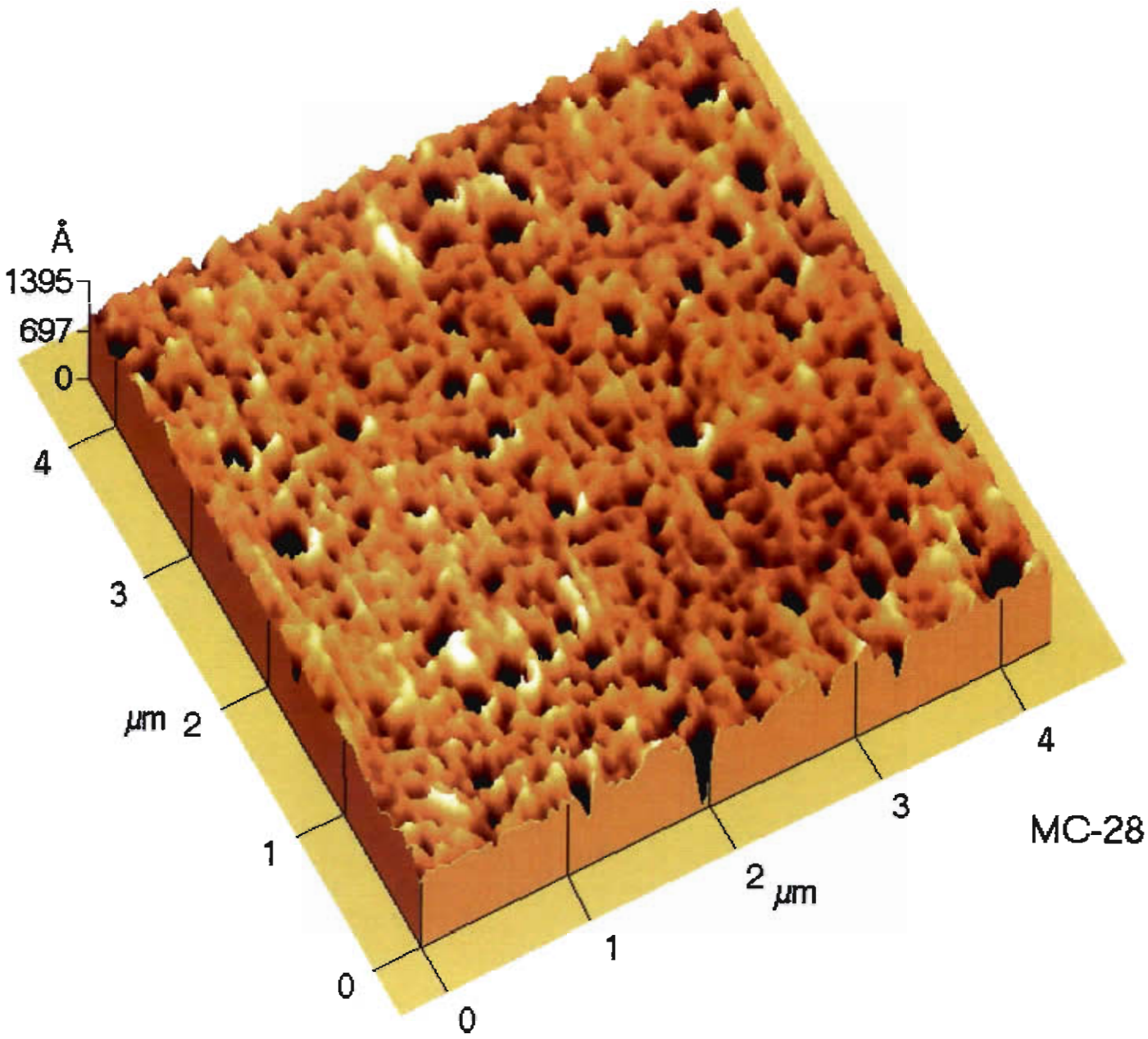
Å
1395
697
0
4
3
µm 2
1
0
0
1
2 µm
3
4
MC-28

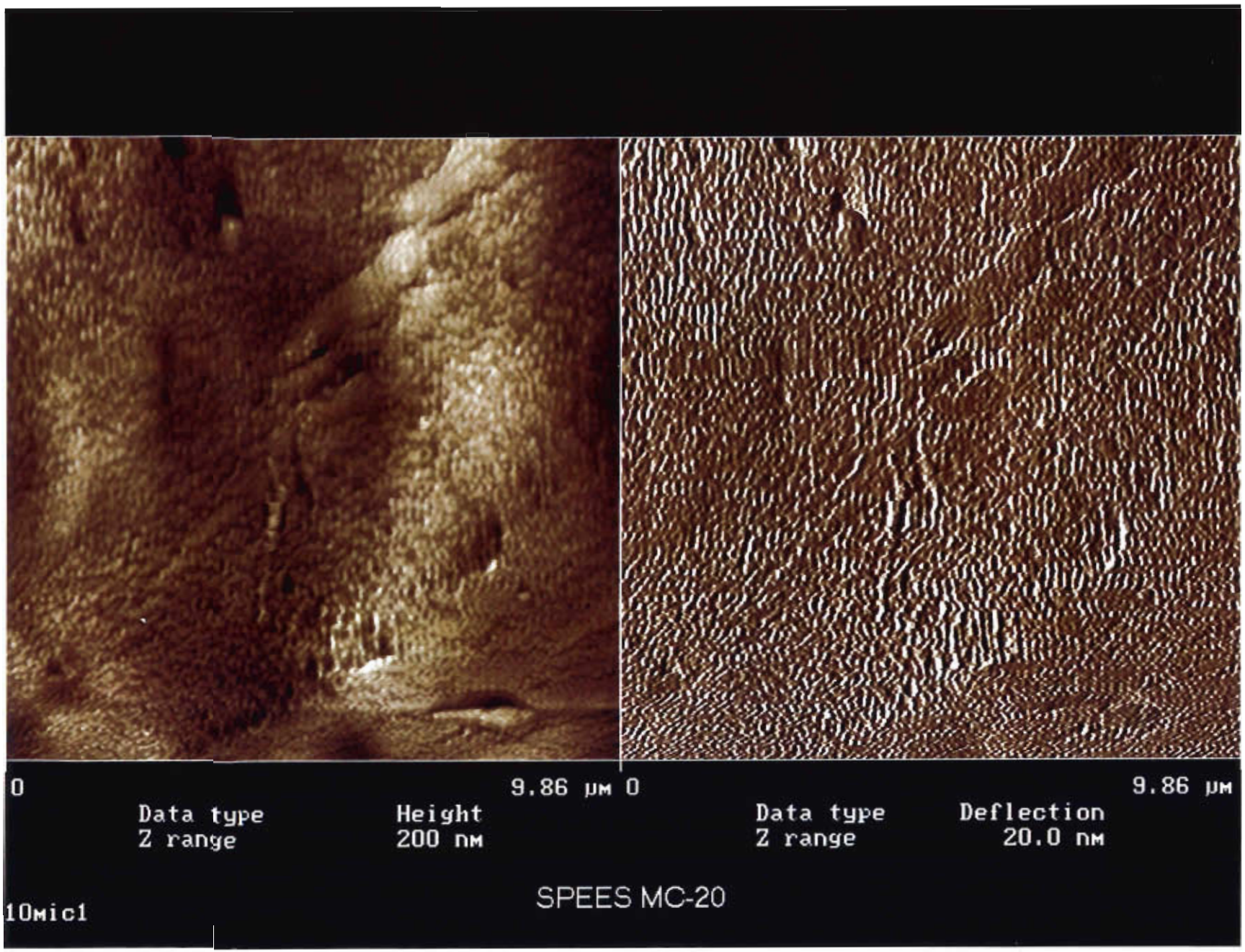
0
9.86 µm 0
9.86 µm
Data type
Z range
Height
200 nm
Data type
Z range
Deflection
20.0 nm
SPEES MC-20
10mic1

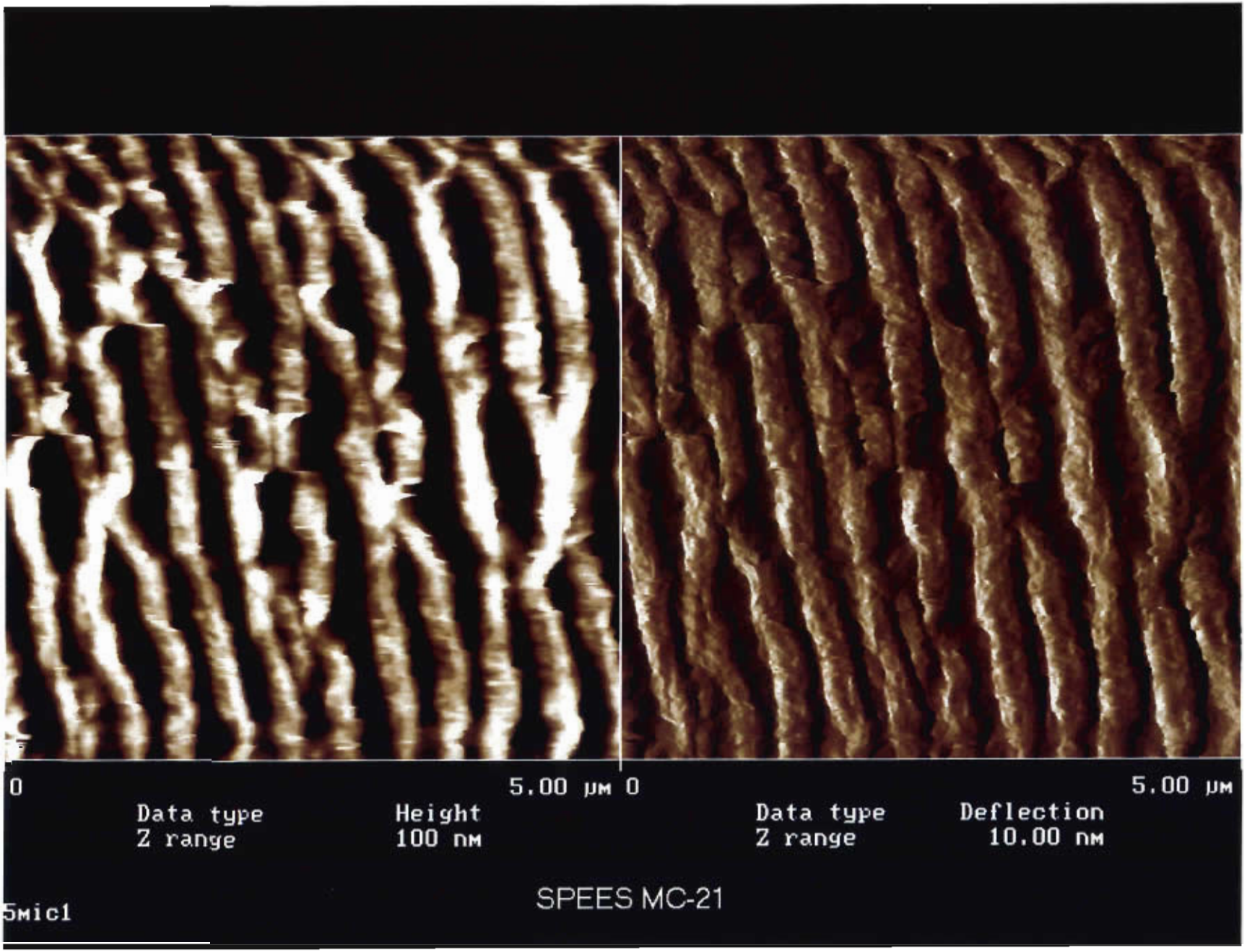
0
5.00 µм
Data type
Height
Z range
100 nм
0
5.00 µм
Data type
Deflection
Z range
10.00 nм
SPEES MC-21
5mic1

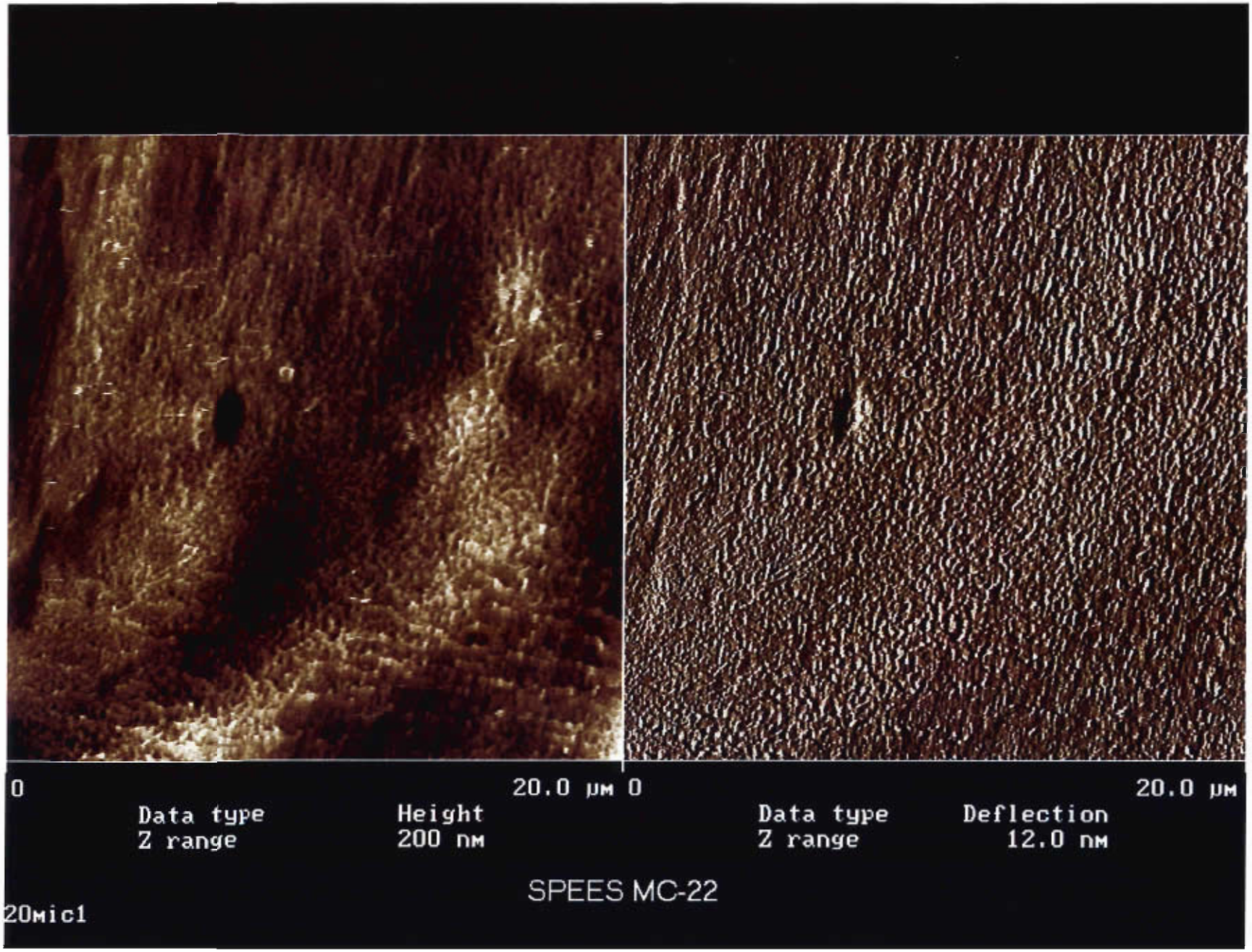
0
20.0 µm
Data type
Height
Z range
200 nm
0
20.0 µm
Data type
Deflection
Z range
12.0 nm
SPEES MC-22
20mic1

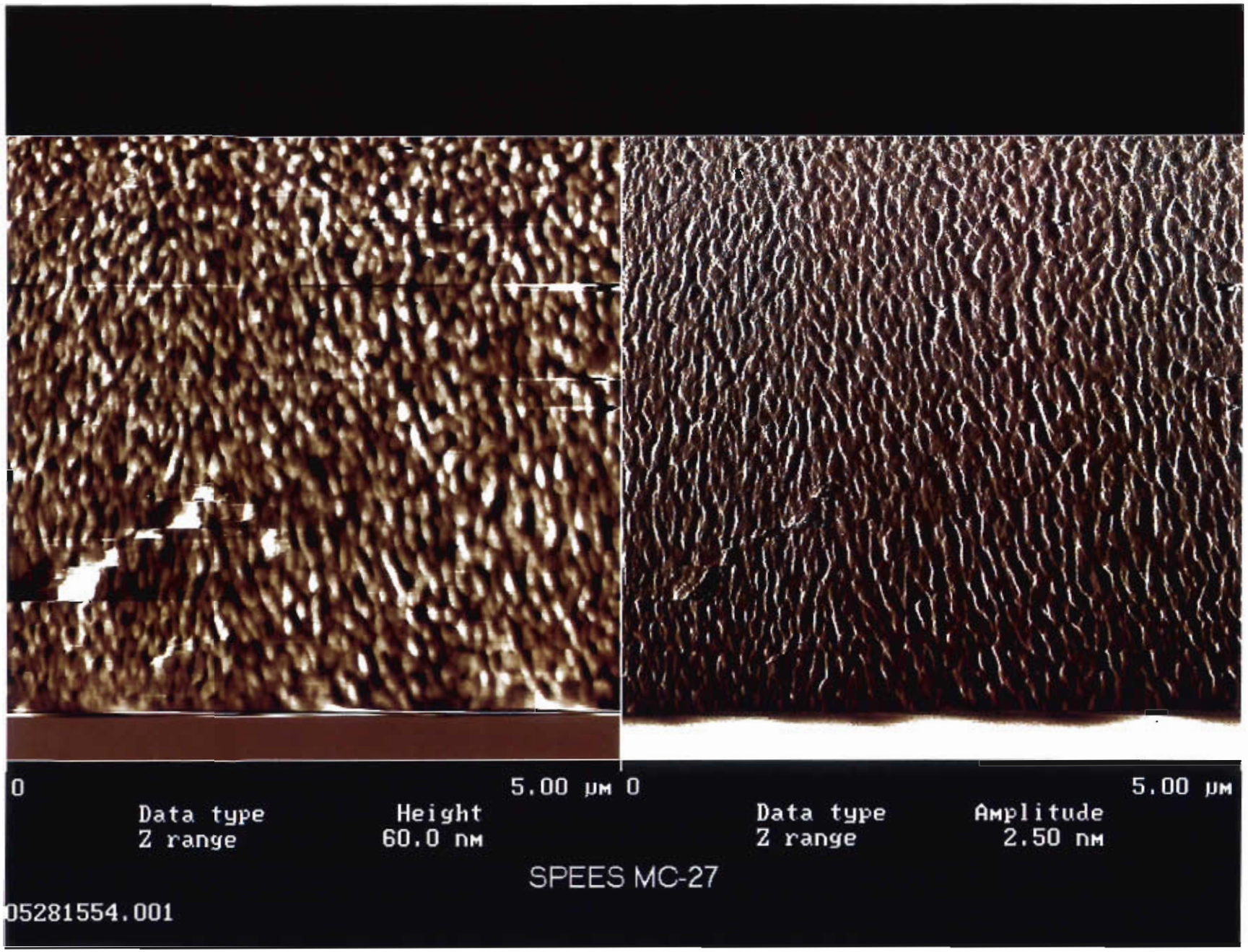
0
5.00 µm
Data type
Height
Z range
60.0 nm
0
5.00 µm
Data type
Amplitude
Z range
2.50 nm
SPEES MC-27
05281554.001

Part III

Results of PVP-PS Series Membranes

Development and Characterization of UF Membranes and Relation of Membrane Properties to Adsorptive Fouling

Subject: PVP-PS series membranes

Principal Investigator: Mark M. Clark

Research Assistants: Kerry Howe, Kwang-Soo Kim, Manish Kumar, Yingge Wang, and Yonghun Lee

JULY, 1999

EXECUTIVE SUMMARY

A series of nine membranes were cast from solutions of polyvinylpyrrolidone (PVP), polysulfone (PS), and N-methyl pyrrolidone (NMP) using the phase inversion process. PVP/PS ratio varied between 0 % and 39 %, while solids (PVP) to solvent (NMP) ratio varied between 18 % and 22 %. Membrane permeability varied from around 23 LMH/psi at the lowest solids content, to around 2 LMH/psi at the highest solids content. There was also a slight increase in permeability with increasing PVP/PS ratio.

Polyethylene glycol (PEG) retention experiments indicated a significant decrease in molecular weight cutoff (MWCO) with increasing solids content, while MWCO increased significantly with increasing PVP/PS ratio. Overall, for the series of 9 membranes, MWCO varied from a low of 2,800 Da (high solids content, PVP/PS ratio = 0) to greater than 10,000 Da (low solids content, high PVP/PS ratio).

Captive bubble contact angle measurements did not indicate a large variation in contact angle with PVP/PS ratio, although contact angle did decrease somewhat with increasing solids content. The average contact angle for all membranes was 37 degrees. Zeta potential measurements indicated a decrease in negative charge with increasing PVP/PS ratio and decreasing pH. Atomic Force Microscopy (AFM) measurements were not able to detect pores in any of the membrane examined; roughness values were in the range of 4 to 48 nm on sample sizes of 20 μm x 20 μm. AFM measurements did suggest the existence of surface damage on certain membrane samples.

Membranes were contacted with humic acid in order to characterize the tendency of natural organic matter to adsorb to the membrane surface. No clear tendencies were found, although the membranes without PVP tended to experience lower adsorption of humic acid. Flux decline during dead end filtration was also studied. Overall, membrane performance tended to become better with increasing PVP/PS ratio. Results for chemical cleaning with NaOH did not show clear difference among the membranes. Rejection of humic acid by all membranes was quite impressive, approximately in the range of 80-95 %.

MEMBRANE CHARACTERIZATION

- Water permeability
- XPS analysis*: elemental composition of membrane surface*
- PolyEthyleneGlycol retention*: estimation of MWCO*
- Contact angle measurements*: hydrophobic/hydrophilic character*
- Streaming potential measurements*: measurement of membrane pore charge*
  evolution of pore charge with pH
- Atomic Force Microscopy*: visualization of membrane surface*

FOULING OF MEMBRANE BY HUMIC ACID

- Adsorption of humic acid without permeation*: interactions between membrane surface and humic acid*
- Stirred deadend filtration tests: *flux decline*

PVP/PS ULTRAFILTRATION MEMBRANES

CASTING PARAMETERS

Fabric: Texlon

Casting conditions: knife gap=7.0 mil, casting speed=20 ft/min, 5 C D.I. water

% solid content ↗

% PVP ↗

PVP HR-1 PVP : 0 % PS : 17.9 % NMP : 82.1 %	**PVP HR-4** PVP : 0 % PS : 19.93 % NMP : 80.07 %	**PVP HR-7** PVP : 0 % PS : 21.93 % NMP : 79.07 %
PVP HR-2 PVP : 2.5 % PS: 15.4 % NMP : 82.1 %	**PVP HR-5** PVP : 2.5 % PS : 17.43 % NMP : 80.07 %	**PVP HR-8** PVP : 2.5 % PS : 19.43 % NMP : 78.07 %
PVP HR-3 PVP : 5 % PS : 12.9 % NMP : 82.1 %	**PVP HR-6** PVP : 5 % PS : 14.93 % NMP : 80.07 %	**PVP HR-9** PVP : 5 % PS : 16.93 % NMP : 78.07 %

What we can expect?

a) PVP/PS ratio ↗ (vertically)
- charge density ↘
- hydrophilicity ↗
- water permeability constant

b) % solid content ↗ (horizontally)
- charge density constant
- hydrophilicity constant
- water permeability ↘

NON-CHARGED HYDROPHILIC BLEND MEMBRANE SERIES

PVP: Polyvinylpyrrolidone (non-charged/hydrophilic)

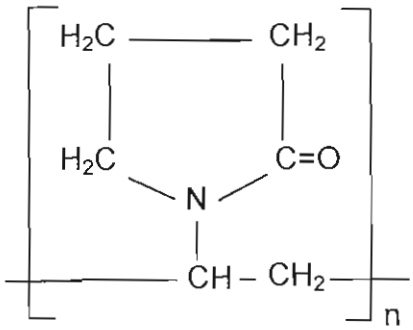

PS: Polysulfone

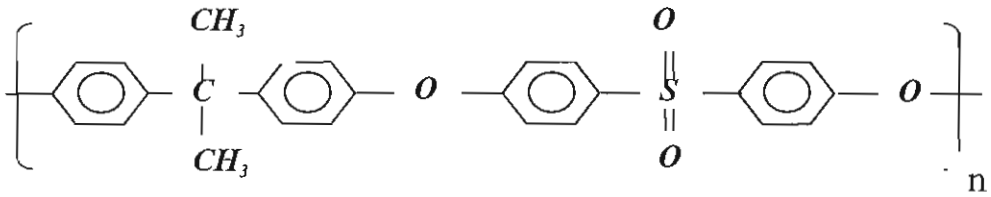

NMP (solvent): N-Methyl Pyrrolidone (C_5H_9NO)

WATER PERMEABILITY

Methods and Material

Filtration tests were performed using a 28.7cm^2 diameter UF cell with magnetic stirrer (Amicon, Minnetonka, MI). The pressure was applied via a compressed nitrogen tank, and was varied between 68.9 kPa and 206.7 kPa (10psi and 30psi).

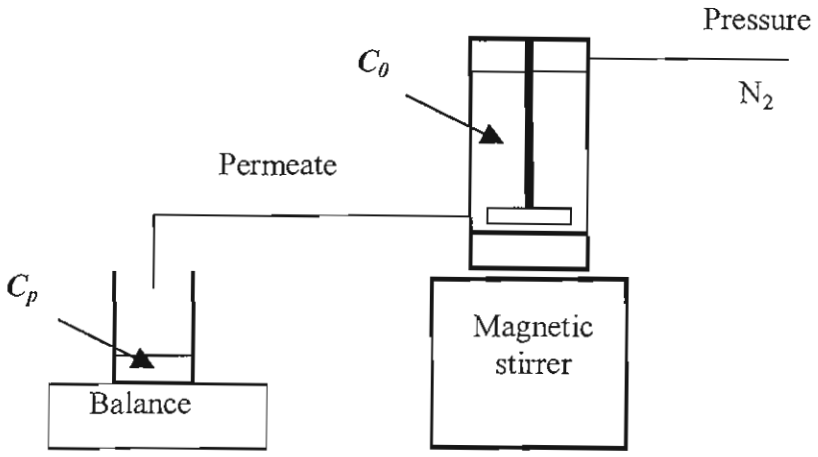

Figure 1 Amicon cell dead-end setup

The variation of water flux was plotted versus applied pressure and the slope represents the membrane water permeability symbolized by Lp.

Results and Summary

Table 1 Water permeability and thickness of membranes

PVP HR-1 Lp (LMH/psi) = 22.1 Total Thickness (μm) = 190.5	**PVP HR-4** Lp (LMH/psi) = 8.2 Total Thickness (μm) = 198.1	**PVP HR-7** Lp (LMH/psi) = 2.1 Total Thickness (μm) = 215.9
PVP HR-2 Lp (LMH/psi) = 21.4 Total Thickness (μm) = 210.8	**PVP HR-5** Lp (LMH/psi) = 13.4 Total Thickness (μm) = 223.5	**PVP HR-8** Lp (LMH/psi) = 6.9 Total Thickness (μm) = 236.2
PVP HR-3 Lp (LMH/psi) = 22.9 Total Thickness (μm) = 218.4	**PVP HR-6** Lp (LMH/psi) = 14.6 Total Thickness (μm) = 287.0	**PVP HR-9** Lp (LMH/psi) = 4.6 Total Thickness (μm) = 254.0

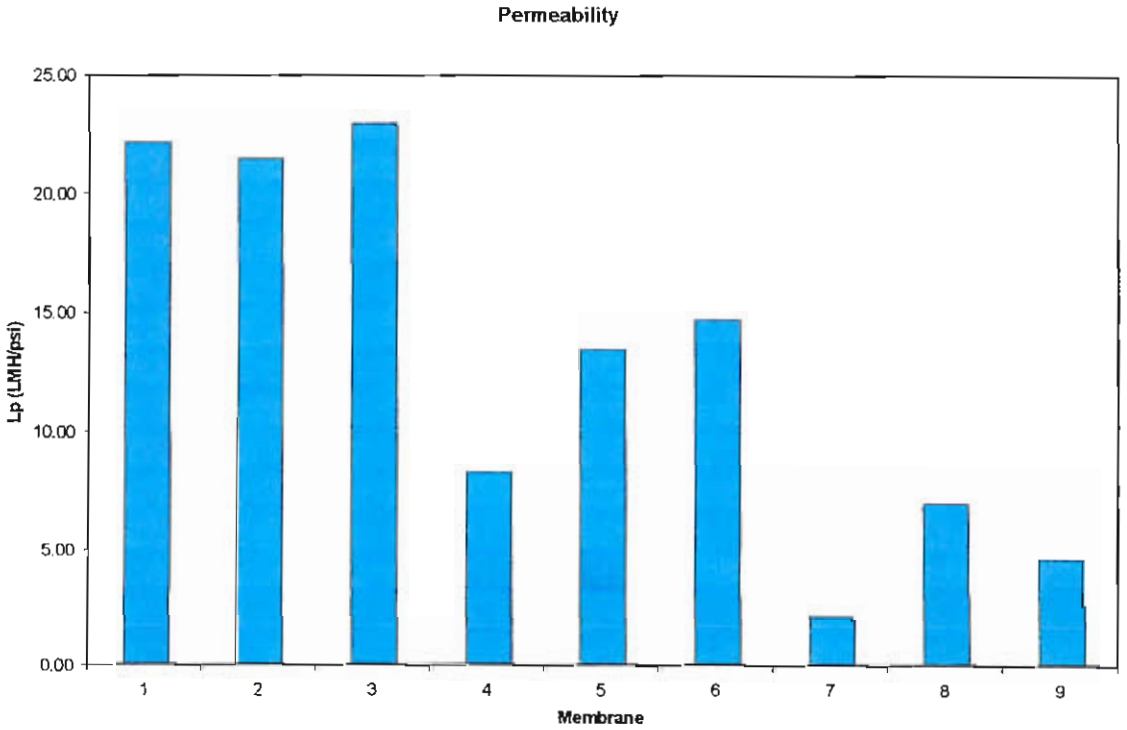

Figure 2 Specific water permeability

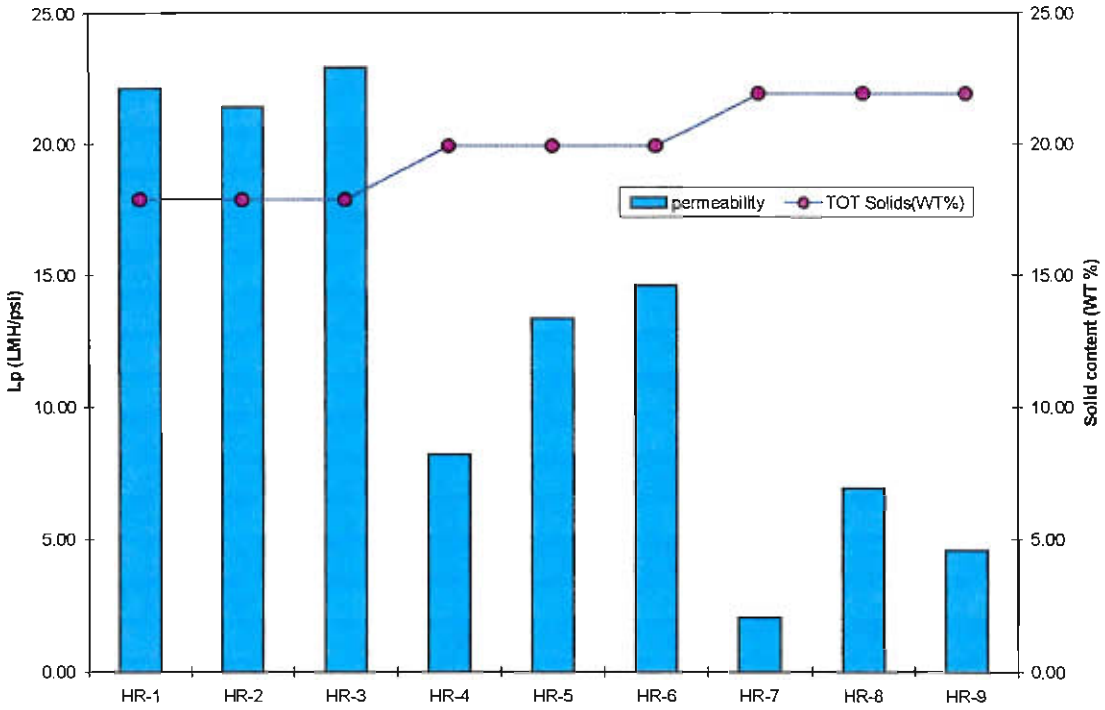

Figure 3 Effect of solid content on water permeability

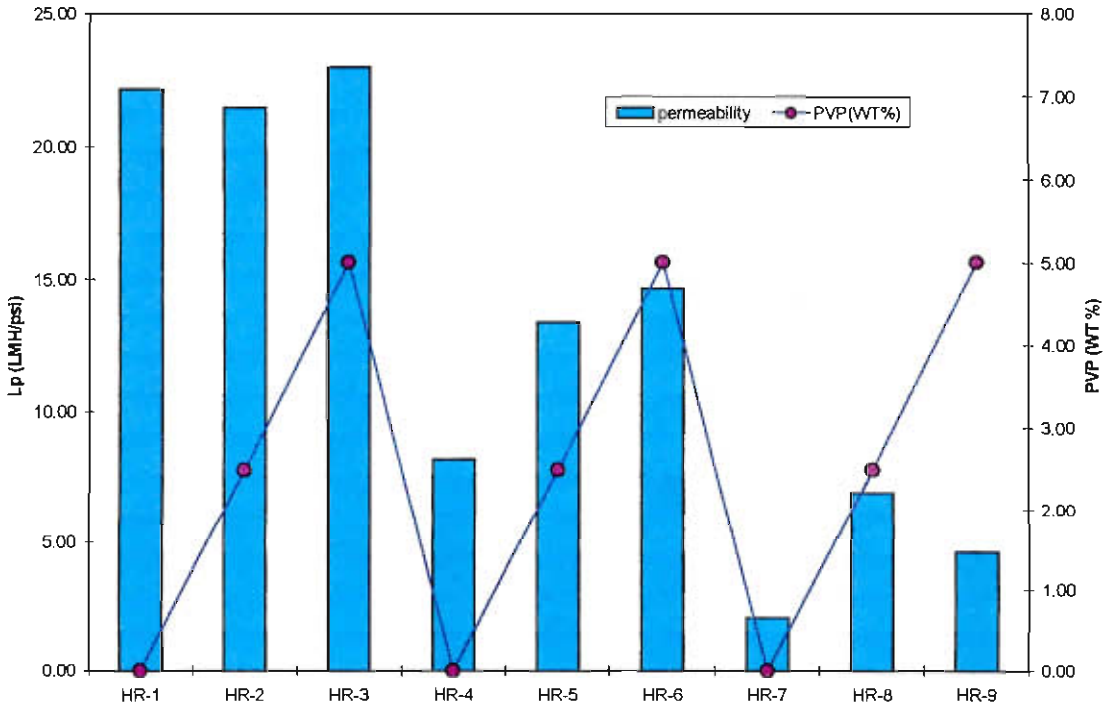

Figure 4 Effect of PVP content on water permeability

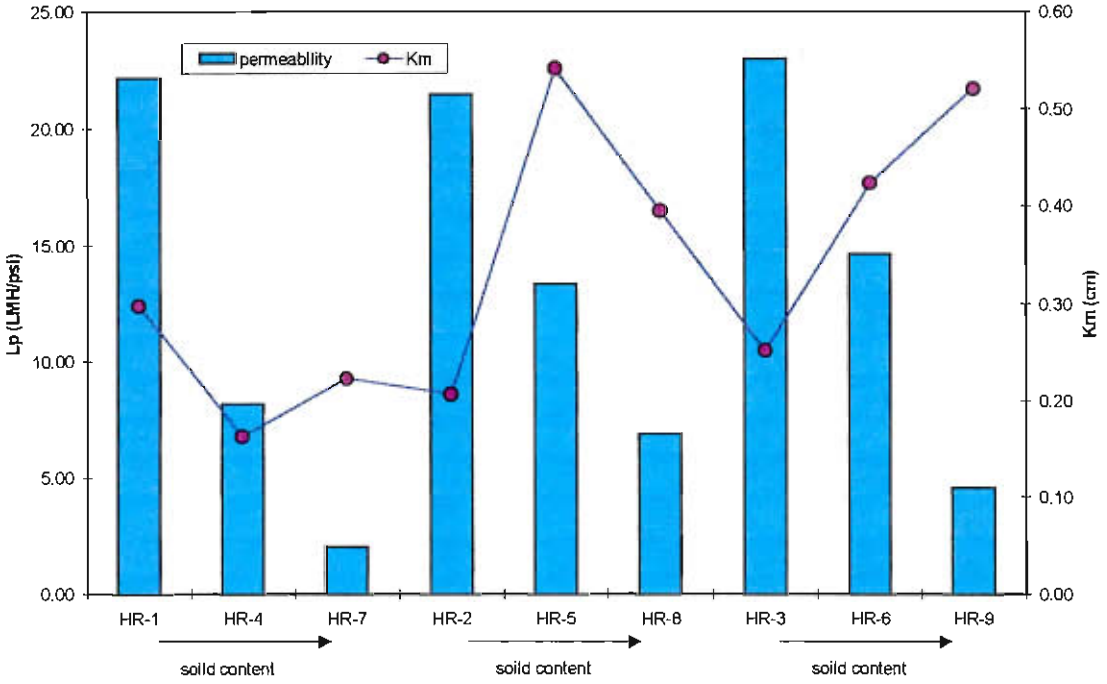

Figure 5 Effect of solid content on interaction parameter

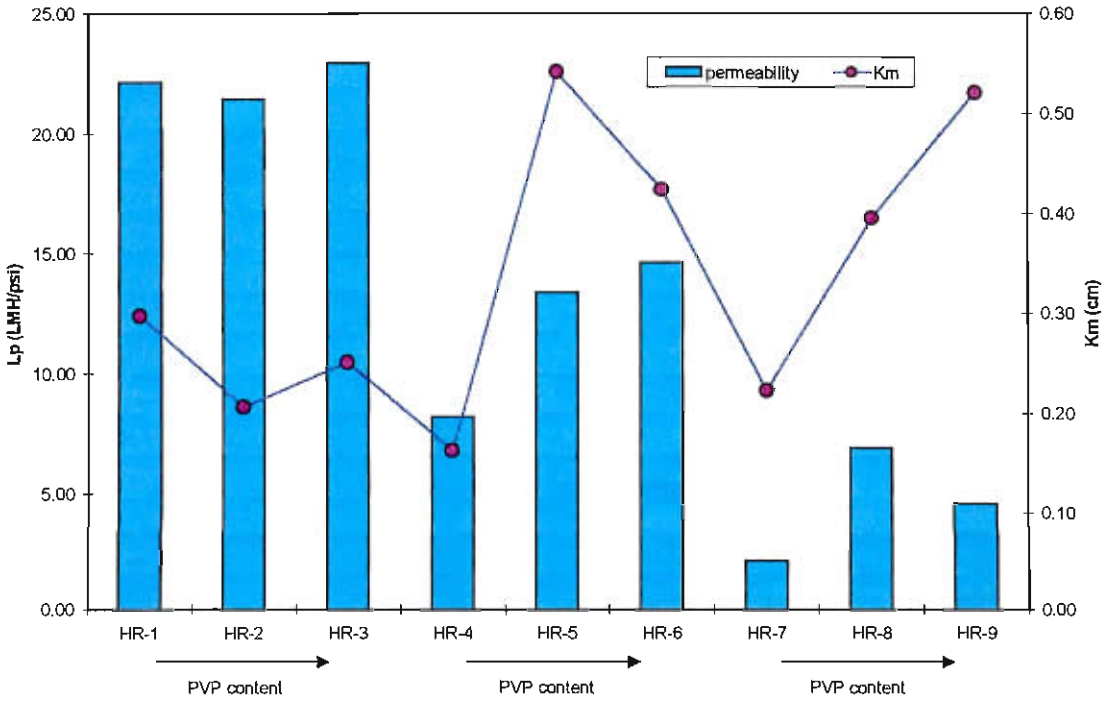

Figure 6 Effect of PVP content on interaction parameter

XPS ANALYSIS: SURFACE ELEMENTARY COMPOSITION

Methods and Material

This technique is used to determine the elementary composition of a surface sample. It is known under several names: X-ray photoelectron spectroscopy (XPS), electron spectroscopy for chemical analysis (ESCA), high-energy photoelectron spectroscopy (HEPS), induced emission spectroscopy (IEES0, photoelectron spectroscopy of the inner shell (PESIS) and energy dispersion system (EDS). The principle is simple: the sample surface is bombing by X-rays and the kinetic energies of photoelectrons ejected are measured. Because the binding energy of those electrons, also called core electrons, is a characteristic of an individual element, each chemical element is identifiable (Oldani and Schock, 1989; Clark and Feast, 1975). For each element, the binding energy depends on the energy level of the core electron, which can be 1s, 2s, $2p_{1/2}$, and/or $2p_{3/2}$. In general, the ESCA spectrum of a given core level consists of well resolved peaks corresponding to electrons escaping without undergoing energy losses, superimposed in a background tailing to lower kinetic energy arising from inelastically scattered electrons.

This technique provides information related to surface, subsurface, or essentially bulk properties, depending on differences in escape depths for photoemitted (or Auger) electrons corresponding to different kinetic energies. By varying the incident energy, it is possible to use ESCA to depth profile samples to investigate their homogeneity. Hence, if an element gives two or more signals from levels with very different escape depths, it ought to be possible to use the relative intensities of the signals to calculate the thickness of the layer containing that element (Clark and Feast, 1975).

The principle advantages of this technique are:

- the sample may be solid, liquid or gas, and the technique is essentially non-destructive
- the sensitivity of this technique is such that a fraction of a monolayer coverage may be detected

• high sensitivity is independent of the spin properties of any nucleus and is applicable in principle to any element of the periodic table. Hydrogen and helium are exceptions, being the only elements for which the core levels are also the valence levels

• information can be obtained on both the core and the valence energy levels of molecules

• only the top 50-100 Å of the samples are analyzed (Clark and Feast, 1975; Stengaardh, 1988)

In our experiments the data were collected by a Perkin-Elmer/Physical Electronics Division model n° 5400 X-ray photoelectron spectrometer with Mg Kα X-radiation, 1253.6 eV (15kV, 400W). For the determination of the atomic composition of each element, data were collected for multiplex spectra at 0.05 eV/step for 100 mses/step with a 35.75 pass energy. The atomic composition was determined using peak area sensitivity factors described by Wagner et al. (1979). The accuracy of the instrument is 0.1 eV, and the minimum detection limit in the relative chemical composition determination is about 0.2%. Prior to analysis pieces of membranes (about 1 cm^2) were put in petri dishes and let at room temperature for one day. Before starting the analysis the samples were placed in a vacuum for about 15 min, under a base pressure of 1 to $1.4.10^{-11}$ psi. The analysis pressure was in the range 0.2 to $1.0.10^{-11}$ psi. In our experiments ESCA measurements were carried out to determine the atomic composition (C, O, S, N) of the clean membranes.

Results and Summary

The elemental composition of the membrane material as calculated and measured is listed in Table 2a and 2b. The calculated elemental composition is based on the chemical formulas for polysulfone and polyvinylpyrrolidone, the percentage of polysulfone and polyvinylpyrrolidone present in the casting solution for each membrane, and as assumption that the N-methylpyrrolidone solvent completely evaporates leaving a solid consisting of only polysulfone and polyvinylpyrrolidone.

The calculated values indicate that the composition should stay the same as the solids concentration of the casting solution increases (membranes HR-2, HR-5, and HR-8), with only a very slight increase in carbon (0.15%) and sulfur (0.2%) and a slight

decrease in nitrogen (0.35%) would theoretically occur under the conditions reported. These differences are too small to be significant, given the variability in casting solution concentration during preparation and the accuracy of the XPS. However, as the fraction of PVP in the casting solution increases, an increase of nitrogen from 0% to 3.43% is expected, whereas a decrease in sulfur from 7.84% to 5.88% is expected.

The XPS measurements show a fairly constant nitrogen concentration of about 4.5% as the fraction of PVP changes. The higher than expected concentration of nitrogen in membrane composition is believed to be the result of the presence of the solvent within the molecular matrix of the membrane material. The higher nitrogen concentration is accompanied by a carbon concentration about 2 to 3 percent higher than predicted by chemical formulas. The higher nitrogen and carbon concentrations are offset by lower than expected sulfur concentrations. The sulfur concentrations did show the expected trend with respect to increasing PVP fraction, although the effect was very slight.

Table 2a Elementary composition obtained by XPS of some PVP/PS membranes

Membrane	HR-2	HR-4	HR-5	HR-6	HR-8
Carbon	78.2 %	78.3 %	77.6 %	77.9 %	79.9%
Oxygen	15.1 %	15.2 %	16.2 %	15.3 %	14.0 %
Nitrogen	3.8 %	4.5 %	4.7 %	4.5 %	3.9 %
Sulfur	1.7 %	2.2 %	1.6 %	1.5 %	1.9 %
Silicon	1.3 %			0.8 %	0.3 %

Table 2b Calculated elementary composition (assuming all solvent completely evaporates)

Membrane	HR-2	HR-4	HR-5	HR-6	HR-8
% PVP	14.0 %	0 %	12.5 %	25.0 %	11.4 %
% PS	86.0 %	100.0 %	87.5 %	75.0 %	88.6 %
Carbon	75.7 %	76.5 %	75.7 %	75.0 %	75.8 %
Oxygen	15.7 %	15.7 %	15.7 %	15.7 %	15.7 %
Nitrogen	1.9 %	0 %	1.7 %	3.4 %	1.6 %
Sulfur	6.8 %	7.8 %	6.9 %	5.9 %	7.0 %

PEG RETENTION: DETERMINATION OF MWCO

Methods and Material

In order to characterize the membrane pore size, molecular weight cut-off (MWCO) was determined using model solutes. Synthetic polymers, such as polyethylene glycol (PEG), dextran, polyvinylpyrrolidone are usually chosen because they do not interact strongly with the membrane material. In this study we used a group of four PEG, with molecular weights of 300, 600, 3350 and 10000 Da purchased from Sigma (St Louis, MO). Lentsch et al. (1993) used an empirical equation to calculate the Stokes radius of PEG. Experimental PEG diffusion coefficient measurements were combined with the Stokes-Einstein law to give the following relation:

$$r_s = 0.045\ M^{0.44} \tag{1}$$

where r_s: PEG Stokes radius (nm)

M: molecular weight (Da)

The Stokes radii calculated for the PEG used in this study are presented in Table 3.

Table 3: Solute radius of PEG calculated by empirical Lentsch's equation (1)

MW (Da)	300	600	3350	10000
r_s (nm)	0.5	0.75	1.6	2.6

Filtration tests were performed using a 28.7cm^2 diameter UF cell with magnetic stirrer (Amicon, Minnetonka, MI). The pressure was applied via a compressed nitrogen tank, and was varied between 68.9 kPa and 206.7 kPa (10psi and 30psi). Membrane water permeability was measured before and after each filtration experiment in order to check for membrane fouling by PEG. For each applied pressure, PEG concentrations in the retentate and permeate were measured by a TOC analyzer (Phoenix 8000, Dohrmann) and PEG retentions were calculated using the following equation:

$$R = 1 - \frac{C_p}{C_0} \tag{2}$$

Because of concentration polarization occurring in the retentate side, an intrinsic retention must be defined by:

$$R^* = 1 - \frac{C_p}{C_m} \tag{3}$$

where C_m represents the concentration at the membrane surface [14]. The film model is used to relate R and R^*:

$$\ln\left(\frac{1-R}{R}\right) = \ln\left(\frac{1-R^*}{R^*}\right) + \frac{J}{k} \tag{4}$$

R^* is obtained by the intercept of the slope of $\ln\left(\frac{1-R}{R}\right)$ versus flux J. The plot of intrinsic retention versus flux is used to determine the membrane MWCO.

In order to get the average corresponding pore radius, we used a model of steric exclusion as presented by Ferry (Deen, 1987). When size exclusion is the only selectivity phenomena the intrinsic retention extrapolated to no flux is equal to

$$R^*_{J=0} = \left(1 - (1-\lambda)^2\right)^2 \tag{5}$$

with $\lambda = \frac{r_s}{r_p}$ r_s solute radius, r_p pore radius

The first approximation is to consider that the membrane pores are all the same size. In this case an average pore radius can be calculated from the values of R^* determined by the retention experiments and PEG radius. This method allows the calculation of the pore radius of the homogeneous membrane equivalent to the membrane tested. This is a good method in our case where we want to compare different membranes.

Results and Summary

Three PEG with molecular weights of 600, 3,350 and 10,000 were used in the solute retention experiments to determine the MWCO for PVP-HR membranes. Figure 7 shows the PEG retention curves for each membrane. The MWCO value is obtained at 90% rejection. However, in the case of HR-1 and HR-3, the retention coefficient for PEG 10,000 is less than 50%, thus no MWCO values can be determined from the retention curve. Obviously, their MWCO will be larger than 10,000. These two membranes have very broad MW distribution compared to the other membranes.

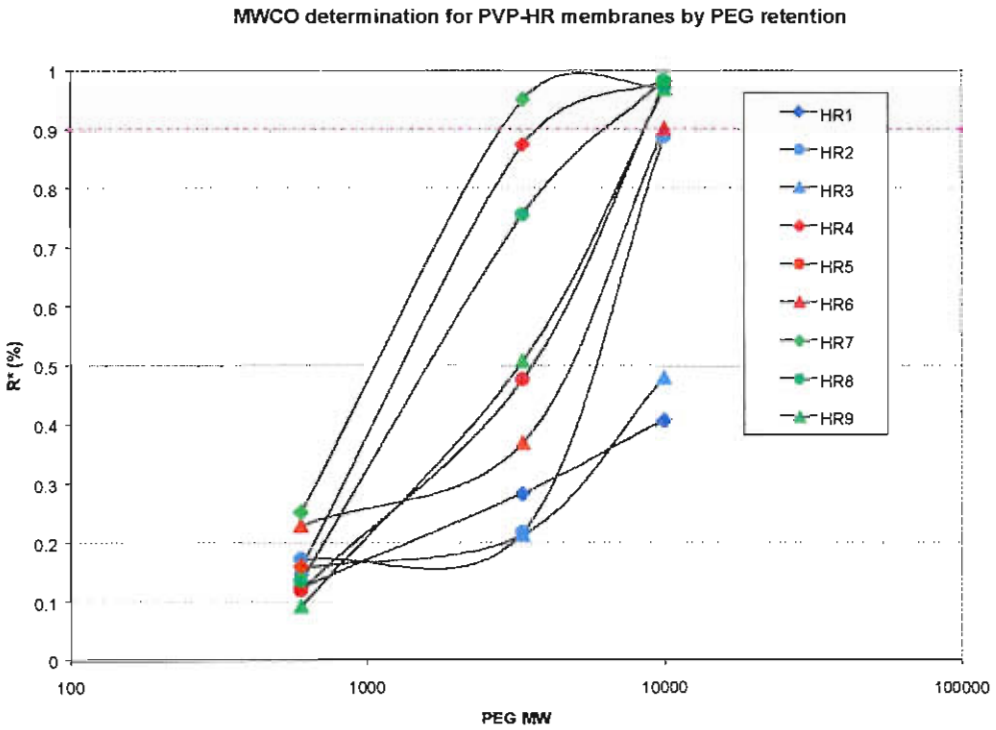

Figure 7 MWCO determination for PVP-HR membranes by PEG retention experiments

Table 4 shows the MWCO and pore radius for PVP-HR membranes. The pore radius is calculated from Eqs. (1) and (5) using the $R^*_{j=0}$ values. As expected, as the total solid content increases (for series HR1-4-7, HR2-5-8, and HR3-6-9, moving across the table from left to right), the average pore size becomes smaller and the MWCO decreases. This is consistent with our expectation and the water permeability measurements (Table 1).

Table 4 MWCO and pore radius determined by PEG retention experiments

HR-1 MWCO (Da) > 10,000 r_p (nm) > 3.13	HR-4 MWCO (Da) = 3,750 r_p (nm) = 2.03	HR-7 MWCO (Da) = 2,800 r_p (nm) = 1.79
HR-2 MWCO (Da) = 10,000 r_p (nm) = 3.13	HR-5 MWCO (Da) = 8,600 r_p (nm) = 2.93	HR-8 MWCO (Da) = 6,300 r_p (nm) = 2.56
HR-3 MWCO (Da) >10,000 r_p (nm) > 3.13	HR-6 MWCO (Da) =10,000 r_p (nm) = 3.13	HR-9 MWCO (Da) = 8,600 r_p (nm) = 2.93

The pressure effects on the MWCO determination were evaluated by applying three different pressures (10, 20, and 30 psi) during the experiment. As demonstrated in Figures 8 through 10, the true rejection R* obtained for different pressures does not vary too much. This indicates that the pressure does not play an important role for the true rejection curves in the PEG retention experiments.

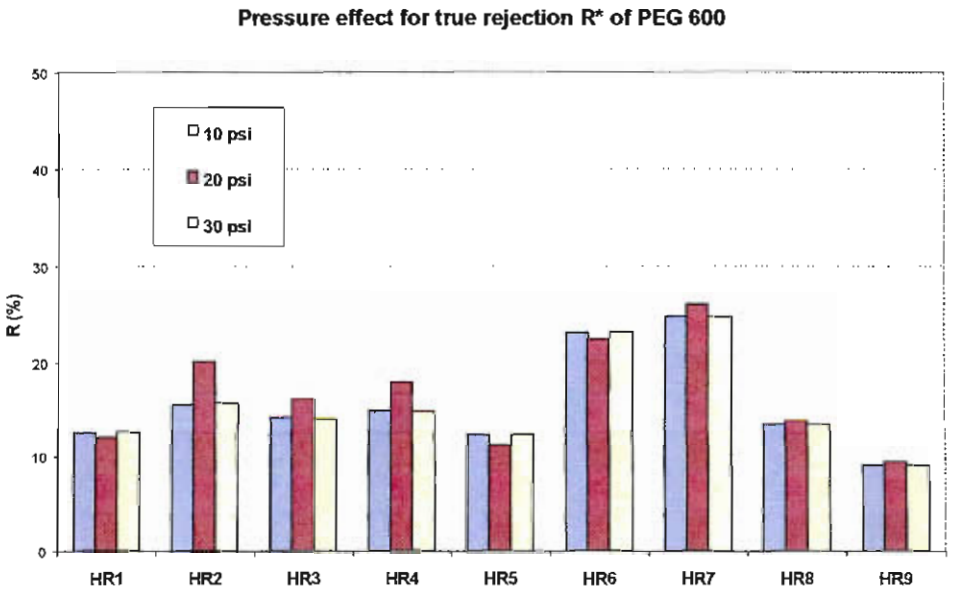

Figure 8 Pressure effect on true rejection R^* of PEG 600

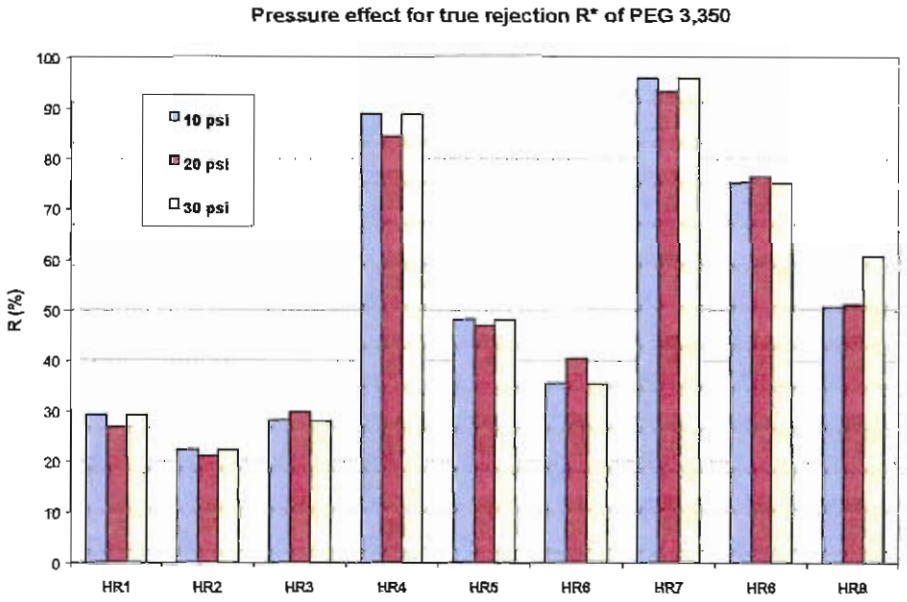

Figure 9 Pressure effect on true rejection R^* of PEG 3,350

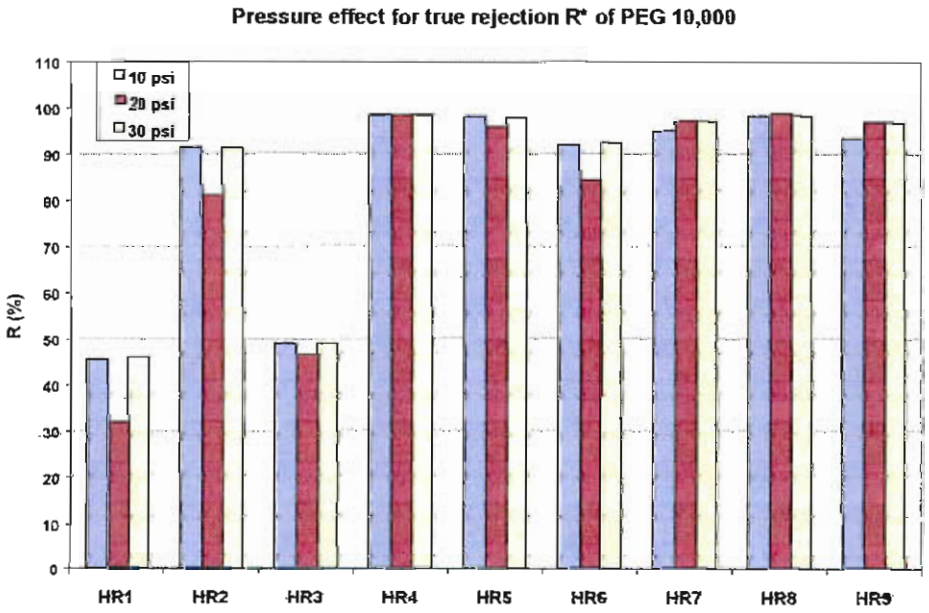

Figure 10 Pressure effect on true rejection R^* of PEG 10,000

CONTACT ANGLE (CAPTIVE AIR BUBBLE METHOD): HYDROPHOBICITY

Methods and Material

Contact angle measurements have been completed on the PVP series of membranes. A new contact angle cell was used for the measurements of this membrane series. The method used on previous membrane series used a liquid cell that required the contact angle to be determined by aligning the crosshairs of a goniometer with the tangent point between an air bubble and the membrane surface. The measurement scale on the goniometer was small, so the resolution of angle measurement was difficult. The new method involves the use of a new contact angle liquid cell and a CCD camera. The liquid cell has optical-quality glass on one face that allows better quality imaging of the air bubble. The new contact angle cell also allows better control of the size and placement of the air bubble. An image of the bubble was then captured with a CCD camera, stored on a computer, and printed for determination of the point of tangency and contact angle. To assure that all surface contamination was cleaned from the membrane surface, the membranes were prepared by sonicating in distilled water for 30 minutes, with the water being replaced with fresh water every 10 minutes. Ten measurements were taken of each membrane. The new method had a 95 percent confidence interval between 2.0 and 3.7 degrees for the various membranes in this series.

Results and Summary

Contact angle measurements show a slight increase in hydrophobicity for the series HR-1 to HR-3, which correspond to increasing quantity of PVP in the solution. As PVP is a more hydrophilic material than polysulfone, this result is the opposite of the expectations. The difference in hydrophobicity was slight, however, with a difference only 2 degrees for each sequential membrane in the series. A contact angle difference of 2 degrees is not anticipated to be significant in the performance of the membrane. The remaining 6 membranes in this series (HR-4 to HR-9) showed greater hydrophilicity than membranes HR-1 through HR-3. Each membrane between HR-4 and HR-9 had a contact angle that was 8 to 10 degrees lower than the contact angles for HR-1 to HR-3. HR-4 to HR-9 contained higher solids concentrations in the casting solution. The difference in

contact angles within this group of 6 membranes was not significant and did not show any trends with increasing PVP fraction or with a increase of total solids from 20 to 20 percent.

Overall, the contact angle measurements for this membrane series ranged from 29 to 45 degrees. Literature values for polysulfone range from 40 to 60 degrees, but the addition of PVP would be expected to lower the contact angle. As a control, contact angle measurements were conducted on several other materials. Laboratory parafilm contact angle measurements ranged from 108 to 116 degrees compared to a measurement of 113 degrees reported in the literature. Teflon ranged from 103 to 110 degrees, compared to 112 degrees reported in the literature.

Table 5 Contact angle and its standard deviation obtained by captive air bubble

HR-1 CA = 41 ± 5.9	HR-4 CA = 34 ± 3.2	HR-7 CA = 35 ± 4.9
HR-2 CA = 43 ± 5.0	HR-5 CA = 34 ± 3.3	HR-8 CA = 29 ± 3.7
HR-3 CA = 45 ± 4.2	HR-6 CA = 35 ± 3.9	HR-9 CA = 38 ± 3.6

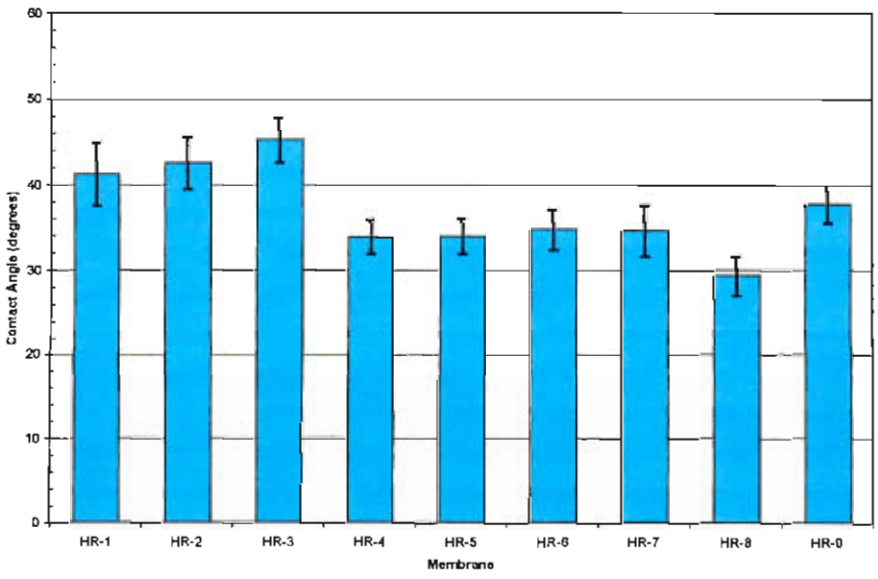

Figure 11 Contact angle measurements of PVP/PS membranes

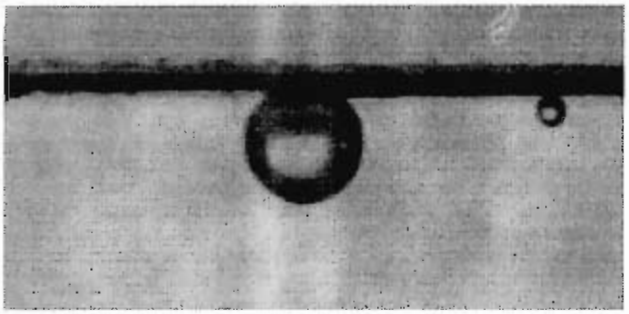

HR-PVP-1-1

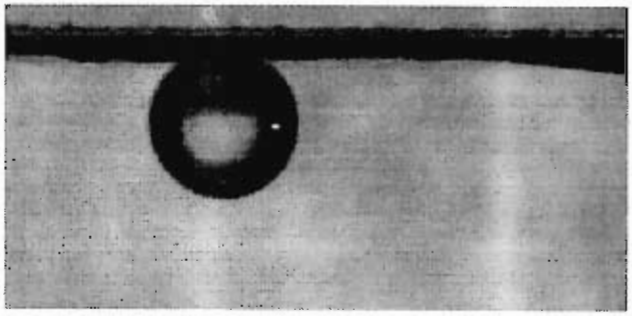

HR-PVP-1-2

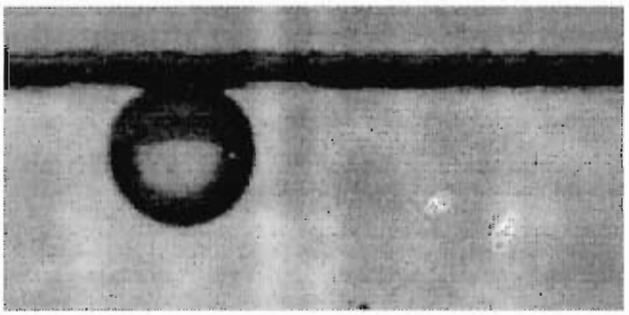

HR-PVP-1-3

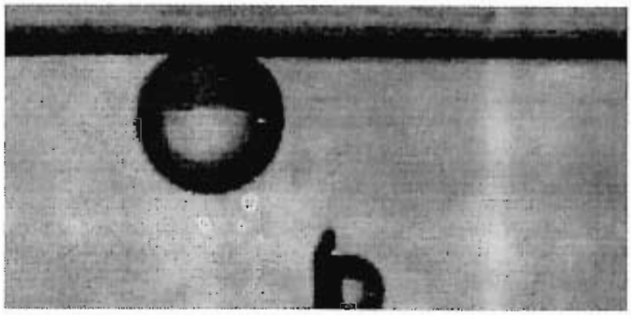

HR-PVP-1-4

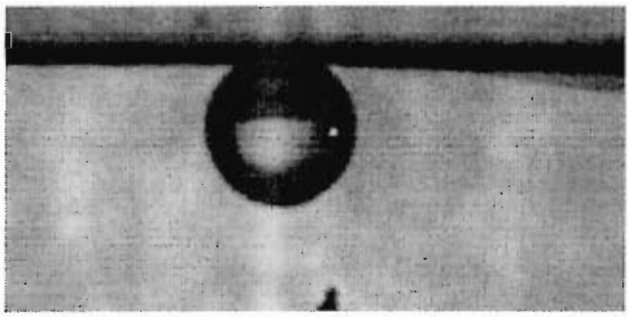

HR-PVP-1-5

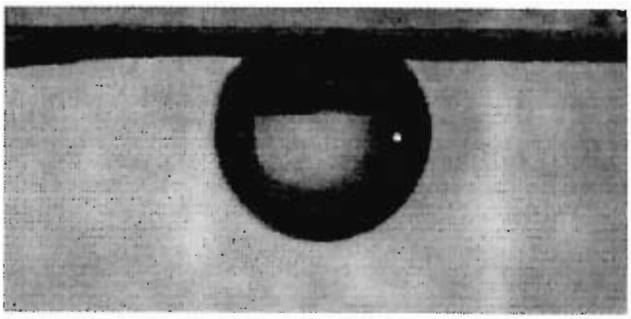

HR-PVP-1-6

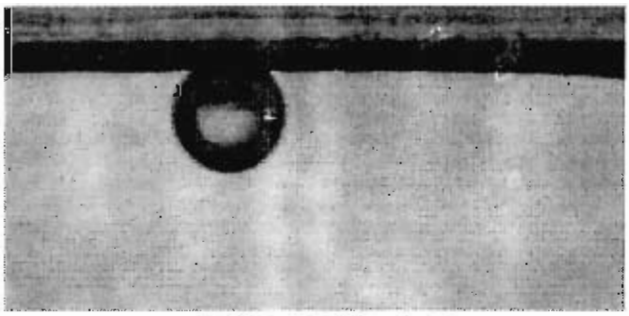

HR-PVP-1-7

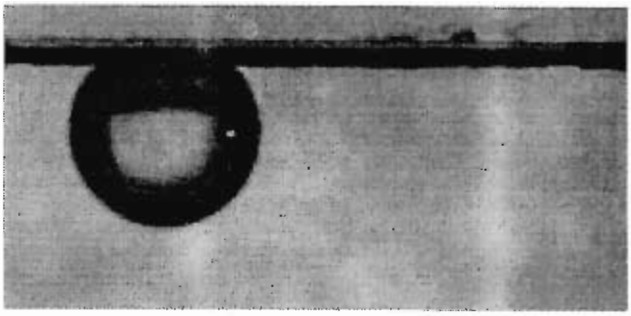

HR-PVP-1-8

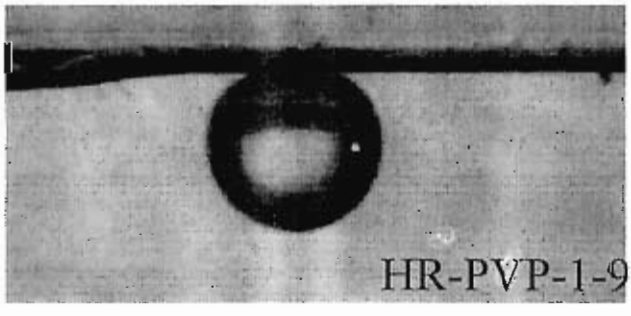

HR-PVP-1-9

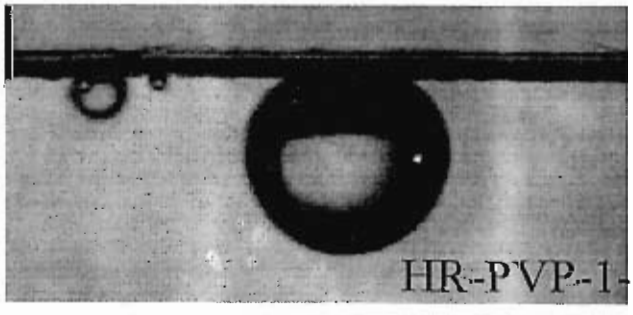

HR-PVP-1-10

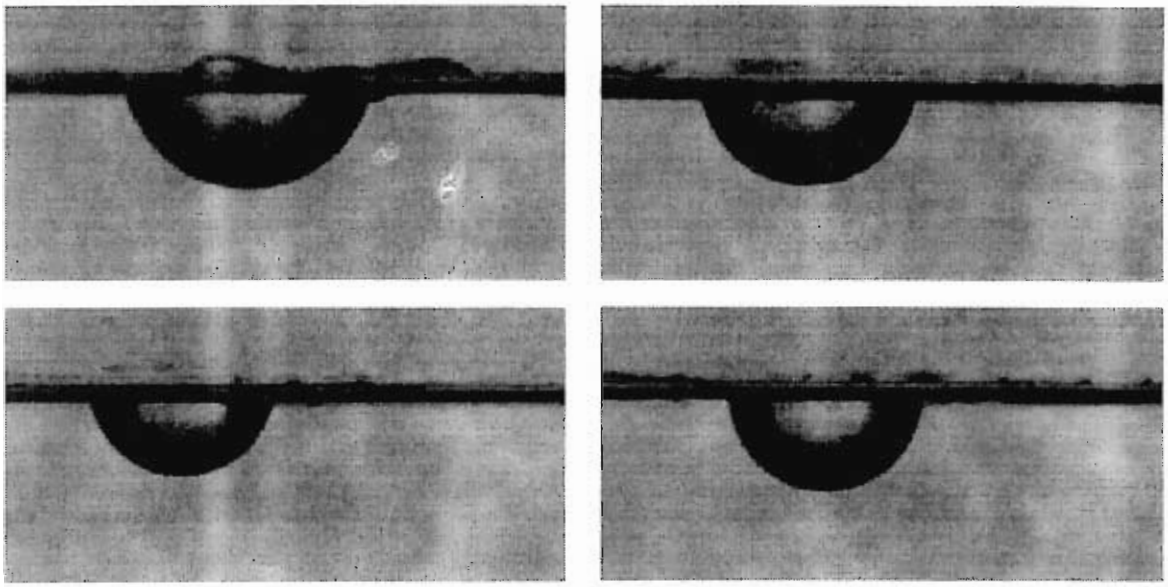

Laboratory Parafilm 3/18/99

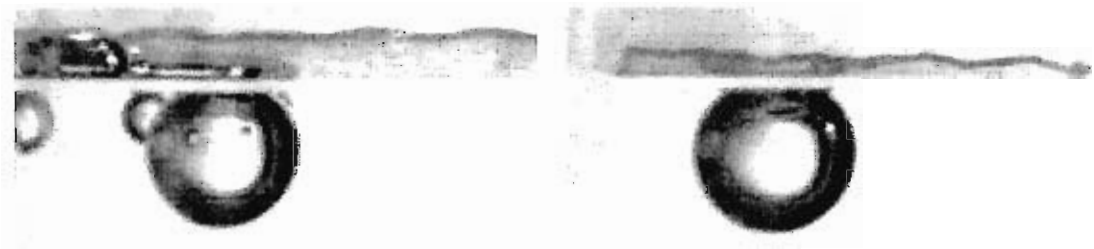

Microscope Slide

Teflon

STREAMING POTENTIAL: PORE CHARGE

Methods and Material

All membranes were stored in 0.01 % sodium azide (Na_3N) solution at all times to prevent biofouling. First, membranes were cut and soaked in the Milli-Q water. Water was exchanged twice every 30 min to remove any trace solvents. Finally, membranes were soaked overnight in the Milli-Q water. The 0.01 M NaCl solution was used as basic electrolyte solution for the streaming potential measurement. Although KCl can be used as a basic electrolyte, NaCl was chosen because it gave more reproducible values than KCl in preliminary tests. To prevent a sudden change of pH during the measurement, the buffer solution of $5*10^{-4}$ M Na_2HPO_4 was added to the basic electrolyte solution. Then, 1N HCl or NaOH solutions were used to adjust to the final pH value.

Zeta potential of membrane pores was obtained from streaming potential measurements using an instrument build according to Nyström (Nyström et al., 1989; Nyström and Zhu, 1997).

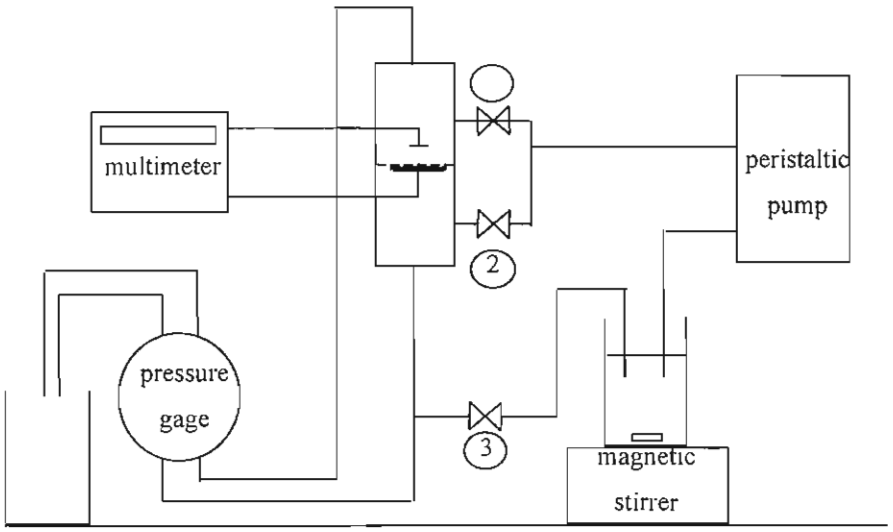

Figure 12 Experimental set-up for zeta potential measurement

The measuring cell consists of two cylindrical half-cells made from plexiglass. To prepare the electrodes, 18 X 18 per linear inch copper mesh is cut into two disks of 17 mm and 29mm diameter. These disks are soldered to a 0.5 mm copper wire. Both disks

and wire are silver plated by electrolysis for 2-6 hours at a total current of 2-0.5 mA. Next, they are chloridized for 30 min by electrolysis in 0.1N HCl at a total current of about 2mA during half an hour (Brown, 1934). After silver plating they are washed for a few hours to eliminate any excess chloride ions until the voltage is constant when no differential pressure is applied.

A peristaltic pump with a variable speed drive (6-600 rpm) is used to pump the liquid from the feed beaker through the cell. The speed is controlled with a speed drive system. Since the flow from the peristaltic pump is not perfectly smooth, a pulse dampener is added in the line to reduce the fluctuations of the flow. The two cell compartments are connected to a Capsuhelic differential pressure gage gage (0-10 psi, accuracy ± 0.3 psi). The voltage is measured with a Fluke 45 dual display multimeter (resolution 0.001mV, accuracy 0.02%).

All our experiments follow the following experimental procedure: the cell is closed without membrane and placed in the instrumental set-up. All the valves are open and the electrolyte solution is pumped until there are no air bubbles left in the system (valves 1 and 2 may be closed at the end of the filling). The pump is then turned off and the cell is opened, without letting air bubbles enter the lower half-cell. A 3.3cm diameter piece of membrane is cut and placed on the lower larger electrode, which serves as a support for the membrane. The cell is closed and the solution is pumped again, in order to fill the upper part of the instrument. The instrument is ready when it is free of air bubbles. Valves 1 and 3 are open, valve 2 is closed.

The electrolyte solution is circulated under no differential pressure until the potential difference between the two half cells remains constant (about 30 min). The conductivity of the solution is measured using the CDM 230 conductivity meter. The conductivity meter was calibrated with 0.01 M KCl every week. The pressure is increased up to 4.0 to 5.0 psi by adjusting the valve 2, and the potential difference was measured. The pressure is decreased by an increment of 0.5 psi and the corresponding potential difference is measured each time. At the end of the experiment, the conductivity and temperature are checked and the pressure is released. The system is completely emptied and flushed with the Milli-Q water before any other measurement.

The Helmoltz-Smoluchowski equation was used to calculate the zeta potential from these measurements:

$$\xi = \frac{\eta \ \kappa \Delta E}{\varepsilon_0 \ \varepsilon_r \ \Delta P} \tag{6}$$

Where T= temperature

η = viscosity ($kg.m^{-1}.s^{-1}$)

ε_0 = permittivity of vacuum

ε_r = dielectric constant

ΔE = potential difference (mV)

ΔP = pressure difference (psi)

κ = conductivity ($mS.cm^{-1}$)

ξ = zeta potential (mV)

The Helmoltz-Smoluchowski equation tends to underestimate the zeta potential value (Bowen *et al.*, 1998). Therefore, this value is called a 'relative', 'apparent', 'equivalent' or 'nominal' zeta potential. Although this value is a little underestimated, it can be used in the qualitative comparison if other experimental conditions such as electrolyte concentration and buffer concentration are held constant. Bowen *et al.* (1998) calculated theoretical correction factors for the Helmoltz-Smoluchowski equation. However, we did not apply any correction factor to our calculations because the relative potential value is enough to investigate the effect of PVP content on membrane charge.

Results and Summary

The charge of membranes was evaluated by measuring streaming potential. Streaming potential can be converted to zeta potential with the Helmholtz-Smoluchowski equation. Experiments were also carried out at different pHs to examine the effect of pH on the membrane charge (see Figure 13).

The ratio of polyvinylpyrrolidone (PVP) to polysulfone (PS) was controlled during manufacture in order to investigate the effect of non-charged component on the membrane charge and fouling. The PVP is known as a hydrophilic and non-charged compound. As the ratio of PVP to PS increases, the zeta potential of the membrane tends to decrease (becomes less negative). The membrane without PVP (polysulfone membrane) has a zeta potential between –7 to -9 mV at pH 7 (see PVP HR1, 4, 7), which is almost in the same range as our previous measurements of polysulfone membranes. A small increase of the PVP content caused a dramatic change in zeta potential. HR 2, 5,

and 8 have zeta potential ranging from –1.2 to –3.5 mV at pH 7, which is relatively small compared to membranes with polysulfone only. However, an additional increase of PVP ratio did not cause a significant change in zeta potentials (see HR 3, 6). No significant trend in zeta potentials was observed when the solid content of membranes was increased.

The pH effect on the membrane charge was also investigated. In preliminary tests of titration, there was a sudden pH change around pH=4. A sudden change of conductivity was also observed around this pH value. The conductivity depends on ion species in solution (Atkins, 1978), and the changes of major ion species around this pH may cause a sudden change of pH and conductivity. So, pH 4.5 was chosen as a minimum pH.

As the electrolyte's pH decreases, the zeta potential of the membranes tends to decrease (i.e., become less negative). The pH dependence of zeta potential may come from the shift of proton equilibrium at the membrane surface (Szymczyk et al., 1998). However, the effect of pH is less significant in the case of the PVP membranes (HR 2, 5, 8 or HR 3, 6) compared to membranes with polysulfone only (HR 1, 4, 7).

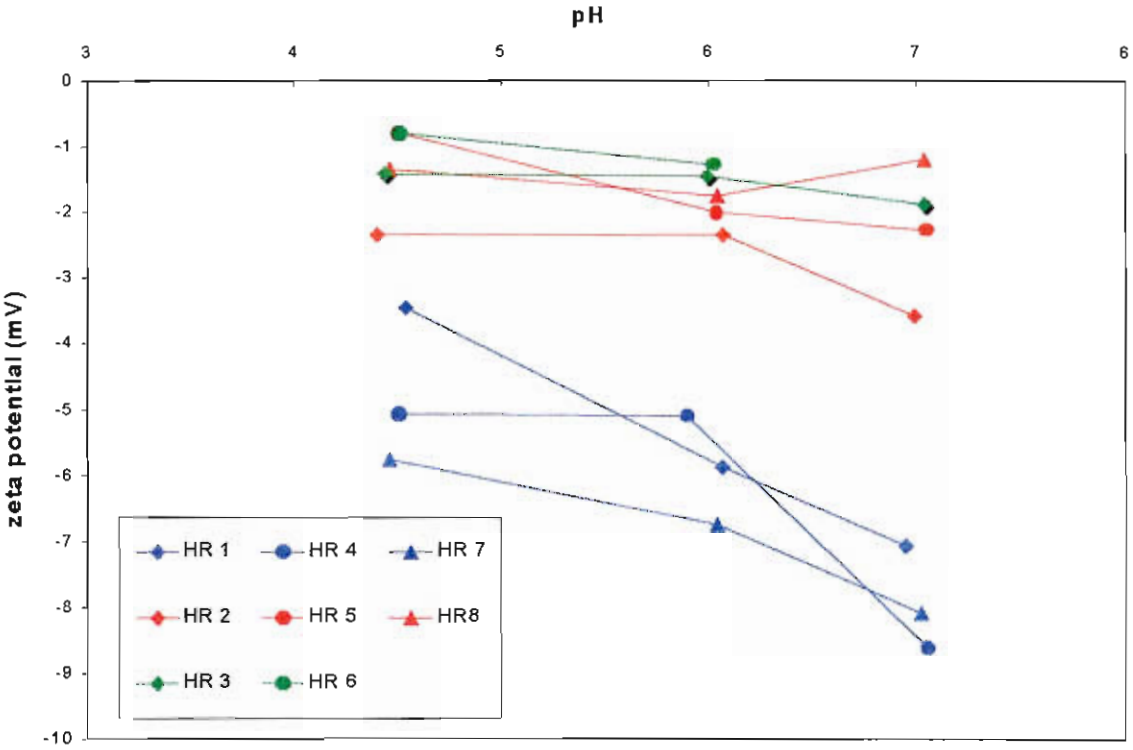

Figure 13 Zeta potential mesurements ([NaCl]=0.01M and [Na_2HPO_4]=0.0005M)

a) PVP to PS ratio ↗ (vertically) charge density ↘ because of an increase in non-charge component

b) % solid content ↗ (horizontally) no significant evolution

AFM: MEAN DIAMETER AND ROUGHNESS

Methods and Material

Atomic Force Microscopy (AFM) is used for direct analysis of membrane surface properties, such as pore size distribution, pore shape, and surface roughness. This technique does not require any special preparation of the sample, and the sample can be imaged in either air or liquid.

The membranes were imaged under water since the membranes should be studied in their working environment in order to get the best resolution. The wet membranes are studied in contact mode. In this case the probe tip scans across the sample surface and is in direct physical contact with the sample. It can then respond to very short-range repulsive interactions with the sample.

The AFM observations were performed on a Digital Nanoscope II instrument. Cantilevers, made from silicon nitride, are 200μm long and have a triangular shape. The spring constant of the narrow cantilever is k=0.032N/m. The tip is also made of silicon nitride and has a pyramidal shape. Square pieces (5mm*5mm) of the membrane were cut and attached to the magnetic holder using doubled-sided tape. The wet membrane surface was studied by contacting the surface with a drop of ultrapure water after sample mounting. For studies in liquids, a liquid tube scanner is used. The liquid tube scanner allows simple and routine imaging in liquids, without the need for ancillary equipment or a closed chamber.

Pore sizes are estimated from AFM images and calculated by AFM surface analysis software. Line profiles are selected to traverse the AFM image and pass through the pores. To determine pore size, the operator must choose points on each height profile where the pore is considered to start and end. The pore radius is then the horizontal distance between these points. The porosity of the membrane was estimated using the measured average pore diameter and the "lakes analysis" included with the software.

Results and Summary

Atomic Force Microscopy (AFM) was completed on the PVP series membranes with a Digital Instruments AFM. Oxide-sharpened tips were used. AFM was conducted in both contact mode and tapping mode. Scan size ranged from 0.2 μm to 20 μm, for an ultimate resolution of 0.4 nm to 40 nm.

The PVP membrane material appears to be a soft material that yields under the force of the AFM tip. Many of the images appear to be fuzzy or out of focus. Several images appear quite rough, but inspection reveals that the features have a repeating sinusoidal shape which cannot be reproduced if the imaging proceeds from a different direction. It is believed that this sinusoidal roughness was caused by interactions between the tip and the soft material and not by the actual topology of the membrane. It is possible that the fuzzy images and sinusoidal features are caused by the lack of a solid interaction between the tip and surface. In essence, the soft material allows the AFM to receive different feedback in terms of the force applied as it contacts different points on the surface, which would prevent sharp clarity in the images. It addition, it is possible for the tip to physically rearrange the surface to the extent that repetitive imaging of fine details on the surface is not possible. No features were observed on any of the membranes which could be identified as pores. It is believed that the interactions between the AFM tip and the soft material as described above was responsible for the inability to distinguish pores in this material.

Many of the membrane samples showed various kinds of surface damage. The damage included linear scraps in the surface ranging from 0.1 to 3 μm in width and 2 to 20 μm in length as well as sharp-edged punctures of various shapes and sizes. This surface damage could have occurred during fabrication of the membranes, during preparation for the AFM, or during routine handling of the membranes. Every effort was made during AFM preparation and imaging to avoid touching the surface that was to be imaged; however, surface damage appeared on many of the membranes anyway. The surface damage can probably be attributed to the soft material as described above. The surface of several membranes also showed what appeared to be large pores (1 μm or larger). Due to the large size of these features, however, it is believed that they are not pores but are only circular indentations in the membrane surface. The circular shape of

these features makes it appear that they were formed during the fabrication process. One possible explanation is that they were formed by droplets of pure solvent that subsequently evaporated.

Table 6 Pore diameter (dp in nm) and average roughness (Z and Rms in nm) measured after AFM images.

HR-1	HR-4	HR-7
dp =	dp =	dp =
Z = 517	Z = 95	Z = 82 (16)
Rms = 47.7	Rms = 7.4	Rms = 2.7 (1.7)
HR-2	HR-5	HR-8
dp =	dp =	dp =
Z = 210 (56)	Z = 276 (99)	Z = 37
Rms = 8.2 (5.7)	Rms = 11.4 (4.9)	Rms = 3.5
HR-3	HR-6	HR-9
dp =	dp =	dp =
Z = 261	Z = 143	Z = 187
Rms = 6.4	Rms = 6.6	Rms = 14.7

a) PVP to PS ratio ↗ pore diameter

(vertically) roughness

b) % solid content ↗ pore diameter constant

(horizontally) roughness ↘

ADSORPTION EXPERIMENTS

Methods and Material

First membrane water permeability was measured. In these experiments the organic matter was Suwannee River reference humic acid purchased from the International Humic Substances Society. A solution of this humic acid was placed in a glass jar with the membrane on the top, the skin side facing the interior of the jar. A Teflon sheet covered by one sheet of Parafilm and three sheets of aluminum foil was then placed on the membrane. The jar was closed and turned upside down, in order to contact the solution and membrane. The aluminum sheets were required to avoid any leakage from the jar. The jar was then placed on a gyrator shaker in the dark at 22 ± 2°C and it was shaken during the time of the experiment.

After the adsorption period the membrane was removed from the jar. The humic acid concentration of the supernatant was measured by UV absorption (254nm) and the percent of mass adsorbed was calculated by:

$$\%\ mass\ adsorbed = 100 * \frac{UV_0 - UV_f}{UV_0} \tag{7}$$

with UV_0: UV measurement of feed solution before adsorption

UV_f: UV measurement of supernatant after adsorption

Water permeability was measured and compared with the value obtained with the clean membrane. The membrane resistances were calculated and the adsorptive resistance, i.e. the resistance due to the adsorbed humic acid is obtained by:

$$R_a = R_t - R_m \tag{8}$$

with R_a: membrane adsorptive resistance

R_t: total membrane resistance after adsorption

R_m: clean membrane resistance

R_a is plotted on the figures as a percent of the total resistance R_t.

Results and Summary

The adsorption kinetics curves for PVP HR1-9 series are shown in Figures 15 through 18. A one-dimensional diffusion and partitioning model developed by Clark and Lucas (1998) was used to model those curves. An interaction parameter km was first introduced in their model to characterize the interaction between the humic acid and membranes. The higher the km value, the more humic acid adsorbs on the membrane. It correctly accounts for the variation in initial mass of adsorbate or other conditions, thus offers a better comparison of adsorption than directly using "% mass adsorbed". Therefore, we use the 'km' values as an important parameter in our study of humic acid adsorptive fouling on PVP-HR membranes.

Table 7 shows the interaction parameter km values determined from the adsorption experiments. As the PVP content increases, moving down the third column in the table, the km values increases moving from membrane HR-7 to HR-8 to HR-9. This is not consistent to our expectation. Since an increasing in PVP content will result in increasing membrane hydrophlicity, one expects that less adsorption should be found on the HR-9 compared to the HR-7. However, note that the zeta potential measurements indicate that in most cases, the charge density decreases (becomes less negative) moving down columns in the table. For example, the HR-9 is less negative charged than the HR-7 or HR8, which suggests that a higher adsorption occurs on HR-9 because of less repulsion in the case of the HR-9. This agrees well with the results we got from the adsorption tests of HR7-9 (see also Figure 18).

No clear tendencies were found moving down the other columns. According to the literature, it is common to associate increased negative charge and increased hydrophilicity with decreased adsorptive fouling by natural organic matter (Combe et al., 1999). In our case, one could postulate that a cancellation of beneficial effects here, i.e. the positive effect of increased hydrophilicity with PVP contents was offset by the negative effect of the decreased membrane surface charge density. It seems that the charge effects outweigh the increasing hydroplicity effects caused by PVP content. On the other hand, from the contact angle measurements, increasing PVP content does not show that the membrane become more hydrophilic. We may conclude that the amount of

PVP added is not large enough to substantially change the membrane properties with regards to adsorption.

Moving across the third row of the table, the km value increases moving from HR-3 to HR-6 and HR-9. This may be explained by the fact that the hydrophobicity of the membrane increases with increasing PS content. However, no clear trends were found for the other two rows.

During the experiment, the clean water flux before and after the adsorption tests has been measured and compared. The decrease in clean water flux was due to the adsorption of humic acid on the membrane. The adsorptive resistance R_a, which represents the increased resistance caused by adsorptive fouling, was calculated from R_t and R_m using Eq. (8). The R_a results were plotted as the percent of the total resistant R_t versus time. As shown in the attached Figures, in most cases, the R_a value reaches an equilibrium point within one day of adsorption, and then either remains constant or decreases slightly as the adsorption approaches equilibrium. We expect to see a higher adsorptive resistance for the membrane which shows a higher adsorption. This trend can be seen for the series of HR1-3 (see Figures 21 and 22). The HR-1 adsorbed slightly more humic acid than the HR-2 and 3, and correspondingly, showed the highest R_a. The same trend can be seen for the series HR7-9 at the early stage of adsorption (see Figures 25 and 26).

Adsorption resistance measurements show consistency with the flux decline data. For example, the greatest flux decline during the stirred dead-end filtration test corresponds to the largest adsorptive resistance (HR-1). As shown in Figure 29, the flux decline for series HR2-5-8 is not distinguishable, which corresponds to no significant difference of adsorptive resistance as shown in Figure 27.

Table 7 Interaction parameter (Km)

HR-1 Km = 0.30	HR-4 Km = 0.16	HR-7 Km = 0.22
HR-2 Km = 0.21	HR-5 Km = 0.54	HR-8 Km = 0.40
HR-3 Km = 0.25	HR-6 Km = 0.42	HR-9 Km = 0.52

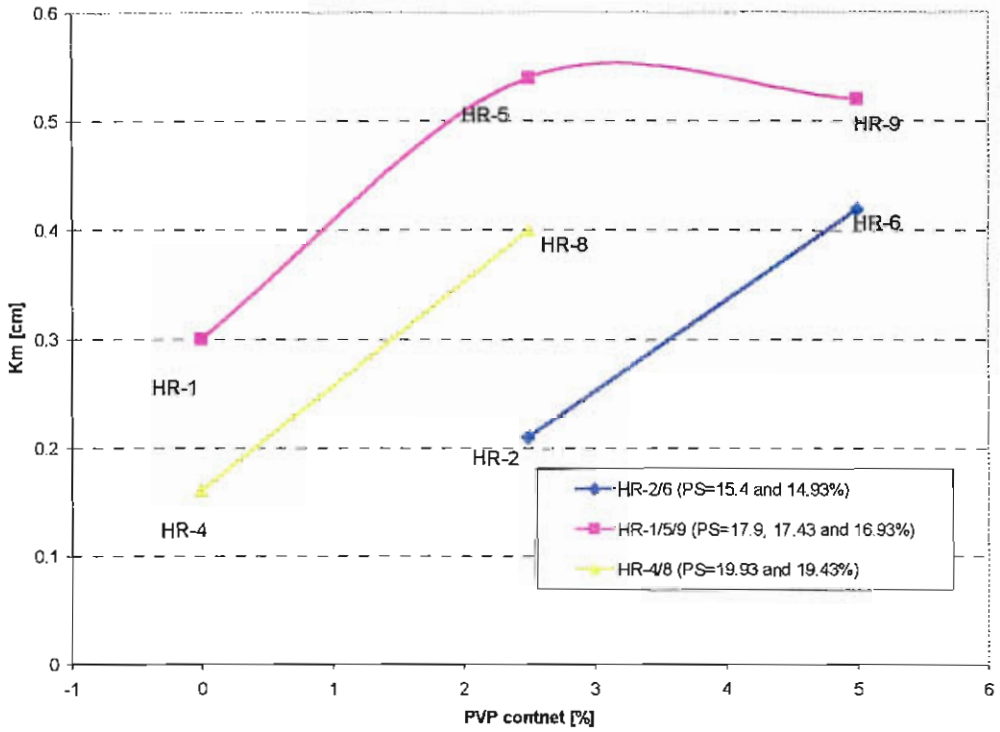

Figure 14 Effect of PVP content on interaction parameter (PS content=constant)

a) PVP content ↗ (diagonally) interaction ↗

b) solid content ↗ (diagonally) interaction ↗

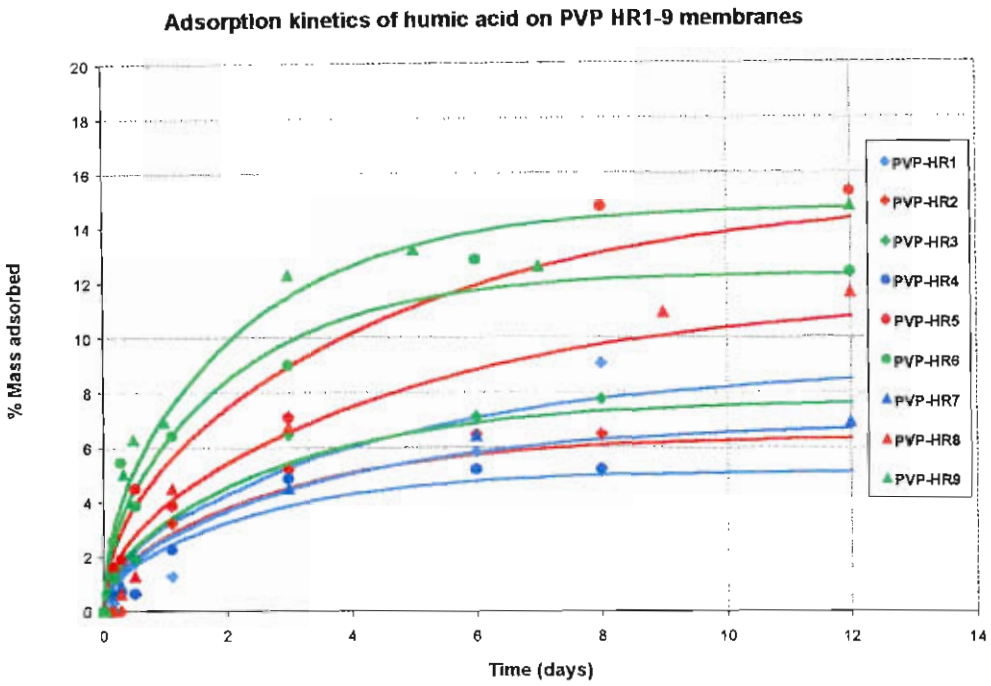

Figure 15 Model fitting of humic acid adsorption on PVP HR membranes

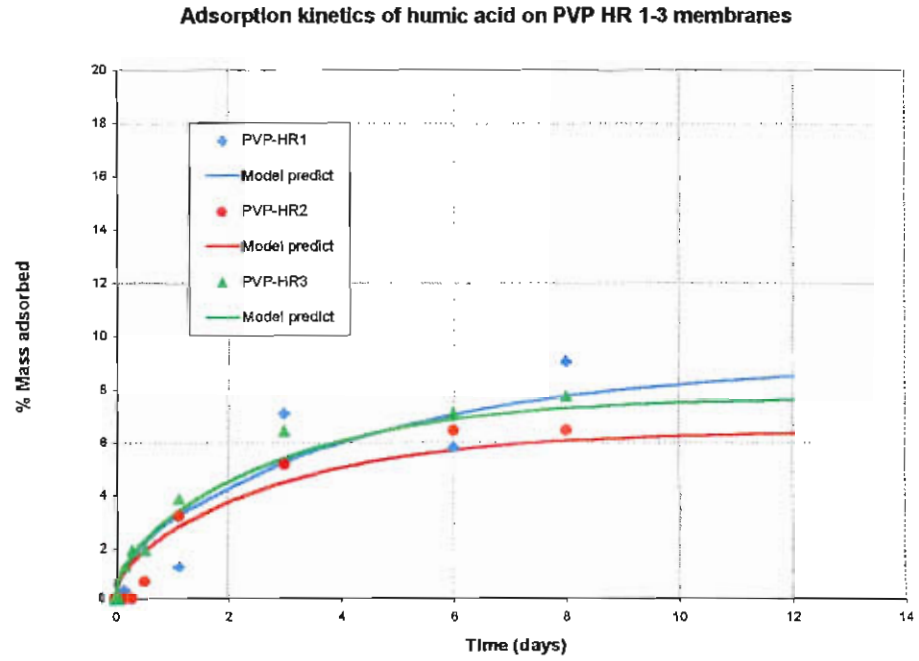

Figure 16 Model fitting of humic acid adsorption on PVP HR 1-3 membranes

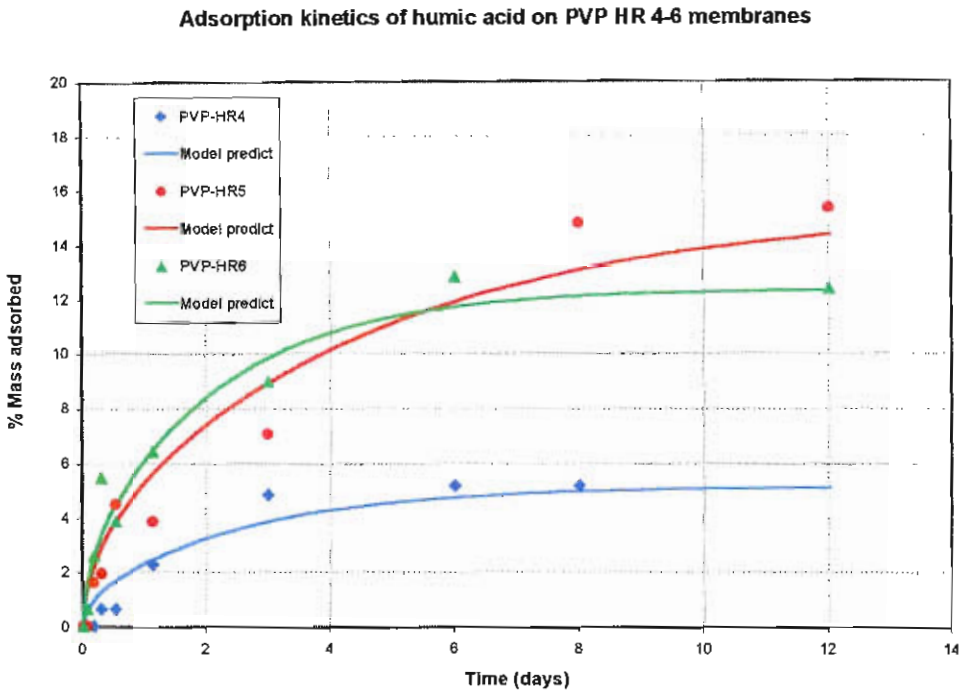

Figure 17 Model fitting of humic acid adsorption on PVP HR 4-6 membranes

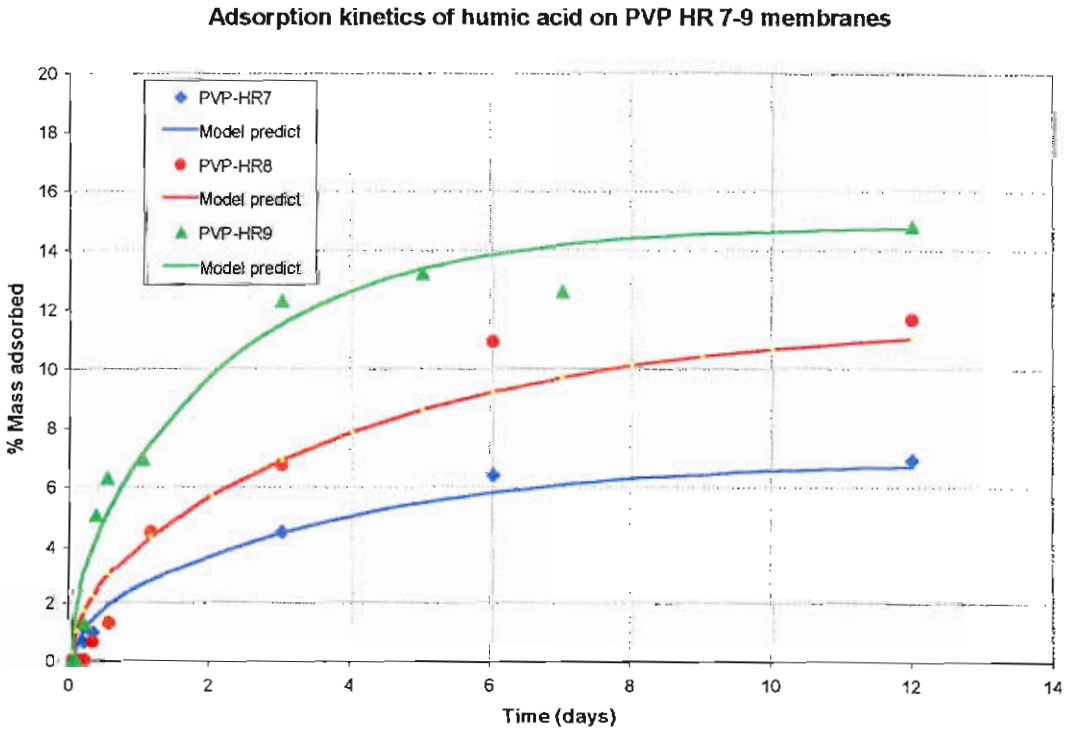

Figure 18 Model fitting of humic acid adsorption on PVP HR 7-9 membranes

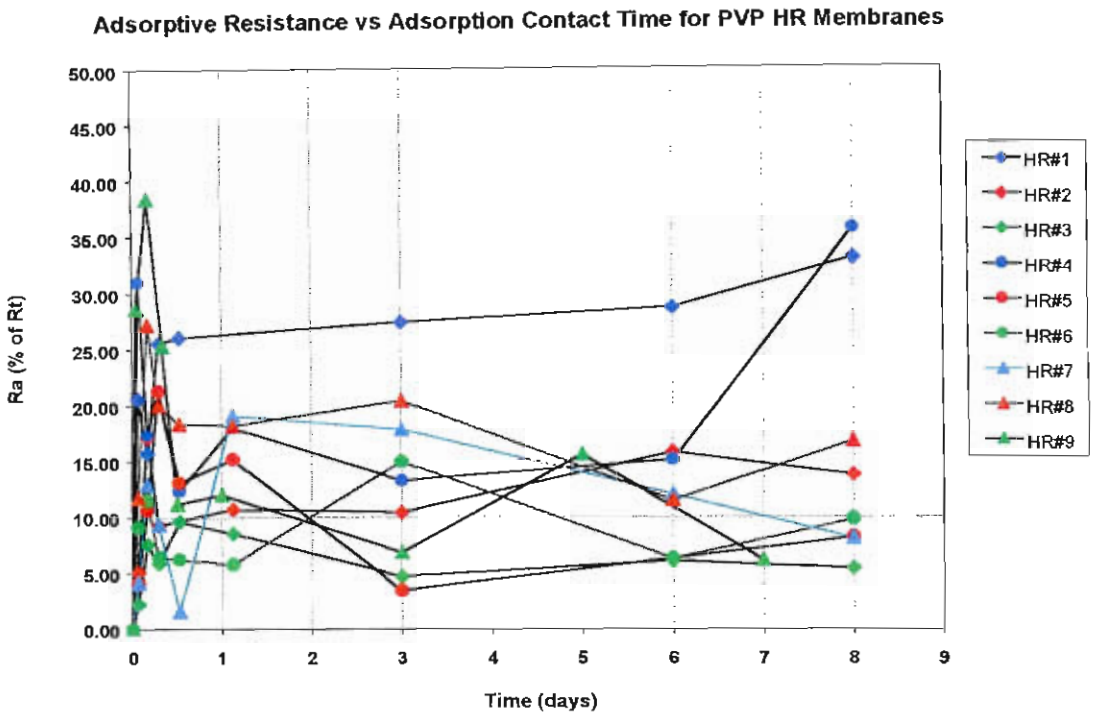

Figure 19 Adsorptive resistance of PVP HR membranes

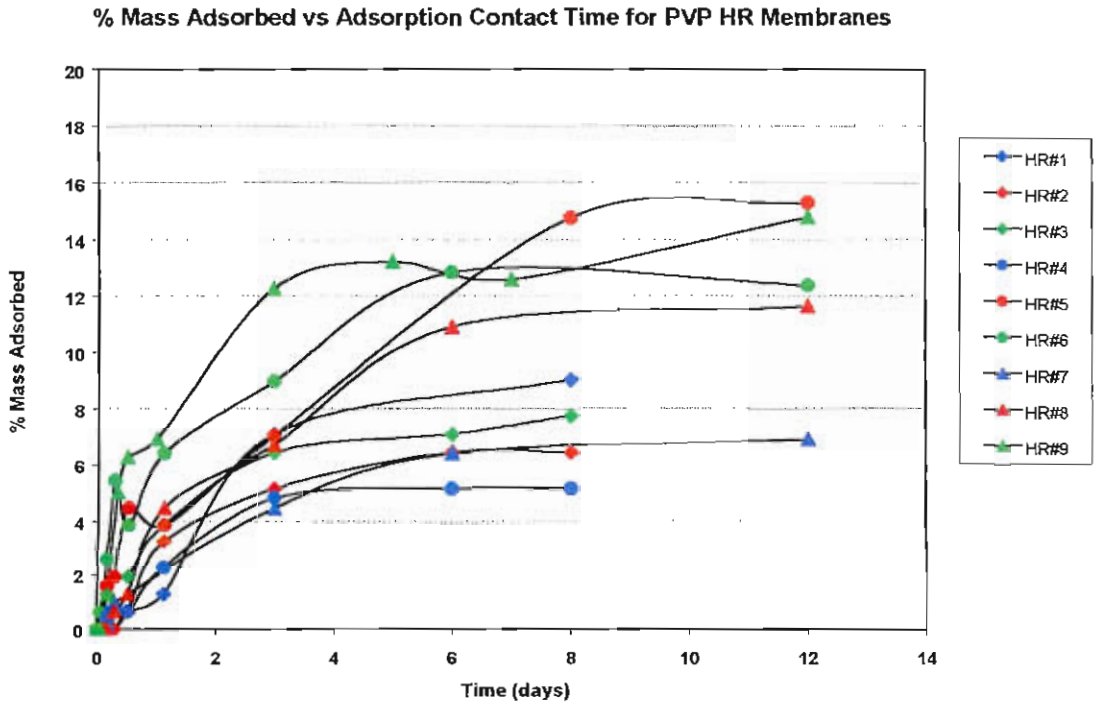

Figure 20 Percentage of mass adsorbed on PVP HR membranes

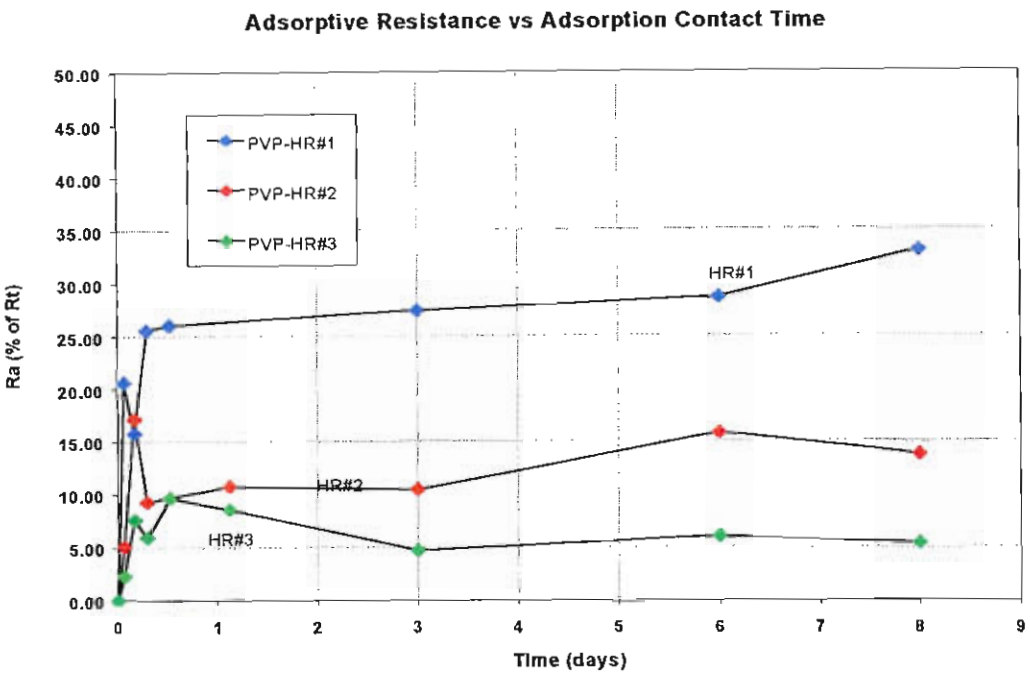

Figure 21 Adsorptive resistance of PVP HR 1-3 membranes

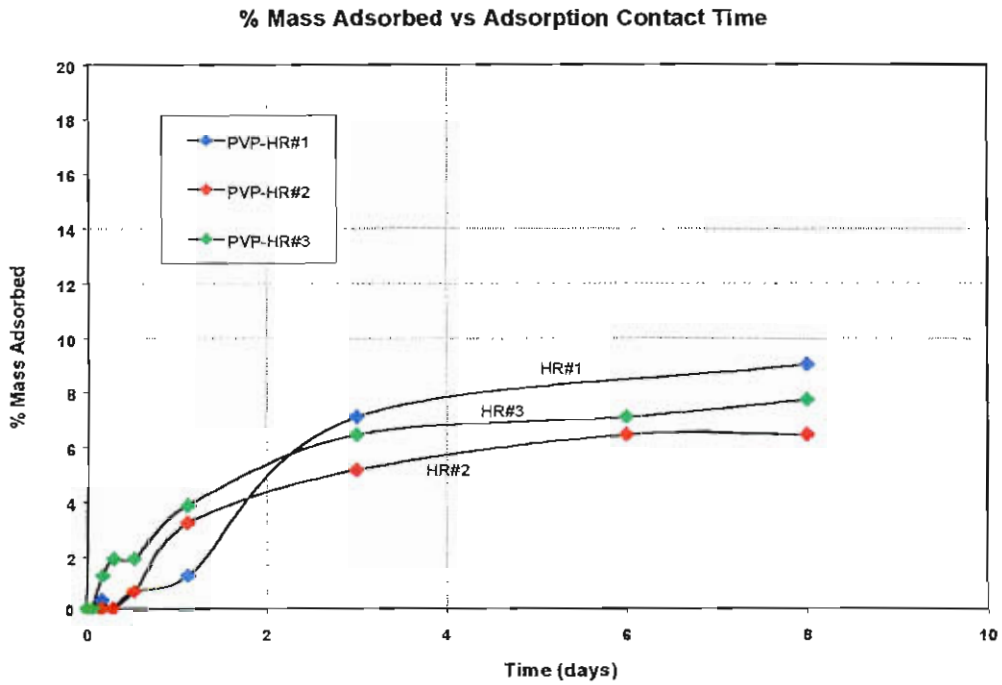

Figure 22 Percentage of mass adsorbed on PVP HR 1-3 membranes

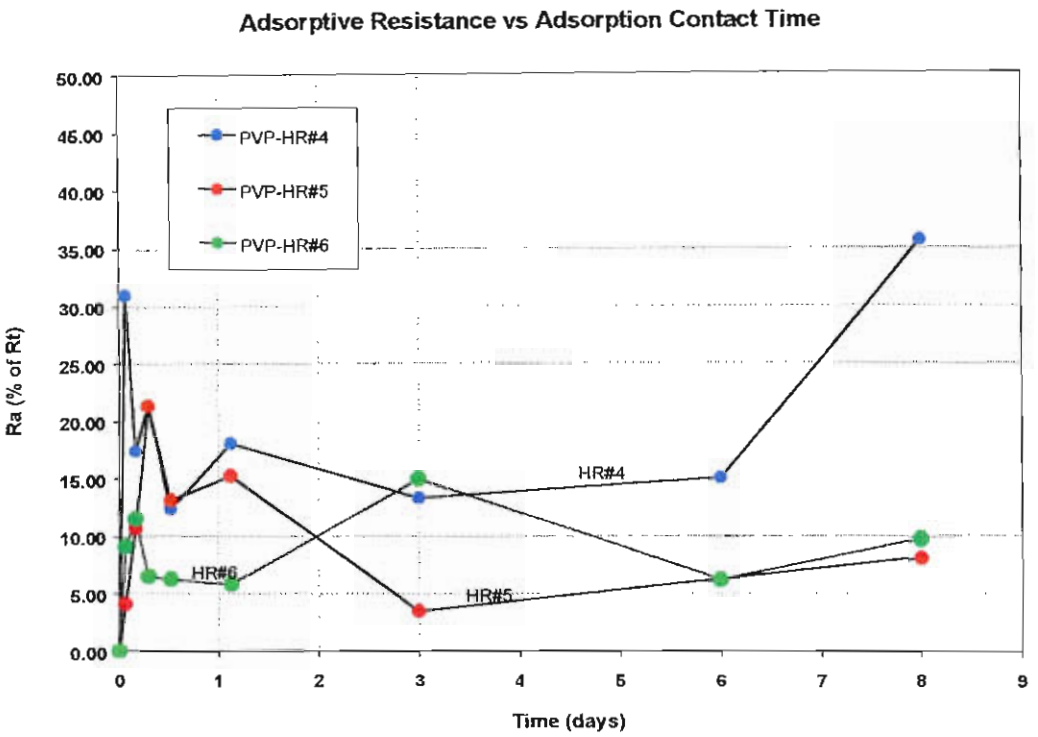

Figure 23 Adsorptive resistance of PVP HR 4-6 membranes

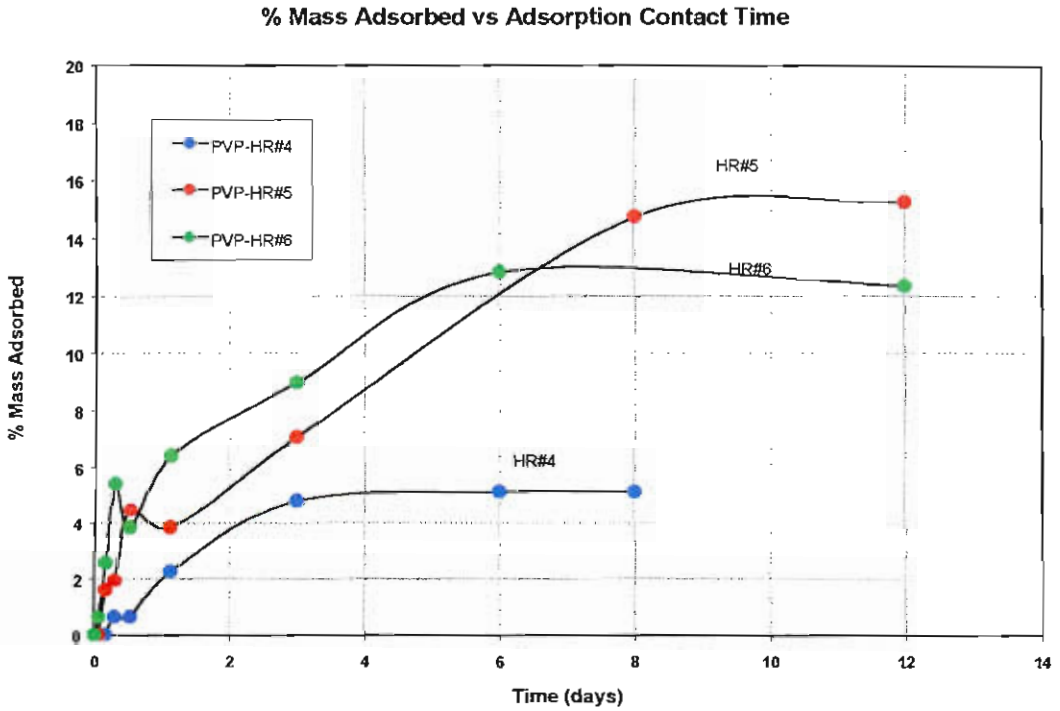

Figure 24 Percentage of mass adsorbed on PVP HR 4-6 membranes

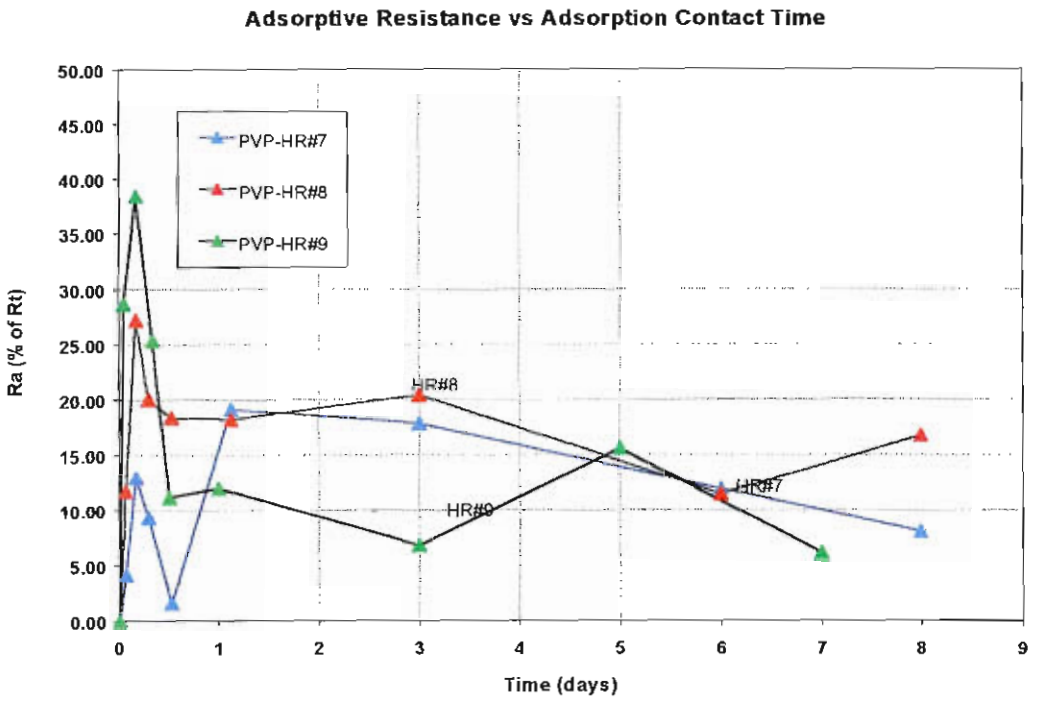

Figure 25 Adsorptive resistance of PVP HR 7-9 membranes

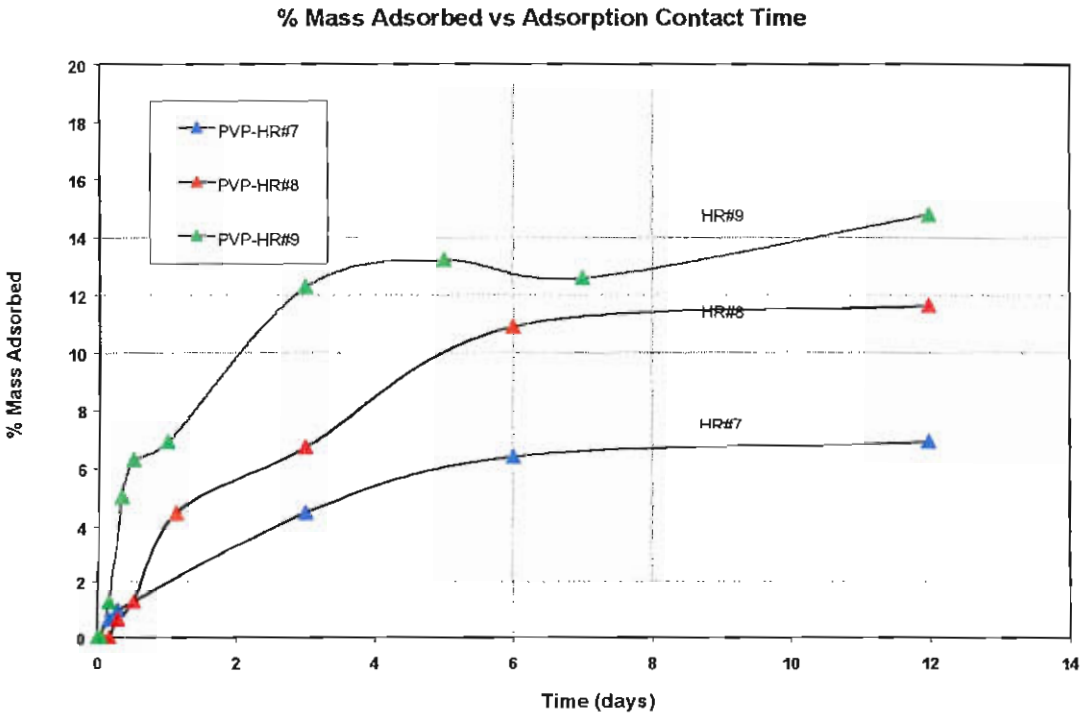

Figure 26 Percentage of mass adsorbed on PVP HR 7-9 membranes

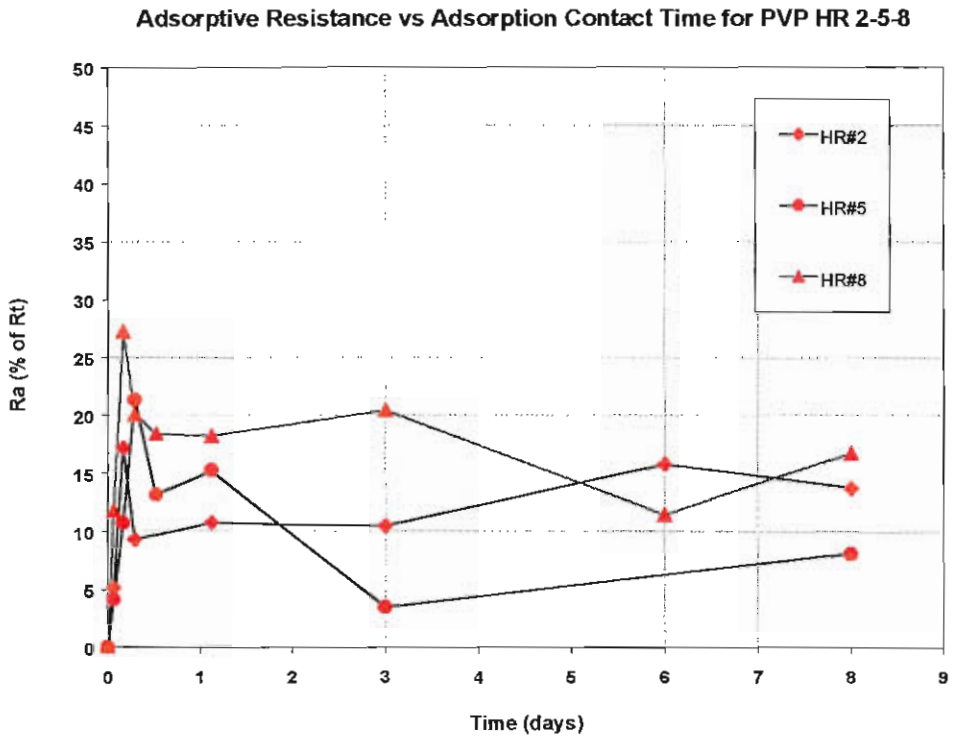

Figure 27 Comparison of Adsorptive Resistance of PVP HR 2-5-9

STIRRED DEADEND FILTRATION TESTS: FLUX DECLINE

Methods and Materials

Flux decline experiments were carried out using the Amicon deadend cell (Amicon, Minnetonka, MI). The experimental set up was same as the water permeability set up (see Figure 1). The permeate volume was measured by an electrical balance. To minimize solute build-up near the membrane surface (i.e. concentration polarization), the solution is stirred using a magnetic stirrer near the membrane surface.

Before the deadend filtration test, membranes were flushed with Milli-Q water at 20 psi for 10 minutes. An initial clean water flux was fixed at 150-200 LMH by adjusting transmembrane pressure in order to compare the relative flux declines of each membrane. Flux was monitored by measuring the total accumulated permeate weight every 30 seconds during the filtration of 300 ml of solution. Permeate samples were taken at total accumulated permeate volumes of 50, 100, 200, and 300 ml. Rejection was obtained by measuring retentate concentration at the end of experiment.

After flux decline tests, the surface of the membrane was observed in order to examine the pattern of gel layer formation. Then, the membrane was rinsed carefully with milli-Q water. The membrane was put back into the Amicon cell with the skin-side down and backflushed with Milli-Q water at 10 psi for 10 minutes. After backflushing, clean water flux was measured again at the same transmembrane pressure to check for any reversible fouling. The backflushed membrane was soaked in the 0.1 M NaOH solution for 0.5, 1, 2, and 4 hours to investigate the flux recovery rate by chemical cleaning. After chemical cleaning, the membrane was washed carefully with milli-Q water. Again, clean water flux was measured at the same transmembrane pressure to check flux recovery by chemical cleaning.

Results and Summary

Flux Decline

The PVP content of the membranes has a dramatic effect on flux decline (see Figure 28). The membrane with PS only (PVP HR 1) showed the highest flux decline

compared to other PVP membranes (PVP HR 2 and 3). A hydrophobic membrane tends to adsorb more humic substances than a hydrophilic membrane (Jucker and Clark, 1994). Therefore, in the case of hydrophobic membranes (PVP HR 1), a reduction of pore size or an increase of adsorptive resistance becomes greater, which results in a higher flux decline. An additional increase in the PVP content seemed to have no significant effect on flux decline (compare the flux decline curves of PVP HR 2 and 3). The PVP HR 2 membrane showed a little more flux decline compared to the PVP HR 3 membrane.

After filtration, the gel layer formation on the membrane surface was observed. The membrane with polysulfone only (PVP HR 1) showed a little darker color change than the other PVP membranes, which implies that the PS membranes adsorbed more SRHA than the PVP membranes. The membranes with PVP showed very little color change, and the gel was removed easily by spraying with clean water. For all membranes, there was a darker color change at the center of membranes, which implies that stirring at was not uniform across the membrane.

In order to investigate the effect of solids content on the flux decline, the membranes with the same amount of PVP content and with a different amount of PS content were also tested (PVP HR 2, 5, and 8). Regardless of solids content, no significant differences of flux decline were observed (see Figure 29).

Rejection and Flux Recovery

Rejection was calculated in two different ways. One is based on the retentate concentration after filtration (actual rejection, $r_{act} = \frac{C_r - C_p}{C_r}$), and the other is based on the feed concentration (apparent rejection, $r_{app} = \frac{C_f - C_p}{C_f}$). The membrane with PS only (PVP HR 1) showed a little higher rejection than the other PVP membranes (PVP HR 2 and 3). This higher rejection could be explained by more adsorption of SRHA in the case of polysulfone membrane, which would result in greater reduction of effective pore size. An additional increase of PVP content did not show any significant change in rejection. The rejection tends to increase with the solids content (from PVP HR 2 to PVR HR 5 and 8) as a result of decreased MWCO (see Table 4).

Overall, all these membranes showed a higher rejection (i.e. above 60 % rejection) compared to the SPEES-PS membranes (a previous set of membranes). In addition, the rejection in all cases did not change significantly during filtration, which implies that most of the adsorption occurred during the initial filtration stage, and the flux reached steady state quickly. A rejection value based on the retentate concentration was a little higher than a rejection based on the feed concentration because the concentration of the retentate increased as filtration proceeded.

After backflushing, most of the membranes except PVP HR 5 and 8 showed little flux recovery. However, most of adsorbed humic substances were not detached during backflushing. After chemical cleaning, most of color on the membrane surface were easily removed except for PVP HR 1. After soaking in 0.01M NaOH for 30 min, flux was recovered a little, but an additional period of chemical cleaning did not help flux recovery. Overall, the chemical cleaning as well as backflushing could not recover the flux completely, which implies that a considerable portion of adsorption results in very strong irreversible fouling.

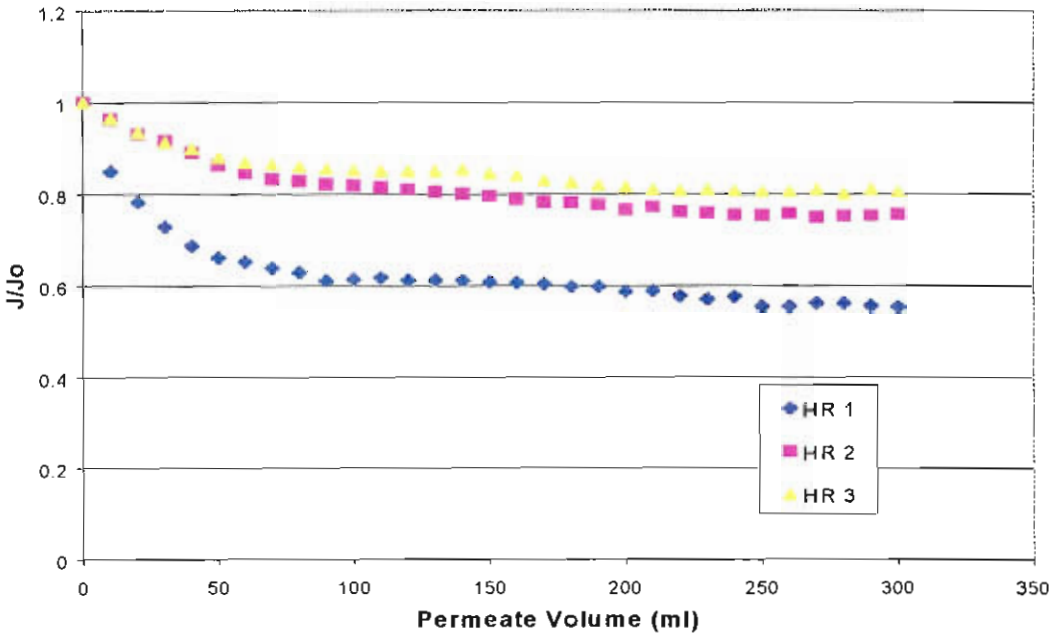

Figure 28 The effect of PVP on flux decline

(Humic Acid 5 mg/L, Ca^{2+} 5mg/L, Na_2HPO_4 0.001 M, pH 6.5)

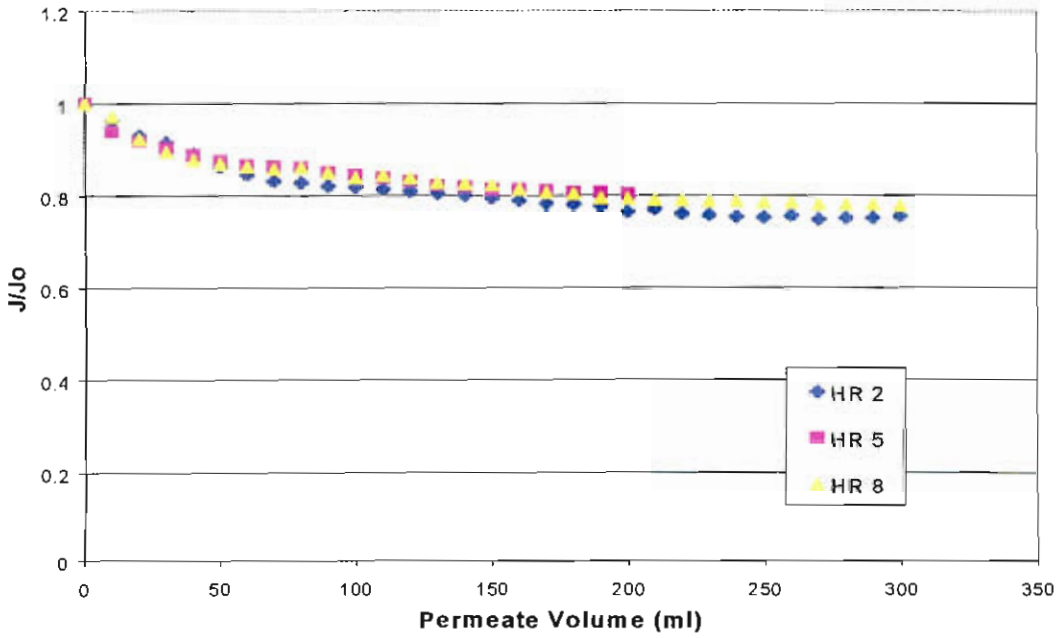

Figure 29 The effect of solid content on flux decline

(Humic Acid 5 mg/L, Ca^{2+} 5mg/L, Na_2HPO_4 0.001M, pH 6.5)

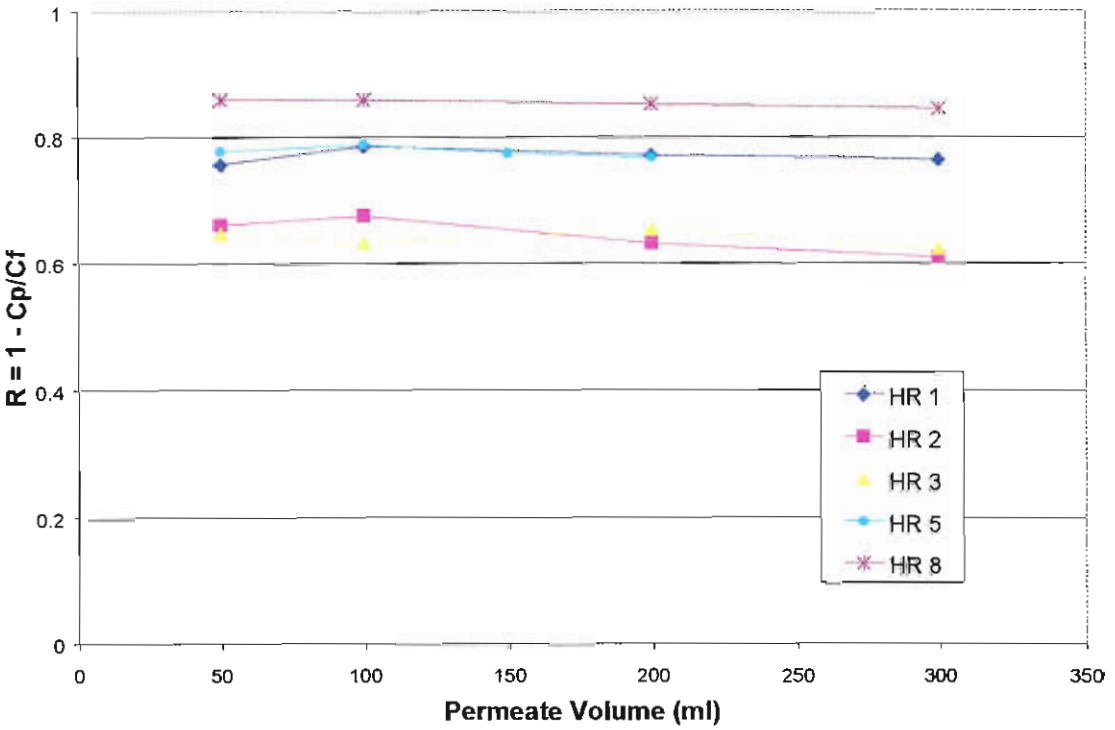

Figure 30a Apparent rejection (C_p permeate concentration, C_f : feed concentration)

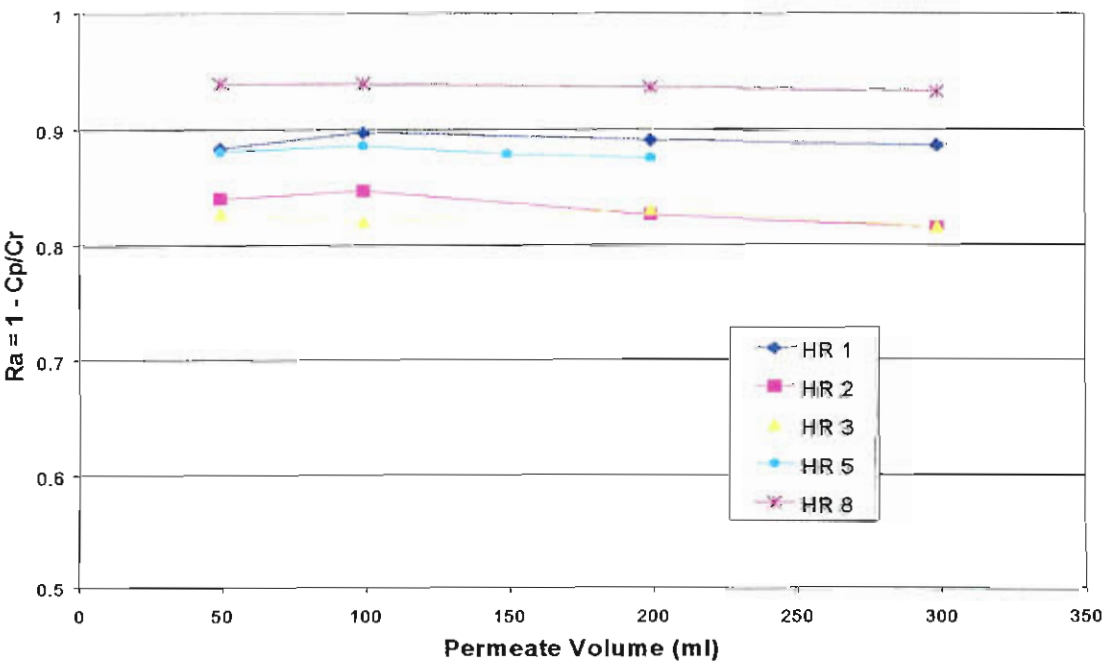

Figure 30b Actual Rejection

(C_p : permeate concentration, C_r : retentate concentration after filtration)

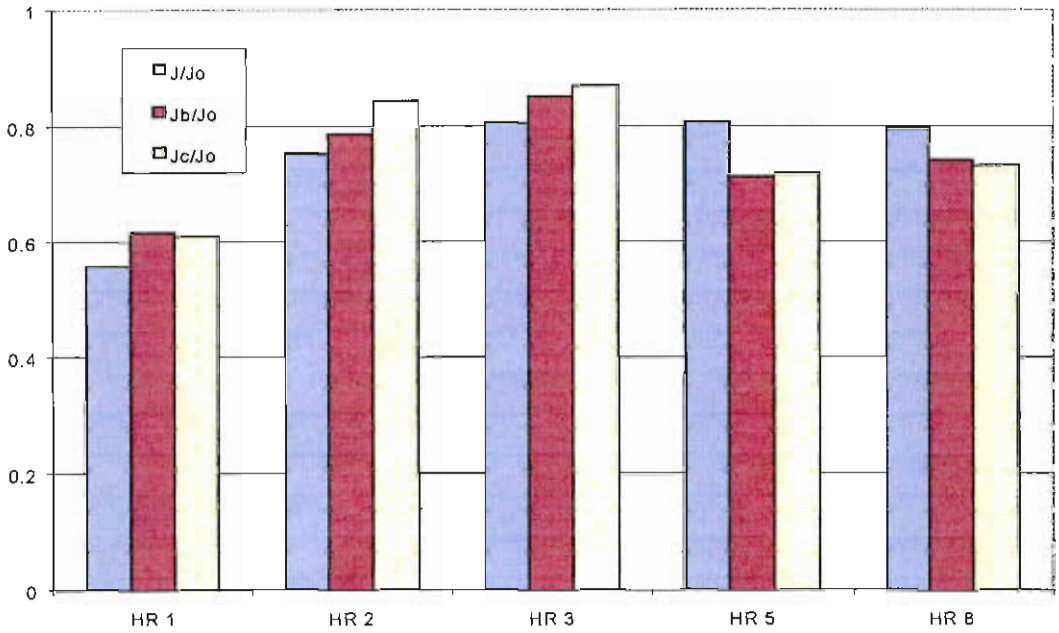

Figure 31 Flux recovery

(J : flux after filtration, J_0 : initial flux, J_b : flux after backflush, J_c : flux after 30 min. chemical cleaning with 0.1M NaOH)

BIBLIOGRAPHY

M. Oldani, G. Schock, *Characterization of ultrafiltration membranes by infrared spectroscopy, ESCA, and contact angle measurements*, Journal of Membrane Science, 43 (1989) 243.

D.T. Clark, W.J. Feast, *Application of ESCA to studies of structure and bonding in polymeric systems*, Rev. Macromol. Chem., C12(2) (1975) 191.

F.F. Stengaardh, *Characteristics and performance of new types of ultrafiltration membranes with chemically modified surfaces*, Desalination, 70 (1988) 207.

C.D. Wagner, W.M. Riggs, L.E. Davis, J.F. Moulder, G.E. Mullenberg, in *Handbook of X-ray photoelectron spectroscopy*, Perkin Elmer Corp., Physical Electronics Div., Eden Pririe, MN, (1979).

S. Lentsch, P. Aimar, J.L. Orozco, *Separation albumin-PEG: transmission of PEG through ultrafiltration membranes, Biotechnology and Bioengineering*, 41 (1993) 1039.

W.M. Deen, *Hindered transport of large molecules in liquid-filled pores*, AIChE Journal, 33 (1987) 1409.

M. Nyström, M. Lindström, E. Mathiasson, *Streaming potential as a tool in the characterization of ultrafiltration membranes*, Colloids Surfaces, 36 (1989), 297.

M. Nyström, H. Zhu, *Characterization of cleaning results using combined flux and streaming potential methods*, Journal of Membrane Science, 131 (1997) 195.

A.S. Brown, *A type of silver chloride electrode suitable for use in dilute solutions*, Journal of American Chemical Society, 56 (1934) 646

W.R. Bowen, X. Cao, *Electrokinetic effects in membrane pores and the determination of zeta-potential*, Journal of Membrane Science, 140 (1998) 267

C. Jucker and M.M. Clark, *Adsorption of aquatic humic substances on hydrophobic ultrafiltration membranes*, Journal of membrane Science 97 (1994) 37

K.J. Kim, A.G. Fane, C.J.D. Fell, and D.C. Joy, *Fouling mechanism of membranes during protein ultrafiltration*, Journal of Membrane Science, 68 (1992) 79

M. Cheryan, *Ultrafiltration and microfiltration handbook*, Technomic Publishing Co., (1998)

P.W. Akins, Physical Chemistry, Oxford University Press (1978)

A. Szymczyk, P. Fievet, M. Mullet, J.C. Reggiani, and J. Pagetti, *Comparison of two electrokinetic methods-electoosmosis and streaming potential-to determine the zeta-potential of plane ceramic membranes*, Journal of Membrane Science, 143 (1998) 189

Appendix AFM images of PVP-PS membranes

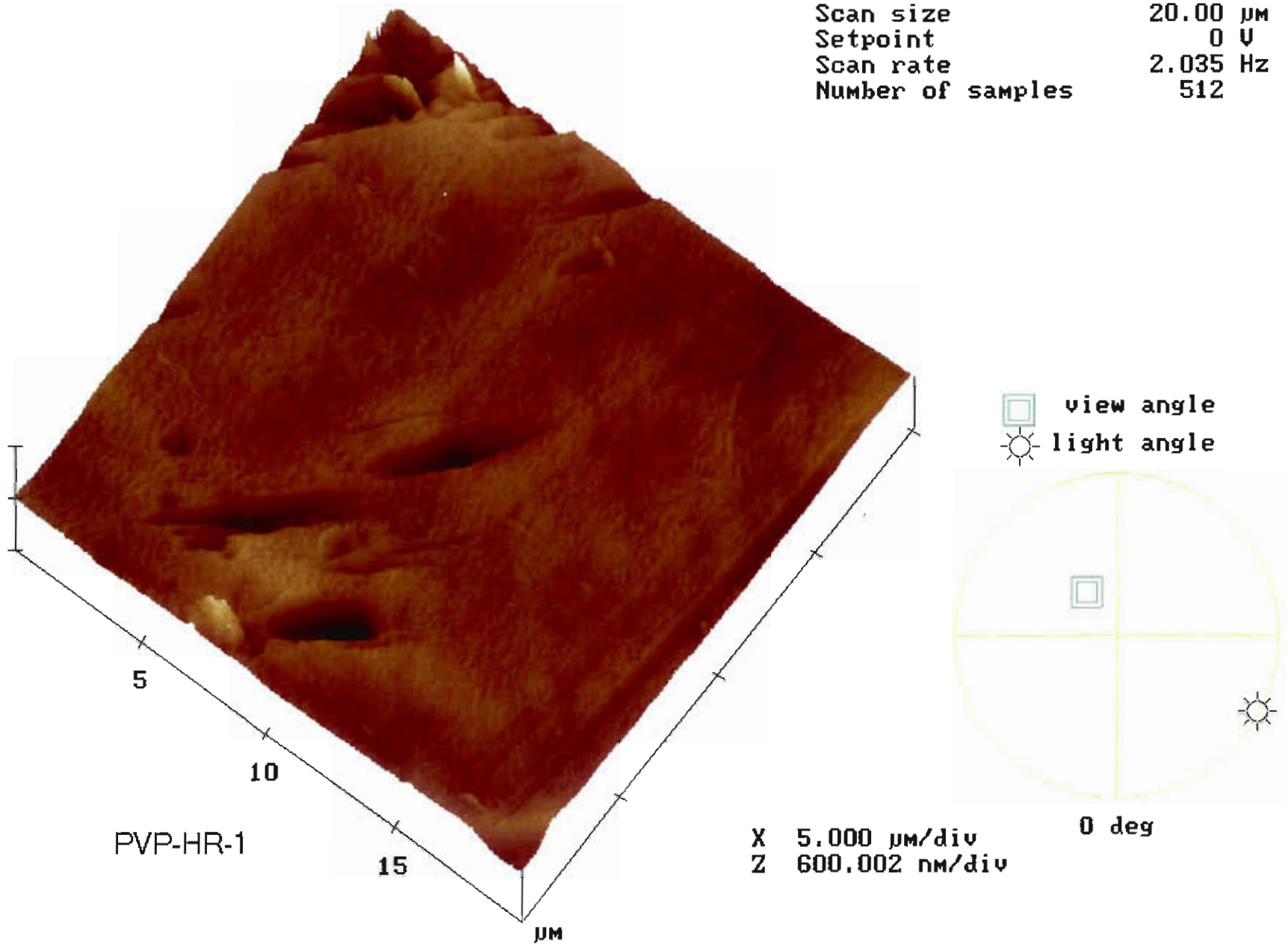
NanoScope Contact AFM
Scan size 20.00 µm
Setpoint 0 V
Scan rate 2.035 Hz
Number of samples 512
view angle
light angle
5
10
15
µm
PVP-HR-1
X 5.000 µm/div
Z 600.002 nm/div
0 deg

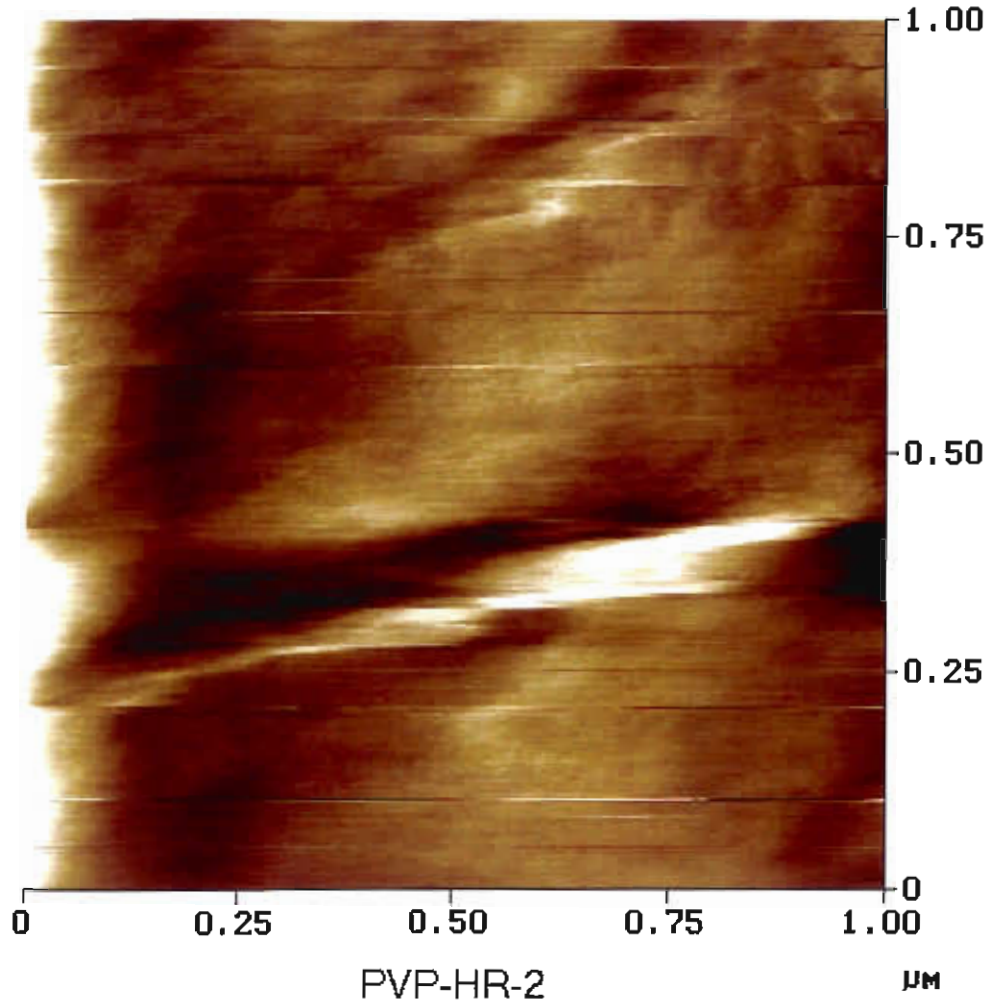

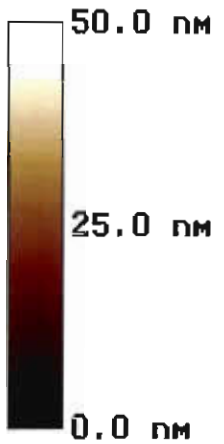

NanoScope	Contact AFM
Scan size	1.000 µm
Setpoint	9.000 V
Scan rate	2.035 Hz
Number of samples	512

pvp0201.001

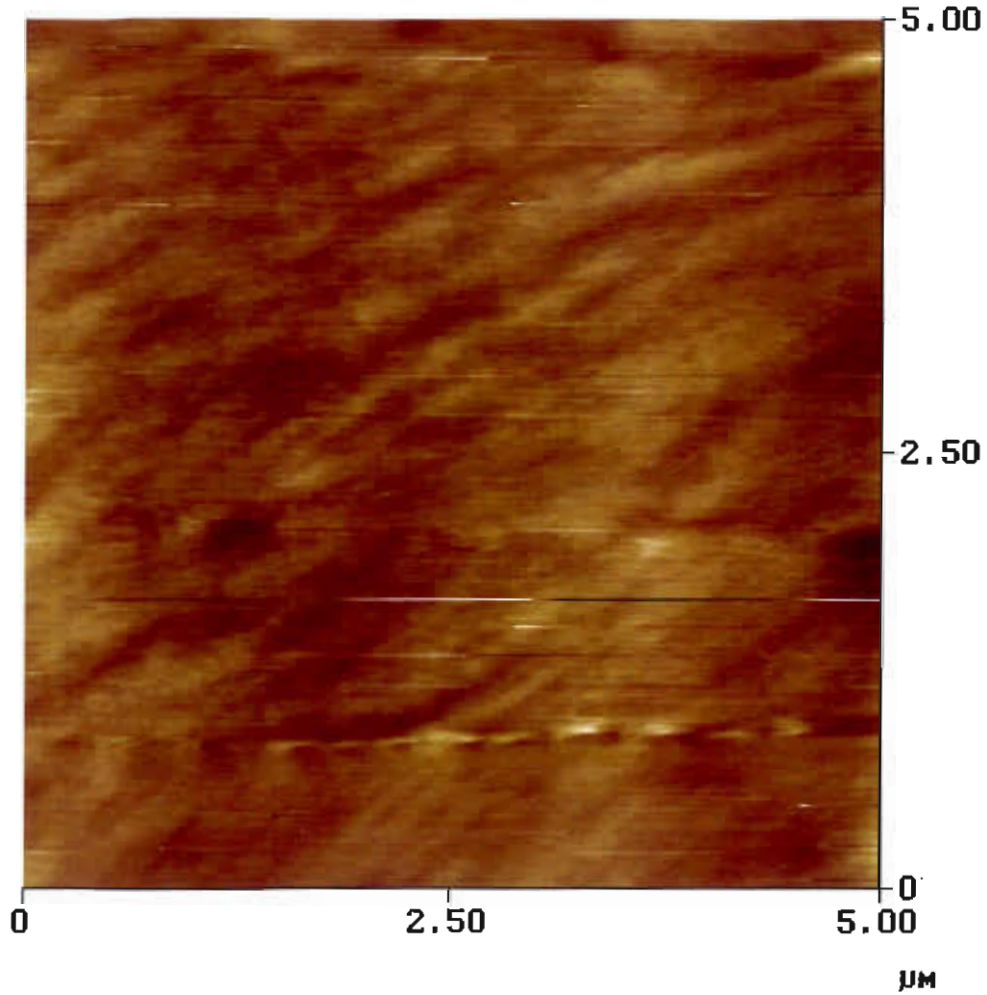

PVP-HR-3

NanoScope	Contact AFM
Scan size	5.000 µm
Setpoint	9.000 V
Scan rate	2.035 Hz
Number of samples	512

pvp0305.001

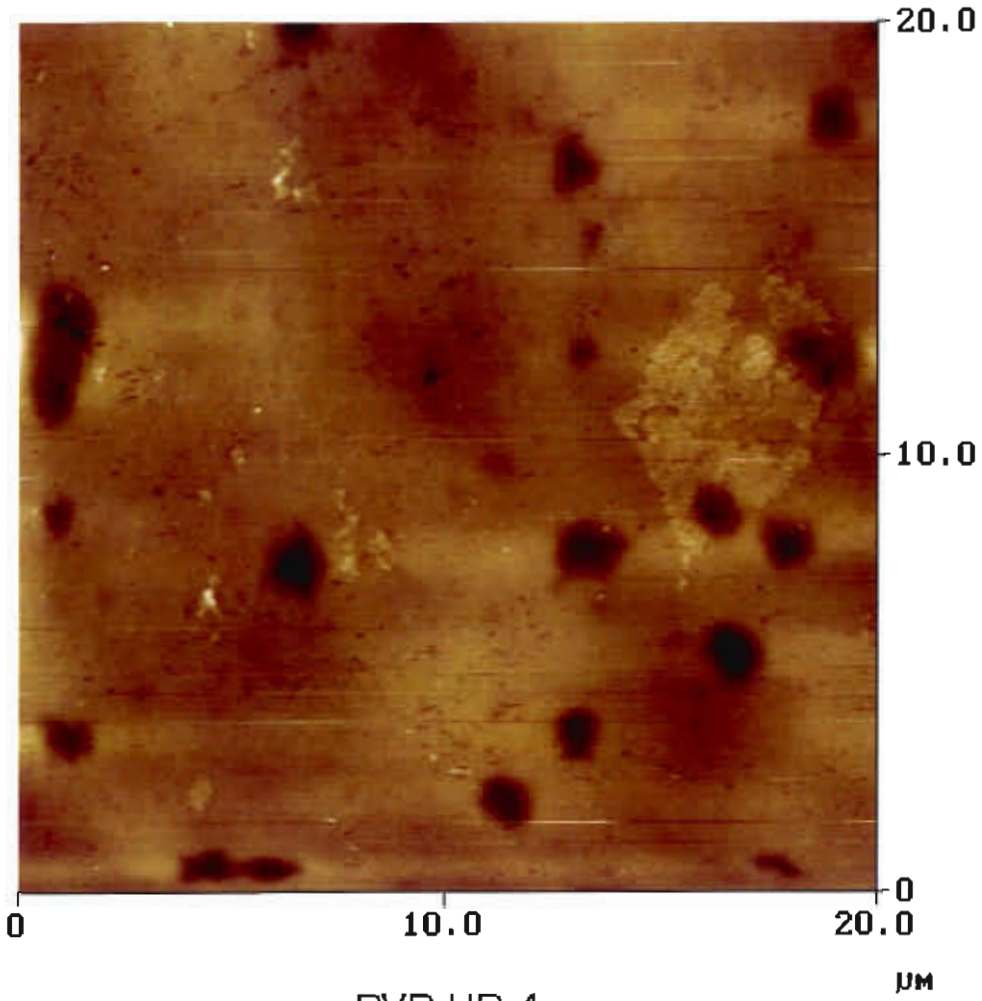

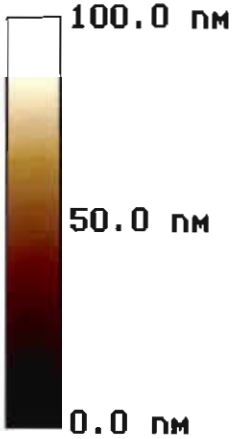

NanoScope	Tapping AFM
Scan size	20.00 µm
Setpoint	0.4468 V
Scan rate	1.077 Hz
Number of samples	512

PVP-HR-4

12021657.001

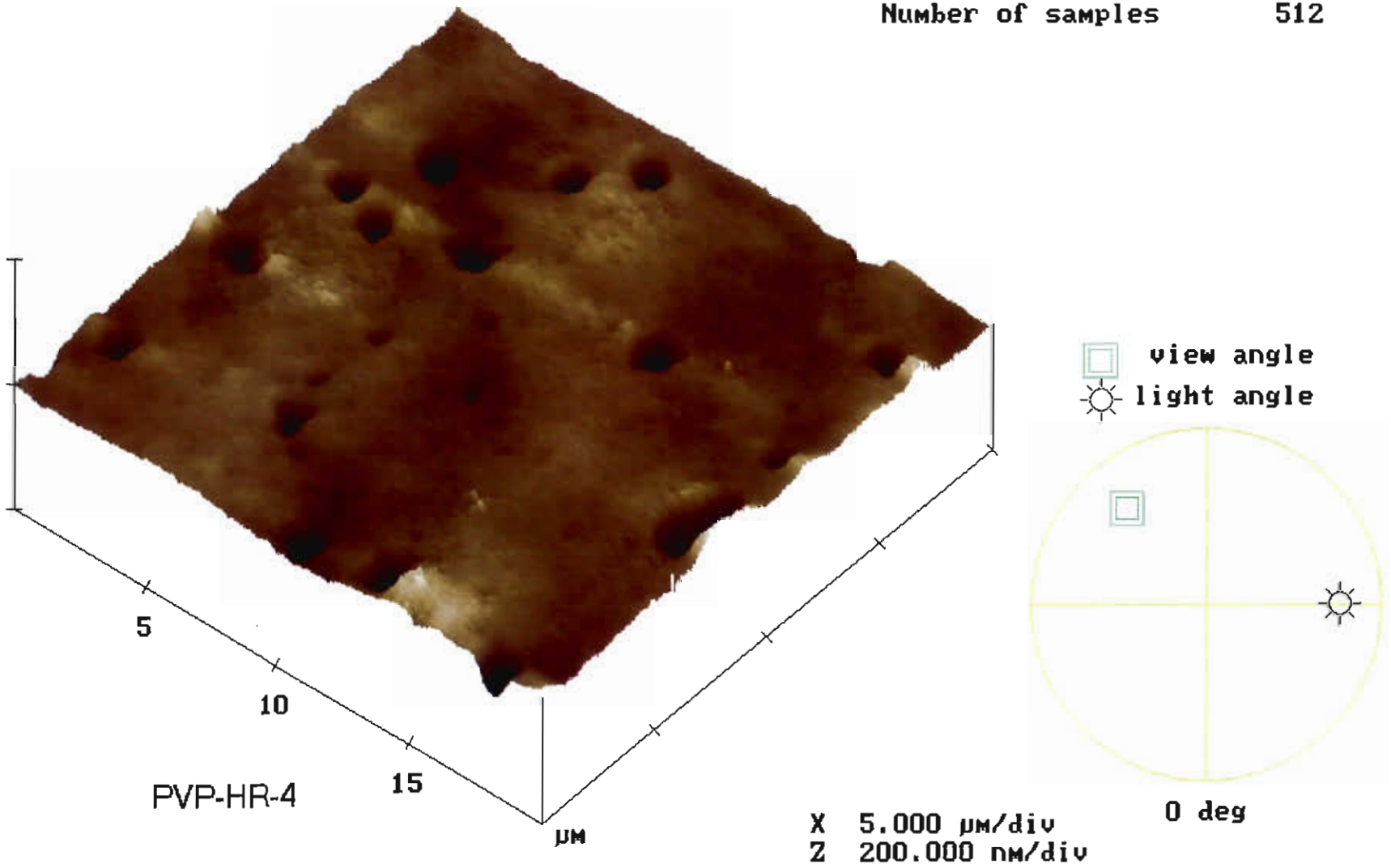
NanoScope Tapping AFM
Scan size 20.00 µm
Setpoint 0.3468 V
Scan rate 3.052 Hz
Number of samples 512
5
10
15
µm
PVP-HR-4
view angle
light angle
0 deg
X 5.000 µm/div
Z 200.000 nm/div

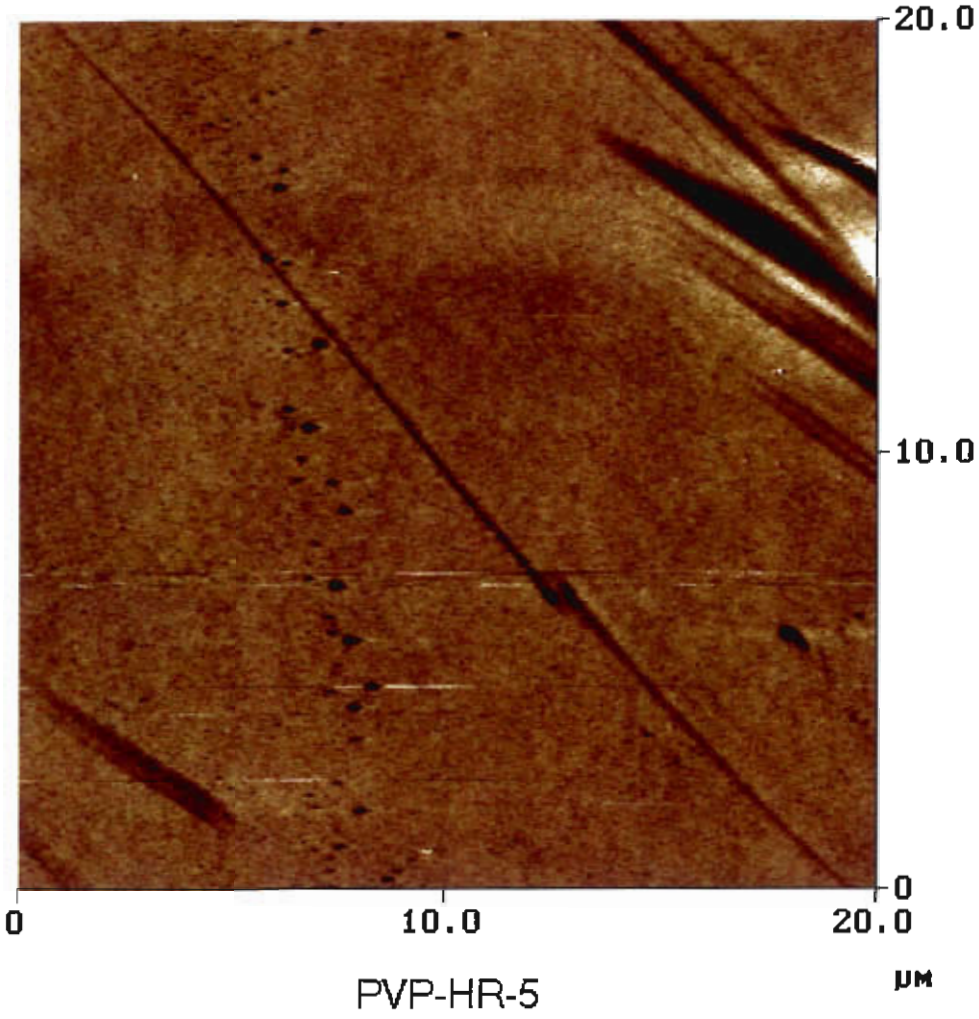

NanoScope	Tapping AFM
Scan size	20.00 µm
Setpoint	0.3451 V
Scan rate	3.052 Hz
Number of samples	512

12021958.001

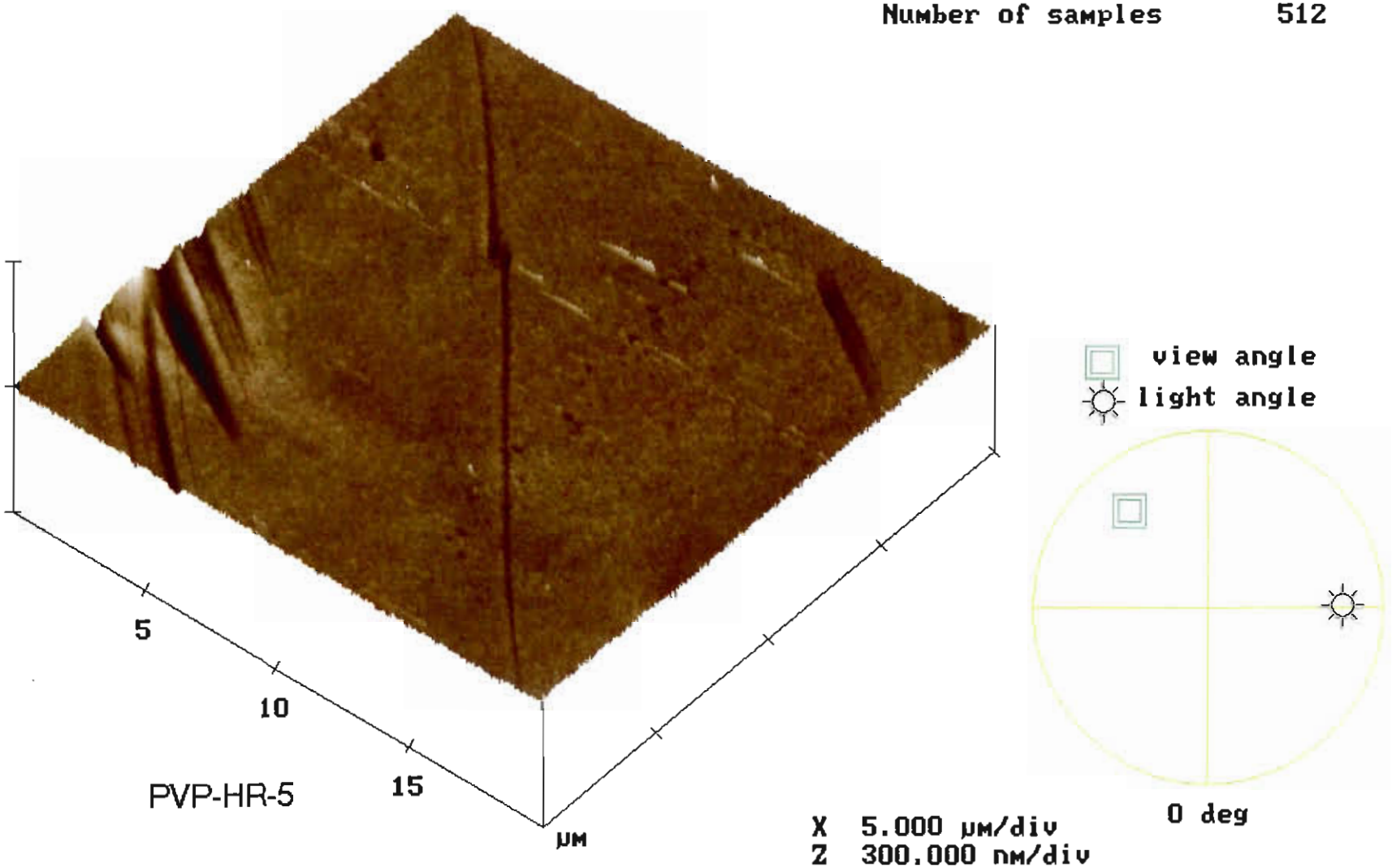
NanoScope Tapping AFM
Scan size 20.00 µm
Setpoint 0.3451 V
Scan rate 3.052 Hz
Number of samples 512
5
10
15
µm
PVP-HR-5
view angle
light angle
0 deg
X 5.000 µm/div
Z 300.000 nm/div

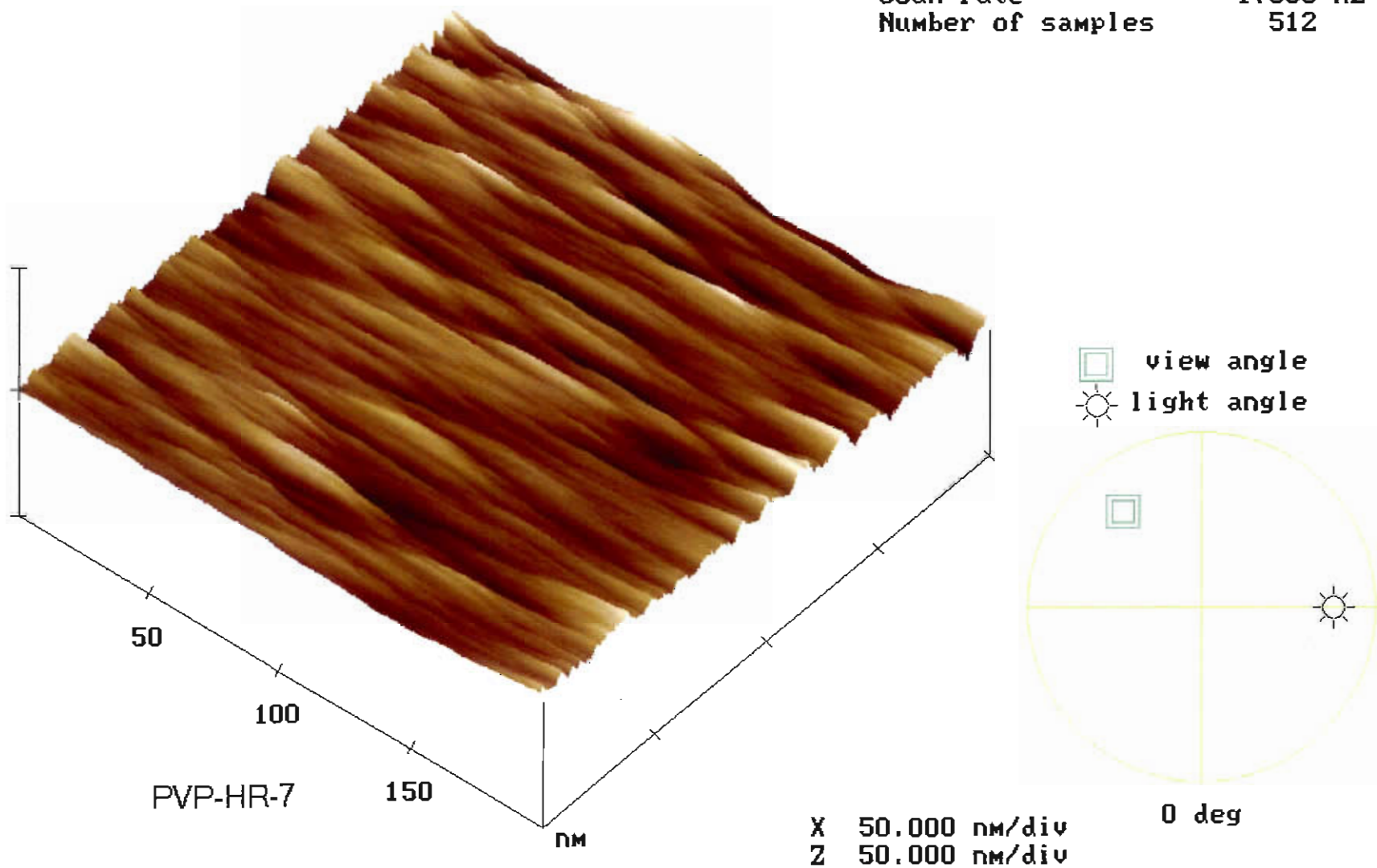
NanoScope Tapping AFM
Scan size 200.0 nm
Setpoint 0.1676 V
Scan rate 1.969 Hz
Number of samples 512
50
100
150
PVP-HR-7
nm
view angle
light angle
0 deg
X 50.000 nm/div
Z 50.000 nm/div

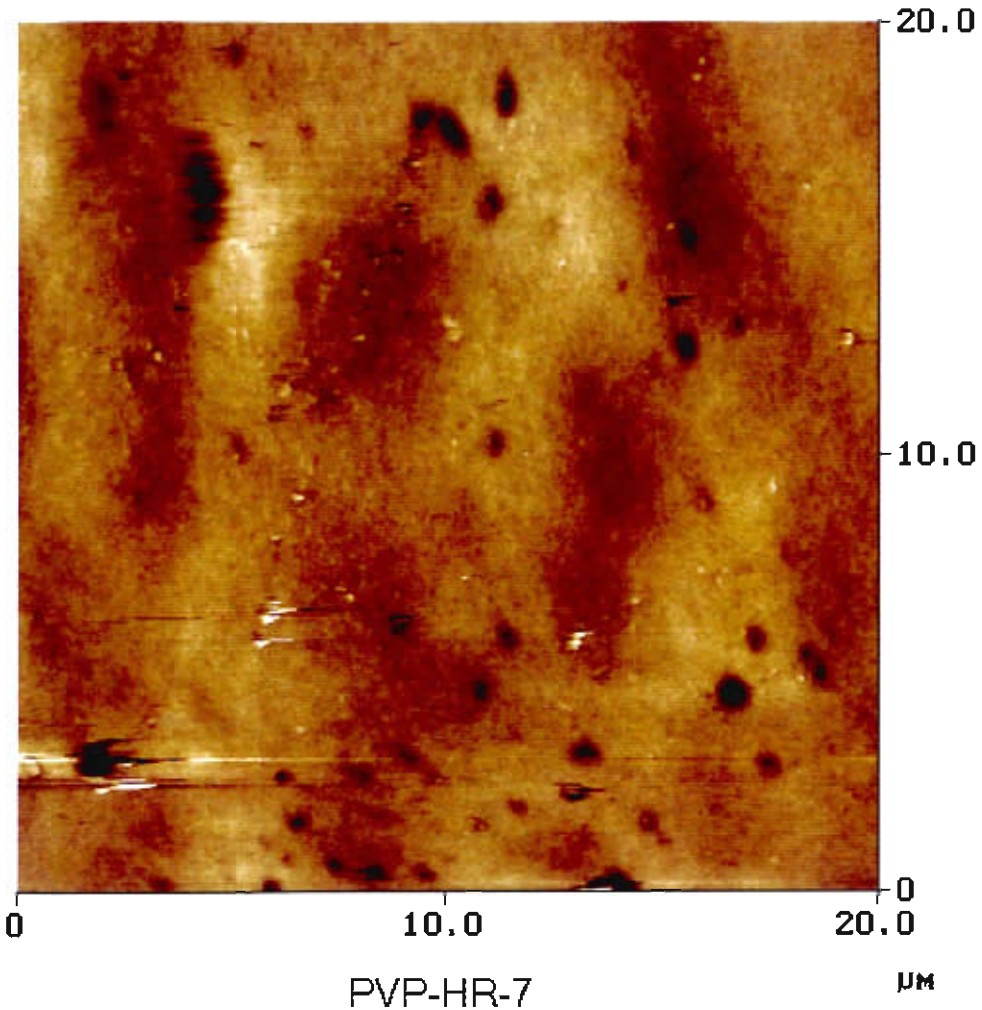

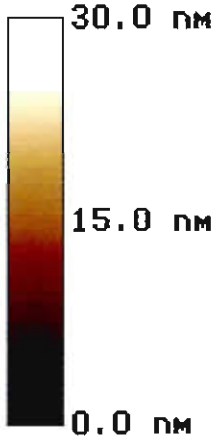

NanoScope	Tapping AFM
Scan size	20.00 µm
Setpoint	0.09801 V
Scan rate	1.969 Hz
Number of samples	512

02031807.001

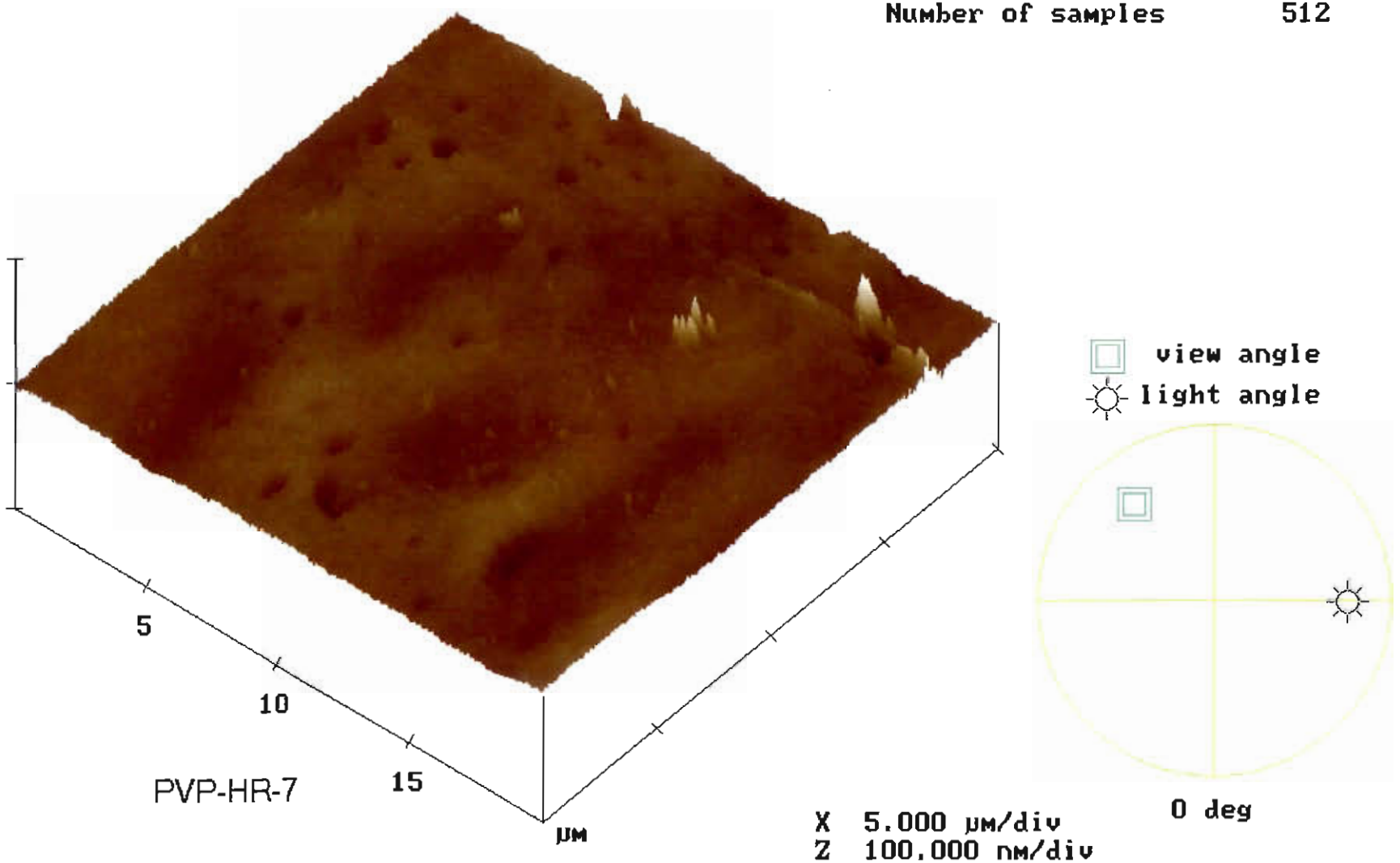
NanoScope Tapping AFM
Scan size 20.00 µm
Setpoint 0.09801 V
Scan rate 1.969 Hz
Number of samples 512
5
10
15
µm
PVP-HR-7
view angle
light angle
0 deg
X 5.000 µm/div
Z 100.000 nm/div

Part IV

The Effect of pH and Ionic Strength on the Diffusion Coefficient of Humic Acid, submitted to Environmental Science and Technology, 1999

The Effects of pH and Ionic Strength on the Diffusion Coefficient of Humic Acid

Yingge Wang, Corine Combe and Mark M. Clark*
Department of Civil and Environmental Engineering, University of Illinois
205 N. Mathews Avenue, Urbana, IL 61801, USA

ABSTRACT

Humic acid is a major component of natural organic matter in surface water and can cause serious fouling problems in membrane filtration processes for drinking water treatment. The transport of humic acid to the membrane surface and within membrane pores is related to its diffusivity. Thus, the diffusion coefficient of humic acid is an important mass transport parameter. Clark and Lucas (*J. Membr. Sci.*, 1998, *143*, 13-25) studied the diffusion and partitioning of humic acid into a porous ultrafiltration membrane and developed a model to predict how humic acid diffusivity changes under different pH and ionic strength conditions. In this work, the diffusion coefficient of humic acid was directly measured and compared to the predictions of the Clark and Lucas model. The experiments were conducted in a two-chamber diffusion cell separated by a track-etched membrane. The results show that the diffusivity of humic acid increases with decreasing pH and increasing ionic strength, which can be explained by the compaction of humic acid molecules at low pH and high ionic strength. The experimental measurements strongly support the predictions of the Clark and Lucas model.

* Corresponding author phone: 217 333-3629, email: m-clark3@uiuc.edu

1. Introduction

Humic substances are predominant species of natural organic matter (NOM). The properties of humic substances vary from source to source, because they are heterogeneous mixtures of biochemical degradation products from plant and animal residues, and synthesis activities of microorganisms (*1-4*). Suwannee River humic acid has been used in numerous environmental studies (*4-10*). Suwannee River humic acid is reported to contain 4.9 meq/g of carboxylic (COOH) and 2.9 meq/g of phenolic OH groups (*7*). Using small angle X-ray scattering, Thurman et al. (*8*) estimated that Suwannee River humic acid has a molecular weight of 5,000-10,000 Daltons. On the other hand, Bechett et al. (*4*) used the flow field fractionation method and estimated Suwannee River humic acid has a number average molecular weight (M_n) of 1,490 Daltons.

Humic acid has been implicated in fouling problems in the application of membrane technology for drinking water treatment. Previous studies showed that membrane fouling by humic acid is affected by many factors, including the hydrodynamic and operating conditions, the characteristics of the humic acid and membranes, and the pH and ionic strength of the feed (*6, 9, 10*). The transport of humic acid near the membrane and within the pores is related to its diffusivity, thus diffusion coefficient is an important mass transfer parameter. Uncertainties in diffusivity data can lead to serious errors in predicting the flux, especially in laminar flow system where the mass transfer coefficient is highly dependent on diffusivity (*11*).

For macromolecules like humic acid, solution chemistry, such as pH and ionic strength can affect the conformation and hydration of the molecules, and therefore will have an impact on the diffusivity (*11*). At neutral to high pH, humic acids are more negatively charged due to the ionization of COOH and phenolic OH groups. At low pH values, these functional groups are mostly protonated which makes humic acid less negatively charged and reduces intramolecular electrical repulsion (*6*). Metal ions such as calcium can bind to the negatively charged carboxylic groups, resulting in charge reduction and coiling of the molecule (*5*). Ghosh and Schnitzer (*12*) concluded that humic molecules can change from a large, flexible and linear shape at high pH, low ionic strength and low humic concentration, to a small, rigid and spherical shape at low pH, high ionic strength and high humic concentration.

There is limited work focused on the effects of pH and ionic strength on humic acid diffusivity. Cornel et al. (*1*) studied Aldrich humic acid adsorption in a fixed-bed granular activated-carbon adsorber and measured the external mass transfer coefficient, from which the diffusion coefficient of humic acid was estimated. They also determined the humic acid apparent molecular weight (MW) distribution by membrane fractionation. They found that humic acid MW decreased at high ionic strength; correspondingly, humic acid diffusivity was found to increase for these same conditions (*1*). More recently, Clark and Lucas (*5*) studied the kinetics of Suwannee River humic acid adsorption in a porous ultrafiltration membrane. They developed a one-dimensional diffusion and partitioning model which can be used to predict how humic acid diffusivity changes under different values of pH and ionic strength. Their model also predicts that humic acid

diffusivity will increase with decreasing pH and increasing ionic strength. However, the sources of humic acid in the studies of Cornel et al. (*1*) and Clark et al. (*5*) are different, so quantitative comparison of their results is not straightforward.

In this work, we directly measured the diffusion coefficient of humic acid. Several methods for measuring diffusion coefficient are described in the literature. Cussler (*13*) gave a thorough review on those techniques, including the diffusion cell, capillary method, infinite couple, Taylor dispersion analysis, and methods using Gouy, Mach-Zehnder and Rayleigh interferometers. The diffusion cell method is chosen in this research, because the equipment is easy to build and the technique is accurate (*13*).

There have been extensive studies on measurement of diffusion coefficient with diffusion cells (*13-22*). The original cell was built by Northrup and Anson in 1928 using a sintered disc (*14*). Their analysis is based on the assumption that the only mass transfer resistance is related to the solute transport through the sintered disc by molecular diffusion. This assumption requires no bulk flow through the sintered disc and no mass transfer limitation in boundary layers adjacent to the disk (*15*). This method required calibration with solutes of known diffusion coefficient, from which the cell constant was measured and further used to determine the diffusivity of other solutes. In the 1950s, Stokes (*16,17*) carefully investigated the operation of the diffusion cell and developed a new set-up using magnetic stirring to eliminate boundary layer effects. Malone and Anderson (*18*) further studied mass transfer in a diffusion cell and found that the cell constant was not really a constant even with intense mixing. A model was developed that considers the

total mass transfer resistance as the sum of resistances from the membrane itself, boundary layers and end effects (*18, 19*). Deen et al. (*19*) improved the resistance model by incorporating three constants k_1, k_2 and k_3 which characterized the mass transfer in the diffusion cell. They measured those constants and used them to determine the unknown diffusion coefficient of dextran (*19*). More recent work using diffusion cell method can be found in a paper by Lebrun and Junter (*20*). They simplified the resistance model by assuming that the stirring is sufficiently high and the membrane is porous enough so that the boundary layer resistances and end effect resistances could be neglected.

2. Materials and Methods

2.1 Diffusion Experiments

2.1.1 Diffusion cell

The diffusion cell constructed for this work (Figure 1) is a rectangular two-chamber Plexiglas cell with a membrane separating the left and right cells. Each chamber is 8.4 cm high, 6.6 cm long, and 7.1 cm wide. The exposed membrane area in the cell is 12.6 cm^2. At the beginning of the experiment, the left chamber in the cell was filled with a 300 ml solution, while the right chamber was filled with the same volume of Milli-Q water. Temperature was controlled by immersing the cell in a water bath connected to a Polystat Refrigerated Constant Temperature Circulator (model #12101-00, Cole Parmer). The solutions in both chambers were vigorously stirred by two magnetic stirrers positioned under the bath and cell. The stirrer bars are 3.81 cm long and 0.95 cm in diameter with a

ridge around in the middle. For all the diffusion tests, the stirring speed was fixed at 960 rpm, approximately the maximum speed attainable.

2.1.2 Membrane used in the diffusion cell

A track-etched Nuclepore polycarbonate membrane was used in the diffusion cell (model #111110, Costar, Inc). This type of membrane is created by bombarding a polycarbonate film with high energy heavy ions followed by chemical etching (*11*). The well distributed pores have a very uniform size and appear to have a straight cylindrical shape. This kind of membrane is considered ideal for diffusion cell measurements (*18-19, 21-22*). According to the manufacturer, the 111110 Nuclepore membrane used in this research had a pore diameter $d = 1$ μm, a thickness $l = 11$ μm, and a porosity $\varepsilon = 0.157$. After each test, the membrane was rinsed several times with Milli-Q water, then put into a beaker containing a 0.01% NaN_3 solution and stored in the refrigerator before being reused.

2.1.3. The mass transfer resistance model

The model used in the diffusion experiment begins with a pseudo steady state application of Fick's First Law. The solute diffuses across the membrane from the left to right chamber because of the concentration gradient. For one-dimensional diffusion through a porous membrane with uniform, parallel, and straight cylindrical pores, the flux across the membrane J is given by (*13, 18*):

$$J = k(C_l - C_r) \tag{1}$$

Where C_l and C_r are the concentration of the solution in left and right chamber respectively, and k is the mass transfer coefficient.

Mass balance equations for the left and right chambers can be written as (*13*):

$$V\frac{dC_l}{dt} = -JA \qquad V\frac{dC_r}{dt} = JA \tag{2}$$

Where V is the volume of the solution in the left and right chambers, and A is the membrane area in the cell. Combing equations (1) and (2) one obtains:

$$ln\frac{(C_l - C_r)_o}{(C_l - C_r)_t} = \frac{2Ak}{V}t \tag{3}$$

Hence, by plotting $ln\frac{(C_l - C_r)_o}{(C_l - C_r)_t}$ versus time, the slope $\frac{2Ak}{V}$ can be determined by linear regression analysis, and the value of k can be determined knowing the membrane area A and volume V. The total mass transfer resistance R_t is then:

$$R_t = \frac{1}{k} = \frac{2A}{V \times slope} \tag{4}$$

In a study of KCl diffusion, Malone and Anderson (*18*) modeled the total resistance to the mass transfer as the sum of the membrane resistance R_m, the boundary layer resistance R_b, and the end effect resistance R_e:

$$R_t = \frac{1}{k} = R_m + 2R_b + 2R_e \tag{5}$$

Where $$R_m = \frac{l}{D_p \varepsilon} \quad (6)$$

$$R_b = \frac{l}{k_b} = \frac{\delta}{D} \quad (7)$$

$$R_e = \frac{\pi r / 4}{D\varepsilon} \quad (8)$$

Here r is the pore radius, δ is the boundary layer thickness, D_p is the hindered diffusion coefficient in the pores, and D is the molecular diffusion coefficient of the solute. Both Malone and Anderson (*18*) and Deen et al. (*19*) pointed out that the boundary layer mass transfer coefficient k_b can be correlated with:

$$\frac{k_b a}{D} = \alpha \, N_{R_e}^{\gamma} \, N_{S_c}^{1/3} \quad (9)$$

Where $$N_{R_e} = \omega a^2 / \nu \quad (10)$$

And $$N_{S_c} = \nu / D \quad (11)$$

N_{Re} is the Reynolds Number based on the stirring speed ω and membrane radius a, N_{Sc} is the Schmidt Number, α and γ are dimensionless empirical constants, and ν is the kinematic viscosity of the solution. From the relationship between k_b and D shown in Eqn. (9), k_b can be expressed in terms of $D^{2/3}$, and Eqn. (5) can be taken as (*19*):

$$R_t = \frac{k_1}{D_p} + \frac{k_2}{D^{2/3}} + \frac{k_3}{D} \quad (12)$$

As pointed out by Deen et al. (*19*), k_1 k_2 and k_3 should depend on the membrane properties, the cell geometry and the stirring speed, but not on the nature of the solutes. They directly determined the values of k_1 and k_3 from independent measurement of r, ε,

and 1 as shown in equations (6) and (8) for Nuclepore track-etched polycabonate membranes. They used ^{14}C-sucrose, ^{14}C -glucose, and ^{14}C-urea to determine k_2.

In our experiments, membranes with 1 μm diameter pores were used in the diffusion cell. From the Renkin equation (*18, 21-22*):

$$\frac{D_p}{D} = (1-\lambda)^2(1-2.1044\lambda+2.0888\lambda^3-0.948\lambda^5) \tag{13}$$

where $$\lambda = \frac{r_s}{r} \tag{14}$$

and r_s is the Stokes-Einstein radius of the solute molecule. This equation shows that at the infinite pore size limit ($\lambda \to 0$), the diffusion coefficient in the pores D_p equals the bulk solution value D. Since in our experiments, $r >>> r_s$, $D_p \approx D$, and Eqn. (12) can be simplified to:

$$R_t = \frac{k_1+k_3}{D} + \frac{k_2}{D^{2/3}} \tag{15}$$

Since R_t can be directly measured from diffusion experiments, once we know constants (k_1+k_3) and k_2, D can be calculated from Eqn. (15). Considering the difficulty in directly verifying membrane properties, we decided to use solutes with known diffusion coefficients to determine the constants (k_1+k_3) and k_2, and then use these constants to determine the unknown diffusion coefficient of other solutes under the same experimental conditions.

2.1.4 Determination of the constants (k_1+k_3) and k_2

In the calibration tests, KCl, NaCl, $CaCl_2$, and sucrose were used to determine constants (k_1+k_3) and k_2. Their diffusion coefficients can be easily found in the literature (*23*). Diffusion coefficient values can be adjusted for small temperature changes with (*11*):

$$D_{T_2} = \frac{T_2 \mu_1}{T_1 \mu_2} D_{T_1} \tag{16}$$

Where, μ is the viscosity of the solution, which is also a function of temperature (*23*):

$$\log \frac{\mu_T}{\mu_{20}} = \frac{1.3272(20-T) - 0.001053(T-20)^2}{T+105} \tag{17}$$

For the salt diffusion experiments, the concentrations of NaCl, KCl and $CaCl_2$ were measured with a conductivity meter (model MC 230, Radiometer Analytical S.A. France). The conductivity probe was put directly into the right chamber to measure the increase of concentration due to the solute diffusion. The concentration in the left chamber was calculated from a mass balance. The conductivity of the solution was recorded every 5 minutes. The whole experiment lasted about 1 to 2 hours.

For the sugar diffusion test, the concentration of sucrose in each cell was measured by a TOC analyzer (Phoenix 8000, Dohrmann). Because the samples were consumed during TOC measurement, the volume of the solution in the diffusion cell decreased slightly after each sampling. During the test, 0.4 ml of solution was taken every 30 minutes from both chambers and then diluted 100 times by adding 39.6 ml of Milli-Q water to each sample. In this case, the overall loss of the solution in the cell was about 2% and its effect on the results of the diffusion test could be neglected. The experiment lasted about 8 hours. The accuracy of the TOC analyzer is approximately 0.5%.

2.1.5 Determination of diffusivity of humic acid

The humic acid in this study was Suwannee Humic Acid Reference purchased from the International Humic Substances Society. Appropriate amounts of humic acid powder, $CaCl_2$, and Na_2HPO_4 (10^{-3} M Na_2HPO_4 served as buffer in all experiments) were measured and put into a beaker. Milli-Q water was then added to about 80% of the total volume required. The solution in the beaker was well mixed by a magnetic stirrer for about 1 hour. Then a solution of 0.1 N HCl was added by pipet to adjust the pH to the desired values. The pH was determined with an Orion pH meter. When the pH stabilized, the solution in the beaker was carefully transferred to a clean flask, and Mill-Q water was added to the calibration line of the flask. A magnetic bar was then put into the flask and the solution was stirred overnight. A sheet of aluminum was used to completely cover the flask. The pH was checked again just before using the solution. Because we were only interested in humic acid diffusion, a solution containing the same concentrations of $CaCl_2$ and Na_2HPO_4 at the same pH was prepared with Milli-Q water, and served as the feed solution in the right chamber. Therefore, the pH and ionic strength in the solutions of both chambers were the same.

Membranes calibrated with the salts and sucrose were used for humic acid diffusion experiments. At the beginning of the diffusion experiment, the left chamber in the cell was filled with a 300 ml humic acid solution; and the right one was filled with the same volume of the corresponding solution described above. All humic acid solutions used in the experiments are described in Table 1.

The concentration of humic acid was measured with a Perkin Elmer Lambda 3b UV/VIS spectrophotometer (Perkin Elmer Oak Brook Instrument Division) in a 1-cm path-length quartz cell. The reference cell was filled with Milli-Q water. Two 3 ml samples were taken every 30 minutes from both chambers at the same time and poured back into the cell immediately after the UV measurement. The whole experiment lasted about 8 hours. The conductivity and temperature of HA solutions were monitored during the experiment. The pH of the final solutions was also checked. After termination of an experiment, the membrane was cleaned several times with Milli-Q water. A salt diffusion test was then conducted in the diffusion cell to check for fouling of the Nuclepore membrane by humic acid.

2.2 Adsorption

2.2.1 Adsorption experiments

The adsorption experiments were designed to investigate adsorptive fouling of porous and hydrophobic ultrafiltration membranes by humic acid. The reader is referred to two previous papers for a thorough description of the adsorption kinetics experiments (*5, 9*). The source of humic acid and the solution concentrations were identical to those used in the diffusion experiments. 250 ml of one of the humic acid solution shown in Table 1 was poured into a 473 ml semi-transparent glass jar, and a cleaned membrane was placed over the jar mouth, with the skin side facing the interior of the jar. A Teflon sheet and several sheets of aluminum foil were then placed over the membrane. The jar lid was then screwed on and the jar was turned upside down in order to contact the solution and

membrane. It was then placed on a gyrator shaker and was shaken during the entire adsorption period. The adsorption experiment usually lasted about 12 to 16 days depending on whether the final solution had reached equilibrium. The temperatures for all adsorption experiments were maintained at 22±2°C in a dark chamber (*5, 9, 24*). The ultrafiltration membrane used in this study was a polysulfone PM30 membrane (Amicon) with a nominal molecular-weight cut off of 30,000 Daltons. Atomic Force Microscope (AFM) images show that the surface of this membrane is smooth and porous. Humic acid concentration of the supernatant was measured by UV absorption (254nm). The difference of the concentration between the solution in the jar and the initial solution was used to determine the uptake of humic acid by the porous membrane over time.

2.2.2 Modeling the adsorption kinetics

The adsorption of humic acid on the PM30 membrane was modeled as one-dimensional diffusion and partitioning in a porous medium from a well stirred liquid without permeation (*5, 25*). With appropriate boundary and initial conditions, the solution of the diffusion equation with linear partitioning is (*5, 25*):

$$\frac{M_t}{M_e} = 1 - \sum_{n=1}^{\infty} \frac{2\alpha(1+\alpha)}{1+\alpha+\alpha^2 q_n^2} exp\left(-\frac{q_n^2 t}{\tau}\right) \qquad (18)$$

Here, M_t is the mass adsorbed at time t, M_e is the mass adsorbed at the equilibrium, and α is the ratio of mass adsorbed on the membrane to the mass remaining in the bulk solution. The fractional uptake of humic acid on the membrane at the equilibrium is (*5, 9*):

$$Fractional\ uptake = \frac{UV_0 - UV_f}{UV_0} = \frac{1}{1+\alpha} \tag{19}$$

Where UV_0 is the UV value at time = 0, and UV_f is the value at some point during adsorption. τ is the diffusion time scale defined as:

$$\tau = \frac{m^2}{D_{eff}} \tag{20}$$

and q_n are the roots of the generating function:

$$\tan q_n = -\alpha q_n \tag{21}$$

Here m is the membrane thickness and D_{eff} is the effective diffusion coefficient inside the membrane. The best fit of Eqn. (18) to the experimental data was obtained by adjusting the parameter τ until the difference between the measured and modeled values was minimized (*5*).

Clark and Lucas identified a new parameter in their analysis, the interaction parameter Km, which characterizes the strength of interaction between humic acid and the membrane. Km is the product of the membrane thickness and the linear partition coefficient K, and is calculated simply as (*5*):

$$Km = \frac{h}{\alpha} \tag{22}$$

Where h is the solution depth.

3. Results and Discussion

3.1 Diffusion Experiments

3.1.1 Determination of constants (k_1+k_3) and k_2

As shown in Figures 2 and 3, the plots of data from the salt and sugar calibration tests showed good linear relationships. In all cases, the regression coefficient R^2 was higher than 0.99. R_t values were then calculated from the slopes of the lines by linear regression. Using Eqn. (15), several combinations of two solutes can be used to obtain values of (k_1+k_3) and k_2. Table 2 provides the calculated (k_1+k_3) and k_2 values. We then averaged the three sets of data to provide the final values for (k_1+k_3) and k_2.

The constant (k_1+k_3) value is comparable to the one obtained by direct calculation ($7.08*10^{-3}$ cm) using data provided by the manufacturer and equations (6) and (8). In order to check the accuracy of these constants, we put them back into Eqn. (15) to recalculate the diffusion coefficients of the salts and sugar. The results were then compared to literature values corrected for temperature (*23*). As shown in Table 3, the differences between the calculated and published diffusion coefficients were quite small.

3.1.2 Determination of diffusion coefficient for humic acid

As shown in Figure 4, plots of data from the humic acid diffusion tests also demonstrated good linear relationships. R_t values were then calculated from the slope of each line, and using (k_1+k_3) and k_2 values determined from the calibration tests, the diffusion coefficients of humic acid solutions were calculated using Eqn. (15) and the Solver program in the EXCEL Spreadsheet. KCl diffusion tests prior to and after each humic

acid diffusion experiment showed that there was no pore narrowing due to humic acid adsorption in the Neclepore membrane pores. The pH and conductivity did not vary during the humic acid diffusion experiments. Table 4 gives the experimental conditions and measured diffusion coefficient values for humic acid.

The measured diffusion coefficients are comparable to the literature values (*1, 4*). Cornel et al. (*1*) estimated diffusion coefficients of Aldrich humic acid (with 0-100 mM NaCl and 1 mM Na_2HPO_4) to be in a range of approximately $2.3*10^{-6}$ to $3.3*10^{-7}$ cm^2/sec for pH between 5 and 10. Using the flow field-flow fractionation method, Beckett et al. (*4*) determined a diffusion coefficient for Suwannee humic acid of $3.23*10^{-6}$ cm^2/s, which falls within the range of values shown in Table 4. However, they used 0.05 M tris (hydroxy-methyl) aminomethane (TRISMA) as the carrier solvent. The concentration of humic acid was about 250 mg/l, pH was about 7.9 and the ionic strength was higher than that used here (*4*).

Figure 5 shows the effect of pH and calcium concentration on the diffusion coefficient of humic acid. When the pH of the humic acid solution is lowered or the calcium concentration is increased, the diffusivity of humic acid increases. This can be explained by the theory of Gosh and Schnitzer (*12*). They proposed that at low pH and high ionic strength, humic molecules become more coiled and compact, either due to the neutralization of carboxylic and phenolic OH groups or due to the complexation of humic acid with calcium ions. Thus, the diffusion coefficient of humic acid increases.

3.2. Adsorption Experiment

Measured and fitted values for the adsorption experiments are provided in Table 5. A comparison of Km parameters indicates that the interaction between the humic acid and PM30 membrane increases as the pH decreases or ionic strength increases. This can be explained in several ways. At lower pH, the carboxylic groups of humid acid are protonated and the charge of humic acid molecules becomes less negative. The membrane charge also becomes less negative as the pH is lowered. Thus the electrostatic barrier to the adsorption of humic acid on the membrane is weakened as pH decreases (*5, 9, 24*). At high ionic strength, the complexation of calcium ions with humic acid compacts the molecule and reduces the charge. This could presumably result in a denser packing of humic acid during adsorption, leading to greater overall humic acid adsorption (*5*).

3.3 Comparison of results from diffusion and adsorption experiments

With the adsorption and partitioning model (*5*), we can also estimate ratios of molecular diffusion coefficients at various physicochemical conditions using the fitted diffusion time scale τ and interaction parameter Km values. The molecular diffusion coefficient is related to the effective diffusion coefficient D_{eff} in a porous medium by the following equation (*26*):

$$D_{eff} = \frac{DT}{R} \tag{23}$$

Here T is the torturosity of the diffusion path in the membrane and R is the retardation coefficient (*26*):

$$R = 1 + \frac{K}{\varepsilon} \tag{24}$$

where K is the linear partition coefficient and ε is the membrane porosity. Assuming m and T are constant for a given membrane, manipulation of equations (20), (23), and (24) yields (*5*):

$$\frac{D^{(pH_1)}}{D^{(pH_2)}} = \frac{\tau^{(pH_2)}}{\tau^{(pH_1)}} \frac{Km^{(pH_1)}}{Km^{(pH_2)}} \tag{25}$$

where the subscripts 1 and 2 represent two different physicochemical condition. For humic acid solutions at different pH (but constant calcium concentration), we can calculate the ratio of molecular diffusion coefficient using Km and τ values (Table 5) and Eqn. (25). Those ratios can then be compared with the results of direct diffusion coefficient measurements in Table 4:

HA = 8mg/l, [Ca] = 33mg/l, pH from 4.8 → 6,

Model prediction (Eqn. 25): $D^{pH=4.8}/D^{pH=6} = 1.58$

Direct measurement: $D^{pH=4.8}/D^{pH=6} = 1.63$

HA = 8mg/l, [Ca] = 11mg/l, pH from 4.8 → 6,

Model prediction (Eqn. 25): $D^{pH=4.8}/D^{pH=6} = 1.08$

Direct measurement: $D^{pH=4.8}/D^{pH=6} = 1.22$

These results show that the ratios of humic acid diffusivity at different pH predicted using Eqn. (25) are comparable to those obtained by direct measurement in the diffusion cell.

In order to investigate the effect of ionic strength on the diffusivity of humic acid, we can make further calculations for humic acid solutions at the same pH but different calcium concentrations (substitute calcium concentration 1 for pH_1 and calcium concentration 2 for pH_2):

HA = 8mg/l, pH = 4.8, [Ca] from 33mg/l → 11mg/l

Model prediction (Eqn. 25): $D^{Ca=33}/D^{Ca=11} = 1.53$

Direct measurement: $D^{Ca=33}/D^{Ca=11} = 1.44$

HA = 8mg/l, pH = 6.0, [Ca] from 33mg/l → 11mg/l

Model prediction (Eqn. 25): $D^{Ca=33}/D^{Ca=11} = 1.05$

Direct measurement: $D^{Ca=33}/D^{Ca=11} = 1.07$

Again, the model predictions (Eqn. 25) are quite comparable to the direct measurements. The direct measurement of humic acid diffusivity as a function of the pH and ionic strength lends support to the diffusion and partitioning model developed previously (*5*).

4. Acknowledgement

The authors thank the National Water Research Institute, Lyonnaise des Eaux, and the American Water Works Association Research foundation for their financial support. We would also like to thank Professors Francis DiGiano and John Anderson for sharing some of their ideas on measurement of diffusion coefficient.

Reference:

[1] Cornel, P.K., Summers, R.S., and Roberts, P.V. *J. Colloid Interface Sci.*, **1986**, *110(1)*, 149-164.

[2] Aiken, G. and Cotsaris, E. *Jour. AWWA,* **1995**, *87(1)*, 36-45.

[3] Avena, M.J. and Koopal, L.K. *Environ. Sci. Technol*, **1998**, *32*, 2572-2577.

[4] Beckett, R., Zhang, J. and Giddings, J.C. *Environ. Sci. Technol.*, **1987**, *21(3)*, 289-295.

[5] Clark, M.M. and Lucas, P. *J. Membr. Sci.,* **1998**, *143*, 13-25.

[6] Braghetta, A., DiGiano, F. A., and Ball, W.P. *J. Environ. Eng.*, July **1997**, *123(7)*, 628-641.

[7] Thorn, K.A., in R.C. Averret, J.A. Leenheer, D.M. McKnight and K.A. Thorn (Eds), Humic substances in the Suwannee River, Geogia: interactions, properties, and proposed structures, Open-File Rep. U.S. Geol. Surv., **1989**, No. 87-557, 251-311.

[8] Thurman, E.M., Wershaw, R.L., Malcolm, R.L. and Pinckney, D.J. *Org. Geochem.*, **1982**, *4*, 27-35.

[9] Jucker, C. and Clark, M.M. *J. Membr. Sci.*, **1994**, *97*, 37-52.

[10] Combe, C., Molis, E., Lucas, P., Riley, R., and Clark, M.M. *J. Membr. Sci.,* **1999**, *154*, 73-87.

[11] Cheryan, M. Ultrafiltration and microfiltration handbook. Technomic Publishing Co. Inc., **1998**, p. 52, 159-162.

[12] Ghosh, K., and Schnitzer, M. *Soil Sci.*, **1980**, *129(5)*, 266-276.

[13] Cussler, E. L. Diffusion: mass transfer in fluid systems. Cambridge University Press, **1984**, 132-143.

[14] Mills, R.and Woolf, L.A. The diaphragm cell: theory and practice of the diaphragm cell for liquid diffusion measurements. Diffusion Research Unit, Research School of Physics Sciences, Australian National University, Canberra, A.C.T., Australia, **1968**, p.1-3, 22, 44.

[15] Holmes, J.T., Wilke, C.R., and Olander, D.R. *J. Phys. Chem.*, **1963**, *67*, 1469-1472.

[16] Stokes, R.H. *J. Am. Chem. Soc.*, **1950**, *72*, 763-767.

[17] Stokes, R.H. *J. Am. Chem. Soc.*, **1950**, *72*, 2243-2247.

[18] Malone, D.M., and Anderson, J.L. *AIChE Journal*, **1977**, *23(2)*, 177-184.

[19] Deen, W.M., Bohrer, M.P., and Epsteen, N.B. *AIChE Journal*, **1981**, *27(6)*, 952-959.

[20] Lebrun, L. and Junter G.A. *J. Membr. Sci.*, **1994**, *88*, 253-261.

[21] Kathawalla, I.A., Anderson, J.L. *Ind. Eng. Chem. Res.*, **1988**, *27(5)*, 866-871.

[22] Kathawalla, I.A., Anderson, J.L. and Lindsey, J.S. *Macromolecules*, **1989**, *22(3)*, 1215-1219.

[23] Handbook of chemistry and physics, 56th edition, **1975-1976**, F-60 and F-49.

[24] Jucker, C.A., Interactions between aquatic humic substances and ultrafiltration membranes. Master's thesis, University of Illinois at Urbana Champaign, **1993**.

[25] Crank, J. The mathematics of diffusion. Oxford University Press, Inc., New York, **1975**, p. 56-57.

[26] Clark, M.M. Transport modeling for environmental engineers and scientists. John Wiley & Sons, Inc., New York, **1996**, p. 270.

List of tables:

List of figures:

Table 1. Initial humic acid solutions in the left chamber

HA (mg/l)	Na_2HPO_4 (M)	[Ca] (mg/l)	pH
8	10^{-3}	11	3.0
8	10^{-3}	11	4.8
8	10^{-3}	11	6.0
8	10^{-3}	33	3.0
8	10^{-3}	33	4.8
8	10^{-3}	33	6.0

Table 2. Model constants using sucrose, NaCl, KCl and $CaCl_2$

	NaCl and sucrose	$CaCl_2$ and sucrose	KCl and sucrose	Average
k_2 ($cm^{1/3}s^{1/3}$)	0.2526	0.2725	0.2952	0.2734
k_1+k_3 (cm)	$8.008*10^{-3}$	$7.668*10^{-3}$	$7.281*10^{-3}$	$7.652*10^{-3}$

Table 3. Comparison between literature and calculated diffusion coefficients

Solute	Temperature (°C)	D from literature (cm^2/s)	D calculated (cm^2/s)	Difference (%)
0.01M KCl	22.5	$1.79*10^{-5}$	$1.762*10^{-5}$	1.6
0.01M NaCl	24.0	$1.50*10^{-5}$	$1.525*10^{-5}$	1.7
0.01M $CaCl_2$	23.0	$1.126*10^{-5}$	$1.13*10^{-5}$	< 0.1
0.38% Sucrose	23.0	$4.94*10^{-6}$	$5.183*10^{-6}$	4.9

Table 4. Diffusion coefficients of humic acid solutions at various pH and ionic strength

HA (mg/l)	[Ca] (mg/l)	pH	T (°C)	Slope (1/min)	R_t (s/cm)	D ($10^{-6}cm^2/s$)
8	11	6.0	23.2-23.8	102.65	4896.63	2.30
8	11	4.8	23.4-23.6	122.83	4092.16	2.80
8	11	3.0	21.7-22.2	159.71	3147.20	3.79
8	33	6.0	23.5-24	108.4	4636.90	2.46
8	33	4.8	23.4-23.9	169.85	2959.32	4.02
8	33	3.0	23.7-24.1	186.61	2693.53	4.52

Table 5. Measured and fitted parameters for adsorption tests

HA (mg/l)	[Ca] (mg/l)	pH	Fractional uptake	α	τ (days)	Km (cm)
8	11	6.0	0.12	7.0	2.9	0.97
8	11	4.8	0.29	2.5	8	2.9
8	33	6.0	0.32	2.1	9.4	3.3
8	33	4.8	0.39	1.6	8.1	4.5

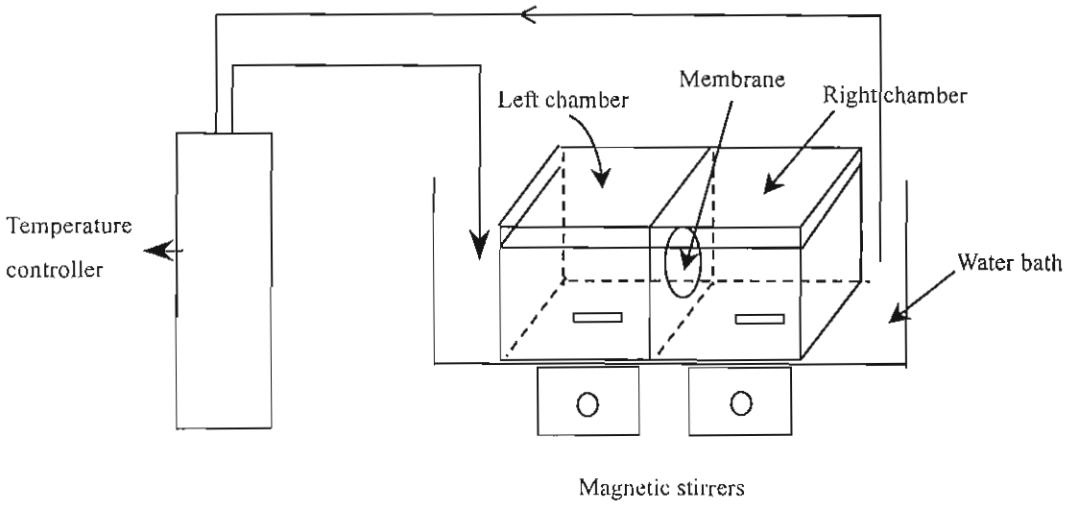

Figure 1. The schemetic representation of the diffusion cell

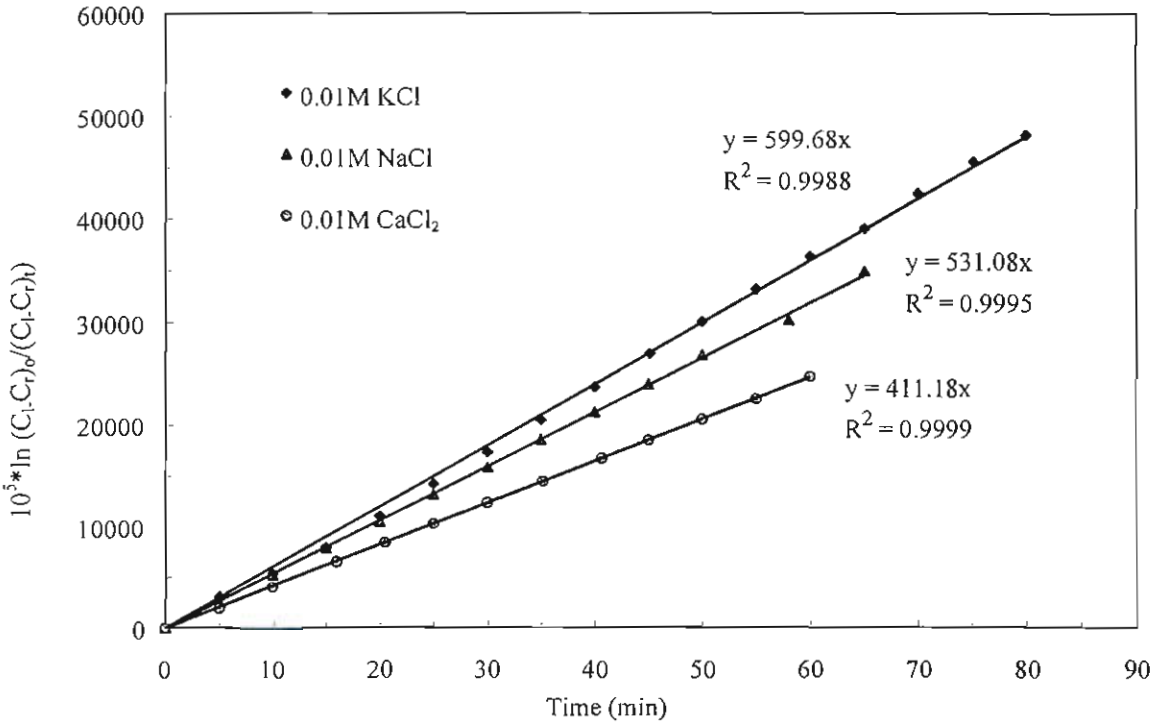

Figure 2. Diffusion cell calibration, KCl, NaCl and $CaCl_2$

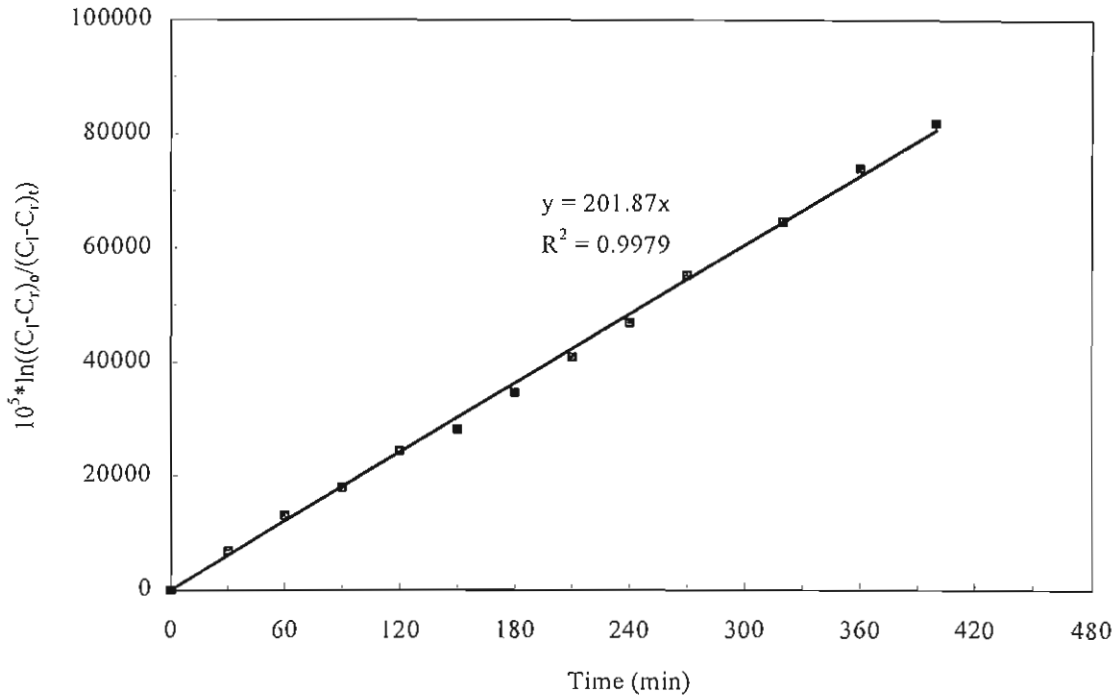

Figure 3. Diffusion cell calibration, 0.38% sucrose solution

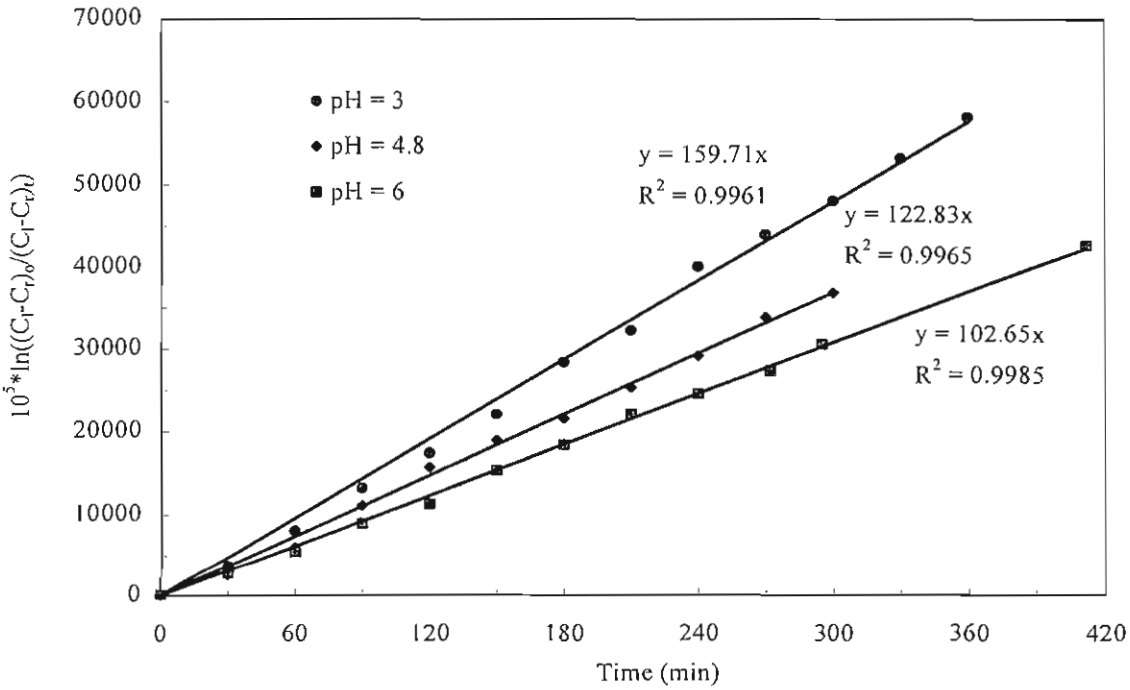

Figure 4. Humic acid diffusion experiments: [HA] = 8 mg/l, [Ca] = 11 mg/l

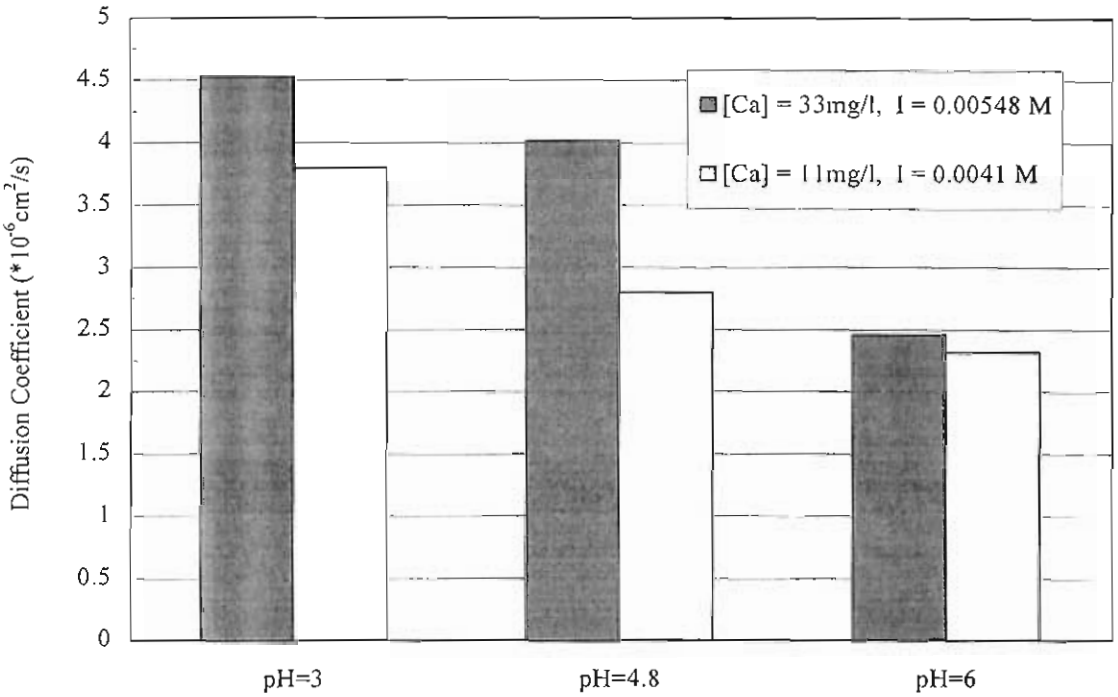

Figure 5. The effects of pH and ionic strength on the diffusion coefficients of 8 mg/l humic acid solutions